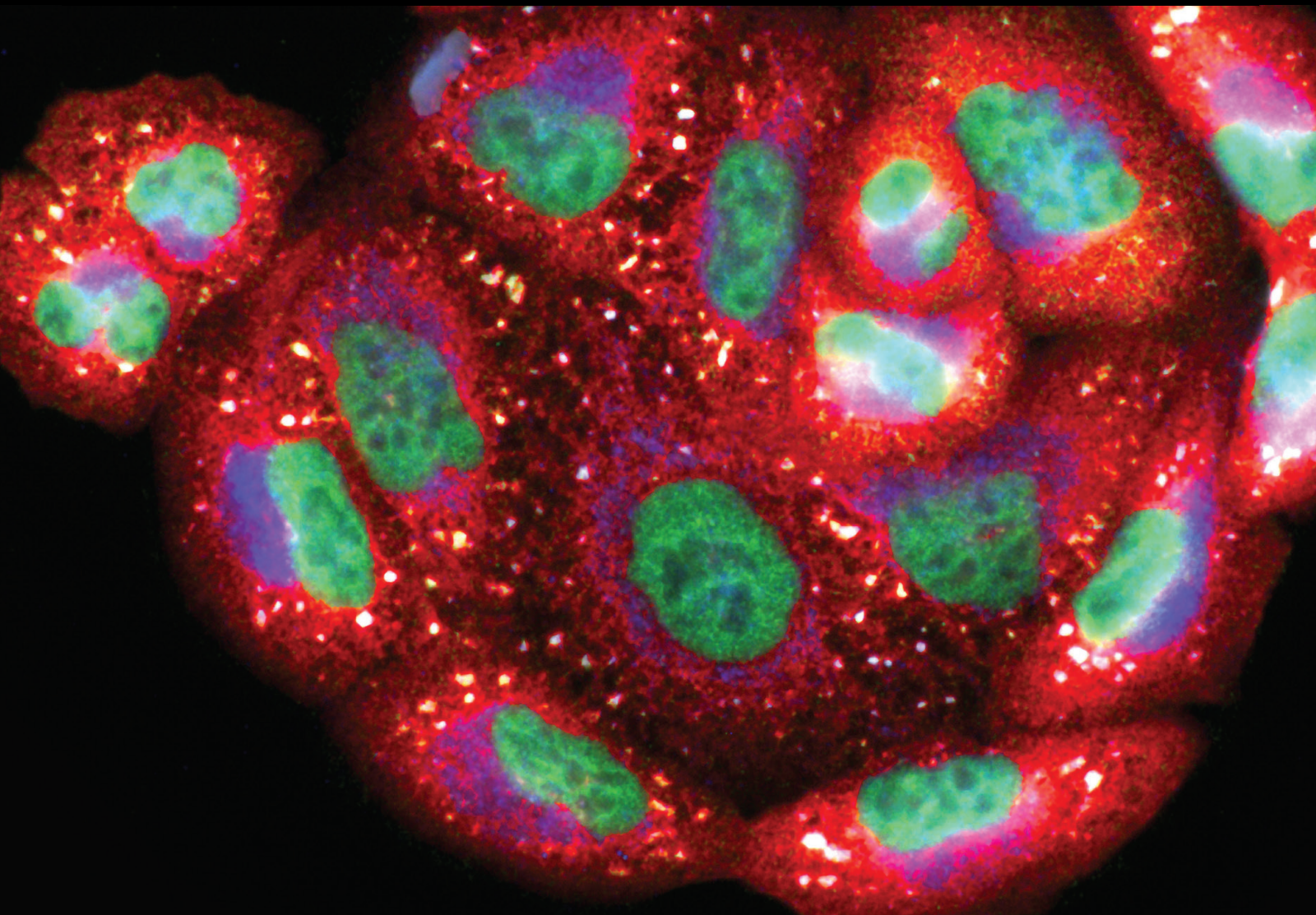


Oxidative Stress and Inflammation Interaction in Ischemia Reperfusion Injury: Role of Programmed Cell Death 2020

Lead Guest Editor: Weifeng Yao

Guest Editors: Xue Han, Hong Zheng, Wai Lydia Tai, Margaret H Hastings,
and Ziqing Hei





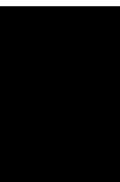
**Oxidative Stress and Inflammation Interaction
in Ischemia Reperfusion Injury: Role of
Programmed Cell Death 2020**

Oxidative Medicine and Cellular Longevity

**Oxidative Stress and Inflammation
Interaction in Ischemia Reperfusion
Injury: Role of Programmed Cell Death
2020**

Lead Guest Editor: Weifeng Yao

Guest Editors: Xue Han, Hong Zheng, Wai Lydia
Tai, Margaret H Hastings, and Ziqing Hei



Copyright © 2021 Hindawi Limited. All rights reserved.

This is a special issue published in "Oxidative Medicine and Cellular Longevity" All articles are open access articles distributed under the Creative Commons Attribution License, which permits unrestricted use, distribution, and reproduction in any medium, provided the original work is properly cited.

Chief Editor

Jeannette Vasquez-Vivar, USA

Associate Editors

Amjad Islam Aqib, Pakistan
Angel Catalá , Argentina
Cinzia Domenicotti , Italy
Janusz Gebicki , Australia
Aldrin V. Gomes , USA
Vladimir Jakovljevic , Serbia
Thomas Kietzmann , Finland
Juan C. Mayo , Spain
Ryuichi Morishita , Japan
Claudia Penna , Italy
Sachchida Nand Rai , India
Paola Rizzo , Italy
Mithun Sinha , USA
Daniele Vergara , Italy
Victor M. Victor , Spain

Academic Editors

Ammar AL-Farga , Saudi Arabia
Mohd Adnan , Saudi Arabia
Ivanov Alexander , Russia
Fabio Altieri , Italy
Daniel Dias Rufino Arcanjo , Brazil
Peter Backx, Canada
Amira Badr , Egypt
Damian Bailey, United Kingdom
Rengasamy Balakrishnan , Republic of Korea
Jiaolin Bao, China
Ji C. Bihl , USA
Hareram Birla, India
Abdelhakim Bouyahya, Morocco
Ralf Braun , Austria
Laura Bravo , Spain
Matt Brody , USA
Amadou Camara , USA
Marcio Carcho , Portugal
Peter Celec , Slovakia
Giselle Cerchiaro , Brazil
Arpita Chatterjee , USA
Shao-Yu Chen , USA
Yujie Chen, China
Deepak Chhangani , USA
Ferdinando Chiaradonna , Italy

Zhao Zhong Chong, USA
Fabio Ciccarone, Italy
Alin Ciobica , Romania
Ana Cipak Gasparovic , Croatia
Giuseppe Cirillo , Italy
Maria R. Ciriolo , Italy
Massimo Collino , Italy
Manuela Corte-Real , Portugal
Manuela Curcio, Italy
Domenico D'Arca , Italy
Francesca Danesi , Italy
Claudio De Lucia , USA
Damião De Sousa , Brazil
Enrico Desideri, Italy
Francesca Diomede , Italy
Raul Dominguez-Perles, Spain
Joël R. Drevet , France
Grégory Durand , France
Alessandra Durazzo , Italy
Javier Egea , Spain
Pablo A. Evelson , Argentina
Mohd Farhan, USA
Ioannis G. Fatouros , Greece
Gianna Ferretti , Italy
Swaran J. S. Flora , India
Maurizio Forte , Italy
Teresa I. Fortoul, Mexico
Anna Fracassi , USA
Rodrigo Franco , USA
Juan Gambini , Spain
Gerardo García-Rivas , Mexico
Husam Ghanim, USA
Jayeeta Ghose , USA
Rajeshwary Ghosh , USA
Lucia Gimeno-Mallench, Spain
Anna M. Giudetti , Italy
Daniela Giustarini , Italy
José Rodrigo Godoy, USA
Saeid Golbidi , Canada
Guohua Gong , China
Tilman Grune, Germany
Solomon Habtemariam , United Kingdom
Eva-Maria Hanschmann , Germany
Md Saquib Hasnain , India
Md Hassan , India


Tim Hofer , Norway
John D. Horowitz, Australia
Silvana Hrelia , Italy
Dragan Hrnčić, Serbia
Zebo Huang , China
Zhao Huang , China
Tarique Hussain , Pakistan
Stephan Immenschuh , Germany
Norsharina Ismail, Malaysia
Franco J. L. , Brazil
Sedat Kacar , USA
Andleeb Khan , Saudi Arabia
Kum Kum Khanna, Australia
Neelam Khaper , Canada
Ramoji Kosuru , USA
Demetrios Kouretas , Greece
Andrey V. Kozlov , Austria
Chan-Yen Kuo, Taiwan
Gaocai Li , China
Guoping Li , USA
Jin-Long Li , China
Qiangqiang Li , China
Xin-Feng Li , China
Jialiang Liang , China
Adam Lightfoot, United Kingdom
Christopher Horst Lillig , Germany
Paloma B. Liton , USA
Ana Lloret , Spain
Lorenzo Loffredo , Italy
Camilo López-Alarcón , Chile
Daniel Lopez-Malo , Spain
Massimo Lucarini , Italy
Hai-Chun Ma, China
Nageswara Madamanchi , USA
Kenneth Maiese , USA
Marco Malaguti , Italy
Steven McAnulty, USA
Antonio Desmond McCarthy , Argentina
Sonia Medina-Escudero , Spain
Pedro Mena , Italy
V́ctor M. Mendoza-Núñez , Mexico
Lidija Milkovic , Croatia
Alexandra Miller, USA
Sara Missaglia , Italy

Premysl Mladenka , Czech Republic
Sandra Moreno , Italy
Trevor A. Mori , Australia
Fabiana Morroni , Italy
Ange Mouithys-Mickalad, Belgium
Iordanis Mourouzis , Greece
Ryoji Nagai , Japan
Amit Kumar Nayak , India
Abderrahim Nemmar , United Arab Emirates
Xing Niu , China
Cristina Nocella, Italy
Susana Novella , Spain
Hassan Obied , Australia
Pál Pacher, USA
Pasquale Pagliaro , Italy
Dilipkumar Pal , India
Valentina Pallottini , Italy
Swapnil Pandey , USA
Mayur Parmar , USA
Vassilis Paschalis , Greece
Keshav Raj Paudel, Australia
Ilaria Peluso , Italy
Tiziana Persichini , Italy
Shazib Pervaiz , Singapore
Abdul Rehman Phull, Republic of Korea
Vincent Pialoux , France
Alessandro Poggi , Italy
Zsolt Radak , Hungary
Dario C. Ramirez , Argentina
Erika Ramos-Tovar , Mexico
Sid D. Ray , USA
Muneeb Rehman , Saudi Arabia
Hamid Reza Rezvani , France
Alessandra Ricelli, Italy
Francisco J. Romero , Spain
Joan Roselló-Catafau, Spain
Subhadeep Roy , India
Josep V. Rubert , The Netherlands
Sumbal Saba , Brazil
Kunihiro Sakuma, Japan
Gabriele Saretzki , United Kingdom
Luciano Saso , Italy
Nadja Schroder , Brazil

Anwen Shao , China
Iman Sherif, Egypt
Salah A Sheweita, Saudi Arabia
Xiaolei Shi, China
Manjari Singh, India
Giulia Sita , Italy
Ramachandran Srinivasan , India
Adrian Sturza , Romania
Kuo-hui Su , United Kingdom
Eisa Tahmasbpour Marzouni , Iran
Hailiang Tang, China
Carla Tatone , Italy
Shane Thomas , Australia
Carlo Gabriele Tocchetti , Italy
Angela Trovato Salinaro, Italy
Rosa Tundis , Italy
Kai Wang , China
Min-qi Wang , China
Natalie Ward , Australia
Grzegorz Wegrzyn, Poland
Philip Wenzel , Germany
Guangzhen Wu , China
Jianbo Xiao , Spain
Qiongming Xu , China
Liang-Jun Yan , USA
Guillermo Zalba , Spain
Jia Zhang , China
Junmin Zhang , China
Junli Zhao , USA
Chen-he Zhou , China
Yong Zhou , China
Mario Zoratti , Italy








Contents

1-O-Hexyl-2,3,5-Trimethylhydroquinone Ameliorates the Development of Preeclampsia through Suppression of Oxidative Stress and Endothelial Cell Apoptosis

Lai Jiang, Yanping Gong, Jie Rao, Qihong Yang, Na Gao, Guiyang Li, and Yuyan Ma 


Research Article (12 pages), Article ID 8839394, Volume 2021 (2021)

Neuroprotection Effect of Astragaloside IV from 2-DG-Induced Endoplasmic Reticulum Stress

Yu Fu , Jianhang Cai , Mengyao Xi , Yifei He , Yang Zhao , Yi Zheng , Yidong Zhang , Jinkun Xi , and Yonggui He 

Research Article (11 pages), Article ID 9782062, Volume 2020 (2020)

Pharmacological Modulation of Cardiac Remodeling after Myocardial Infarction

Wei Zhao, Jia Zhao, and Jianhui Rong 




Review Article (11 pages), Article ID 8815349, Volume 2020 (2020)

Involvement of the miR-137-3p/CAPN-2 Interaction in Ischemia-Reperfusion-Induced Neuronal Apoptosis through Modulation of p35 Cleavage and Subsequent Caspase-8 Overactivation

He Wang , Qian Yu , Zai-Li Zhang , Hong Ma , and Xiao-Qian Li 






Research Article (17 pages), Article ID 2616871, Volume 2020 (2020)

A Preclinical Systematic Review of Curcumin for Protecting the Kidney with Ischemia Reperfusion Injury

Zi-Hao Wang, Li-Hui Deng, Chang-Wei Chi, Hong Wang , Yue-Yue Huang , and Qun Zheng 


Research Article (17 pages), Article ID 4546851, Volume 2020 (2020)

Implication of Gut Microbiota in Cardiovascular Diseases

Wenyi Zhou , Yiyu Cheng, Ping Zhu , M. I. Nasser , Xueyan Zhang , and Mingyi Zhao 


Review Article (14 pages), Article ID 5394096, Volume 2020 (2020)

Dexmedetomidine Improves Lung Function by Promoting Inflammation Resolution in Patients Undergoing Totally Thoracoscopic Cardiac Surgery

Junji Cui, Mintai Gao, Hongqian Huang, Xiaoyan Huang, and Qingshi Zeng 



Research Article (10 pages), Article ID 8638301, Volume 2020 (2020)

MG53 Protects against Sepsis-Induced Myocardial Dysfunction by Upregulating Peroxisome Proliferator-Activated Receptor- α





Xue Han, Daili Chen, Ning Liufu, Fengtao Ji, Qingshi Zeng, Weifeng Yao , and Minghui Cao 

Research Article (16 pages), Article ID 7413693, Volume 2020 (2020)

Electroacupuncture Pretreatment Attenuates Intestinal Injury after Autogenous Orthotopic Liver Transplantation in Rats via the JAK/STAT Pathway

Lili Jia , Wenli Yu , Hongli Yu, and Yiqi Weng

Research Article (11 pages), Article ID 9187406, Volume 2020 (2020)

MiR-181c-5p Promotes Inflammatory Response during Hypoxia/Reoxygenation Injury by Downregulating Protein Tyrosine Phosphatase Nonreceptor Type 4 in H9C2 Cardiomyocytes
Sheng Wang , Liang Ge, Dengwen Zhang, Lin Wang, Hao Liu, Xiaodong Ye, Wanling Liang, Jun Li, Haichun Ma , Yin Cai , and Zhengyuan Xia 
Research Article (13 pages), Article ID 7913418, Volume 2020 (2020)

Research Article

1-O-Hexyl-2,3,5-Trimethylhydroquinone Ameliorates the Development of Preeclampsia through Suppression of Oxidative Stress and Endothelial Cell Apoptosis

Lai Jiang,¹ Yanping Gong,² Jie Rao,³ Qihong Yang,⁴ Na Gao,¹ Guiyang Li,¹ and Yuyan Ma¹ 

¹Department of Obstetrics and Gynecology, Qilu Hospital, Cheeloo College of Medicine, Shandong University, Jinan, Shandong 250012, China

²Department of Obstetrics and Gynecology, The First Affiliated Hospital of USTC, Division of Life Sciences and Medicine, University of Science and Technology of China, Hefei, Anhui 230001, China

³Department of Echocardiography, The First Affiliated Hospital of USTC, Division of Life Sciences and Medicine, University of Science and Technology of China, Hefei, Anhui 230001, China

⁴Department of Obstetrics and Gynecology, Jinan Maternity and Child Care Hospital, Jinan, Shandong 250001, China

Correspondence should be addressed to Yuyan Ma; yuyanma@sdu.edu.cn

Received 4 September 2020; Revised 26 December 2020; Accepted 6 January 2021; Published 20 January 2021

Academic Editor: Ziqing Hei

Copyright © 2021 Lai Jiang et al. This is an open access article distributed under the Creative Commons Attribution License, which permits unrestricted use, distribution, and reproduction in any medium, provided the original work is properly cited.

1-O-Hexyl-2,3,5-trimethylhydroquinone (HTHQ), a potent nuclear factor-E2-related factor 2 (Nrf2) activator, has potent antioxidant activity by scavenging reactive oxygen species (ROS). However, the role of HTHQ on the development of preeclampsia (PE) and the underlying mechanisms have barely been explored. In the present study, PE model was induced by adenovirus-mediated overexpression of soluble fms-like tyrosine kinase 1 (sFlt-1) in pregnant mice. The results showed that HTHQ treatment significantly relieved the high systolic blood pressure (SBP) and proteinuria and increased the fetal weight and fetal weight/placenta weight in preeclamptic mice. Furthermore, we found that HTHQ treatment significantly decreased soluble endoglin (sEng), endothelin-1 (ET-1), and activin A and restored vascular endothelial growth factor (VEGF) in preeclamptic mice. In addition, HTHQ treatment inhibited oxidative stress and endothelial cell apoptosis by increasing the levels of Nrf2 and its downstream haemoxygenase-1 (HO-1) protein. In line with the data *in vivo*, we discovered that HTHQ treatment attenuated oxidative stress and cell apoptosis in human umbilical vein endothelial cells (HUVECs) following hypoxia and reperfusion (H/R), and the HTHQ-mediated protection was lost after transfected with siNrf2. In conclusion, these results suggested that HTHQ ameliorates the development of preeclampsia through suppression of oxidative stress and endothelial cell apoptosis.

1. Introduction

Preeclampsia (PE) is a serious complication of pregnancy, which is one of the important causes of morbidity and mortality of pregnant women and perinatal infants. It refers to a group of clinical syndromes with hypertension and proteinuria as the main clinical manifestations after 20 weeks of pregnancy [1–4]. PE adversely affects maternal health and leads to substantial complications, such as eclampsia, ischemic heart disease, renal failure, liver injury, central nervous system injury, stroke, pulmonary edema, respiratory distress syndrome, and other complications. It also increases the risks

of fetus growth restriction, placental abruption, prematurity, and even perinatal mortality, all of which negatively mediate fetal health [5–7]. Clinical data revealed that PE affects roughly 5% to 7% of pregnant women worldwide and led to the deaths of more than 70,000 maternal and 50,000 fetal every year [8]. Therefore, great attention has been addressed to the identification of novel therapeutic targets and agents against the maternal syndrome of PE.

Although the pathophysiology of PE remains is not wholly clear, it is known that oxidative stress plays a pivotal role of PE development. Oxidative stress is characterized by the imbalance between the generation of reactive oxygen

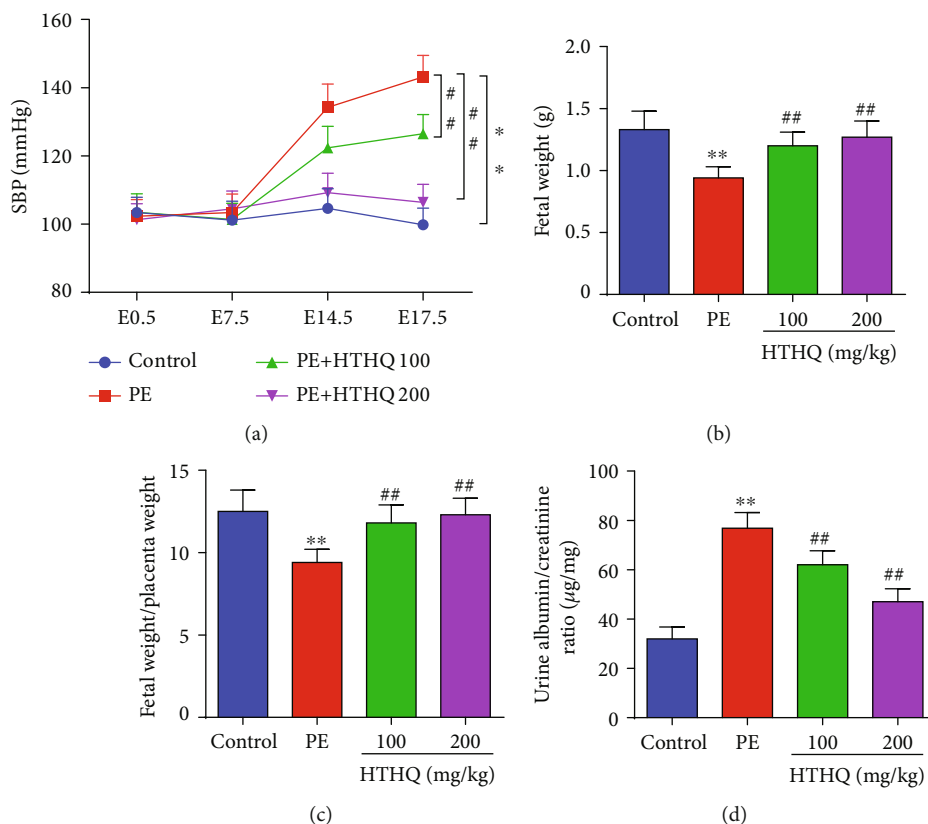


FIGURE 1: HTHQ treatment ameliorated PE development in vivo. (a) The systolic blood pressure (SBP) of mice was detected in each group ($n = 8$). (b) The fetal weight of mice was detected in each group ($n = 8$). (c) The fetal weight/placenta weight ratio of mice was detected in each group ($n = 8$). (d) The proteinuria of mice was detected in each group ($n = 8$). ** $P < 0.01$ vs. the control group; # $P < 0.05$ and ## $P < 0.01$ vs. the PE group.

species (ROS) and the antioxidant defence system, [9, 10]. ROS can induce placental dysfunction by suppression of placental angiogenesis, induction endothelial damage, and immune malfunction, which are suggested to be the underlying of PE development [11–13]. Several studies have found suppressing oxidative stress, and scavenging ROS represents potential therapeutic opportunities for the treatment of PE development [11] [14].

1-O-Hexyl-2,3,5-trimethylhydroquinone (HTHQ), a derivative of vitamin E, has potent antioxidant activity by directly reacting with ROS and scavenging them to form more stable free radicals [15]. HTHQ is a potent nuclear factor-E2-related factor 2 (Nrf2) activator and induces the haemoxygenase-1 (HO-1) expression [16, 17]. In addition, HTHQ has positive effects on various diseases and conditions, including diabetes [18], hepatic cirrhosis [19], neurodegenerative diseases [20], and cancer [21, 22]. Previous researches showed that Nrf2/HO-1 pathway plays an important role in the development of PE [23, 24]. However, the effects of HTHQ on PE development remain unclear. Hence, the aim of this study was to investigate the effects of HTHQ on PE development as well as the associated mechanisms.

2. Materials and Methods

2.1. Animal and Model Establishment. Female (8–10 weeks) and male (for mating purposes only) C57BL/6 mice were

purchased from Beijing Vital River Laboratory Animal Technology Co., Ltd. (Beijing, China). All mice were housed with a controlled environment and maintained in 12-hour light and dark cycles. Virgin female mice were mated with males, and the next morning, a white or faint yellow vaginal plug was detected in the 0.5 embryonic day (E0.5). The PE model was prepared by injection with 3×10^9 PFU/100 μ L of adenovirus to overexpress sFlt-1 (Ad-sFlt-1) through the tail vein at days 7 to 8 of gestation as described in a previous study [25]. The mice in the control group were injected with 3×10^9 PFU/100 μ L of adenovirus encoding murine Fc protein (Ad-Fc). In PE group, the mice were orally administered with HTHQ (100 or 200 mg/kg) every day from days E0.5 to E17.5 of pregnancy. The systolic blood pressure (SBP) was measured by noninvasive blood pressure analysis system and repeated at least three times. Albumin and creatinine levels were determined following the manufacturer's instructions on E17.5. All animal care and experimental procedures were conducted in strict according to the National Institutes of Health Guide for the Care and Use of Laboratory Animals and approved by the animal ethics and welfare committee of Anhui Medical University.

2.2. Plasma and Tissue Assays. On day 17.5 of pregnancy, the animals were euthanized, and peripheral blood was collected for further analysis. The mice were dissected; fetal and placentas were obtained to evaluate the weight. The circulating

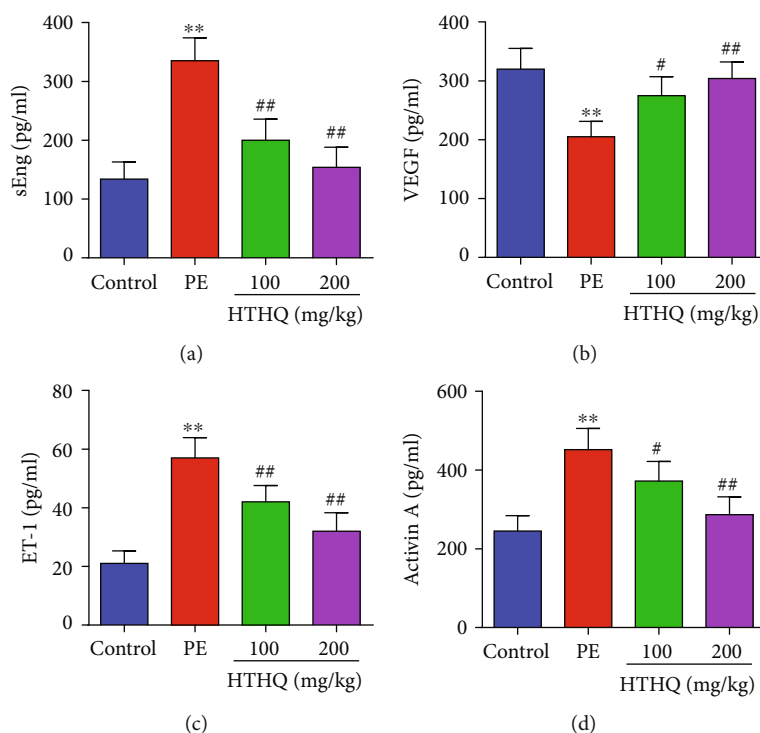


FIGURE 2: HTHQ treatment attenuated decreases the concentration of sEng, ET-1, and activin A levels and restored VEGF levels in blood from PE animals. ELISA was used to detect the concentration of sEng (a), VEGF (b), ET-1 (c), and activin A (d) in serum of mice in each group ($n = 6$). ** $P < 0.01$ vs. the control group; # $P < 0.05$ and ## $P < 0.01$ vs. the PE group.

levels of soluble endoglin (sEng), vascular endothelial growth factor (VEGF), endothelin-1 (ET-1), and activin A were measured using enzyme-linked immunosorbant assay (ELISA) kits according to the manufacturer's instructions.

2.3. TUNEL Staining. Placenta tissues were fixed by perfusion with 10% formalin and embedded in paraffin and then cut into $4 \mu\text{m}$ slides. Apoptotic cells were measured using a terminal deoxynucleotidyl transferase dUTP nick-end labeling (TUNEL) detection kit. All images were analyzed using a quantitative digital image analysis system.

2.4. Cell Culture and Treatment. Human umbilical vein endothelial cells (HUVECs) were purchased and cultured in Medium 199 supplemented with 20% fetal bovine serum, 1% antibiotics, and L-glutamine at 37°C under 5% CO_2 and 100% humidity [26]. To knockdown the genes, the cells were transfected with si-Nrf2 using Lipofectamine 2000 according to the protocol recommended. After transfection with siRNA for 18 h, the HUVECs were treated with HTHQ for 6 h before hypoxia and reperfusion (H/R) insult. Briefly, the cells were cultured in preconditioned hypoxic medium under 5% CO_2 and 95% N_2 in a humidified chamber for 8 h and then replaced with fresh medium, and the cells were cultured under normal growth conditions for 16 h of reoxygenation.

2.5. Oxidative Stress Detection. Dihydroethidium (DHE) staining was performed to assess the ROS production as described in a previous study [27]. In addition, placenta tissues and HUVEC concentrations of superoxide dismutase

(SOD), catalase (CAT), malondialdehyde (MDA), and glutathione (GSH) were measured using commercially available kits.

2.6. Western Blotting. The total proteins were separated on SDS-PAGE gel, blotted onto PVDF membrane, and then blocked with 5% nonfat milk. Subsequently, the membranes were incubated with antibodies Bax (1:1000, Abcam), Bcl-2 (1:1000, Abcam), Nrf2 (1:1000, Abcam), HO-1 (1:1000, Abcam), and β -actin (1:1000, Abcam). The membranes were incubated goat anti-rabbit IgG secondary antibody (LI-COR) and analyzed by a two-color infrared imaging system (Odyssey; LICOR) to quantify protein expression.

2.7. Statistical Analysis. The data are presented as the means \pm standard deviation (SD). Statistical differences between 2 groups were determined by Student's t -test. Statistical comparisons among multiple groups were compared by one-way analysis of variance (ANOVA) tests with a post hoc Tukey test. P values less than 0.05 were considered to indicate a statistically significant.

3. Results

3.1. HTHQ Treatment Ameliorated PE Development In Vivo. As shown in Figure 1, the PE group has increased SBP and the proteinuria and decreased the fetal weight and fetal weight/placenta weight compared with the control group, indicative of successful model establishment. We further found that HTHQ treatment significantly relieved the high

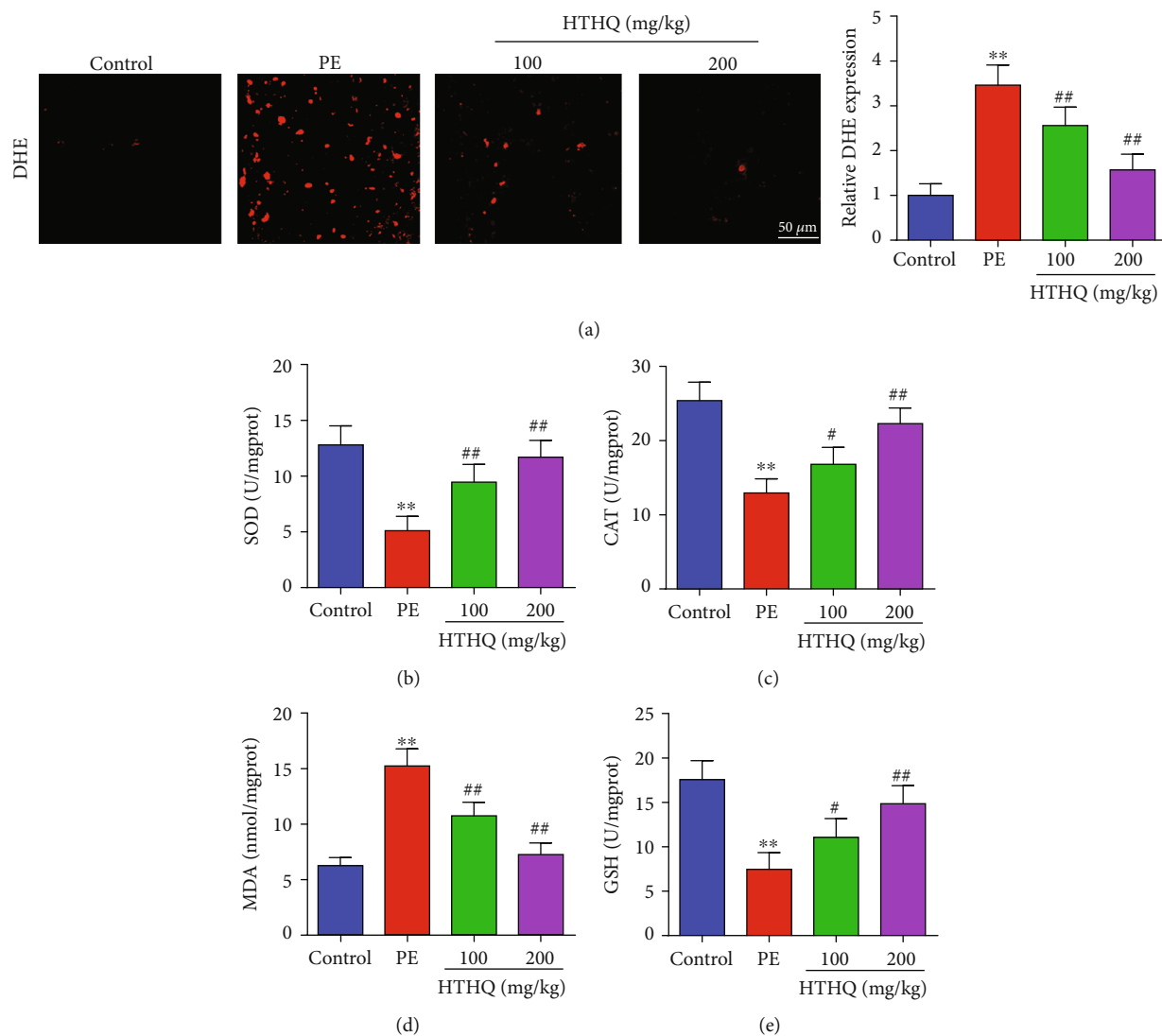


FIGURE 3: HTHQ treatment attenuated oxidative stress induced by PE. DHE staining was used to assess the ROS production in each group ($n=6$). The levels of SOD (b), CAT (c), MDA (d), and GSH (e) in each group ($n=6$). ** $P < 0.01$ vs. the control group; # $P < 0.05$ and ## $P < 0.01$ vs. the PE group.

SBP and proteinuria and increased the fetal weight and the fetal weight and fetal weight/placenta weight in a dose-dependent manner (Figure 1). Notably, HTHQ treatment significantly decreased sEng, ET-1, and activin A levels and restored VEGF concentrations compared with the PE group (Figure 2), suggested that HTHQ treatment is able to relieve the symptoms of PE.

3.2. HTHQ Treatment Attenuated Oxidative Stress Induced by PE. Then, DHE staining was performed to assess ROS production, and the results showed that the DHE expression in the PE group was higher than that in the control group, which was mitigated by HTHQ (Figure 3(a)). In addition, the SOD, CAT, and GSH levels in the PE group were significantly lower, and MDA levels were significantly higher than those in the control group (Figures 3(b)–3(e)). However, HTHQ treatment significantly upregulated SOD, CAT, and

GSH levels and reduced MDA levels compared with the PE group (Figures 3(b)–3(e)).

3.3. HTHQ Treatment Decreased Placental Apoptosis. To further assess the protective effects of HTHQ, we used the TUNEL staining to measure the placental apoptosis. The results demonstrated that the apoptotic index in the PE group was obviously increased compared with that in the control group, while HTHQ treatment significantly decreased placental apoptosis induced by PE (Figure 4(a)). The results of western blot also showed that HTHQ treatment significantly increased Bax levels and decreased the expression of Bcl-2 in the PE group (Figure 4(b)).

3.4. HTHQ Treatment Attenuated Oxidative Stress and Apoptosis in HUVECs following H/R. To further assess the effects of HTHQ on oxidative stress following H/R, we measured the SOD, CAT activities, and MDA contents in

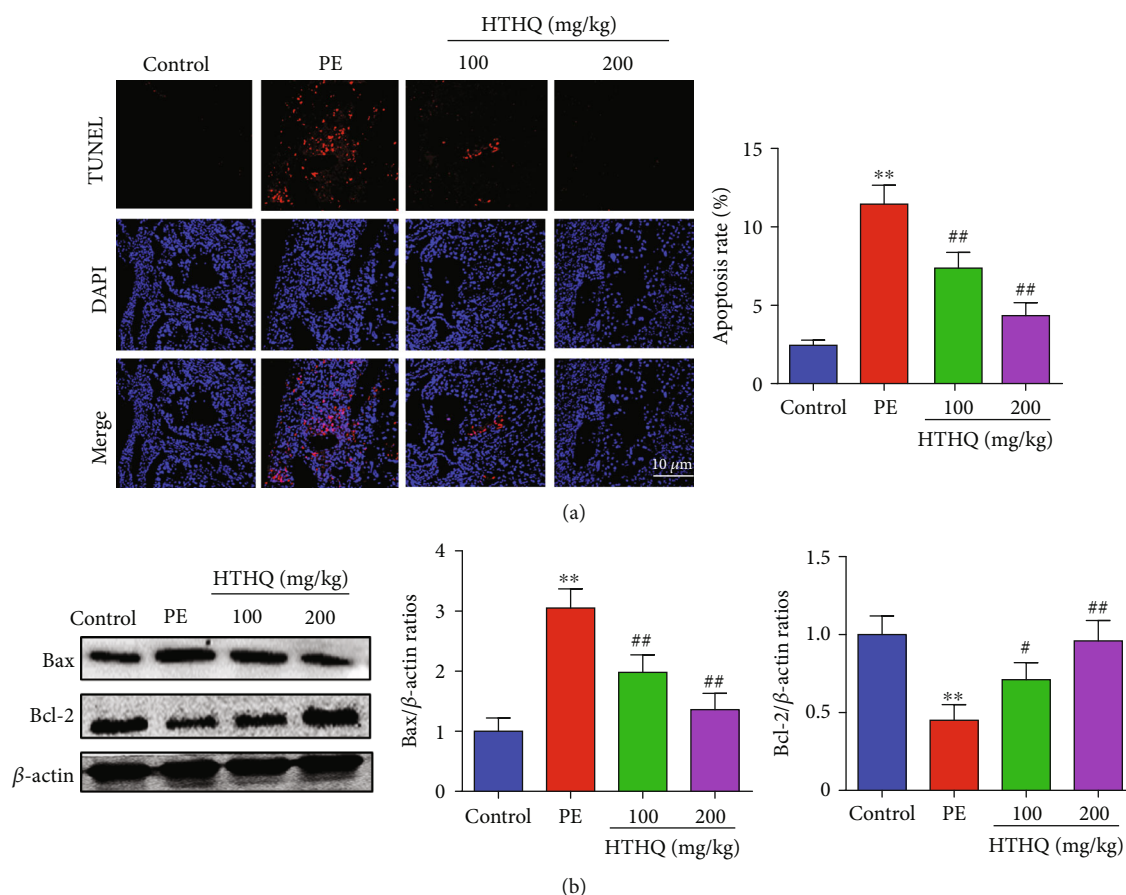


FIGURE 4: HTHQ treatment decreased placental apoptosis. (a, b) TUNEL staining was used to measure the placental apoptosis in each group ($n = 4$). ** $P < 0.01$ vs. the control group; # $P < 0.05$ and ## $P < 0.01$ vs. the PE group.

HUVECs. The results revealed that the SOD and CAT activities in the H/R group were significantly lower, and MDA contents were significantly higher than those in the control group (Figures 5(a)–5(c)). However, HTHQ treatment significantly restored SOD and CAT activities and decreased MDA contents compared with the H/R group (Figures 5(a)–5(c)). In addition, HTHQ treatment significantly decreased endothelial cell apoptosis following H/R (Figure 5(d)).

3.5. HTHQ Activates Nrf2 Antioxidant Pathway. Recent evidence has strongly suggested that HTHQ is a potent nuclear Nrf2 activator and has positive effects on oxidative stress-related diseases [16, 17]. Thus, we investigated whether HTHQ protect against PE is associated with Nrf2 antioxidant pathway. The results showed that the expression of Nrf2 and HO-1 was also significantly increased after HTHQ treatment (Figure 6(a)). In line with the data in vivo, we found that HTHQ treatment increased Nrf2 and HO-1 expression after following H/R (Figure 6(b)), indicated that HTHQ regulates PE via Nrf2 antioxidant pathway.

3.6. HTHQ Induces Translocation of Nrf2. Then, we evaluated the effects of HTHQ on Nrf2 transcription. The results of western blots showed that the level of nuclear-Nrf2 was decreased, while the level of cytoplasm-Nrf2 was increased

in the PE group compared with the sham group. In addition, HTHQ treatment significantly increased the level of nuclear-Nrf2, while decreasing the cytoplasm-Nrf2 expression (Figures 7(a) and 7(b)). The results of immunofluorescence staining also showed that HTHQ has effectively induced the nuclear translocation and transcriptional activity of Nrf2 (Figure 7(c)).

3.7. The Protection of HTHQ Involves the Nrf2/HO-1 Pathway. To confirm the role of Nrf2/HO-1 pathway in HTHQ-mediated protection effects, we measured the oxidative stress and cell apoptosis after si-Nrf2 transfection. The results showed that HUVECs were more vulnerable to H/R-induced oxidative stress after si-Nrf2 transfection. Meanwhile, the HTHQ-mediated protection was lost in HUVECs transfected with siNrf2 (Figures 8(a) and 8(b)). In consistent, the knockdown of Nrf2 increased the apoptosis ratio after H/R, and HTHQ treatment did not affect neuronal apoptotic in HUVECs transfected with siNrf2 (Figures 8(a) and 8(b)), indicated that the protective effects of HTHQ is involved activation of Nrf2/HO-1 pathway.

4. Discussion

The present study investigated the effects of HTHQ treatment on the regulation of oxidative stress and endothelial cell

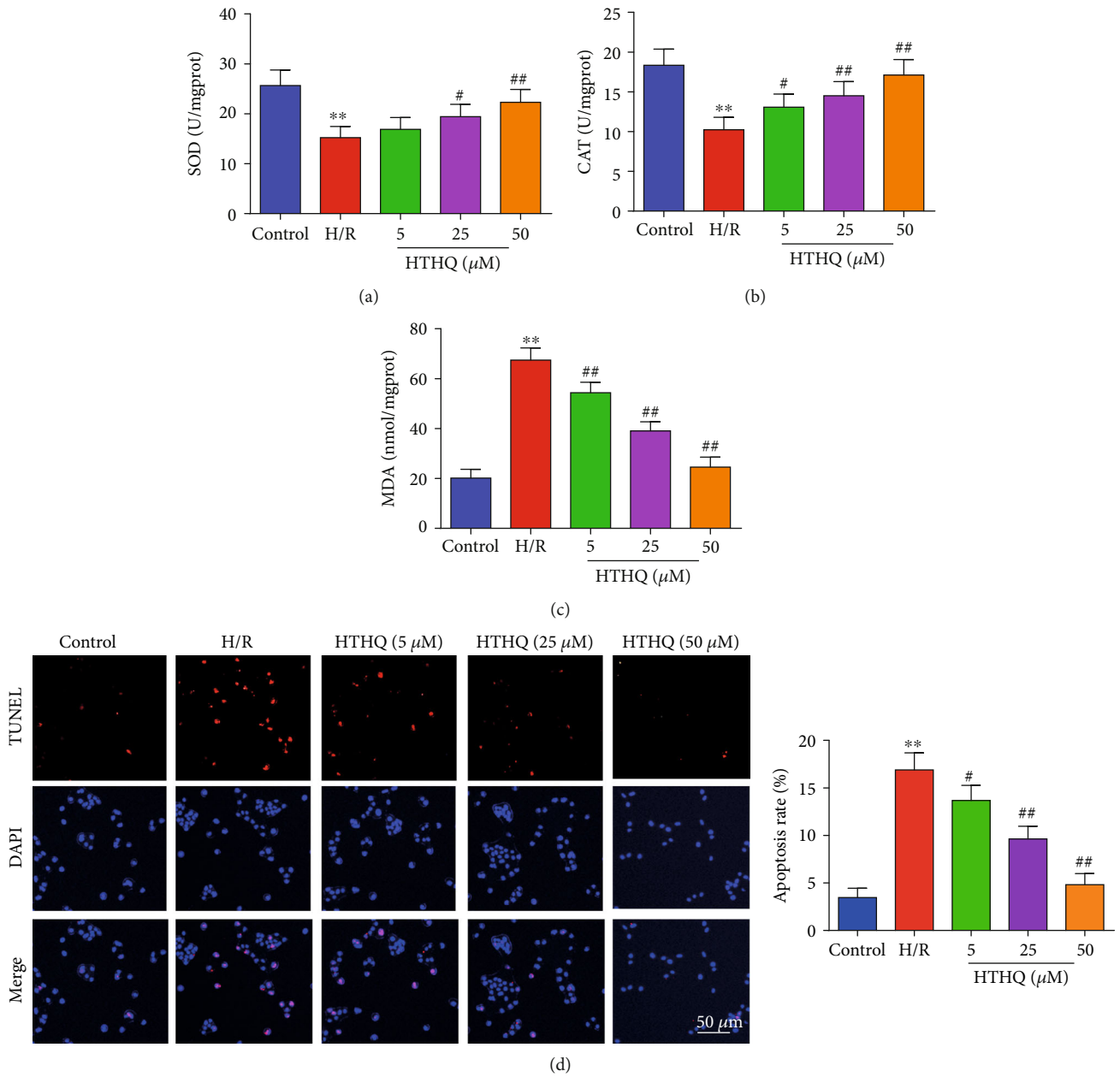


FIGURE 5: HTHQ treatment attenuated oxidative stress and apoptosis in HUVECs following H/R. The levels of SOD (a), catalase CAT (b), and MDA (c) in each group ($n = 6$). (d) Images and quantifications of TUNEL staining in each group ($n = 6$). ** $P < 0.01$ vs. the control group; # $P < 0.05$ and ## $P < 0.01$ vs. the H/R group.

apoptosis in preeclamptic mice. The results showed that HTHQ treatment is able to relieve the high SBP and reduce proteinuria in a dose-dependent manner and thus improve PE. Further, we found that HTHQ treatment significantly decreased sEng, ET-1, and activin A levels and restored VEGF in preeclamptic mice. In addition, HTHQ treatment decreases oxidative stress and endothelial cell apoptosis by increasing the levels of Nrf2 and HO-1, and the HTHQ-mediated protection was lost in HUVECs transfected with siNrf2. These data provided evidence supporting HTHQ activating the Nrf2 signaling pathway, thereby protecting cells against oxidative stress injury.

ROS, the most important factor for oxidative stress, represents a family of oxygen containing molecules [28, 29]. Excessive ROS can induce placental dysfunction by suppression of placental angiogenesis, induction endothelial damage, and immune malfunction, which are suggested to be the underlie of PE development [11] [30]. In order to maintain cellular redox homeostasis, cells are equipped with antioxidant enzymes or nonenzymatic antioxidants, including SOD, CAT, and GSH, which can scavenge ROS and inhibit free radical formation [31, 32]. Previous study demonstrated that the levels of SOD, CAT, and GSH were significantly lower in women with PE than in healthy women, suggesting

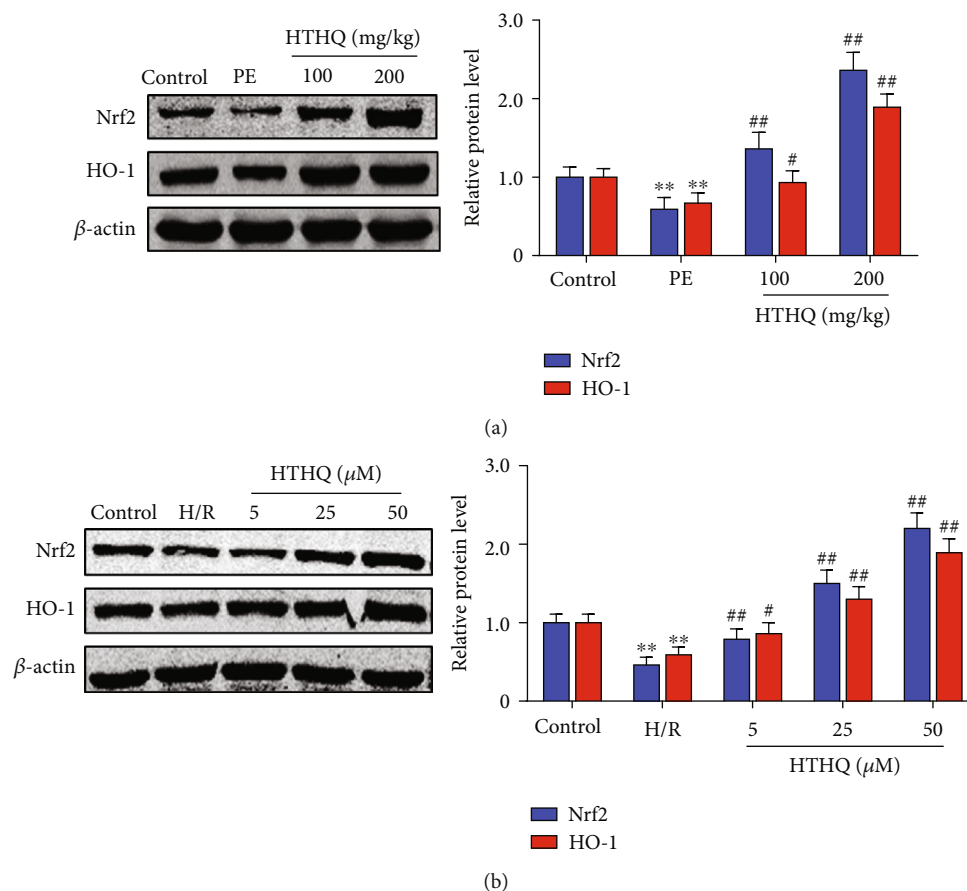


FIGURE 6: HTHQ activates Nrf2 antioxidant pathway. (a) Western blots showing the level of Nrf2 and HO-1 in mice of each group ($n = 4$). (b) Western blots showing the level of Nrf2 and HO-1 in each group ($n = 4$). ** $P < 0.01$ vs. the control group; ## $P < 0.01$ vs. the H/R group.

that the antioxidant protective capacity was decreased in women with preeclampsia [33–35]. MDA, a product of lipid peroxidation, is an important feature to estimate the degree of lipid peroxidation caused by free radical attacks [36]. Feng et al. reported that increased MDA levels could be associated with increased generation of toxic lipid peroxides and contributed to the development of PE [37].

HTHQ is a novel synthesized vitamin E derivative and has a potent antioxidant and anti-lipid-peroxidative activity. Previous research indicated that HTHQ has been considered as a promising therapeutic agent for oxidative stress-induced diseases [16] [38]. Jung et al. reported that HTHQ treatment significantly attenuated dimethylnitrosamine-induced liver fibrosis by inhibiting ROS formation and reducing lipid peroxidation. In this study, DHE staining was performed to assess the ROS production, and the results showed that the DHE expression in the PE group was higher than that in the control group, which was mitigated by HTHQ. In addition, the SOD, CAT, and GSH activities were significantly decreased, whereas MDA level was increased in PE mice and HUVECs after H/R. Interestingly, HTHQ treatment significantly reduced the extent of oxidative stress by increasing cellular antioxidants SOD, CAT, and GSH activity and decreasing MDA level, indicated that HTHQ suppressed oxidative stress induced by PE. Nevertheless, the precise mechanisms on how HTHQ exerts protection effects still unclear.

Endothelial cells are important cell types of human placenta and contribute to the regulation of vascular tone and function. Previous research showed that endothelial damage has been proposed to be the important underlie of PE and involved in major symptoms of PE, including hypertension, proteinuria, and edema [39, 40]. Thus, improving maternal endothelial function has been proposed to be an effective therapeutic strategy to ameliorate the clinical outcomes of PE [41, 42]. In this study, we detected the role of HTHQ on endothelial function. The results showed that HTHQ treatment attenuates oxidative stress in HUVECs following H/R. In addition, H/R obviously induced the apoptosis of HUVECs, while HTHQ treatment significantly decreased endothelial cell apoptosis following H/R, indicated that HTHQ could suppress endothelial dysfunction.

Nrf2 is a transcription factor and protects cells against oxidative stress, electrophiles, and carcinogenic substances [43, 44]. Under regular conditions, Nrf2 is bound to Kelch-like ECH-associated protein 1 (Keap1) in the cytosol and forms an E3 ubiquitin ligase complex, which leads to ubiquitination and proteasomal degradation of Nrf2 [45, 46]. However, when cells are exposed to oxidative and electrophilic challenges, Nrf2 is activated, released from Keap1, and binds to the ARE sequences then recruits the transcription of antioxidant defence genes [47–49]. Several evidences have shown the Nrf2 signaling pathway is a mediator of protection to

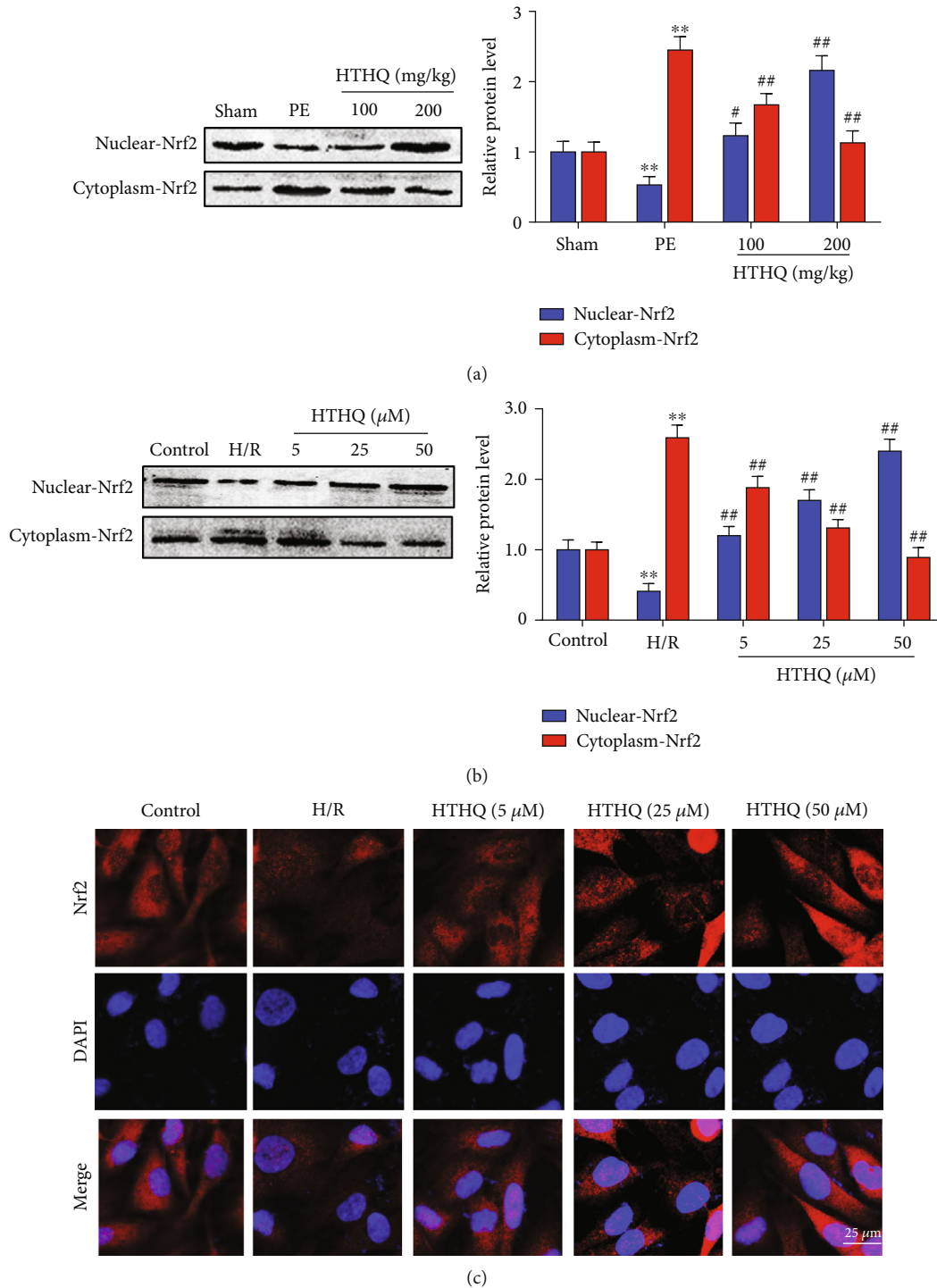


FIGURE 7: HTHQ induces translocation of Nrf2. (a) Western blots showing the level of nuclear-Nrf2 and cytoplasm-Nrf2 in mice of each group ($n = 4$). (b) Western blots showing the level of nuclear-Nrf2 and cytoplasm-Nrf2 in each group ($n = 4$). (d) Immunofluorescence staining was used to assess the translocation of Nrf2 in each group ($n = 6$). * $P < 0.05$ vs. the control group; ** $P < 0.01$ vs. the PE or H/R group.

counteract oxidative stress and maintain redox homeostasis in the placenta [50, 51]. Yu et al. reported that the Nrf2 and HO-1 expressions were lower in the PE placenta compared with the healthy women, and Nrf2 overexpression protected the placenta by upregulating the antioxidant genes in the murine PE model [50]. Onda et al. reported that sofalcone decreased sEng production and ameliorated placenta dys-

function by activate Nrf2 and HO-1 pathway. These researches further highlight that Nrf2 is a promising therapeutic target for the treatment of PE [51].

In the present study, we investigated the role of HTHQ treatment in Nrf2/HO-1 signaling pathway. The results showed that HTHQ treatment significantly increased the expression of Nrf2 and HO-1. In addition, HTHQ has

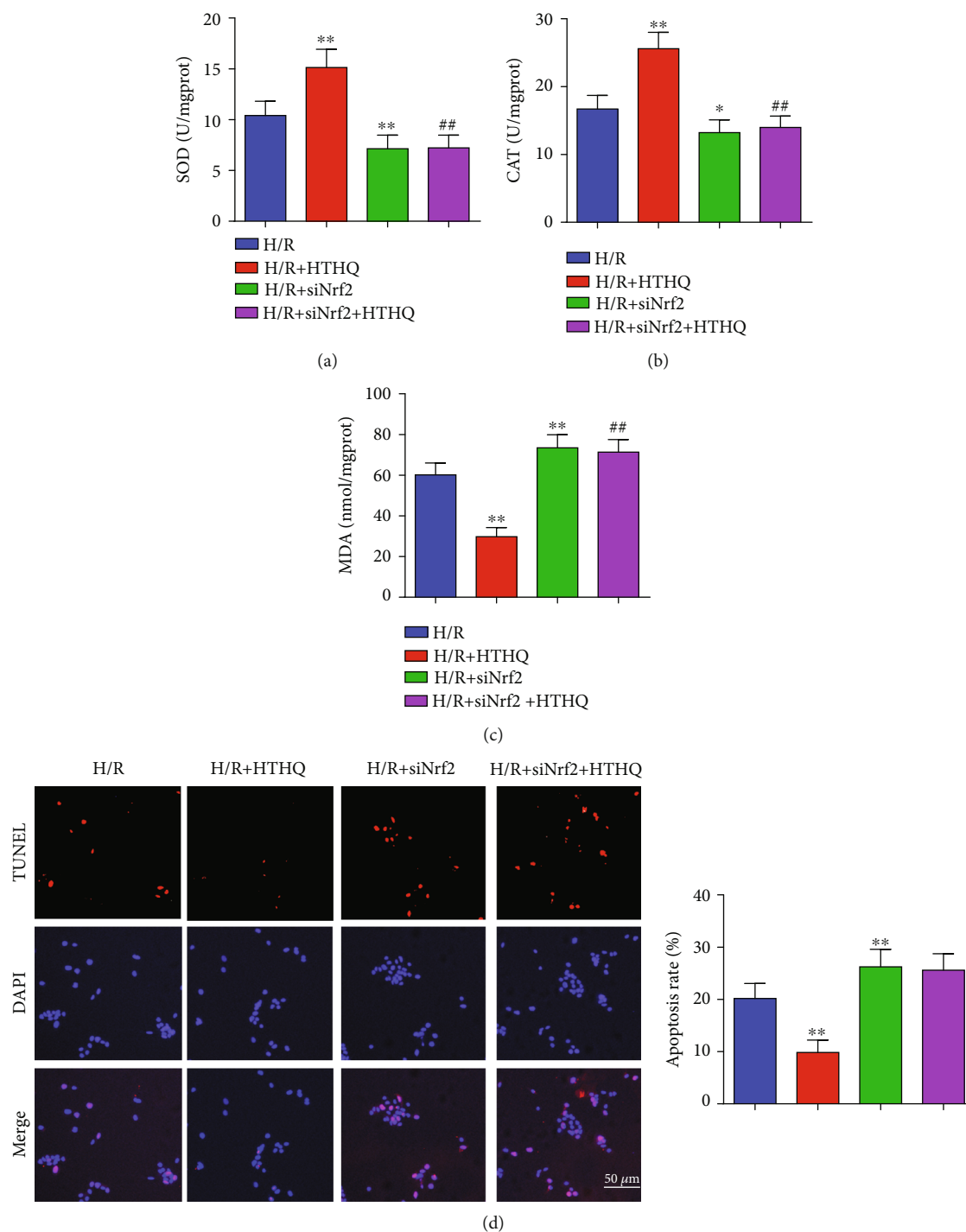


FIGURE 8: The protection of HTHQ involves the Nrf2/HO-1 pathway. The levels of SOD (a), catalase CAT (b), and MDA (c) in HUVECs after si-Nrf2 transfection ($n = 6$). (d) Images and quantifications of TUNEL staining in HUVECs after si-Nrf2 transfection ($n = 6$). * $P < 0.05$ vs. the H/R group; ** $P < 0.01$ vs. the H/R group.

effectively induced the nuclear translocation and transcriptional activity of Nrf2. As shown in our study, knockdown of Nrf2 could increase the level of oxidative stress and apoptosis of HUVECs under H/R. In addition, the HTHQ treatment mediated protective effect that was lost in HUVECs transfected with siNrf2. HO-1, which is regulated by Nrf2, has antioxidant and antiapoptotic activities by restoring

redox homeostasis and reducing inflammation response [52, 53]. Researches showed that activation of HO-1 protects placental cells against oxidative stress injury that can improve hypertension and placental ischemia in rodents PE model [54, 55]. In this study, we also found that HTHQ treatment significantly increased the HO-1 expression in the placenta of PE. Taken together, we propose that the protective

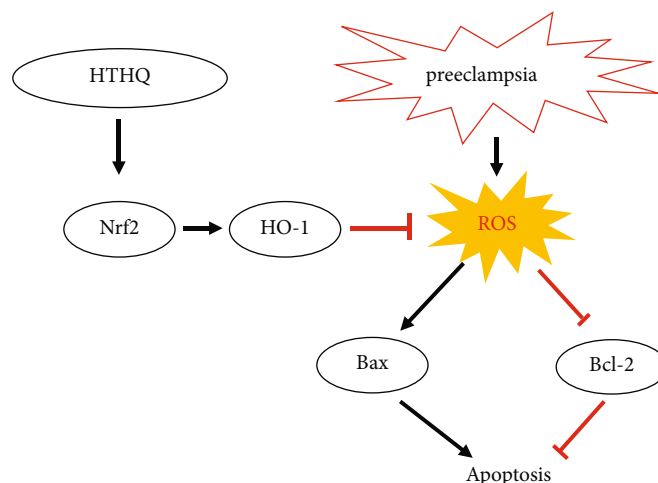


FIGURE 9: HTHQ suppresses oxidative stress and endothelial cell apoptosis and subsequent improvement of PE through activation of Nrf2/HO-1 signaling.

action of HTHQ is related to an antioxidant and antiapoptotic effect, and the mechanism is involved in Nrf2/HO-1 signaling pathway.

In summary, we have shown that HTHQ suppresses oxidative stress and endothelial cell apoptosis and subsequent improvement of PE through activation of Nrf2/HO-1 signaling (Figure 9). These findings suggest that HTHQ could be a potential pharmacological agent for PE therapy.

Data Availability

We declare that the materials described in the manuscript, including all relevant raw data, will be freely available to any scientist wishing to use them for noncommercial purposes, without breaching participant confidentiality.

Conflicts of Interest

The authors declare that there is no conflict of interest regarding the publication of this article.

Authors' Contributions

Lai Jiang and Yanping Gong contributed equally to this work.

Acknowledgments

The authors are grateful for the enthusiastic support of Mr. Kai Zhang's contribution to design the graphics. This study was supported by grants from the Anhui Province Postdoctoral Science Foundation (Grant No. 2019B324) and the Fundamental Research Funds for the Central Universities (Grant No. WK9110000044).

References

- [1] S. Wedenoja, M. Yoshihara, H. Teder et al., "Fetal_HLA-G-mediated immune tolerance and interferon response in preeclampsia," *EBioMedicine*, vol. 59, p. 102872, 2020.
- [2] W. N. Phoswa, "Dopamine in the Pathophysiology of Preeclampsia and Gestational Hypertension: Monoamine Oxidase (MAO) and Catechol-O-methyl Transferase (COMT) as Possible Mechanisms," *Oxidative Medicine and Cellular Longevity*, vol. 2019, Article ID 3546294, 8 pages, 2019.
- [3] S. Yang, L. Song, X. Shi, N. Zhao, and Y. Ma, "Ameliorative effects of pre-eclampsia by quercetin supplement to aspirin in a rat model induced by L-NAME," *Biomedicine & Pharmacotherapy*, vol. 116, p. 108969, 2019.
- [4] X. Yang, Y. Yang, Y. Yuan, L. Liu, and T. Meng, "The Roles of Uterine Natural Killer (NK) Cells and KIR/HLA-C Combination in the Development of Preeclampsia: A Systematic Review," *BioMed Research International*, vol. 2020, Article ID 4808072, 10 pages, 2020.
- [5] S. Viana-Mattioli, P. Nunes, R. Cavalli, and V. Sandrim, "Analysis of SIRT1 Expression in Plasma and in an In Vitro Model of Preeclampsia," *Oxidative Medicine and Cellular Longevity*, vol. 2020, Article ID 4561083, 7 pages, 2020.
- [6] S. Choi, J. A. Kim, S. Oh, M. H. Park, G. J. Cho, and S. H. Suh, "Internalization and Transportation of Endothelial Cell Surface KCa3.1 and KCa3.2 in Normal Pregnancy and Preeclampsia," *Oxidative Medicine and Cellular Longevity*, vol. 2019, Article ID 5820839, 13 pages, 2019.
- [7] H. Zhao, L. Gong, S. Wu et al., "The Inhibition of Protein Kinase C β Contributes to the Pathogenesis of Preeclampsia by Activating Autophagy," *EBioMedicine*, vol. 56, p. 102813, 2020.
- [8] S. Rana, E. Lemoine, J. P. Granger, and S. A. Karumanchi, "Preeclampsia: pathophysiology, challenges, and perspectives," *Circulation Research*, vol. 124, no. 7, pp. 1094–1112, 2019.
- [9] T. Silberstein, B. Hamou, S. Cervil, T. Barak, A. Burg, and O. Saphier, "Colostrum of Preeclamptic Women Has a High Level of Polyphenols and Better Resistance to Oxidative Stress in Comparison to That of Healthy Women," *Oxidative Medicine and Cellular Longevity*, vol. 2019, Article ID 1380605, 2019.
- [10] X. Xie, Z. He, N. Chen, Z. Tang, Q. Wang, and Y. Cai, "The Roles of Environmental Factors in Regulation of Oxidative Stress in Plant," *BioMed Research International*, vol. 2019, Article ID 9732325, 11 pages, 2019.

- [11] M. B. Tenório, R. C. Ferreira, F. A. Moura, N. B. Bueno, A. C. M. de Oliveira, and M. O. F. Goulart, "Cross-Talk between Oxidative Stress and Inflammation in Preeclampsia," *Oxidative Medicine and Cellular Longevity*, vol. 2019, Article ID 8238727, 26 pages, 2019.
- [12] D. Ardalic, A. Stefanovic, G. Banjac et al., "Lipid profile and lipid oxidative modification parameters in the first trimester of high- risk pregnancies - possibilities for preeclampsia prediction," *Clinical Biochemistry*, vol. 81, pp. 34–40, 2020.
- [13] M. Hodel, P. R. Blank, P. Marty, and O. Lapaire, "sFlt-1/PlGF ratio as a predictive marker in women with suspected preeclampsia: an economic evaluation from a Swiss perspective," *Disease Markers*, vol. 2019, Article ID 4096847, 10 pages, 2019.
- [14] X. Yang and T. Meng, "Long Noncoding RNA in Preeclampsia: Transcriptional Noise or Innovative Indicators?," *BioMed Research International*, vol. 2019, Article ID 5437621, 7 pages, 2019.
- [15] T. Hino, S. Kawanishi, H. Yasui, S. Oka, and H. Sakurai, "HTHQ (1-O-hexyl-2,3,5-trimethylhydroquinone), an anti-lipid-peroxidative compound: its chemical and biochemical characterizations," *Biochimica et Biophysica Acta*, vol. 1425, no. 1, pp. 47–60, 1998.
- [16] C. Tang, Y. Hu, H. Lyu et al., "Neuroprotective effects of 1-O-hexyl-2,3,5-trimethylhydroquinone on ischaemia/reperfusion-induced neuronal injury by activating the Nrf2/HO-1 pathway," *Journal of Cellular and Molecular Medicine*, vol. 24, no. 18, pp. 10468–10477, 2020.
- [17] J. Kim, S.-H. Shin, Y.-E. Ko et al., "HX-1171, a Novel Nrf2 Activator, Induces NQO1 and HMOX1 Expression," *Journal of Cellular Biochemistry*, vol. 118, no. 10, pp. 3372–3380, 2017.
- [18] J. Kim, S. H. Shin, J. K. Kang, and J. W. Kim, "HX-1171 attenuates pancreatic β -cell apoptosis and hyperglycemia-mediated oxidative stress via Nrf2 activation in streptozotocin-induced diabetic model," *Oncotarget*, vol. 9, no. 36, pp. 24260–24271, 2018.
- [19] J. An, G.-G. Feng, L. Huang et al., "Effects of 1-O-hexyl-2,3,5-trimethylhydroquinone on carbon tetrachloride-induced hepatic cirrhosis in rats," *Hepatology Research*, vol. 40, no. 6, pp. 613–621, 2010.
- [20] H. Park, J. Kang, and M. Lee, "1-O-Hexyl-2,3,5-Trimethylhydroquinone Ameliorates 1-DOPA-Induced Cytotoxicity in PC12 Cells," *Molecules*, vol. 24, no. 5, p. 867, 2019.
- [21] H. Yada, M. Hirose, S. Tamano et al., "Effects of Antioxidant 1-O-Hexyl-2,3,5-trimethylhydroquinone or Ascorbic Acid on Carcinogenesis Induced by Administration of Aminopyrine and Sodium Nitrite in a Rat Multi-organ Carcinogenesis Model," *Japanese Journal of Cancer Research*, vol. 93, no. 12, pp. 1299–1307, 2002.
- [22] M. Futakuchi, M. Hirose, K. Imaida et al., "Chemoprevention of 2-amino-1-methyl-6-phenylimidazo- [4,5-b]pyridine-induced colon carcinogenesis by 1-O-hexyl-2,3,5-trimethylhydroquinone after initiation with 1,2-dimethylhydrazine in F344 rats," *Carcinogenesis*, vol. 23, no. 2, pp. 283–287, 2002.
- [23] M. Nezu, T. Souma, L. Yu et al., "Nrf2 inactivation enhances placental angiogenesis in a preeclampsia mouse model and improves maternal and fetal outcomes," *Science Signaling*, vol. 10, no. 479, p. eaam5711, 2017.
- [24] N. Kweider, B. Huppertz, M. Kadyrov, W. Rath, T. Pufe, and C. J. Wruck, "A possible protective role of Nrf2 in preeclampsia," *Annals of Anatomy - Anatomischer Anzeiger*, vol. 196, no. 5, pp. 268–277, 2014.
- [25] M. Shashar, A. Zubkov, T. Chernichovski et al., "Profound decrease in glomerular arginine transport by CAT (cationic amino acid transporter)-1 contributes to the FLT-1 (FMS-like tyrosine kinase 1) induced preeclampsia in the pregnant mice," *Hypertension*, vol. 73, no. 4, pp. 878–884, 2019.
- [26] R. Lim, R. Acharya, P. Delpachitra et al., "Activin and NADPH-oxidase in preeclampsia: insights from in vitro and murine studies," *American Journal of Obstetrics and Gynecology*, vol. 212, no. 1, pp. 86.e1–86.e12, 2015.
- [27] Y. Feng, R. Cui, Z. Li et al., "Methane Alleviates Acetaminophen-Induced Liver Injury by Inhibiting Inflammation, Oxidative Stress, Endoplasmic Reticulum Stress, and Apoptosis through the Nrf2/HO-1/NQO1 Signaling Pathway," *Oxidative Medicine and Cellular Longevity*, vol. 2019, Article ID 7067619, 14 pages, 2019.
- [28] H. Chen, H. Yoshioka, G. S. Kim et al., "Oxidative Stress in Ischemic Brain Damage: Mechanisms of Cell Death and Potential Molecular Targets for Neuroprotection," *Antioxidants & Redox Signaling*, vol. 14, no. 8, pp. 1505–1517, 2011.
- [29] M. Gyurászová, A. G. Kovalčíková, E. Renczés et al., "Oxidative Stress in Animal Models of Acute and Chronic Renal Failure," *Disease Markers*, vol. 2019, Article ID 8690805, 10 pages, 2019.
- [30] F. C. Brownfoot, N. J. Hannan, P. Cannon et al., "Sulfasalazine reduces placental secretion of antiangiogenic factors, up-regulates the secretion of placental growth factor and rescues endothelial dysfunction," *EBioMedicine*, vol. 41, pp. 636–648, 2019.
- [31] C. Tang, G. Yin, C. Huang et al., "Peroxisome proliferator-activated receptor- α ameliorates pressure overload-induced cardiac hypertrophy and fibrosis," *Biomedicine & Pharmacotherapy*, vol. 129, p. 110357, 2020.
- [32] L. Jiang, Y. Gong, Y. Hu et al., "Peroxisome proliferator-activated receptor- α Overexpression Attenuates Doxorubicin-Induced Cardiotoxicity by Inhibiting Oxidative Stress and Cardiomyocyte Apoptosis," *Oxidative Medicine and Cellular Longevity*, vol. 2020, Article ID 2405135, 11 pages, 2020.
- [33] I. M. Ahmad, M. C. Zimmerman, and T. A. Moore, "Oxidative stress in early pregnancy and the risk of preeclampsia," *Pregnancy Hypertension*, vol. 18, pp. 99–102, 2019.
- [34] N. Z. Đorđević, G. M. Babić, S. D. Marković et al., "Oxidative stress and changes in antioxidant defense system in erythrocytes of preeclampsia in women," *Reproductive Toxicology*, vol. 25, no. 2, pp. 213–218, 2008.
- [35] J. Zhang, M. Masciocchi, D. Lewis, W. Sun, A. Liu, and Y. Wang, "Placental anti-oxidant gene polymorphisms, enzyme activity, and oxidative stress in preeclampsia," *Placenta*, vol. 29, no. 5, pp. 439–443, 2008.
- [36] D. Del Rio, A. J. Stewart, and N. Pellegrini, "A review of recent studies on malondialdehyde as toxic molecule and biological marker of oxidative stress," *Nutrition, Metabolism and Cardiovascular Diseases*, vol. 15, no. 4, pp. 316–328, 2005.
- [37] Y. Feng, J. Xu, Q. Zhou et al., "Alpha-1 antitrypsin prevents the development of preeclampsia through suppression of oxidative stress," *Frontiers in Physiology*, vol. 7, 2016.
- [38] Y. R. Jung, Y. J. Lee, N. J. Lee et al., "Inhibitory effect of 1-O-hexyl-2,3,5-trimethylhydroquinone on dimethylnitrosamine-induced liver fibrosis in male SD rats," *Toxicology Research*, vol. 26, no. 3, pp. 193–201, 2010.
- [39] D. S. Boeldt and I. M. Bird, "Vascular adaptation in pregnancy and endothelial dysfunction in preeclampsia," *Journal of Endocrinology*, vol. 232, no. 1, pp. R27–R44, 2017.

- [40] J. S. Possomato-Vieira and R. A. Khalil, "Mechanisms of endothelial dysfunction in hypertensive pregnancy and preeclampsia," *Advances in Pharmacology*, vol. 77, pp. 361–431, 2016.
- [41] K. McLaughlin, M. C. Audette, J. D. Parker, and J. C. Kingdom, "Mechanisms and clinical significance of endothelial dysfunction in high-risk pregnancies," *The Canadian Journal of Cardiology*, vol. 34, no. 4, pp. 371–380, 2018.
- [42] S. R. Hobson, S. Gurusinghe, R. Lim et al., "Melatonin improves endothelial function in vitro and prolongs pregnancy in women with early-onset preeclampsia," *Journal of Pineal Research*, vol. 65, no. 3, p. e12508, 2018.
- [43] T. Kiesslich, C. Mayr, and D. Neureiter, "NRF2: The key to tumor- and patient-dependent chemosensitivity in biliary tract cancer?," *EBioMedicine*, vol. 49, pp. 9–10, 2019.
- [44] P. R. D. V. Godoy, A. P. Khavari, M. Rizzo, E. T. Sakamoto-Hojo, and S. Haghdoost, "Targeting NRF2, Regulator of Antioxidant System, to Sensitize Glioblastoma Neurosphere Cells to Radiation-Induced Oxidative Stress," *Oxidative Medicine and Cellular Longevity*, vol. 2020, pp. 1–25, 2020.
- [45] E. H. M. Hassanein, A. M. Sayed, O. E. Hussein, and A. M. Mahmoud, "Coumarins as Modulators of the Keap1/Nrf2/ARE Signaling Pathway," *Oxidative Medicine and Cellular Longevity*, vol. 2020, Article ID 1675957, 17 pages, 2020.
- [46] M.-x. Wang, J. Zhao, H. Zhang et al., "Potential Protective and Therapeutic Roles of the Nrf2 Pathway in Ocular Diseases: An Update," *Oxidative Medicine and Cellular Longevity*, vol. 2020, Article ID 9410952, 22 pages, 2020.
- [47] A. Kobayashi, M.-I. Kang, Y. Watai et al., "Oxidative and Electrophilic Stresses Activate Nrf2 through Inhibition of Ubiquitination Activity of Keap1," *Molecular and Cellular Biology*, vol. 26, no. 1, pp. 221–229, 2006.
- [48] K.-C. Cheng, R.-J. Lin, J.-Y. Cheng et al., "FAM129B, an anti-oxidative protein, reduces chemosensitivity by competing with Nrf2 for Keap1 binding," *EBioMedicine*, vol. 45, pp. 25–38, 2019.
- [49] S. Habtemariam, "The Nrf2/HO-1 axis as targets for flavanones: neuroprotection by pinocembrin, naringenin, and eriodictyol," *Oxidative Medicine and Cellular Longevity*, vol. 2019, Article ID 4724920, 15 pages, 2019.
- [50] L. Yu, T. Wang, R. Que et al., "The potentially protective role of ATP-binding cassette transporters in preeclampsia via Nrf2," *Pregnancy Hypertension*, vol. 18, pp. 21–28, 2019.
- [51] K. Onda, S. Tong, A. Nakahara et al., "Sofalcone upregulates the nuclear factor (erythroid-derived 2)-like 2/heme oxygenase-1 pathway, reduces soluble fms-like tyrosine kinase-1, and quenches endothelial dysfunction: potential therapeutic for preeclampsia," *Hypertension*, vol. 65, no. 4, pp. 855–862, 2015.
- [52] X. Fan and L. Mu, "The role of heme oxygenase-1 (HO-1) in the regulation of inflammatory reaction, neuronal cell proliferation and apoptosis in rats after intracerebral hemorrhage (ICH)," *Neuropsychiatric Disease and Treatment*, vol. 13, pp. 77–85, 2017.
- [53] E. Amata, V. Pittalà, A. Marrazzo et al., "Role of the Nrf2/HO-1 axis in bronchopulmonary dysplasia and hyperoxic lung injuries," *Clinical Science*, vol. 131, no. 14, pp. 1701–1712, 2017.
- [54] E. M. George, M. Arany, K. Cockrell, M. V. Storm, D. E. Stec, and J. P. Granger, "Induction of heme oxygenase-1 attenuates sFlt-1-induced hypertension in pregnant rats," *American Journal of Physiology. Regulatory, Integrative and Comparative Physiology*, vol. 301, no. 5, pp. R1495–R1500, 2011.
- [55] E. M. George, K. Cockrell, M. Arany, E. Csongradi, D. E. Stec, and J. P. Granger, "Induction of heme oxygenase 1 attenuates placental ischemia-induced hypertension," *Hypertension*, vol. 57, no. 5, pp. 941–948, 2011.

Research Article

Neuroprotection Effect of Astragaloside IV from 2-DG-Induced Endoplasmic Reticulum Stress

Yu Fu ^{1,2}, Jianhang Cai ^{1,3}, Mengyao Xi ⁴, Yifei He ¹, Yang Zhao ¹, Yi Zheng ¹,
Yidong Zhang ¹, Jinkun Xi ¹ and Yonggui He ¹

¹Clinic School of Medicine and Affiliated Hospital, North China University of Science and Technology, Tangshan 063000, China

²Hebei Key Laboratory for Chronic Diseases, North China University of Science and Technology, Tangshan 063000, China

³Department of Neurology, Dongming People's Hospital, Dongming 274501, China

⁴School of Nursing, Dalian Medical University, Dalian 116044, China

Correspondence should be addressed to Jinkun Xi; jinkunxi@126.com and Yonggui He; heyonggui-1994@163.com

Received 29 May 2020; Revised 15 November 2020; Accepted 12 December 2020; Published 31 December 2020

Academic Editor: Weifeng Yao

Copyright © 2020 Yu Fu et al. This is an open access article distributed under the Creative Commons Attribution License, which permits unrestricted use, distribution, and reproduction in any medium, provided the original work is properly cited.

Objective. Astragaloside IV shows neuroprotective activity, but its mechanism remains unclear. To investigate whether astragaloside IV protects from endoplasmic reticulum stress (ERS), we focus on the regulation of glycogen synthase kinase-3 β (GSK-3 β) and mitochondrial permeability transition pore (mPTP) by astragaloside IV in neuronal cell PC12. **Methods and Results.** PC12 cells treated with different concentrations of ERS inducer 2-deoxyglucose (2-DG) (25-500 μ M) showed a significant increase of glucose-regulated protein 78 (GRP 78) and GRP 94 expressions and a decrease of tetramethylrhodamine ethyl ester (TMRE) fluorescence intensity and mitochondrial membrane potential ($\Delta\Psi$ m), with the peak effect seen at 50 μ M, indicating that 2-DG induces ERS and the mPTP opening. Similarly, 50 μ M of astragaloside IV increased the GSK-3 β phosphorylation at Ser9 most significantly. Next, we examined the neuroprotection of astragaloside IV by dividing the PC12 cells into control group, 2-DG treatment group, astragaloside IV plus 2-DG treatment group, and astragaloside IV only group. PC12 cells treated with 50 μ M 2-DG for different time courses (0-36 hr) showed a significant increase of Cleaved-Caspase-3 with the peak at 6 hr. 2-DG significantly induced cell apoptosis and increased the green fluorescence intensity of Annexin V-FITC, and these effects were reversed by astragaloside IV. Such a result indicates that astragaloside IV protected neural cell survival from ERS. 2-DG treatment significantly increased the expressions of inositol-requiring ER-to-nucleus signal kinase 1 (IRE1), phosphor-protein kinase R-like ER kinase (p-PERK), but not affect the transcription factor 6 (ATF6) expression. 2-DG treatment significantly decreased the phosphorylation of GSK-3 β and significantly reduced the TMRE fluorescence intensity and $\Delta\Psi$ m, following mPTP open. Astragaloside IV significantly inhibited the above effects caused by 2-DG, except the upregulation of ATF6 protein. Taken together, astragaloside IV significantly inhibited the ERS caused by 2-DG. **Conclusion.** Our data suggested that astragaloside IV protects PC12 cells from ERS by inactivation of GSK-3 β and preventing the mPTP opening. The GRP 78, GRP 94, IRE1, and PERK signaling pathways but not ATF6 are responsible for GSK-3 β inactivation and neuroprotection by astragaloside IV.

1. Introduction

Astragaloside IV is the most active saponin compound with a molecular formula C₄₁H₆₈O₁₄. It is soluble in highly polar organic solution [1, 2]. Previous studies have shown protective effects of astragaloside IV on various organs such as heart [3, 4], kidney [5, 6], brain [7, 8], and nerve [9-11].

Endoplasmic reticulum (ER) is an important organelle folding cell surface and secreted protein in eukaryotic cells [12]. Imbalance of ER steady state leads to ERS [13] with the hall markers GRP 78 and GRP 94, which participates in nerve damage [14-16].

Mitochondria are the energy warehouse of eukaryotic cells [17]. Mitochondria are vital in nerve damage [18, 19], which opens mPTP on the mitochondrial membrane and

leads to the destruction of mitochondrial structure and cell damage [20–22]. Cross-talk between the endoplasmic reticulum and mitochondria are critical to resist apoptosis and cell stress [23, 24]. GSK-3 β controls cell growth, survival, and neuronal plasticity in the nervous system [25, 26]. Inactivation of GSK-3 β to prevent mPTP opening is vital for neuroprotection [18].

ERS causes the accumulation of unfolded or misfolded proteins in the ER, triggering unfolded protein response (UPR) [27]. PERK, IRE1, and ATF6 are the molecular markers of three signaling pathways of ERS. UPR activated IRE1 and damages endothelial cells [28, 29]. PERK and ATF6 pathways participate in the protection of the ischemic brain [30, 31].

Astragaloside IV is a potent neuroprotective saponin compound, which reduces ERS, but the mechanism remains unclear. This study tested whether astragaloside IV inhibits ERS by inactivating GSK-3 β and preventing mPTP from opening.

2. Material and Methods

2.1. Cell Culture. Rat adrenal pheochromocytoma-derived PC12 cell was purchased from Baoshide (Wuhan, China). Cells were cultured in Dulbecco's modified Eagle's medium (DMEM) supplemented with 10% fetal bovine serum (FBS) (Invitrogen) and 100 U penicillin/streptomycin at 37°C in a humidified 5% CO₂-95% air atmosphere. Culture medium changed every 2 to 3 days. Cells were passaged using 0.25% trypsin when cell density reaches about 90%.

2.2. Reagents. Following chemicals were used in this study: astragaloside IV (cat. no. HQJG-20110507, Tianjin Mark Biotechnology Co.), 2-Deoxy-D-glucose (cat. no. D6134, Sigma), Tetramethylrhodamine ethylester (cat. no. T669, Molecular Probes), Annexin V-FITC Apoptosis Detection kit (cat. no. C1062 L, Beyotime Biotechnology), Cell culture reagents DMEM (cat. no. C11995500BT), FBS (cat. no. 16140071), 0.25% trypsin-EDTA (cat. no. 25200-056), and penicillin/streptomycin (cat. no. 15140-122) were purchased from Gibco BRL.

All rabbit antibodies were obtained from Cell Signaling Technology Inc. Monoclonal antibody against: GRP 78 (cat. no. 3177), GRP 94 (cat. no. 20292), p-PERK (cat. no. 3179), ATF6 (cat. no. 65880), IRE1 (cat. no. 3294), p-GSK-3 β (cat. no. 9323), GSK-3 β (cat. no. 12456), and GADPH (cat. no. 5174). Polyclonal antibody against: Cleaved Caspase-3 (cat. no. 9661), Caspase-3 (cat. no. 9662), and anti-rabbit IgG (cat. no. 14708). All antibodies were used at 1 : 1,000 dilution.

2.3. Drug Treatment Group. PC12 cells were grown to 90% confluence and treated as follows. To determine the optimal concentration of 2-DG, PC12 cells were treated with 25, 50, 100, 150, 200, and 500 μ M 2-DG or vehicle only for 30 min. To determine the optimal concentration of astragaloside IV, PC12 cells were treated with 25, 50, 75, and 100 μ M astragaloside IV or vehicle only for 20 min.

To observe the effect of astragaloside IV on ERS, PC12 cells were divided into 4 groups: (1) control group: treat with

vehicle only; (2) 2-DG group: treat with 50 μ M 2-DG for 30 min; (3) astragaloside IV+2-DG group: treat with 50 μ M astragaloside IV for 20 min then 50 μ M 2-DG for 30 min; (4) astragaloside IV group: treat with 50 μ M astragaloside IV for 20 min.

2.4. Drug Treatment Schedule. PC12 cell culture was washed twice with PBS and then incubated in Tyrode solution for 2 hours prior to other treatments. To examine the effect of astragaloside IV on protein expressions of GRP 78, GRP 94, IRE1, p-PERK, ATF6, p-GSK-3 β , and GSK-3 β , PC12 cells were exposed to 2-DG (50 μ M) for 30 min. Astragaloside IV (50 μ M) was applied 20 min before exposure to 2-DG. PC12 cells were exposed to 50 μ M 2-DG for 30 min before $\Delta\Psi_m$ measurement and 6 hr before apoptosis measurement, respectively.

2.5. Western Blotting. After drug treatment, PC12 cells were washed twice with PBS, and cell pellets were lysed on ice for 30 min with 50 μ L of fresh cell lysis buffer (Cell Signaling Technology, cat. no. 9803). The lysate was ultrasonicated and then centrifuged at 12 000 r (4°C) for 15 min. Protein concentration was measured using a BCA kit and then divided into equal protein amount for boiling and loading. After electrophoresis, protein was transferred to PVDF membrane and incubated in 10% nonfat milk at room temperature for 90 min. Blot membranes were incubated with primary antibodies against GRP 78, GRP 94, IRE1, p-PERK, ATF6, p-GSK-3 β , and GSK-3 β overnight at 4°C. After incubating the secondary antibody at room temperature for 1 h, ECL fluorescence was developed and the blot image was captured and analyzed with Biospectrum Imaging System (UVP, Upland, USA).

2.6. Confocal Imaging of Mitochondrial Membrane Potential. Mitochondrial membrane potential ($\Delta\Psi_m$) was measured by loading PC12 cells with cell permeable, cationic mitochondria probe TMRE, as reported previously [32]. TMRE is accumulated specifically by the mitochondria in proportion to mitochondrial membrane potential ($\Delta\Psi_m$) [33]. Loss of $\Delta\Psi_m$ is caused by the mPTP opening [34]. Briefly, PC12 cell culture in a temperature-controlled culture dish (MatTek, MA, USA) was incubated with TMRE (100 nM) in standard Tyrode solution containing (mM) NaCl 140, KCl 6, MgCl₂ 1, CaCl₂ 1, HEPES 5, and glucose 5.8 (pH 7.4) for 20 minutes. Cells were washed several times with fresh Tyrode solution. The dish was then mounted on the stage of an Olympus FLUOVIEW FV-1000 laser scanning confocal microscope with a 543 nm excitation (Olympus Corporation, Tokyo, Japan). Fluorescence intensity of 10 random-picked cells in each field was measured by FLUOVIEW FV-1000 software at 0 min and measured the average fluorescence intensity value at 0 and 30 min. The changes of fluorescence intensity were expressed as the ratio of average fluorescence intensity of the 10 picked cells at 30-minute over that at 0-minute.

2.7. Confocal Imaging of Apoptosis. Apoptosis of PC12 cells was measured using Annexin V-FITC Apoptosis Detection kit following the manual. Briefly, cell culture in a temperature-controlled culture dish (MatTek, MA, USA)

was incubated with Annexin V-FITC and PI (Propidium Iodide) for 20 minutes with binding solution at RT in the dark and was washed 3 times with PBS according to the manual. The dish was then mounted on the stage of an Olympus FLUOVIEW FV-1000 laser scanning confocal microscope with 488 and 543 nm excitation (Olympus Corporation, Tokyo, Japan). Quantitative analysis of fluorescence intensity changes by FLUOVIEW FV-1000 -software.

2.8. Cell Survival Analysis. Cell survival was assessed by staining cells with Annexin V-FITC Apoptosis Detection kit according to the manufacturer's instructions using flow cytometry (FACScalibur, Becton Dickinson, NJ). Fluorescence intensity was measured at the excitation wavelengths of 488 and 543 nm, respectively. Cells were treated the same as confocal imaging of apoptosis.

2.9. Statistical Analysis. Results obtained from 6 experiments are expressed as mean \pm SD. Statistical significance was determined using one-way ANOVA followed by Tukey's test. $P < 0.05$ was considered as statistically significant.

3. Results

3.1. Effects of 2-DG on ERS and mPTP Opening. PC12 cells were treated with different concentrations (0, 25, 50, 100, 150, and 200 μ M) of 2-DG to induce ERS. The expressions of GRP 78 and GRP 94 increased most significantly in cells treated with 50 μ M 2-DG (Figure 1(a)). Similarly, the intensity of TMRE red fluorescence decreases the most in cells treated with 2-DG at 50 μ M (Figure 1(b)). According to these results, we treated PC12 cells with 50 μ M 2-DG in the subsequent experiments.

3.2. Effect of Astragaloside IV on GSK-3 β Phosphorylation. PC12 cells were treated with astragaloside IV at different concentrations (25, 50, 75, and 100 μ M) to find out the concentration with the most neuroprotection effect. We found the expression of p-GSK-3 β increased most significantly in cells treated with astragaloside IV at 50 μ M (Figure 2). Therefore, we use 50 μ M astragaloside IV in the subsequent experiments.

3.3. Effect of Astragaloside IV on PC12 Cell Survival from ERS. 2-DG in different times (0-36 hr) showed a significant increase of Cleaved-Caspase-3 with the peak at 6 hr (Figure 3(a)). 2-DG significantly reduced Cleaved-Caspase-3 expression (Figure 3(b)) and increased the green fluorescence intensity of Annexin V-FITC (Figure 3(c)) and apoptosis rate (Figure 3(d)); these effects were reversed by astragaloside IV, respectively, indicating that astragaloside IV protected PC12 cells from ERS-induced apoptosis.

3.4. Effect of Astragaloside IV on PC12 Cells from ERS. 2-DG significantly increased GRP 78 and GRP 94 expressions while astragaloside IV reduced the increasement induced by 2-DG (Figure 4), indicating that astragaloside IV induced neuroprotection on PC12 cells by preventing ERS.

3.5. Effect of Astragaloside IV on ERS-Induced mPTP Opening. We determined the ERS-induced loss of $\Delta\Psi_m$ by

monitoring change in TMRE fluorescent intensity with confocal microscopy. 50 μ M of 2-DG induced a remarkable decrease in TMRE fluorescence in PC12 cells. Cells pretreated with 50 μ M astragaloside IV showed less reduction in TMRE fluorescence after 2-DG treatment (Figure 5), suggesting that astragaloside IV may protect PC12 cells by preventing the ERS-induced mPTP opening.

3.6. Effect of Astragaloside IV on ERS. We examined IRE1, p-PERK, and ATF6 expressions by western blotting. 2-DG significantly increased their expressions, while astragaloside IV significantly inhibited 2-DG-induced increasement of IRE1 and p-PERK, but not ATF6 (Figure 6). These results suggest that the IRE1/PERK but not the ATF6 signaling pathway is necessary for astragaloside IV to protect PC12 cells from ERS.

3.7. Effect of Astragaloside IV on GSK-3 β Phosphorylation from ERS. To determine the role of GSK-3 β in the neuroprotection of astragaloside IV, we tested the expression of phosphorylated GSK-3 β . Astragaloside IV significantly increased the phosphorylation of GSK-3 β (Figure 7), suggesting that the inactivation of GSK-3 β is necessary for astragaloside IV to protect PC12 cells from ERS.

4. Discussion

Stroke is one of the cerebrovascular diseases whose total mortality increases every year, with a high demand of neuroprotection. Ischemia-reperfusion injury (IRI) plays a key role in nerve damage caused by cerebral infarction [35, 36]. Endoplasmic reticulum stress-induced unfolded protein response is the main adaptive regulatory mechanism [37].

Nonmetabolizable glucose analogue 2-DG blocks glycolysis and glucose metabolism and inhibits protein glycosylation and ER quality control [38]. 2-DG significantly reduces ATP activity, inducing ERS in cells and inhibiting tumor growth and its anticancer or antiviral were tested in multiple studies [39, 40]. We found that 2-DG treatment significantly reduced the PC12 cell survival. We determined the effects of different concentrations (0, 25, 50, 100, 150, 200, and 500 μ M) of 2-DG treatment on the expressions of ERS chaperones GRP 78 and GRP 94 and found 50 μ M of 2-DG increased GRP 78 and GRP 94 expressions most significantly. In addition, we found 50 μ M of 2-DG decreased the red fluorescence of mitochondrial TMRE most significantly.

The main bioactive substance of *Astragalus membranaceus bunge*, a herb possessing protective activities for thousands of years [41], astragaloside IV demonstrates potent protective effect on focal cerebral ischemia/reperfusion [42], cardiovascular disease [43], pulmonary disease [44], liver fibrosis [45], and diabetic nephropathy [46] through several mechanisms including anti-inflammatory [47], antifibrotic [44], and antioxidative stress [48]. Our previous results have shown that 50 μ M of astragaloside IV treatment protects H9c2 cardiac cells by inhibition of GSK-3 β and prevention of the mPTP opening [32].

Previous studies have shown that astragaloside IV has a neuroprotective effect on cortical neurons by inducing Nrf2

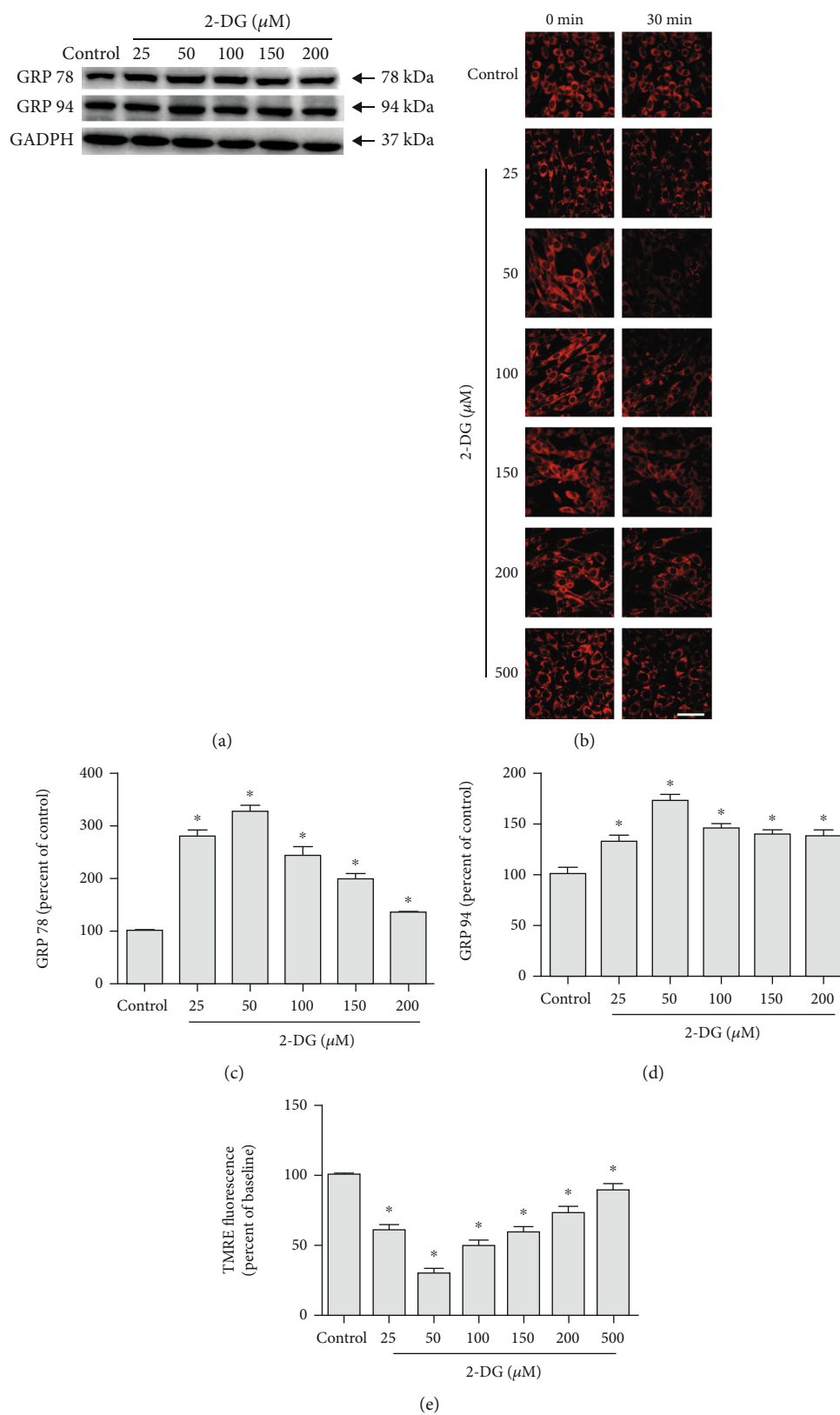


FIGURE 1: Effects of 2-DG on ERS and the mPTP opening. (a) Western blot images of GRP 78 and GRP 94 expression in PC12 cells treated with vehicle control and 25, 50, 100, 150, 200, and 500 μM 2-DG. (b) Confocal fluorescence images of cells incubating TMRE for 20 minutes in PC12 cells treated with 0, 25, 50, 100, 150, 200, and 500 μM 2-DG. (c, d) Quantification of (a). Each protein expression level was normalized with GAPDH. (e) Quantification of (b). Data are mean \pm SD of 6 independent experiments. * $P < 0.05$ compared to vehicle control. Scale bar, 50 μm .

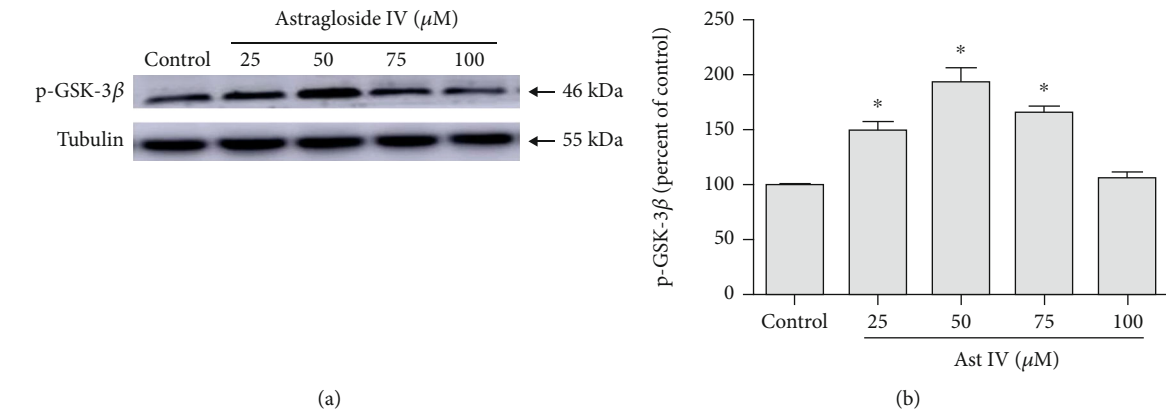


FIGURE 2: Effect of astragaloside IV on GSK-3β phosphorylation. (a) Western blot image of p-GSK-3β expression in PC12 cells treated with vehicle control and 25, 50, 75, and 100 μM astragaloside IV. (b) Quantification of (a). Each protein expression level was normalized with Tubulin. Data are mean ± SD of 6 independent experiments. *P < 0.05 compared to vehicle control.

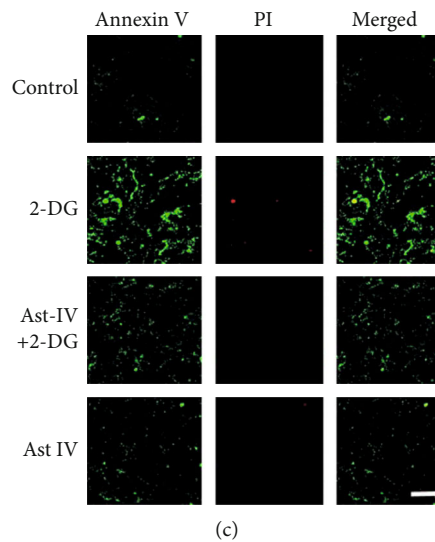
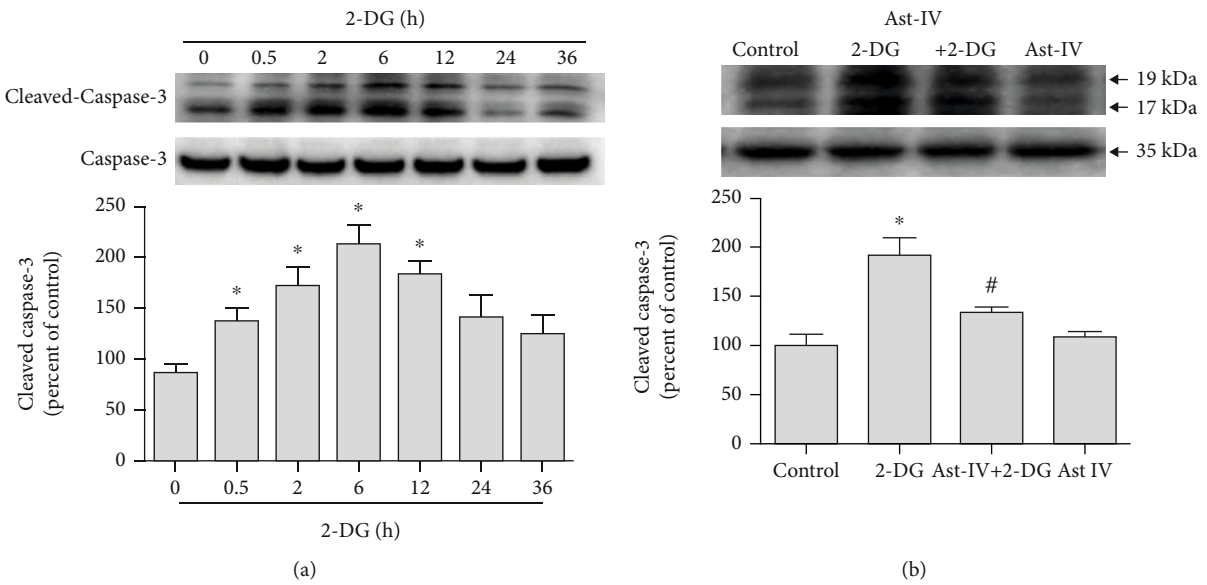


FIGURE 3: Continued.

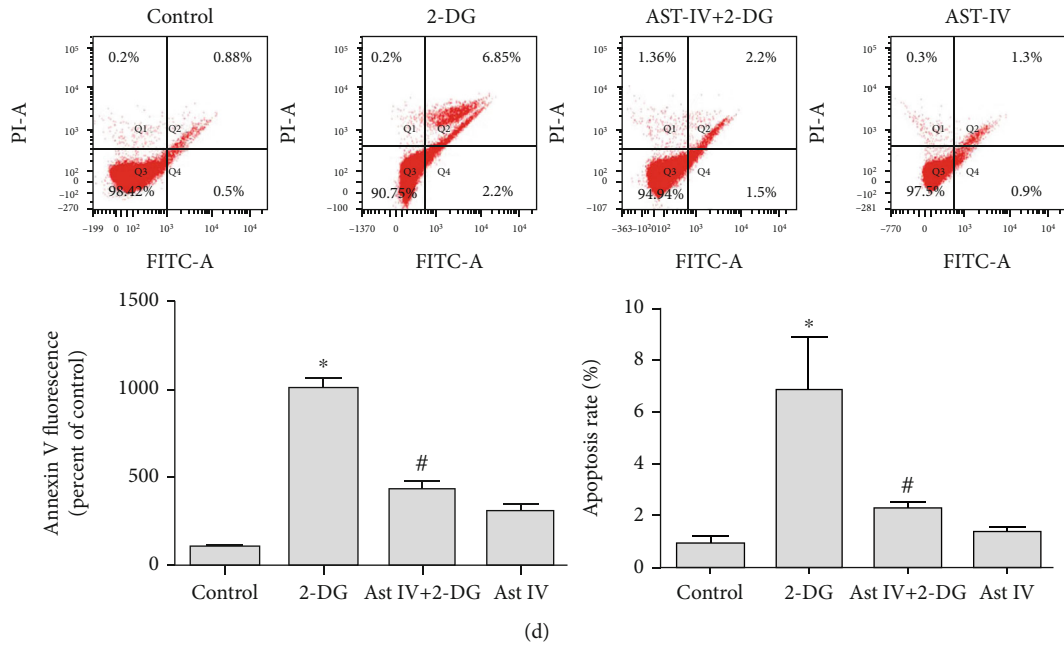


FIGURE 3: Effect of astragaloside IV on PC12 cell survival from ERS. (a) Representative Western blot images of Cleaved-Caspase-3 in PC12 cells treated with 2-DG in different times. (b) Representative Western blot images of Cleaved-Caspase-3 in PC12 cells treated with 2-DG and astragaloside IV. (c, d) Confocal fluorescence images and flow cytometry of Annexin V-FITC Apoptosis Detection kit in PC12 cells treated with 2-DG and astragaloside IV. Cells were preloaded with Annexin V and PI for 20 minutes before other treatments. PC12 cell culture was placed on the temperature-controlled stage and treated with astragaloside IV for 20 minutes and 2-DG for 6 h. Data are mean \pm SD of 6 independent experiments. * $P < 0.05$ compared to control; # $P < 0.05$ compared to 2-DG. Scale bar, 50 μ m.

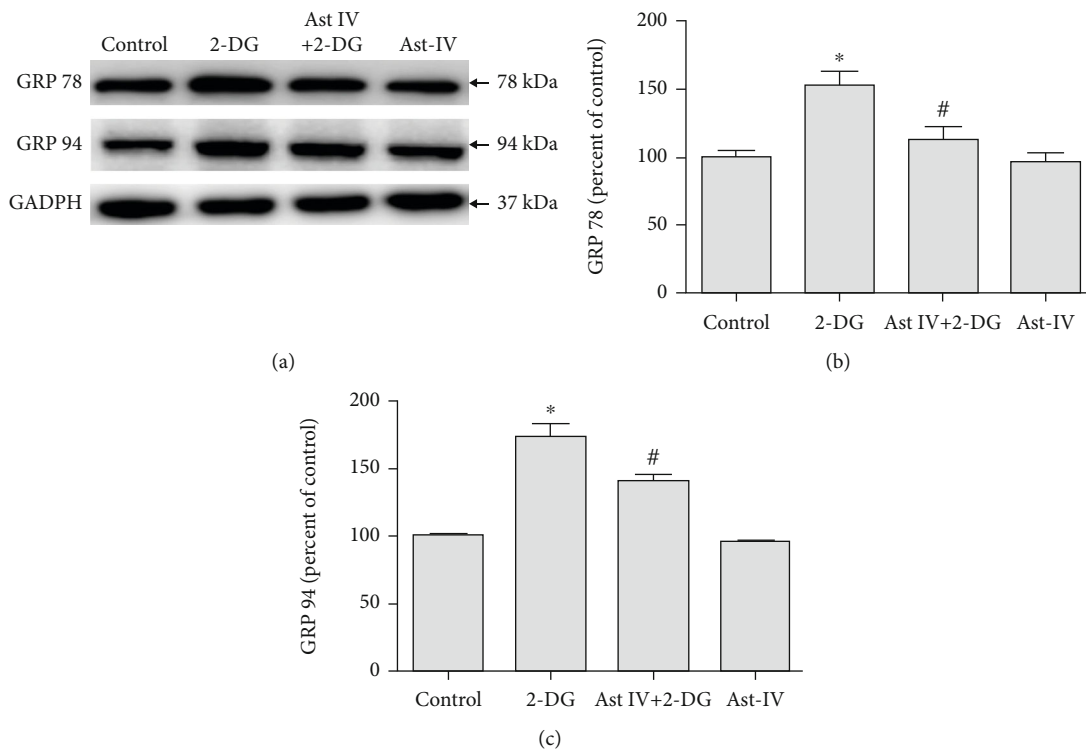


FIGURE 4: Effect of astragaloside IV on PC12 cells from ERS. (a) Western blot images of ER chaperone proteins GRP 78 and GRP 94 in PC12 cells treated with 2-DG and astragaloside IV. (b, c) Quantification of (a). Each protein expression level was normalized with GAPDH. Data are mean \pm SD of 6 independent experiments. * $P < 0.05$ compared to vehicle control; # $P < 0.05$ compared to 2-DG.

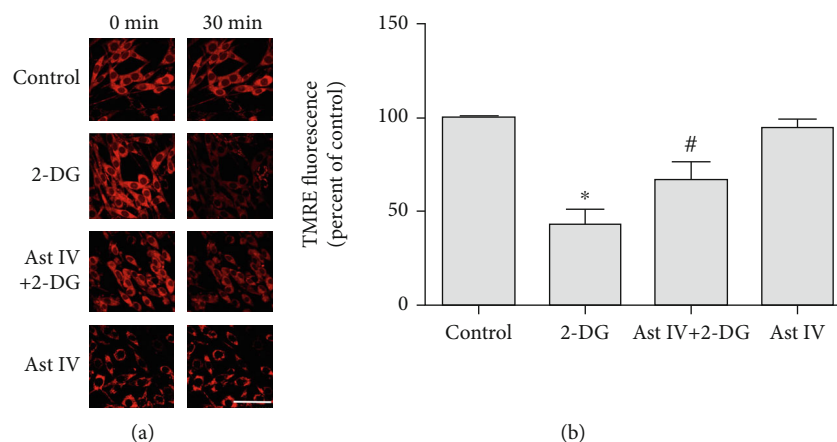


FIGURE 5: Effect of astragaloside IV on PC12 cells from ERS-induced mPTP opening. (a) Confocal images of TMRE probe in PC12 cells treated with 2-DG and astragaloside IV. Cells were preloaded with TMRE probe for 20 minutes before other treatments. PC12 cell culture was placed on the temperature-controlled stage and treated with astragaloside IV for 20 minutes and 2-DG for 30 minutes. (b) Quantification of TMRE Red fluorescence expressed as % of the control. The fluorescence intensity value was calculated as 30-minute normalized to 0-minute. Data are mean \pm SD of 6 independent experiments. * $P < 0.05$ compared to control; # $P < 0.05$ compared to 2-DG. Scale bar, 50 μ m.

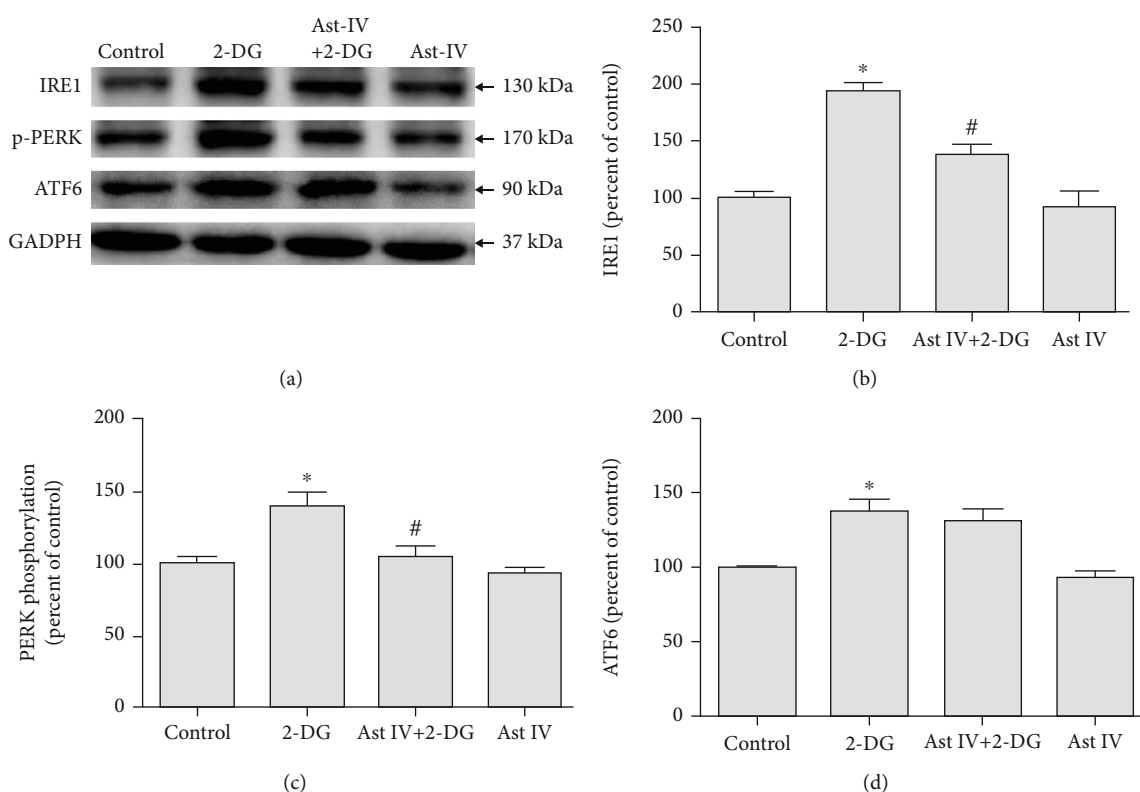


FIGURE 6: Effect of astragaloside IV on ERS signaling pathway. (a) Representative Western blot images of IRE1, p-PERK, and ATF6 in PC12 cells treated with 2-DG and astragaloside IV. (b–d) Quantification of (a). Each protein expression level was normalized with GAPDH. Data are mean \pm SD for 6 independent experiments. * $P < 0.05$ compared to vehicle control; # $P < 0.05$ compared to 2-DG.

activation [9]. Astragaloside IV reduced glutamate-induced neurotoxicity and hypoxia-induced damage through the Raf-MEK-ERK pathway and miR-124 in PC12 cells [10, 11]. We examined the effect of different concentrations (0, 25, 50, 75, and 100 μ M) of astragaloside IV on GSK-3 β phos-

phorylation in PC12 cells. Among different concentrations of astragaloside IV treatment, 50 μ M of astragaloside IV was most significant to induce GSK-3 β phosphorylation.

The endoplasmic reticulum of eukaryotic cells is a membrane-bound organelle, performing various functions

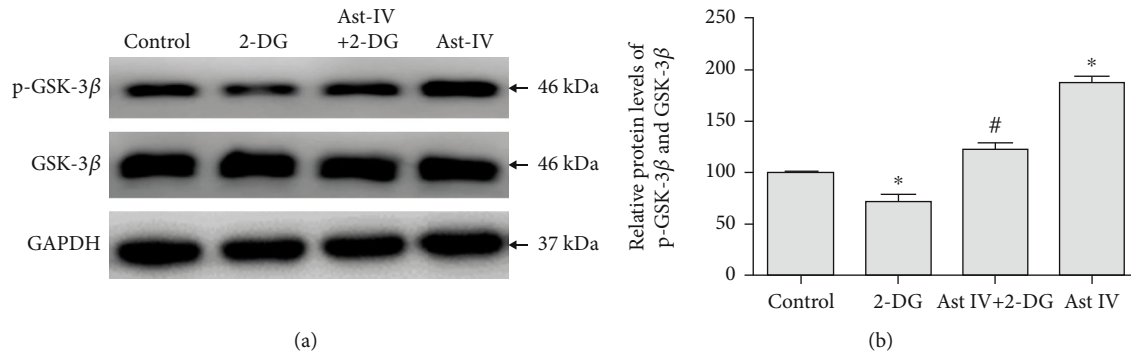


FIGURE 7: Effect of astragaloside IV on GSK-3 β phosphorylation from ERS. (a) Representative Western blot image of p-GSK-3 β in PC12 cells treated with 2-DG and astragaloside IV. (b) Quantification of (a). The relative level of p-GSK-3 β was normalized with GAPDH and then to that of GSK-3 β . Data are mean \pm SD for 6 independent experiments. * P < 0.05 compared to vehicle control; # P < 0.05 compared to 2-DG.

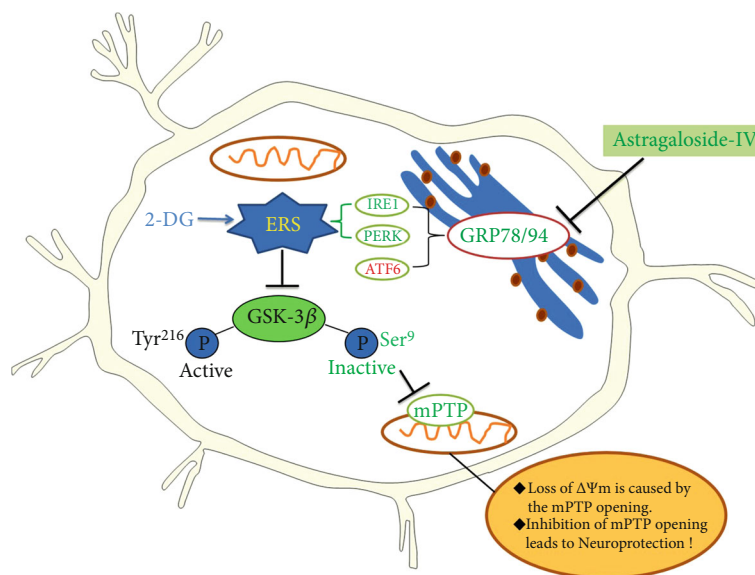


FIGURE 8: Mechanism of astragaloside IV-mediated neuroprotection on PC12 cells from ERS. Astragaloside IV protects PC12 cells from ERS by inactivation of GSK-3 β and preventing the mPTP opening. The GRP 78, GRP 94, IRE1, and PERK signaling pathways but not ATF6 are responsible for GSK-3 β inactivation and neuroprotection by astragaloside IV.

including synthesis of proteins to degradation of xenobiotics. Bioaccumulation of drugs/chemicals/xenobiotics in the cytosol can trigger ERS [49]. GRP 78 and GRP 94 are chaperone proteins for protein synthesis and termination in ERS. Previous studies show that Fluoxetine [14], sulforaphane [15], and Harpagide [16] protect neurons from hypoxia-reoxygenation-induced neuron apoptosis by reducing ERS. To investigate whether astragaloside IV could inhibit ERS to protect neuronal cells, we examined the expressions of ERS-related proteins. We found 2-DG treatment significantly increased the expressions of both GRP 78 and GRP 94 in PC12 cells, while astragaloside IV inhibited this increment.

Mitochondria are the key organelles in eukaryotic cells and contribute to cellular stress responses. Misfunction of mitochondria plays a key role in ERS and nerve damage [50]. mPTP is a nonspecific pore opening in the mitochondrial inner membrane when ERS occurs. The opening of

mPTP allows molecules smaller than 1.5 kDa, including protons, to enter mitochondria freely, affecting membrane potential and causing cell death [51]. Studies have shown that selective inhibition of mPTP prevents neurodegeneration in experimental multiple sclerosis [20]. Low temperature-induced neuroprotection is associated with a decrease in mitochondrial membrane potential [21]. Here, we showed that 2-DG significantly weakened the red fluorescence intensity of TMRE, while astragaloside IV pretreatment inhibited the decrease caused by 2-DG. These results suggested that astragaloside IV suppressed the ERS-induced mitochondrial membrane potential decrease, which prevents mPTP opening and protects PC12 cells.

Prolonged ERS induces cell apoptosis through PERK, ATF, and CHOP [52]. The mitochondrial pathway mediated the ERS-induced apoptosis [53, 54]. Our recent studies showed that resveratrol inhibited ERS-related apoptotic protein CHOP, Caspase12, and JNK expressions induced by 2-

DG [55]. In the present study, we checked the neuroprotection effect of astragaloside IV on PC12 cells from 2-DG-induced apoptosis. We found 50 μM of 2-DG treatment for 2-12 hr significantly increased Cleaved-Caspase-3 level with the peak at 6 hr. Astragaloside IV treatment inhibits PC12 cell apoptosis induced by 2-DG. In our study, we observed 2-DG significantly increased the Annexin V-FITC fluorescence in both confocal image and flow cytometry, these effects were significantly blocked by astragaloside IV. Therefore, these data suggested that chronic ERS caused neuronal damages in PC12 cells and astragaloside IV-induced neuroprotection via antiapoptosis. In our cell survival assay, we confirmed that 50 μM of astragaloside IV is well tolerated in PC12 cell with minimal apoptosis detected (Figure 3(d)), and suggesting such a concentration is neuroprotective with low adverse effects.

Dysregulation of ER functions leads to the accumulation of misfolded-or unfolded-protein in the ER lumen and UPR. IRE1, PERK, and ATF6 are three UPR downstream pathways regulating the gene expressions to maintain ER homeostasis [56]. Unmitigated ERS leads to cell apoptosis [57]. Studies have shown that the PERK pathway plays a neuroprotective role in the brain injury caused by experimental cerebral hemorrhage [31]. Notoginsenoside R1 regulates ATF6/Akt pathway through estrogen receptor and reduces OGD/R-induced neuronal damage. RACK1 upregulation induces neuroprotection by activating the IRE1-XBP1 pathway in rat traumatic brain injury [58]. We found that 2-DG significantly increased the expressions of IRE1, p-PERK, and ATF6, while astragaloside IV inhibited the increases of IRE1 and p-PERK, but not ATF6. These data suggested that IRE1 and PERK pathways are involved in the neuroprotection by astragaloside IV.

GSK-3 β kinase is a key signaling molecule regulating structural and functional synaptic plasticity in the normal brain [25]. Furthermore, the prevention of mPTP opening induced by GSK-3 β phosphorylation is important to reduce cell damage. Grape seed-derived proanthocyanidins reduce neuronal oxidative damage by inhibiting the GSK-3 β -dependent mPTP opening [18]. We found 2-DG significantly reduced GSK-3 β phosphorylation, while astragaloside IV inhibited such phosphorylation. Our data suggested that astragaloside IV protects PC12 cells through GSK-3 β phosphorylation.

In conclusion, astragaloside IV protected PC12 cell survival from ERS by inactivating GSK-3 β and preventing mPTP opening. We further show that IRE1 and PERK but not ATF6 is important for neuroprotection of astragaloside IV (Figure 8). Our *in vitro* results warrant the further study of neuroprotective mechanisms of astragaloside IV using *in vivo* models.

Data Availability

The data used to support the findings of this study are included within the article.

Conflicts of Interest

The authors declare no conflict of interest associated with this manuscript.

Authors' Contributions

Yu Fu and Jianhang Cai contributed equally to this work.

Acknowledgments

This work was supported by grants from the National Natural Science Foundation of China (81570275), the Natural Science Foundation of Hebei Province (H2018209309 and H2020209172), the Research Project of Education Department of Hebei Province (ZD2020110), the Science Foundation for Returned Scholars of Hebei Province (C20200508), and the Talents Project of Tangshan (A202006016).

References


- [1] S. Ren, H. Zhang, Y. Mu, M. Sun, and P. Liu, "Pharmacological effects of astragaloside IV: a literature review," *Journal of Traditional Chinese Medicine*, vol. 33, no. 3, pp. 413–416, 2013.
- [2] L. Li, X. Hou, R. Xu, C. Liu, and M. Tu, "Research review on the pharmacological effects of astragaloside IV," *Fundamental and Clinical Pharmacology*, vol. 31, no. 1, pp. 17–36, 2017.
- [3] Z. Dong, P. Zhao, M. Xu et al., "Astragaloside IV alleviates heart failure via activating PPAR α to switch glycolysis to fatty acid beta-oxidation," *Scientific Reports*, vol. 7, no. 1, p. 2691, 2017.
- [4] Y. B. Sui, Y. Wang, L. Liu, F. Liu, and Y. Q. Zhang, "Astragaloside IV alleviates heart failure by promoting angiogenesis through the JAK-STAT3 pathway," *Pharmaceutical Biology*, vol. 57, no. 1, pp. 48–54, 2019.
- [5] C. Ji, Y. Luo, C. Zou, L. Huang, R. Tian, and Z. Lu, "Effect of astragaloside IV on indoxyl sulfate-induced kidney injury in mice via attenuation of oxidative stress," *BMC Pharmacology and Toxicology*, vol. 19, no. 1, p. 53, 2018.
- [6] W. Yan, Y. Xu, Y. Yuan et al., "Renoprotective mechanisms of astragaloside IV in cisplatin-induced acute kidney injury," *Free Radical Research*, vol. 51, no. 7-8, pp. 669–683, 2017.
- [7] H. Li, P. Wang, F. Huang et al., "Astragaloside IV protects blood-brain barrier integrity from LPS-induced disruption via activating Nrf2 antioxidant signaling pathway in mice," *Toxicology and Applied Pharmacology*, vol. 340, pp. 58–66, 2018.
- [8] Y. Zhang, Y. Zhang, X.-f. Jin et al., "The role of astragaloside IV against cerebral ischemia/reperfusion injury: suppression of apoptosis via promotion of P62-LC3-autophagy," *Molecules*, vol. 24, no. 9, 2019.
- [9] D. M. Gu, P. H. Lu, K. Zhang et al., "EGFR mediates astragaloside IV-induced Nrf2 activation to protect cortical neurons against in vitro ischemia/reperfusion damages," *Biochemical and Biophysical Research Communications*, vol. 457, no. 3, pp. 391–397, 2015.
- [10] R. Yue, X. Li, B. Chen et al., "Astragaloside IV attenuates glutamate-induced neurotoxicity in PC12 cells through Raf-MEK-ERK pathway," *PLoS One*, vol. 10, no. 5, article e0126603, 2015.
- [11] W. Yu, Z. Lv, L. Zhang et al., "Astragaloside IV reduces the hypoxia-induced injury in PC-12 cells by inhibiting expression of miR-124," *Biomedicine & Pharmacotherapy*, vol. 106, pp. 419–425, 2018.

- [12] D. S. Schwarz and M. D. Blower, "The endoplasmic reticulum: structure, function and response to cellular signaling," *Cellular and Molecular Life Sciences*, vol. 73, no. 1, pp. 79–94, 2016.
- [13] M. Wang and R. J. Kaufman, "Protein misfolding in the endoplasmic reticulum as a conduit to human disease," *Nature*, vol. 529, no. 7586, pp. 326–335, 2016.
- [14] F. Xu, G. Zhang, J. Yin et al., "Fluoxetine mitigating late-stage cognition and neurobehavior impairment induced by cerebral ischemia reperfusion injury through inhibiting ERS-mediated neurons apoptosis in the hippocampus," *Behavioural Brain Research*, vol. 370, p. 111952, 2019.
- [15] L. Tang, X. Ren, Y. Han et al., "Sulforaphane attenuates apoptosis of hippocampal neurons induced by high glucose via regulating endoplasmic reticulum," *Neurochemistry International*, vol. 136, p. 104728, 2020.
- [16] K. Wang, Y. Lou, H. Xu, X. Zhong, and Z. Huang, "Harpagide from *Scrophularia* protects rat cortical neurons from oxygen-glucose deprivation and reoxygenation-induced injury by decreasing endoplasmic reticulum stress," *Journal of Ethnopharmacology*, vol. 253, p. 112614, 2020.
- [17] P. Kramer and P. Bressan, "Our (mother's) mitochondria and our mind," *Perspectives on Psychological Science*, vol. 13, no. 1, pp. 88–100, 2018.
- [18] Q. Sun, N. Jia, X. Li, J. Yang, and G. Chen, "Grape seed proanthocyanidins ameliorate neuronal oxidative damage by inhibiting GSK-3 β -dependent mitochondrial permeability transition pore opening in an experimental model of sporadic Alzheimer's disease," *Aging*, vol. 11, no. 12, pp. 4107–4124, 2019.
- [19] A. Cheng, Y. Hou, and M. P. Mattson, "Mitochondria and neuroplasticity," *ASN Neuro*, vol. 2, no. 5, article e00045, 2010.
- [20] J. Warne, G. Pryce, J. M. Hill et al., "Selective inhibition of the mitochondrial permeability transition pore protects against neurodegeneration in experimental multiple sclerosis," *The Journal of Biological Chemistry*, vol. 291, no. 9, pp. 4356–4373, 2016.
- [21] P. Gong, R. Hua, Y. Zhang et al., "Hypothermia-induced neuroprotection is associated with reduced mitochondrial membrane permeability in a swine model of cardiac arrest," *Journal of Cerebral Blood Flow and Metabolism*, vol. 33, no. 6, pp. 928–934, 2013.
- [22] A. Agarwal, P.-H. Wu, E. G. Hughes et al., "Transient opening of the mitochondrial permeability transition pore induces microdomain calcium transients in astrocyte processes," *Neuron*, vol. 93, no. 3, pp. 587–605.e7, 2017.
- [23] A. A. Rowland and G. K. Voeltz, "Endoplasmic reticulum-mitochondria contacts: function of the junction," *Nature Reviews: Molecular Cell Biology*, vol. 13, no. 10, pp. 607–615, 2012.
- [24] T. Simmen and M. S. Herrera-Cruz, "Plastic mitochondria-endoplasmic reticulum (ER) contacts use chaperones and tethers to mould their structure and signaling," *Current Opinion in Cell Biology*, vol. 53, pp. 61–69, 2018.
- [25] T. Jaworski, E. Banach-Kasper, and K. Gralac, "GSK-3 β at the Intersection of Neuronal Plasticity and Neurodegeneration," *Neural Plasticity*, vol. 2019, Article ID 4209475, 14 pages, 2019.
- [26] K. Yang, Z. Chen, J. Gao et al., "The key roles of GSK-3 β in regulating mitochondrial activity," *Cellular Physiology and Biochemistry*, vol. 44, no. 4, pp. 1445–1459, 2017.
- [27] T. Lin, J. Lee, J. Kang, H. Shin, J. Lee, and D. Jin, "Endoplasmic reticulum (ER) stress and unfolded protein response (UPR) in mammalian oocyte maturation and preimplantation embryo development," *International Journal of Molecular Sciences*, vol. 20, no. 2, 2019.
- [28] X. Xu, A. Qimuge, H. Wang et al., "IRE1 α /XBP1s branch of UPR links HIF1 α activation to mediate ANGII-dependent endothelial dysfunction under particulate matter (PM) 2.5 exposure," *Scientific Reports*, vol. 7, no. 1, article 13507, 2017.
- [29] N. Amin-Wetzel, R. A. Saunders, M. J. Kamphuis et al., "A J-protein co-chaperone recruits BiP to monomerize IRE1 and repress the unfolded protein response," *Cell*, vol. 171, no. 7, pp. 1625–1637.e13, 2017.
- [30] Y. Q. Hu, W. Chen, M. H. Yan, J. J. Lai, N. Tang, and L. Wu, "Ischemic preconditioning protects brain from ischemia/reperfusion injury by attenuating endoplasmic reticulum stress-induced apoptosis through PERK pathway," *European Review for Medical and Pharmacological Sciences*, vol. 21, no. 24, pp. 5736–5744, 2017.
- [31] J. Zhang, P. Zhang, C. Meng et al., "The PERK pathway plays a neuroprotective role during the early phase of secondary brain injury induced by experimental intracerebral hemorrhage," *Acta Neurochirurgica. Supplement*, vol. 127, pp. 105–119, 2020.
- [32] Y. He, J. Xi, H. Zheng, Y. Zhang, Y. Jin, and Z. Xu, "Astragaloside IV Inhibits Oxidative Stress-Induced Mitochondrial Permeability Transition Pore Opening by Inactivating GSK-3 via Nitric Oxide in H9c2 Cardiac Cells," *Oxidative Medicine and Cellular Longevity*, vol. 2012, Article ID 935738, 9 pages, 2012.
- [33] R. C. Scaduto Jr. and L. W. Grotyohann, "Measurement of mitochondrial membrane potential using fluorescent rhodamine derivatives," *Biophysical Journal*, vol. 76, no. 1, pp. 469–477, 1999.
- [34] J. C. Corona and M. R. Duchen, "Impaired mitochondrial homeostasis and neurodegeneration: towards new therapeutic targets?," *Journal of Bioenergetics and Biomembranes*, vol. 47, no. 1–2, pp. 89–99, 2015.
- [35] S. Li, T. Wang, L. Zhai et al., "Picroside II exerts a neuroprotective effect by inhibiting mPTP permeability and EndoG release after cerebral ischemia/reperfusion injury in rats," *Journal of Molecular Neuroscience*, vol. 64, no. 1, pp. 144–155, 2018.
- [36] L. Huang, C. Chen, X. Zhang et al., "Neuroprotective effect of curcumin against cerebral ischemia-reperfusion via mediating autophagy and inflammation," *Journal of Molecular Neuroscience*, vol. 64, no. 1, pp. 129–139, 2018.
- [37] I. Bellezza, S. Grottelli, A. L. Mierla et al., "Neuroinflammation and endoplasmic reticulum stress are coregulated by cyclo(His-Pro) to prevent LPS neurotoxicity," *The International Journal of Biochemistry & Cell Biology*, vol. 51, pp. 159–169, 2014.
- [38] H. T. Kang and E. S. Hwang, "2-Deoxyglucose: an anticancer and antiviral therapeutic, but not any more a low glucose mimetic," *Life Sciences*, vol. 78, no. 12, pp. 1392–1399, 2006.
- [39] S. Q. Zhang, K. K. Yung, S. K. Chung, and S. S. Chung, "Aldo-keto reductases-mediated cytotoxicity of 2-deoxyglucose: a novel anticancer mechanism," *Cancer Science*, vol. 109, no. 6, pp. 1970–1980, 2018.
- [40] H. Liu, M. Kurtoglu, Y. Cao et al., "Conversion of 2-deoxyglucose-induced growth inhibition to cell death in normoxic tumor cells," *Cancer Chemotherapy and Pharmacology*, vol. 72, no. 1, pp. 251–262, 2013.
- [41] Q. Yang, J. T. Lu, A. W. Zhou, B. Wang, G. W. He, and M. Z. Chen, "Antinociceptive effect of astragalosides and its

- mechanism of action," *Acta Pharmacologica Sinica*, vol. 22, no. 9, pp. 809–812, 2001.
- [42] M. Li, H. Li, F. Fang, X. Deng, and S. Ma, "Astragaloside IV attenuates cognitive impairments induced by transient cerebral ischemia and reperfusion in mice via anti-inflammatory mechanisms," *Neuroscience Letters*, vol. 639, pp. 114–119, 2017.
- [43] S. Cheng, X. Zhang, Q. Feng et al., "Astragaloside IV exerts angiogenesis and cardioprotection after myocardial infarction via regulating PTEN/PI3K/Akt signaling pathway," *Life Sciences*, vol. 227, pp. 82–93, 2019.
- [44] W. Qian, X. Cai, Q. Qian, W. Zhang, and D. Wang, "Astragaloside IV modulates TGF- β 1-dependent epithelial-mesenchymal transition in bleomycin-induced pulmonary fibrosis," *Journal of Cellular and Molecular Medicine*, vol. 22, no. 9, pp. 4354–4365, 2018.
- [45] T. Guo, Z. L. Liu, Q. Zhao, Z. M. Zhao, and C. H. Liu, "A combination of astragaloside I, levestilide A and calycosin exerts anti-liver fibrosis effects in vitro and in vivo," *Acta Pharmacologica Sinica*, vol. 39, no. 9, pp. 1483–1492, 2018.
- [46] X. Lei, L. Zhang, Z. Li, and J. Ren, "Astragaloside IV/lncRNA-TUG1/TRAF5 signaling pathway participates in podocyte apoptosis of diabetic nephropathy rats," *Drug Design, Development and Therapy*, vol. 12, pp. 2785–2793, 2018.
- [47] Y. Qi, F. Gao, L. Hou, and C. Wan, "Anti-inflammatory and immunostimulatory activities of astragalosides," *American Journal of Chinese Medicine*, vol. 45, no. 6, pp. 1157–1167, 2017.
- [48] C. Yang, Y. Mo, E. Xu et al., "Astragaloside IV ameliorates motor deficits and dopaminergic neuron degeneration via inhibiting neuroinflammation and oxidative stress in a Parkinson's disease mouse model," *International Immunopharmacology*, vol. 75, article 105651, 2019.
- [49] S. V. S. Rana, "Endoplasmic reticulum stress induced by toxic elements—a review of recent developments," *Biological Trace Element Research*, vol. 196, pp. 10–19, 2020.
- [50] J. Nunnari and A. Suomalainen, "Mitochondria: in sickness and in health," *Cell*, vol. 148, no. 6, pp. 1145–1159, 2012.
- [51] A. P. Halestrap, "What is the mitochondrial permeability transition pore?," *Journal of Molecular and Cellular Cardiology*, vol. 46, no. 6, pp. 821–831, 2009.
- [52] Z. W. Liu, H. T. Zhu, K. L. Chen et al., "Protein kinase RNA-like endoplasmic reticulum kinase (PERK) signaling pathway plays a major role in reactive oxygen species (ROS)-mediated endoplasmic reticulum stress-induced apoptosis in diabetic cardiomyopathy," *Cardiovascular Diabetology*, vol. 12, no. 1, p. 158, 2013.
- [53] S. C. Chang, J. Y. Lin, L. Y. Lo, M. L. Li, and S. R. Shih, "Diverse apoptotic pathways in enterovirus 71-infected cells," *Journal of Neurovirology*, vol. 10, no. 6, pp. 338–349, 2004.
- [54] C. Wang, R. Zhou, Z. Zhang, Y. Jin, C. J. Cardona, and Z. Xing, "Intrinsic apoptosis and proinflammatory cytokines regulated in human astrocytes infected with enterovirus 71," *The Journal of General Virology*, vol. 96, no. 10, pp. 3010–3022, 2015.
- [55] Y. He, Y. Fu, M. Xi et al., "Zn(2+) and mPTP mediate resveratrol-induced myocardial protection from endoplasmic reticulum stress," *Metallomics*, vol. 12, no. 2, pp. 290–300, 2020.
- [56] J. S. So, "Roles of endoplasmic reticulum stress in immune responses," *Molecules and Cells*, vol. 41, no. 8, pp. 705–716, 2018.
- [57] P. Walter and D. Ron, "The unfolded protein response: from stress pathway to homeostatic regulation," *Science*, vol. 334, no. 6059, pp. 1081–1086, 2011.
- [58] H. Ni, Q. Rui, Y. Xu et al., "RACK1 upregulation induces neuroprotection by activating the IRE1-XBP1 signaling pathway following traumatic brain injury in rats," *Experimental Neurology*, vol. 304, pp. 102–113, 2018.

Review Article

Pharmacological Modulation of Cardiac Remodeling after Myocardial Infarction

Wei Zhao,^{1,2} Jia Zhao,¹ and Jianhui Rong^{1,3} 

¹School of Chinese Medicine, Li Ka Shing Faculty of Medicine, University of Hong Kong, 10 Sassoon Road, Pokfulam, Hong Kong, China

²Zhujiang Hospital, Southern Medical University, 253 Industrial Road, Guangzhou, Guangdong Province, China

³Shenzhen Institute of Research and Innovation, The University of Hong Kong, Shenzhen, China

Correspondence should be addressed to Jianhui Rong; jrong@hkucc.hku.hk

Received 4 September 2020; Revised 13 November 2020; Accepted 21 December 2020; Published 31 December 2020

Academic Editor: Xue Han

Copyright © 2020 Wei Zhao et al. This is an open access article distributed under the Creative Commons Attribution License, which permits unrestricted use, distribution, and reproduction in any medium, provided the original work is properly cited.

Cardiac remodeling describes a series of structural and functional changes in the heart after myocardial infarction (MI). Adverse post-MI cardiac remodeling directly jeopardizes the recovery of cardiac functions and the survival rate in MI patients. Several classes of drugs are proven to be useful to reduce the mortality of MI patients. However, it is an ongoing challenge to prevent the adverse effects of cardiac remodeling. The present review aims to identify the pharmacological therapies from the existing clinical drugs for the treatment of adverse post-MI cardiac remodeling. Post-MI cardiac remodeling is a complex process involving ischemia/reperfusion, inflammation, cell death, and deposition of extracellular matrix (ECM). Thus, the present review included two parts: (1) to examine the basic pathophysiology in the cardiovascular system and the molecular basis of cardiac remodeling and (2) to identify the pathological aspects of cardiac remodeling and the potential of the existing pharmacotherapies. Ultimately, the present review highlights drug repositioning as a strategy to discover effective therapies from the existing drugs against post-MI cardiac remodeling.

1. Introduction

Acute myocardial infarction (AMI), commonly referred to as a heart attack, is one of the most common cardiovascular diseases and a significant cause of morbidity and mortality, while 7.3 million deaths per year were estimated worldwide [1, 2]. The loss of functional myocardium characterizes the pathology of AMI. The myocardial injury initiates adaptive immune responses so that the heart undergoes structural and functional changes to maintain the cardiac outcome. Such changes in the heart are termed as cardiac remodeling [3]. Although cardiac remodeling was initially created to describe the anatomical changes in the left ventricle of the infarcted hearts, myocardial infarction (MI) is well-known to alter cardiac energy metabolism, impair intramyocardial perfusion, and attenuate diastolic and systolic functions [4].

Post-MI cardiac remodeling involves several pathophysiological processes, such as ischemia/reperfusion, cell death, inflammation, synthesis, and deposition of the extracellular

matrix (ECM), resulting in changes in ventricular morphology, structure, and functions [5, 6]. It is an ongoing challenge to overcome the adverse effects of post-MI cardiac remodeling. Enormous effort has been made to develop effective targeted pharmacological therapies by targeting the basic pathophysiological processes [7–9]. Nevertheless, several existing treatments are often administered simultaneously to achieve satisfactory efficacy. Drugs, including adenosine, nicorandil, nitroprusside, and atrial natriuretic peptide and statins, are administered with other therapies for ischemia/reperfusion injury [10, 11]. Indeed, clinical experience in the past 30 years validated the effectiveness of several existing drugs and interventions to reduce the mortality of AMI patients. However, little is known about the pharmacological approaches for effectively controlling cardiac remodeling [5, 12, 13]. In clinical practice, drugs including angiotensin-converting enzyme inhibitors, angiotensin receptor blockers, aldosterone inhibitors, renin inhibitors, nicorandil, beta-blockers, and statins are administered chronically for

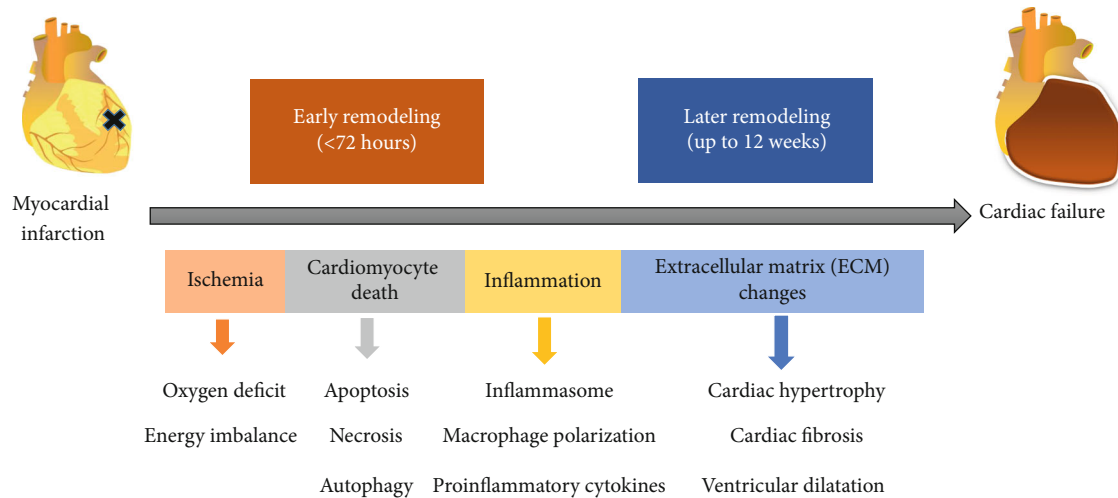


FIGURE 1: The phases and the main pathological changes in post-MI cardiac remodeling. The early remodeling includes ischemia, cell death, and inflammation within hours to days after the acute myocardial insult. The late remodeling is characterized by ECM deposition and causes reactive cardiac hypertrophy, cardiac fibrosis, and ventricular dilatation.

effective treatment of the chronic phase of left ventricular remodeling [14, 15]. It appears that the combination therapy with two or more drugs (e.g., ACE inhibitors/AR blockers, aldosterone antagonist) is currently the preferred strategy for preventing post-MI adverse cardiac remodeling [6]. Therefore, the improvement of therapeutics for myocardial recovery should be achieved based on the comprehensive understanding and analysis of the pathobiology of cardiac remodeling [9, 16]. It is of great interest to identify novel molecular targets in the pathology of cardiac remodeling and dysfunction [17, 18].

The present review basically examined different key pathological aspects of cardiac remodeling and the existing pharmacotherapies in the past 10 years. The findings from this review may pave the avenue to develop effective therapeutics for treating the adverse effects of cardiac remodeling.

2. Key Pathological Alterations in Cardiac Remodeling

Cardiac remodeling is a complex process in which the pathologic stimuli alter cardiac structure, shape, and function [6]. Cardiac remodeling encompasses both the MI-triggered acute events within 90 min of an ST-elevation myocardial infarction as well as the long-standing events in the post-MI period of months or even years [6, 19–21]. In the early phase of MI, cardiac remodeling is driven by the infarct expansion [22]. Early changes are detectable within hours to days after the acute myocardial insult. Myocardial necrosis results in an influx of inflammatory cells, including macrophages and neutrophils [23]. The influx of different inflammatory cells leads to the destruction of the collagen scaffolding, leading to the alteration of ventricular shape, regional thinning, and dilation of the myocardium in the infarcted areas [24]. Over the following weeks to months, the viable myocardium is still challenged by different pathologic events including the activation of proteases and elevated expression of cytokines, especially those that may induce car-

diomyocyte apoptosis and increase the release of the proinflammatory factor. The late phase involves reactive myocyte hypertrophy, interstitial fibrosis, and left ventricular dilatation [25]. Adverse cardiac remodeling is known to impair ventricular function and cause heart failure, representing a significant cause of mortality and morbidity in AMI patients [26]. However, the existing cardiovascular medicines are not designed to target cardiac remodeling due to the lack of understanding of the molecular mechanism of cardiac remodeling [4].

In fact, the post-MI remodeling process involves inflammatory, proliferative, and maturation phases. The pathologic responses in the infarcted heart include but not limited to ischemia, ischemia-reperfusion injury, inflammation (myocarditis), biomechanical stress, excess neurohormonal activation, excess afterload (hypertension, aortic stenosis), and cytokine storm [22, 26]. The post-MI phases and main pathological changes in cardiac remodeling are illustrated in Figure 1.

2.1. Ischemia in the Infarcted Heart. The basic pathology of MI is characterized by ischemia and cardiomyocyte death due to the imbalance between oxygen supply and demand [27, 28]. Myocardial ischemia markedly perturbs the ionic balance in cardiac metabolism [29]. Ischemia is known to cause the sudden cessation of oxidative phosphorylation and forces cardiomyocytes to overrun glycolysis for ATP production. Under physiological conditions, cardiomyocytes possess sufficient energy reserves to maintain contractility against short-time ischemia [30]. The prolonged ischemia disturbs myocardial metabolism and thereby reduces myocardial contractility. Indeed, myocardial ischemia not only causes systolic dysfunction but also reduces the compliance of the ventricle and diastolic dysfunction. When MI occurs, cardiomyocytes undergo necrosis due to initial ischemia and subsequent apoptosis during reperfusion as free radicals activate proapoptotic pathways [31, 32]. During adverse cardiac remodeling, the heart undergoes progressive ventricular

dilatation, cardiac hypertrophy, fibrosis, and deterioration of cardiac performance. Thus, the outcome of cardiac remodeling is determined by interactions between the adaptive modifications and negative adaptations in cardiomyocytes [33].

2.2. Cardiomyocyte Death. The heart represents a well-organized assembly of cardiomyocytes, fibroblasts, endothelial, and smooth muscle cells. The death of cardiomyocytes directly causes post-MI heart failure [34, 35]. Upon MI, cardiomyocytes are damaged by necrosis, apoptosis, and autophagy. Several cellular pathways are activated to drive the progression from cardiac injury to adverse cardiac remodeling [4, 36]. Apoptosis, autophagy, and necroptosis are the regulated forms of cell death in infarcted hearts, although it is difficult to quantify the contributions of individual forms to the infarct size [37–39]. Progressive cell death directly causes cardiac remodeling in chronically overloaded hearts [6, 40]. Apoptosis is an energy-dependent form of cell death with DNA disintegration and without an associated inflammatory response. Apoptosis signal-regulating kinase (ASK) is the key mediator of cell death and susceptibility to heart failure in heart hypertrophy [5]. Necroptosis representing programmed necrosis is recently described as a novel form of regulated cell death and may play a prominent role in cardiovascular diseases [6]. With high relevance to necrosis and apoptosis, necroptosis is uniquely regulated by the activation of specific receptor-interacting protein kinases [41, 42]. Autophagy is another regulated form of cell death, characterized by the orderly degradation and recycling of cellular components, and upregulated in response to nutrient deprivation [43, 44], oxidative stress [45], and hypoxia [46]. A recent study showed that beclin-1 heterozygous deficiency protected mice from adverse cardiac remodeling in the model of I/R via regulating autophagy [47]. During the heart transplantation in mice, mechanical unloading of the LV activates autophagy and of FoxO3, leading to cardiac atrophy [48]. FoxO proteins are critical regulators of autophagy in the regression of cardiac hypertrophy after unloading the hypertrophic stimuli. Upregulation of FoxO proteins may be a novel therapeutic target to reverse cardiac hypertrophy via autophagy-mediated mechanism [33, 48]. Interestingly, the extent of activation determines whether autophagy protects cells from apoptotic death or promotes cell death [6, 49]. Presumably, apoptosis, necrosis, and autophagy coexist in many ways, such as in parallel and sequential in different sequences [50, 51]. Therefore, further investigation should define how much each type of cell death contributes to myocardial remodeling [4].

2.3. Inflammation. Myocardial ischemia and necrosis stimulate robust infiltration of leukocytes, which not only helps to clear necrotic debris but also triggers an intense organized inflammatory response [52, 53]. Such inflammatory cascade involves various components of the innate immunity and affects cardiomyocytes and noncardiomyocyte cells [31, 54]. During the first few days after MI, ischemic or nonischemic cardiomyocytes undergo necrosis and secrete cytokines (e.g., tumor necrosis factor- α (TNF- α), interleukin-1 beta (IL-1 β), and interleukin (IL-6)). These cytokines recruit inflam-

matory cells to the site of injury, leading to adverse cardiac remodeling and dysfunction [4, 53, 55]. Excessive inflammatory response induces myocardial apoptosis and promotes cardiac pathological remodeling [56]. On the other hand, some of the immune cells may contribute to the wound-healing process for post-MI cardiac repair [56].

Post-MI inflammation plays a critical role in determining AMI size and post-MI adverse cardiac remodeling. The detrimental effects of AMI are mediated by several inflammatory mediators, which are important therapeutic targets for cardiac protection [57, 58]. Firstly, the NACHT, LRR, and PYD domain-containing protein 3 (NLRP3) inflammasome is an important ubiquitous intracellular pattern recognition receptor for regulating the inflammatory response during AMI [59]. Particularly, the NLRP3 inflammasome determines the production of IL-1 β and ensures systemic inflammatory response. In the early phase of inflammation, the inflammasome specks are detectable in the endothelial cells, cardiomyocytes, and fibroblasts. The expression of NLRP3 and the activity of the inflammasome in the heart were low within 3 h after AMI in a mouse model of ischemia-reperfusion injury [60, 61]. In this model, the NLRP3 inflammasome was formed in the myocardium within 3–24 h after AMI, contributed to the inflammatory response, and exacerbated the ischemia-reperfusion injury [60]. Importantly, genetic and pharmacological inhibitions of the inflammasome-related components (e.g., caspase 1, IL-1 β , ASC, and NLRP3) are effective to reduce MI size [62–66]. The MI-induced inflammatory response is schematically illustrated in Figure 2.

Neutrophils are well-known to be the first-line defender against invading microorganisms. Within the context of MI, neutrophils are activated to generate oxygen free radicals and secrete chemokines and matrix metalloproteinases (MMPs) [67]. Dysregulation of neutrophils may affect cardiac remodeling due to overproduction of free radicals, insufficient phagocytosis of cell debris, and aberrant degradation of the extracellular matrix.

Secondly, macrophages are known to play a significant role in the pathophysiology of MI, while the timely switch of macrophage polarization is a potential therapeutic target for promoting myocardial healing [62, 68, 69]. Macrophage phenotypes are classified into activated macrophages (M1) and alternatively activated macrophages (M2) [70]. Depending on the pathological environment, M2 macrophages are further differentiated into the following four polarization subtypes: M2a, M2b, M2c, and M2d. Gleissner et al. described another M4 macrophage, which is different from phenotypes M1 and M2 [71]. Although several factors have been identified for regulating macrophage polarization, little is known about the spatiotemporal relationships and functions of the various macrophage subsets in the post-MI cardiac remodeling [72, 73]. A recent study demonstrated that cardio sphere-derived cells decreased proinflammatory M1 macrophages but increased anti-inflammatory M2 macrophages in the infarcted hearts, thereby supporting heart repair [74]. *In vivo* IL-10 infusion significantly improved post-MI cardiac physiology and increased cardiac macrophage M2 polarization and fibroblast activation to moderate

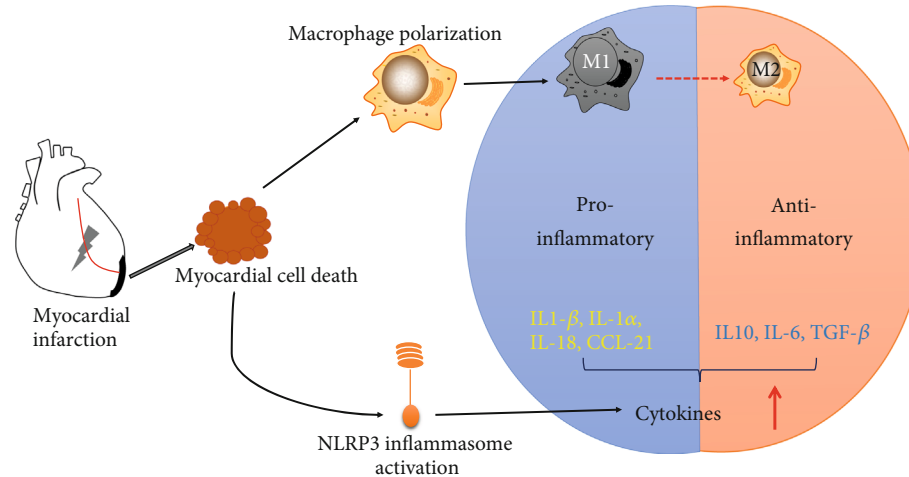


FIGURE 2: Macrophage M1/M2 polarization and the inflammatory response in MI. MI-induced inflammatory response includes the initial proinflammatory and the subsequent anti-inflammatory reparative phase. In the proinflammatory phase, macrophages undergo M1 polarization while activation of the NLRP3 inflammasome increases the release of proinflammatory cytokines (such as IL-1 β , IL-1 α , IL-18, CCL21). In the subsequent anti-inflammatory reparative phase, macrophages undergo M2 polarization while anti-inflammatory factors (such as IL-10, IL6, TGF- β) are produced to execute the resolution of cardiac inflammation.

collagen deposition [74]. Therefore, pharmacological modulation of monocyte differentiation and macrophage polarization could provide anti-inflammatory and reparative therapeutic strategies for the treatment of post-MI cardiac remodeling [62].

2.4. Changes in Cardiac ECM. Cardiac ECM serves as the cellular scaffold to maintain the shape and geometry of the heart [75]. Biochemically, ECM represents a complex network of different cellular components including collagen, MMPs, and cell surface adhesion molecules [76]. The composition of the ECM components determines cardiac remodeling in the infarct heart. In the early phase after MI, cardiac fibroblasts migrate to the infarcted area in response to cytokines, synthesize and secrete ECM components (mainly collagen) to replace the necrotic tissues, stabilize the cardiac structure, and prevent cardiac rupture. Uncontrolled deposition of ECM components promotes the formation of myocardial fibrosis, decreases ventricular compliance, and causes cardiac dysfunction and heart failure over a long time. Moreover, cardiac fibrosis further stimulates the electrophysiological remodeling, inducing arrhythmogenesis and affecting the quality of life.

Different endogenous factors dynamically regulate the synthesis and degradation of ECM components. The healthy cardiac ECM is primarily composed of type I collagen (70%) and type III collagen (12%). Type I, III, IV, V, and VI collagen are increased in the infarct region, while type I collagen and type III collagen are the major components of the myocardial scar [77, 78]. Moreover, ischemia and reperfusion are known to profoundly increase several other ECM proteins, including intermediate cartilage layer protein 1 (CILP1), asporin, adipocyte enhancer-binding protein 1 (AEBP1), and transforming growth factor β -induced gene-h3 (TGFB1) in the border zone at 15 days after reperfusion in a porcine model of ischemia/reperfusion injury [79]. Collectively, the remodeling of the myocardium structure involves the excessive accumulation

of fibrillar collagen matrix in the form of “reparative” and “reactive” fibrosis, causes adverse consequences on ventricular function and arrhythmogenicity, and supports the pathophysiological concept of interstitial heart disease [56].

The proliferative phase of cardiac remodeling is hallmarked by scar formation at 2–7 days for mice and 4–14 days for humans, respectively. Pharmacological intervention is needed to limit pathological ECM remodeling and promote infarct repair. Collagen-based biomaterials may provide mechanical support, improve angiogenesis and tissue integration, reduce inflammation and apoptosis, and limit adverse remodeling and the loss of cardiac function in the animal MI models [80, 81]. On the other hand, recombinant human collagen was also evaluated for the preparation of clinically relevant biomaterials to reduce pathological remodeling and ameliorate post-MI cardiac functions [82].

3. Pharmacological Approaches

Cardiac remodeling contributes to the development and progression of ventricular dysfunction, arrhythmias, and poor prognosis. Uncontrolled cardiac remodeling is a significant cause of mortality and morbidity in AMI patients [67]. Therefore, adverse cardiac remodeling is an important therapeutic target for the treatment of AMI. In fact, the basic pathophysiological processes are targeted for the development of pharmacological treatments [83, 84]. Different existing drugs including β -adrenergic receptor (β -AR) blockers, angiotensin-converting enzyme (ACE) inhibitors, angiotensin-receptor (AR) blockers, mineralocorticoid receptor blockers, hydralazine, nitrates, and cardiac resynchronization therapy have been evaluated for preventing adverse cardiac remodeling [22, 85].

3.1. β -AR Blockers. The activation of β -ARs increases the cAMP synthesis and activates protein kinase A, representing

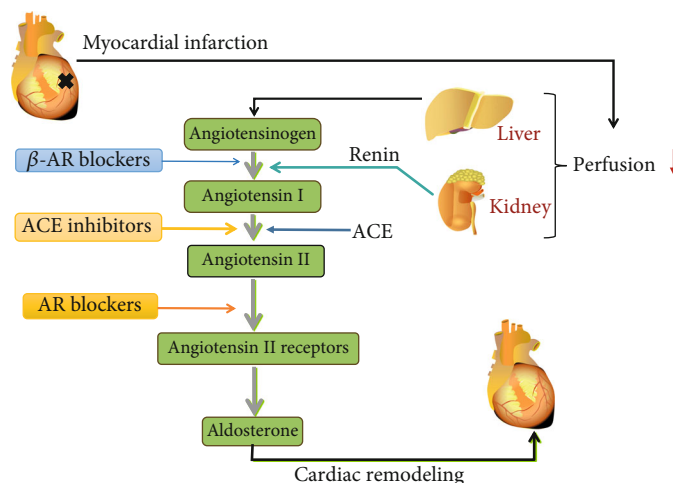


FIGURE 3: MI-induced activation and pharmacologic inhibition of the renin-angiotensin-aldosterone system. Renin-angiotensin-aldosterone system regulates the functions of multiorgans. AMI causes a decrease in cardiac output, reduces tissue perfusion in the kidney and liver, and stimulates renin and angiotensinogen production. Consequently, angiotensin production is increased to stimulate ventricular remodeling. Meanwhile, aldosterone has similar effects on cardiac remodeling.

the primary mechanism for acute enhancement of cardiac reserve to maintain heart function [6]. The β -AR blockers suppress the activation of β -ARs and attenuate adverse cardiac remodeling at the molecular and organ levels [86]. Indeed, several β -AR blockers exhibit potential for reversing cardiac remodeling, although such results should be further validated by clinical trials [87]. A recent report suggested that β -AR blockers reduced the profibrotic potential of resident cardiac progenitor cells in patients [88]. Interestingly, excessive adrenergic stimulation may also affect the *in situ* myofibroblastic potentials of resident progenitors through β 2-AR signaling, resulting in detrimental profibrotic outcomes [89]. Acute overactivation of β -ARs induces inflammasome-dependent production of IL-18 within the myocardium while activates cytokine cascades, macrophage infiltration, and pathological cardiac remodeling [90]. Neutralizing IL-18 at the early stage of β -AR activation successfully prevented inflammatory responses and cardiac injuries. β -adrenergic stimulation on the β -AR-Gas/Src pathway activates the STAT3 pathway for maintaining normal cardiac function and minimizing adverse cardiac remodeling [91]. Cardiac-specific overexpression of β 3-AR inhibits the hypertrophic response to neurohormonal stimulation through a NOS-mediated mechanism [92]. Thus, β 3-AR agonists may have therapeutic potential for the modulation of cardiac remodeling.

3.2. ACE Inhibitors and AR Blockers. The renin-angiotensin system regulates the structural remodeling of the left ventricle for post-MI cardiac healing and long-term prognosis [92]. Interestingly, the renin-angiotensin system is regulated by multiple mechanisms: (1) β -AR blockers inhibit the secretion of renin, (2) renin inhibitors directly diminish the activity of renin, (3) ACE inhibitors block the formation of angiotensin II, and (4) AR blockers dampen the activation of angiotensin II type 1 (AT1) receptor. As shown in Figure 3, these pharmacological mechanisms may inhibit the renin-angiotensin system in a synergistical manner.

It is well-known that acute activation of the renin-angiotensin-aldosterone system alleviates hemodynamic stress. Dysregulation of the renin-angiotensin-aldosterone system is often associated with hypertension, oxidative stress, and adverse cardiac remodeling [93]. The sustained release of angiotensin promotes cardiac fibrosis, cellular necrosis, and cardiomyocyte hypertrophy. Indeed, agents that inhibit either the renin-angiotensin-aldosterone system or sympathetic nervous system reduced mortality in MI patients [94]. ACE inhibitors are widely used in the management of heart failure in the last three decades [95]. Several randomized clinical trials demonstrated the beneficial effect of ACE inhibitors, mineralocorticoid receptor blockers, and AR blockers in the management of heart failure patients [25]. These drugs act at the different points in the signaling cascade of angiotensin II to strop adverse cardiac remodeling regardless of the changes in blood pressure [96]. Others showed that ACE inhibitors favourably altered the loading conditions for LV, reduced progressive LV remodeling, and improved clinical outcomes [97, 98]. AR blockers block the effects of angiotensin II particularly at the receptor subtype 1 level to mediate vasoconstriction, sodium and water retention, cardiac hypertrophy, and cardiac fibrosis [99]. It is noteworthy that randomized trials have not approved the superiority of AR blockers over ACE inhibitors, although angiotensin II antagonism is theoretically favourable in patients with AMI [10, 100].

On the other hand, the stimulation of the renin-angiotensin-aldosterone system leads to the activation of different MMPs in the heart and subsequent degradation of extracellular proteins in the myocardium [37, 101]. MMP-2 and MMP-9 are two typical MMPs for ECM degradation and post-MI cardiac remodeling [102, 103]. Pharmacological inhibition of MMPs is sufficient to limit tissue damage in animal MI models [104, 105].

3.3. Anti-Inflammatory Agents. Inflammation is a critical driving force for post-MI ventricular remodeling [106].

TABLE 1: Summary of pharmacological therapies against adverse post-MI cardiac remodeling.

Drug/target	Mechanism of action	Drug application phase	References
β -AR blockers	Prevent β -ARs/desensitization	Clinical	[86, 87, 89, 90]
ACE inhibitors	Inhibit angiotensin-converting enzyme	Clinical	[95, 97, 98]
AR blockers	Inhibit angiotensin receptor/desensitization	Clinical	[25, 99, 100]
Anti-inflammatory agents	Resistance to an excessive inflammatory response	Clinical	[106, 107, 110, 115]
Probiotics	Regulate gut microbiota	Preclinical	[126, 127, 130, 131]
Antibiotics	Inhibit matrix metalloproteinase/opening mPTP	Clinical	[132–134, 136]
Circadian rhythm regulators	Control cell fate/modulate oxidant stress	Preclinical	[117, 118, 120]
Noncoding RNAs (ncRNAs)	Reduced the cardiac fibrosis/regulating the autophagy signaling	Preclinical	[121–123, 125]

Unrestrained inflammation induces matrix degradation and cardiomyocyte apoptosis in the infarcted myocardium [107]. Prolonged inflammation is known to promote LV dilation, impair LV physiology, and enhance excessive scar formation [108]. Thus, modulation of the inflammatory response represents a potential strategy for intervening post-MI cardiac remodeling. Timely and effective suppression of inflammatory signaling in infarcted hearts is of great importance to protect the myocardium from dilative remodeling and progressive cardiac dysfunction [109]. Indeed, inhibition of the initial proinflammatory responses and promotion of the subsequent anti-inflammatory reparative responses are essential therapeutic strategies to limit MI size and prevent adverse LV remodeling [62]. Therefore, timely resolution of cardiac inflammation is critical to control cardiac remodeling [53].

Therapeutic targets are primarily several cytokines that control the initial proinflammatory response and promote the subsequent anti-inflammatory reparative response. Firstly, IL-1 is an important proinflammatory cytokine for the treatment of atherosclerosis, AMI, and heart failure [110]. Interestingly, blockade of IL-1 β signaling limits adverse cardiac remodeling after AMI [111, 112]. IL-1 α is released from the damaged cardiomyocytes and activates IL-1R1 on cardiac fibroblasts, inducing early myocardial remodeling in AMI [111]. Preclinical research and clinical trials validated the role of IL-1 α in the initiation of post-MI inflammation and the role of IL-1 β in adverse cardiac remodeling and heart failure [63]. Secondly, the CC-chemokine CCL21 interacts with receptor CCR7 to regulate inflammation and immune cell recruitment in response to pressure overload in symptomatic aortic stenosis [113]. Thirdly, IL-10 is an anti-inflammatory cytokine for resolving cardiac inflammation [114]. Myocardial ischemia and reperfusion significantly increased IL-10 in the serum within 6 h in animal models [53]. Finally, the NLRP3 inflammasome is a multiprotein complex for regulating the proteolytic activation of caspase 1 and proinflammatory cytokines such as IL-1 β and IL-18 [64]. NLRP3 inhibition significantly reduced infarct size and preserved cardiac function, suggesting that the early activation of NLRP3 inflammasome may control the downstream inflammatory signaling [115].

3.4. Miscellaneous Aspects

3.4.1. Circadian Rhythm Regulation. Circadian rhythm is known to regulate various biological and cardiovascular rhythms in health and disease and modulates post-MI cardiac remodeling and dysfunction [116, 117]. Circadian rhythms control myocardial homeostasis, apoptosis, autophagy, and necrosis [51]. Circadian rhythm is closely associated with the systems that modulate oxidative stress and may thereby modulate post-MI cardiac remodeling [118]. Melatonin is a well-known circadian rhythm regulator and antioxidant. Several studies demonstrated the cardioprotective activity of melatonin in AMI [119, 120].

3.4.2. Noncoding RNAs (ncRNAs). ncRNAs include small ncRNAs and long ncRNAs (lncRNA) while miRNAs are a class of small ncRNAs [121]. Intravenous miR-144 administration decreased the left ventricular remodeling in post-MI hearts. Further analysis revealed that miR-144 decreased myocardial fibrosis, inflammation, and apoptosis by regulating the autophagy signaling pathways [122]. The lncRNA Wisper reduced the cardiac fibrosis and prevented myocardial remodeling in post-MI hearts [123]. Downregulation of lncRNA Neat1 and AK139328 alleviated the myocardial ischemia/reperfusion injury via regulating the autophagy signaling [124]. The lncRNA Mhrt also protected the heart from cardiac hypertrophy by ATP-dependent chromatin-remodeling [125].

3.4.3. Gut Microbiota. Dysbiosis of the gut microbiota has recently emerged as a novel target for the control of cardiac remodeling [126]. Gut microbiota composition is linked to cardiovascular diseases (CVD) through multiple mechanisms including (1) direct effects of microbial metabolites on atherosclerosis and thrombosis and (2) immune modulation by bacteria and their products [127]. Probiotics may change gut microbiota composition to achieve the maximal beneficial effect on the cardiac remodeling process in MI patients. Lam et al. confirmed the potential effects of microbiota on the post-MI ventricular remodeling [128]. Oral administration of antibiotic vancomycin and probiotic Good belly was containing *Lactobacillus plantarum* and *Bifidobacterium lactis* Bi-07 before ischemia/reperfusion (I/R) injury significantly reduced infarct size and improved myocardial function in rats [129]. An increasing number of recent studies validated the link of gut microbiota to myocardial

function and repair in AMI [130]. Selective gut modulation by probiotic administration improved metabolic dysfunction and attenuated cardiac remodeling in AMI [131].

3.4.4. Antibiotics. Antibiotics may affect ventricular remodeling in the immediate post-MI setting. The “PROVE IT-TIMI22 trial” demonstrated that long-term treatment with gatifloxacin could prevent major adverse cardiovascular events in the subjects with recent acute coronary syndrome [132]. Doxycycline attenuated adverse ventricular remodeling via inhibiting MMPs [133]. Experimental and clinical studies suggested that cyclosporine could attenuate reperfusion injury and prevent adverse left ventricular remodeling [134]. Mechanistically, cyclosporine is a pharmacologic inhibitor of cyclophilin D, a central regulator for the opening of the mitochondrial permeability transition pore (mPTP). Indeed, either genetic or pharmacologic inhibition of cyclophilin D reduced the severity of myocardial reperfusion injury [135, 136].

4. Conclusion and Perspectives

The present review is aimed at identifying drugs for effective treatment of adverse cardiac remodeling in MI. We have summarized the pharmacological therapies on cardiac remodeling after AMI (Table 1). Firstly, the complex pathophysiological processes of cardiac remodeling were investigated to understand better the interactions between the cellular components, signaling molecules, the ECM components, and neurohormonal regulation. Secondly, the capacity of several classes of the existing drugs was assessed to target the vital pathological processes in cardiac remodeling. Surprisingly, different drugs should be combined to achieve efficacy in selected patients. Therefore, a better understanding of the complex pathological process of cardiac remodeling provides the key to develop more effective and safe strategies for the treatment of post-MI cardiac remodeling.

Conflicts of Interest

The authors declare no competing interests.

Acknowledgments

This work was supported by General Research Fund (GRF) grants (17146216, 17100317, 17119619), National Natural Science Foundation of China (81701464, 81703726, 21778046), Health and Medical Research Fund (16171751, 17181231), Midstream Research Programme for Universities (MRP) (053/18X), and the Hong Kong Scholars Program (XJ2019055).

References

- [1] G. W. Reed, J. E. Rossi, and C. P. Cannon, “Acute myocardial infarction,” *The Lancet*, vol. 389, no. 10065, pp. 197–210, 2017.
- [2] G. Maglietta, M. Ardissino, G. Malagoli Tagliazucchi et al., “Long-term outcomes after early-onset myocardial infarction,” *Journal of the American College of Cardiology*, vol. 74, no. 16, pp. 2113–2115, 2019.
- [3] R. Y. Kwong and J. J. Bax, “Unraveling the complex processes of adverse cardiac remodeling,” *Cardiovascular Imaging*, vol. 12, no. 5, article e009086, 2019.
- [4] A. Gonzalez, S. Ravassa, J. Beaumont, B. Lopez, and J. Diez, “New targets to treat the structural remodeling of the myocardium,” *Journal of the American College of Cardiology*, vol. 58, no. 18, pp. 1833–1843, 2011.
- [5] I. Kehat and J. D. Molkentin, “Molecular pathways underlying cardiac remodeling during pathophysiological stimulation,” *Circulation*, vol. 122, no. 25, pp. 2727–2735, 2010.
- [6] L. Schirone, M. Forte, S. Palmerio et al., “A review of the molecular mechanisms underlying the development and progression of cardiac remodeling,” *Oxidative Medicine and Cellular Longevity*, vol. 2017, Article ID 3920195, 16 pages, 2017.
- [7] M. Metra, “April 2016 At a glance. Focus on cardiac remodeling, biomarkers and treatment,” *European Journal of Heart Failure*, vol. 18, no. 4, pp. 345–346, 2016.
- [8] A. A. Gibb and B. G. Hill, “Metabolic coordination of physiological and pathological cardiac remodeling,” *Circulation Research*, vol. 123, no. 1, pp. 107–128, 2018.
- [9] R. M. Mortensen, “Immune cell modulation of cardiac remodeling,” *Circulation*, vol. 125, no. 13, pp. 1597–1600, 2012.
- [10] H. Ishii, T. Amano, T. Matsubara, and T. Murohara, “Pharmacological intervention for prevention of left ventricular remodeling and improving prognosis in myocardial infarction,” *Circulation*, vol. 118, no. 25, pp. 2710–2718, 2008.
- [11] M. A. Pfeffer and J. D. Rutherford, “Therapeutic attenuation of cardiac remodeling after acute myocardial infarction,” *Circulation*, vol. 137, no. 23, pp. 2430–2434, 2018.
- [12] J. N. Cohn, “Inhibiting LV remodeling—the need for a targeted approach,” *Nature Reviews. Cardiology*, vol. 8, no. 5, pp. 248–249, 2011.
- [13] A. M. Shah and D. L. Mann, “In search of new therapeutic targets and strategies for heart failure: recent advances in basic science,” *The Lancet*, vol. 378, no. 9792, pp. 704–712, 2011.
- [14] M. Poncelas, J. Inserte, D. Aluja, V. Hernando, U. Vilardosa, and D. Garcia-Dorado, “Delayed, oral pharmacological inhibition of calpains attenuates adverse post-infarction remodeling,” *Cardiovascular Research*, vol. 113, no. 8, pp. 950–961, 2017.
- [15] G. Tarone, J. L. Balligand, J. Bauersachs et al., “Targeting myocardial remodeling to develop novel therapies for heart failure: a position paper from the working group on myocardial function of the European Society of Cardiology,” *European Journal of Heart Failure*, vol. 16, no. 5, pp. 494–508, 2014.
- [16] G. W. Dorn 2nd, “Novel pharmacotherapies to abrogate postinfarction ventricular remodeling,” *Nature Reviews. Cardiology*, vol. 6, no. 4, pp. 283–291, 2009.
- [17] S. Chen, Y. Zhang, J. K. Lighthouse et al., “A novel role of cyclic nucleotide phosphodiesterase 10a in pathological cardiac remodeling and dysfunction,” *Circulation*, vol. 141, no. 3, pp. 217–233, 2020.
- [18] D. J. Hausenloy and D. M. Yellon, “Targeting myocardial reperfusion injury—the search continues,” *The New England Journal of Medicine*, vol. 373, no. 11, pp. 1073–1075, 2015.
- [19] D. Schuttler, S. Clauss, L. T. Weckbach, and S. Brunner, “Molecular mechanisms of cardiac remodeling and

- regeneration in physical exercise,” *Cells*, vol. 8, no. 10, article 1128, 2019.
- [20] L. V. Kozlovskaya, I. N. Bobkova, M. L. Nanchikееva, N. V. Chebotareva, and O. A. Li, “General molecular and cellular mechanisms for renal and cardiac remodeling in chronic kidney disease: a target for nephrocardioprotection,” *Terapevticheskie Arkhiv*, vol. 85, no. 6, pp. 66–72, 2013.
- [21] Y. Lu, J. J. Liu, and X. J. Yu, “Research progress of molecular mechanisms on cardiac remodeling,” *Sheng Li Ke Xue Jin Zhan [Progress in Physiology]*, vol. 44, no. 1, pp. 23–26, 2013.
- [22] Z. K. Haque and D. Z. Wang, “How cardiomyocytes sense pathophysiological stresses for cardiac remodeling,” *Cellular and Molecular Life Sciences: CMLS*, vol. 74, no. 6, pp. 983–1000, 2017.
- [23] Q. Liu, Y. Chen, M. Auger-Messier, and J. D. Molkenin, “Interaction between NF κ B and Nfat coordinates cardiac hypertrophy and pathological remodeling,” *Circulation Research*, vol. 110, no. 8, pp. 1077–1086, 2012.
- [24] J. H. van Berlo, M. Maillet, and J. D. Molkenin, “Signaling effectors underlying pathologic growth and remodeling of the heart,” *The Journal of Clinical Investigation*, vol. 123, no. 1, pp. 37–45, 2013.
- [25] M. Xie, J. S. Burchfield, and J. A. Hill, “Pathological ventricular remodeling: therapies: part 2 of 2,” *Circulation*, vol. 128, no. 9, pp. 1021–1030, 2013.
- [26] J. B. Muhlestein, “Adverse left ventricular remodeling after acute myocardial infarction: is there a simple treatment that really works?,” *European Heart Journal*, vol. 35, no. 3, pp. 144–146, 2014.
- [27] G. Heusch, “Myocardial ischemia: lack of coronary blood flow or myocardial oxygen supply/demand imbalance?,” *Circulation Research*, vol. 119, no. 2, pp. 194–196, 2016.
- [28] B. R. Weil, R. F. Young, X. Shen et al., “Brief myocardial ischemia produces cardiac troponin I release and focal myocyte apoptosis in the absence of pathological infarction in swine,” *JACC: Basic to Translational Science*, vol. 2, no. 2, pp. 105–114, 2017.
- [29] F. A. C. Seara, E. L. Olivares, and J. H. M. Nascimento, “Anabolic steroid excess and myocardial infarction: from ischemia to reperfusion injury,” *Steroids*, vol. 161, article 108660, 2020.
- [30] B. Shin, D. B. Cowan, S. M. Emani, P. J. Del Nido, and J. D. McCully, “Mitochondrial transplantation in myocardial ischemia and reperfusion injury,” *Advances in Experimental Medicine and Biology*, vol. 982, pp. 595–619, 2017.
- [31] N. G. Frangogiannis, “Pathophysiology of myocardial infarction,” *Comprehensive Physiology*, vol. 5, no. 4, pp. 1841–1875, 2015.
- [32] M. Y. Wu, G. T. Yiang, W. T. Liao et al., “Current mechanistic concepts in ischemia and reperfusion injury,” *Cellular Physiology and Biochemistry*, vol. 46, no. 4, pp. 1650–1667, 2018.
- [33] K. Nishida and K. Otsu, “Autophagy during cardiac remodeling,” *Journal of Molecular and Cellular Cardiology*, vol. 95, pp. 11–18, 2016.
- [34] S. Kostin, L. Pool, A. Elsasser et al., “Myocytes die by multiple mechanisms in failing human hearts,” *Circulation Research*, vol. 92, no. 7, pp. 715–724, 2003.
- [35] G. Takemura and H. Fujiwara, “Role of apoptosis in remodeling after myocardial infarction,” *Pharmacology & Therapeutics*, vol. 104, no. 1, pp. 1–16, 2004.
- [36] I. Shimizu and T. Minamino, “Physiological and pathological cardiac hypertrophy,” *Journal of Molecular and Cellular Cardiology*, vol. 97, pp. 245–262, 2016.
- [37] D. Curley, B. Lavin Plaza, A. M. Shah, and R. M. Botnar, “Molecular imaging of cardiac remodeling after myocardial infarction,” *Basic Research in Cardiology*, vol. 113, no. 2, p. 10, 2018.
- [38] J. Insete, M. Cardona, M. Poncelas-Nozal et al., “Studies on the role of apoptosis after transient myocardial ischemia: genetic deletion of the executioner caspases-3 and -7 does not limit infarct size and ventricular remodeling,” *Basic Research in Cardiology*, vol. 111, no. 2, p. 18, 2016.
- [39] M. Chiong, Z. V. Wang, Z. Pedrozo et al., “Cardiomyocyte death: mechanisms and translational implications,” *Cell Death & Disease*, vol. 2, article e244, 2011.
- [40] R. S. Whelan, V. Kaplinskiy, and R. N. Kitsis, “Cell death in the pathogenesis of heart disease: mechanisms and significance,” *Annual Review of Physiology*, vol. 72, pp. 19–44, 2010.
- [41] J. Liu, P. Wang, L. He et al., “Cardiomyocyte-Restricted Deletion of PPAR β/δ in PPAR α -Null Mice Causes Impaired Mitochondrial Biogenesis and Defense, but No Further Depression of Myocardial Fatty Acid Oxidation,” *PPAR Research*, vol. 2011, Article ID 372854, 13 pages, 2011.
- [42] D. Frank and J. E. Vince, “Pyroptosis versus necroptosis: similarities, differences, and crosstalk,” *Cell Death and Differentiation*, vol. 26, no. 1, pp. 99–114, 2019.
- [43] S. Sciarretta, Y. Maejima, D. Zablocki, and J. Sadoshima, “The role of autophagy in the heart,” *Annual Review of Physiology*, vol. 80, pp. 1–26, 2018.
- [44] Y. Matsui, H. Takagi, X. Qu et al., “Distinct roles of autophagy in the heart during ischemia and reperfusion,” *Circulation Research*, vol. 100, no. 6, pp. 914–922, 2007.
- [45] Y. Maejima, S. Kyoji, P. Zhai et al., “Mst1 inhibits autophagy by promoting the interaction between Beclin1 and Bcl-2,” *Nature Medicine*, vol. 19, no. 11, pp. 1478–1488, 2013.
- [46] H. Zhang, M. Bosch-Marce, L. A. Shimoda et al., “Mitochondrial autophagy is an Hif-1-dependent adaptive metabolic response to hypoxia,” *The Journal of Biological Chemistry*, vol. 283, no. 16, pp. 10892–10903, 2008.
- [47] X. Ma, H. Liu, S. R. Foyil et al., “Impaired autophagosome clearance contributes to cardiomyocyte death in ischemia/reperfusion injury,” *Circulation*, vol. 125, no. 25, pp. 3170–3181, 2012.
- [48] D. J. Cao, N. Jiang, A. Blagg et al., “Mechanical unloading activates Foxo3 to trigger Bnip3-dependent cardiomyocyte atrophy,” *Journal of the American Heart Association*, vol. 2, no. 2, article e000016, 2013.
- [49] A. K. Biala and L. A. Kirshenbaum, “The interplay between cell death signaling pathways in the heart,” *Trends in Cardiovascular Medicine*, vol. 24, no. 8, pp. 325–331, 2014.
- [50] G. Marino, M. Niso-Santano, E. H. Baehrecke, and G. Kroemer, “Self-consumption: the interplay of autophagy and apoptosis, nature reviews,” *Molecular Cell Biology*, vol. 15, no. 2, pp. 81–94, 2014.
- [51] I. Rabinovich-Nikitin, B. Lieberman, T. A. Martino, and L. A. Kirshenbaum, “Circadian-regulated cell death in cardiovascular diseases,” *Circulation*, vol. 139, no. 7, pp. 965–980, 2019.
- [52] S. D. Prabhu and N. G. Frangogiannis, “The biological basis for cardiac repair after myocardial infarction: from inflammation to fibrosis,” *Circulation Research*, vol. 119, no. 1, pp. 91–112, 2016.

- [53] M. Jung, Y. Ma, R. P. Iyer et al., “IL-10 improves cardiac remodeling after myocardial infarction by stimulating M2 macrophage polarization and fibroblast activation,” *Basic Research in Cardiology*, vol. 112, no. 3, p. 33, 2017.
- [54] S. Khodayari, H. Khodayari, A. Z. Amiri et al., “Inflammatory microenvironment of acute myocardial infarction prevents regeneration of heart with stem cells therapy,” *Cellular Physiology and Biochemistry*, vol. 53, no. 5, pp. 887–909, 2019.
- [55] N. G. Frangogiannis, “The immune system and cardiac repair,” *Pharmacological Research*, vol. 58, no. 2, pp. 88–111, 2008.
- [56] K. T. Weber, Y. Sun, S. K. Bhattacharya, R. A. Ahokas, and I. C. Gerling, “Myofibroblast-mediated mechanisms of pathological remodeling of the heart,” *Nature Reviews. Cardiology*, vol. 10, no. 1, pp. 15–26, 2013.
- [57] I. Andreadou, H. A. Cabrera-Fuentes, Y. Devaux et al., “Immune cells as targets for cardioprotection: new players and novel therapeutic opportunities,” *Cardiovascular Research*, vol. 115, no. 7, pp. 1117–1130, 2019.
- [58] Q. Fei, H. Ma, J. Zou et al., “Metformin protects against ischemic myocardial injury by alleviating autophagy-Ros-Nlrp3-mediated inflammatory response in macrophages,” *Journal of Molecular and Cellular Cardiology*, vol. 145, pp. 1–13, 2020.
- [59] I. M. Seropian, S. Toldo, B. W. Van Tassell, and A. Abbate, “Anti-inflammatory strategies for ventricular remodeling following ST-segment elevation acute myocardial infarction,” *Journal of the American College of Cardiology*, vol. 63, no. 16, pp. 1593–1603, 2014.
- [60] S. Toldo, C. Marchetti, A. G. Mauro et al., “Inhibition of the Nlrp3 inflammasome limits the inflammatory injury following myocardial ischemia-reperfusion in the mouse,” *International Journal of Cardiology*, vol. 209, pp. 215–220, 2016.
- [61] O. Sandanger, E. Gao, T. Ranheim et al., “Nlrp3 inflammasome activation during myocardial ischemia reperfusion is cardioprotective,” *Biochemical and Biophysical Research Communications*, vol. 469, no. 4, pp. 1012–1020, 2016.
- [62] S. B. Ong, S. Hernandez-Resendiz, G. E. Crespo-Avilan et al., “Inflammation following acute myocardial infarction: multiple players, dynamic roles, and novel therapeutic opportunities,” *Pharmacology & Therapeutics*, vol. 186, pp. 73–87, 2018.
- [63] L. F. Buckley and A. Abbate, “Interleukin-1 blockade in cardiovascular diseases: a clinical update,” *European Heart Journal*, vol. 39, no. 22, pp. 2063–2069, 2018.
- [64] S. Toldo and A. Abbate, “The Nlrp3 inflammasome in acute myocardial infarction,” *Nature Reviews. Cardiology*, vol. 15, no. 4, pp. 203–214, 2018.
- [65] A. Abbate, S. Toldo, C. Marchetti, J. Kron, B. W. Van Tassell, and C. A. Dinarello, “Interleukin-1 and the inflammasome as therapeutic targets in cardiovascular disease,” *Circulation Research*, vol. 126, no. 9, pp. 1260–1280, 2020.
- [66] J. P. Audia, X. M. Yang, E. S. Crockett et al., “Caspase-1 inhibition by Vx-765 administered at reperfusion in P2y12 receptor antagonist-treated rats provides long-term reduction in myocardial infarct size and preservation of ventricular function,” *Basic Research in Cardiology*, vol. 113, no. 5, p. 32, 2018.
- [67] !!! INVALID CITATION !!!
- [68] S. Adutler-Lieber, T. Ben-Mordechai, N. Naftali-Shani et al., “Human macrophage regulation via interaction with cardiac adipose tissue-derived mesenchymal stromal cells,” *Journal of Cardiovascular Pharmacology and Therapeutics*, vol. 18, no. 1, pp. 78–86, 2012.
- [69] S. Gordon and F. O. Martinez, “Alternative activation of macrophages: mechanism and functions,” *Immunity*, vol. 32, no. 5, pp. 593–604, 2010.
- [70] M. I. Nasser, S. Zhu, H. Huang et al., “Macrophages: first guards in the prevention of cardiovascular diseases,” *Life Sciences*, vol. 250, article 117559, 2020.
- [71] C. A. Gleissner, I. Shaked, K. M. Little, and K. Ley, “Cxc chemokine ligand 4 induces a unique transcriptome in monocyte-derived macrophages,” *Journal of Immunology*, vol. 184, no. 9, pp. 4810–4818, 2010.
- [72] A. Gombozhapova, Y. Rogovskaya, V. Shurupov et al., “Macrophage activation and polarization in post-infarction cardiac remodeling,” *Journal of Biomedical Science*, vol. 24, no. 1, p. 13, 2017.
- [73] J. O. Beitnes, E. Hopp, K. Lunde et al., “Long-term results after intracoronary injection of autologous mononuclear bone marrow cells in acute myocardial infarction: the ASTAMI randomised, controlled study,” *Heart*, vol. 95, no. 24, pp. 1983–1989, 2009.
- [74] A. S. Hasan, L. Luo, C. Yan et al., “Cardiosphere-derived cells facilitate heart repair by modulating M1/M2 macrophage polarization and neutrophil recruitment,” *PLoS One*, vol. 11, no. 10, article e0165255, 2016.
- [75] N. G. Frangogiannis, “The extracellular matrix in ischemic and nonischemic heart failure,” *Circulation Research*, vol. 125, no. 1, pp. 117–146, 2019.
- [76] A. S. Bhatt, A. P. Ambrosy, and E. J. Velazquez, “Adverse remodeling and reverse remodeling after myocardial infarction,” *Current Cardiology Reports*, vol. 19, no. 8, p. 71, 2017.
- [77] P. E. Shamhart and J. G. Meszaros, “Non-fibrillar collagens: key mediators of post-infarction cardiac remodeling?,” *Journal of Molecular and Cellular Cardiology*, vol. 48, no. 3, pp. 530–537, 2010.
- [78] D. J. Luther, C. K. Thodeti, P. E. Shamhart et al., “Absence of type vi collagen paradoxically improves cardiac function, structure, and remodeling after myocardial infarction,” *Circulation Research*, vol. 110, no. 6, pp. 851–856, 2012.
- [79] J. Barallobre-Barreiro, A. Didangelos, F. A. Schoendube et al., “Proteomics analysis of cardiac extracellular matrix remodeling in a porcine model of ischemia/reperfusion injury,” *Circulation*, vol. 125, no. 6, pp. 789–802, 2012.
- [80] N. J. Blackburn, T. Sofrenovic, D. Kuraitis et al., “Timing underpins the benefits associated with injectable collagen biomaterial therapy for the treatment of myocardial infarction,” *Biomaterials*, vol. 39, pp. 182–192, 2015.
- [81] A. Ahmadi, B. McNeill, B. Vulesevic et al., “The role of integrin $\alpha 2$ in cell and matrix therapy that improves perfusion, viability and function of infarcted myocardium,” *Biomaterials*, vol. 35, no. 17, pp. 4749–4758, 2014.
- [82] S. McLaughlin, B. McNeill, J. Podrebarac et al., “Injectable human recombinant collagen matrices limit adverse remodeling and improve cardiac function after myocardial infarction,” *Nature Communications*, vol. 10, no. 1, p. 4866, 2019.
- [83] S. Sciarretta, D. Yee, N. Nagarajan et al., “Trehalose-induced activation of autophagy improves cardiac remodeling after myocardial infarction,” *Journal of the American College of Cardiology*, vol. 71, no. 18, pp. 1999–2010, 2018.

- [84] M. Nakamura and J. Sadoshima, "Mechanisms of physiological and pathological cardiac hypertrophy," *Nature Reviews. Cardiology*, vol. 15, no. 7, pp. 387–407, 2018.
- [85] H. Hashimoto, E. N. Olson, and R. Bassel-Duby, "Therapeutic approaches for cardiac regeneration and repair," *Nature Reviews. Cardiology*, vol. 15, no. 10, pp. 585–600, 2018.
- [86] B. D. Lowes, E. M. Gilbert, W. T. Abraham et al., "Myocardial gene expression in dilated cardiomyopathy treated with beta-blocking agents," *The New England Journal of Medicine*, vol. 346, no. 18, pp. 1357–1365, 2002.
- [87] J. A. Talameh, H. L. McLeod, K. F. Adams Jr., and J. H. Patterson, "Genetic tailoring of pharmacotherapy in heart failure: optimize the old, while we wait for something new," *Journal of Cardiac Failure*, vol. 18, no. 4, pp. 338–349, 2012.
- [88] I. Chimenti, F. Pagano, E. Cavarretta et al., "Beta-blockers treatment of cardiac surgery patients enhances isolation and improves phenotype of cardiosphere-derived cells," *Scientific Reports*, vol. 6, article 36774, 2016.
- [89] F. Pagano, F. Angelini, C. Siciliano et al., "Beta2-adrenergic signaling affects the phenotype of human cardiac progenitor cells through EMT modulation," *Pharmacological Research*, vol. 127, pp. 41–48, 2018.
- [90] H. Xiao, H. Li, J. J. Wang et al., "IL-18 cleavage triggers cardiac inflammation and fibrosis upon β -adrenergic insult," *European Heart Journal*, vol. 39, no. 1, pp. 60–69, 2018.
- [91] W. Zhang, X. Qu, B. Chen et al., "Critical roles of Stat3 in β -adrenergic functions in the heart," *Circulation*, vol. 133, no. 1, pp. 48–61, 2016.
- [92] C. Belge, J. Hammond, E. Dubois-Deruy et al., "Enhanced expression of β 3-adrenoceptors in cardiac myocytes attenuates neurohormone-induced hypertrophic remodeling through nitric oxide synthase," *Circulation*, vol. 129, no. 4, pp. 451–462, 2014.
- [93] S. A. Atlas, "The renin-angiotensin aldosterone system: pathophysiological role and pharmacologic inhibition," *Journal of Managed Care Pharmacy: JMCP*, vol. 13, 8, Supplement B, pp. 9–20, 2007.
- [94] J. Torrado, C. Cain, A. G. Mauro et al., "Sacubitril/valsartan averts adverse post-infarction ventricular remodeling and preserves systolic function in rabbits," *Journal of the American College of Cardiology*, vol. 72, no. 19, pp. 2342–2356, 2018.
- [95] D. M. Reboussin, N. B. Allen, M. E. Griswold et al., "Systematic Review for the 2017 Acc/Aha/Aapa/Abc/Acpm/Ags/Apha/Ash/Aspc/Nma/Pcna Guideline for the Prevention, detection, evaluation, and management of high blood pressure in adults: a report of the American College of Cardiology/American Heart Association Task Force on Clinical Practice Guidelines," *Circulation*, vol. 138, no. 17, pp. e595–e616, 2018.
- [96] J. F. Ainscough, M. J. Drinkhill, A. Sedo et al., "Angiotensin II type-1 receptor activation in the adult heart causes blood pressure-independent hypertrophy and cardiac dysfunction," *Cardiovascular Research*, vol. 81, no. 3, pp. 592–600, 2009.
- [97] Y. Wang, R. Zhou, C. Lu, Q. Chen, T. Xu, and D. Li, "Effects of the angiotensin-receptor neprilysin inhibitor on cardiac reverse remodeling: meta-analysis," *Journal of the American Heart Association*, vol. 8, no. 13, article e012272, 2019.
- [98] T. Sato, A. Kadowaki, T. Suzuki et al., "Loss of apelin augments angiotensin II-Induced cardiac dysfunction and pathological remodeling," *International Journal of Molecular Sciences*, vol. 20, no. 2, 2019.
- [99] S. Ye, W. Luo, Z. A. Khan et al., "Celastrol attenuates angiotensin II-induced cardiac remodeling by targeting Stat3," *Circulation Research*, vol. 126, no. 8, pp. 1007–1023, 2020.
- [100] M. A. Pfeffer, J. J. McMurray, E. J. Velazquez et al., "Valsartan, captopril, or both in myocardial infarction complicated by heart failure, left ventricular dysfunction, or both," *The New England Journal of Medicine*, vol. 349, no. 20, pp. 1893–1906, 2003.
- [101] D. L. Mann, "Inflammatory mediators and the failing heart: past, present, and the foreseeable future," *Circulation Research*, vol. 91, no. 11, pp. 988–998, 2002.
- [102] F. G. Spinale, "Matrix metalloproteinases," *Circulation Research*, vol. 90, no. 5, pp. 520–530, 2002.
- [103] C. Whatling, W. McPheat, and E. Hurt-Camejo, "Matrix management," *Arteriosclerosis, Thrombosis, and Vascular Biology*, vol. 24, no. 1, pp. 10–11, 2004.
- [104] G. V. Halade, Y. F. Jin, and M. L. Lindsey, "Matrix metalloproteinase (MMP)-9: a proximal biomarker for cardiac remodeling and a distal biomarker for inflammation," *Pharmacology & Therapeutics*, vol. 139, no. 1, pp. 32–40, 2013.
- [105] C. Fan, J. Shi, Y. Zhuang et al., "Myocardial-infarction-responsive smart hydrogels targeting matrix metalloproteinase for on-demand growth factor delivery," *Advanced Materials*, vol. 31, no. 40, article e1902900, 2019.
- [106] J. T. Thackeray, H. C. Hupe, Y. Wang et al., "Myocardial inflammation predicts remodeling and neuroinflammation after myocardial infarction," *Journal of the American College of Cardiology*, vol. 71, no. 3, pp. 263–275, 2018.
- [107] I. T. Ramos, M. Henningsson, M. Nezafat et al., "Simultaneous assessment of cardiac inflammation and extracellular matrix remodeling after myocardial infarction," *Circulation: Cardiovascular Imaging*, vol. 11, no. 11, 2018.
- [108] N. G. Frangogiannis, "Targeting the inflammatory response in healing myocardial infarcts," *Current Medicinal Chemistry*, vol. 13, no. 16, pp. 1877–1893, 2006.
- [109] E. A. Liehn, O. Postea, A. Curaj, and N. Marx, "Repair after myocardial infarction, between fantasy and reality: the role of chemokines," *Journal of the American College of Cardiology*, vol. 58, no. 23, pp. 2357–2362, 2011.
- [110] C. A. Dinarello, "Interleukin-1 in the pathogenesis and treatment of inflammatory diseases," *Blood*, vol. 117, no. 14, pp. 3720–3732, 2011.
- [111] S. A. Bageghni, K. E. Hemmings, N. Y. Yuldasheva et al., "Fibroblast-specific deletion of Interleukin-1 Receptor-1 reduces adverse cardiac remodeling following myocardial infarction," *JCI Insight*, vol. 5, 2019.
- [112] L. Kraft, T. Erdenesukh, M. Sauter, C. Tschöpe, and K. Klingel, "Blocking the IL-1 β signalling pathway prevents chronic viral myocarditis and cardiac remodeling," *Basic Research in Cardiology*, vol. 114, no. 2, p. 11, 2019.
- [113] A. V. Finsen, T. Ueland, I. Sjaastad et al., "The homeostatic chemokine Ccl21 predicts mortality in aortic stenosis patients and modulates left ventricular remodeling," *PLoS One*, vol. 9, no. 11, article e112172, 2014.
- [114] L. Yao, K. Huang, D. Huang, J. Wang, H. Guo, and Y. Liao, "Acute myocardial infarction induced increases in plasma tumor necrosis factor- α and interleukin-10 are associated with the activation of poly(ADP-ribose) polymerase of

- circulating mononuclear cell,” *International Journal of Cardiology*, vol. 123, no. 3, pp. 366–368, 2008.
- [115] C. Marchetti, S. Toldo, J. Chojnacki et al., “Pharmacologic inhibition of the NLRP3 inflammasome preserves cardiac function after ischemic and nonischemic injury in the mouse,” *Journal of Cardiovascular Pharmacology*, vol. 66, no. 1, pp. 1–8, 2015.
- [116] D. J. Durgan and M. E. Young, “The cardiomyocyte circadian clock: emerging roles in health and disease,” *Circulation Research*, vol. 106, no. 4, pp. 647–658, 2010.
- [117] N. Khaper, C. D. C. Bailey, N. R. Ghugre et al., “Implications of disturbances in circadian rhythms for cardiovascular health: a new frontier in free radical biology,” *Free Radical Biology & Medicine*, vol. 119, pp. 85–92, 2018.
- [118] J. A. Virag and R. M. Lust, “Circadian influences on myocardial infarction,” *Frontiers in Physiology*, vol. 5, p. 422, 2014.
- [119] A. Dominguez-Rodriguez, M. Garcia-Gonzalez, P. Abreu-Gonzalez, J. Ferrer, and J. C. Kaski, “Relation of nocturnal melatonin levels to C-reactive protein concentration in patients with ST-segment elevation myocardial infarction,” *The American Journal of Cardiology*, vol. 97, no. 1, pp. 10–12, 2006.
- [120] Z. Fu, Y. Jiao, J. Wang et al., “Cardioprotective role of melatonin in acute myocardial infarction,” *Frontiers in Physiology*, vol. 11, p. 366, 2020.
- [121] R. Kumarswamy and T. Thum, “Non-coding RNAs in cardiac remodeling and heart failure,” *Circulation Research*, vol. 113, no. 6, pp. 676–689, 2013.
- [122] J. Li, S. X. Cai, Q. He et al., “Intravenous miR-144 reduces left ventricular remodeling after myocardial infarction,” *Basic Research in Cardiology*, vol. 113, no. 5, p. 36, 2018.
- [123] R. Micheletti, I. Plaisance, B. J. Abraham et al., “The long noncoding RNA Wisper controls cardiac fibrosis and remodeling,” *Science Translational Medicine*, vol. 9, no. 395, 2017.
- [124] H. Zhou, B. Wang, Y. X. Yang et al., “Long noncoding RNAs in pathological cardiac remodeling: a review of the update literature,” *BioMed Research International*, vol. 2019, Article ID 7159592, 11 pages, 2019.
- [125] P. Han, W. Li, C. H. Lin et al., “A long noncoding RNA protects the heart from pathological hypertrophy,” *Nature*, vol. 514, no. 7520, pp. 102–106, 2014.
- [126] J. Moludi, S. Saiedi, B. Ebrahimi, M. Alizadeh, Y. Khajebishak, and S. S. Ghadimi, “Probiotics Supplementation on Cardiac Remodeling Following Myocardial Infarction: A Single-Center Double-Blind Clinical Study,” *Journal of Cardiovascular Translational Research*, 2020.
- [127] A. McMillan and S. L. Hazen, “Gut microbiota involvement in ventricular remodeling post-myocardial infarction,” *Circulation*, vol. 139, no. 5, pp. 660–662, 2019.
- [128] V. Lam, J. Su, S. Kopyrowski et al., “Intestinal microbiota determine severity of myocardial infarction in rats,” *The FASEB Journal*, vol. 26, no. 4, pp. 1727–1735, 2011.
- [129] C. A. Danilo, E. Constantopoulos, L. A. McKee et al., “Bifidobacterium animalis subsp. lactis 420 mitigates the pathological impact of myocardial infarction in the mouse,” *Beneficial Microbes*, vol. 8, no. 2, pp. 257–269, 2017.
- [130] T. W. H. Tang, H. C. Chen, C. Y. Chen et al., “Loss of gut microbiota alters immune system composition and cripples postinfarction cardiac repair,” *Circulation*, vol. 139, no. 5, pp. 647–659, 2019.
- [131] J. Moludi, M. Alizadeh, M. Davari, A. Golmohammadi, and V. Maleki, “The efficacy and safety of probiotics intervention in attenuating cardiac remodeling following myocardial infarction: literature review and study protocol for a randomized, double-blinded, placebo controlled trial,” *Contemporary Clinical Trials Communications*, vol. 15, article 100364, 2019.
- [132] C. P. Cannon, E. Braunwald, C. H. McCabe et al., “Antibiotic treatment of *Chlamydia pneumoniae* after acute coronary syndrome,” *The New England Journal of Medicine*, vol. 352, no. 16, pp. 1646–1654, 2005.
- [133] G. Cerisano, P. Buonamici, R. Valenti et al., “Early short-term doxycycline therapy in patients with acute myocardial infarction and left ventricular dysfunction to prevent the ominous progression to adverse remodelling: the tiptop trial,” *European Heart Journal*, vol. 35, no. 3, pp. 184–191, 2014.
- [134] T. T. Cung, O. Morel, G. Cayla et al., “Cyclosporine before PCI in patients with acute myocardial infarction,” *The New England Journal of Medicine*, vol. 373, no. 11, pp. 1021–1031, 2015.
- [135] C. P. Baines, R. A. Kaiser, N. H. Purcell et al., “Loss of cyclophilin D reveals a critical role for mitochondrial permeability transition in cell death,” *Nature*, vol. 434, no. 7033, pp. 658–662, 2005.
- [136] T. Nakagawa, S. Shimizu, T. Watanabe et al., “Cyclophilin D-dependent mitochondrial permeability transition regulates some necrotic but not apoptotic cell death,” *Nature*, vol. 434, no. 7033, pp. 652–658, 2005.

Research Article

Involvement of the miR-137-3p/CAPN-2 Interaction in Ischemia-Reperfusion-Induced Neuronal Apoptosis through Modulation of p35 Cleavage and Subsequent Caspase-8 Overactivation

He Wang ¹, Qian Yu ², Zai-Li Zhang ¹, Hong Ma ¹ and Xiao-Qian Li ¹

¹Department of Anesthesiology, First Affiliated Hospital, China Medical University, Shenyang, 110001 Liaoning, China

²Department of Thoracic Surgery, Fourth Affiliated Hospital, China Medical University, Shenyang, 110032 Liaoning, China

Correspondence should be addressed to Xiao-Qian Li; shirley037305@hotmail.com

Received 28 May 2020; Revised 20 November 2020; Accepted 26 November 2020; Published 10 December 2020

Academic Editor: Margaret H Hastings

Copyright © 2020 He Wang et al. This is an open access article distributed under the Creative Commons Attribution License, which permits unrestricted use, distribution, and reproduction in any medium, provided the original work is properly cited.

Background. Neuron survival after ischemia-reperfusion (IR) injury is the primary determinant of motor function prognosis. MicroRNA- (miR-) based gene therapy has gained attention recently. Our previous work explored the mechanisms by which miR-137-3p modulates neuronal apoptosis in both *in vivo* and *in vitro* IR models. **Methods.** IR-induced motor dysfunction and spinal calpain (CAPN) subtype expression and subcellular localization were detected within 12 h post IR. Dysregulated miRs, including miR-137-3p, were identified by miR microarray analysis and confirmed by PCR. A luciferase assay confirmed CAPN-2 as a corresponding target of miR-137-3p, and their modulation of motor function was evaluated by intrathecal injection with synthetic miRs. CAPN-2 activity was measured by the intracellular Ca^{2+} concentration and mean fluorescence intensity *in vitro*. Neuronal apoptosis was detected by flow cytometry and TUNEL assay. The activities of p35, p25, Cdk5, and caspase-8 were evaluated by ELISA and Western blot after transfection with specific inhibitors and miRs. **Results.** The IR-induced motor dysfunction time course was closely associated with upregulated expression of the CAPN-2 protein, which was mainly localized in neurons. The miR-137-3p/CAPN-2 interaction was confirmed by luciferase assay. The miR-137-3p mimic significantly improved IR-induced motor dysfunction and decreased CAPN-2 expression, even in combination with recombinant rat calpain-2 (rr-CALP2) injection, whereas the miR-137-3p inhibitor reversed these effects. Similar changes in the intracellular Ca^{2+} concentration, CAPN-2 expression, and CAPN-2 activity were observed when cells were exposed to oxygen-glucose deprivation and reperfusion (OGD/R) and transfected with synthetic miRs *in vitro*. Moreover, double fluorescence revealed identical neuronal localization of CAPN-2, p35, p25, and caspase-8. The decrease in CAPN-2 expression and activity was accompanied by the opposite changes in p35 activity and protein expression in cells transfected with the miR-137-3p mimic, roscovitine (a Cdk5 inhibitor), or Z-IETD-FMK (a caspase-8 inhibitor). Correspondingly, the abovementioned treatments resulted in a higher neuron survival rate than that of untreated neurons, as indicated by decreases in the apoptotic cell percentage and p25, Cdk5, caspase-8, and caspase-3 protein expression. **Conclusions.** The miR-137-3p/CAPN-2 interaction modulates neuronal apoptosis during IR injury, possibly by inhibiting CAPN-2, which leads to p35 cleavage and inhibition of subsequent p25/Cdk5 and caspase-8 overactivation.

1. Introduction

Spinal cord ischemia-reperfusion (IR) injury occurs during operations that require a transient block of blood flow to the spinal cord [1, 2]. Usually, reperfusion cannot prevent ischemia-induced neurological impairment (known as primary insults), but it will further aggravate neurological function (known as secondary insults) during the initial period

[3]. Apart from the high incidence of sensory deficits, IR injury is reported as a major cause of permanent motor dysfunction due to extensive neuronal death after recovery of blood flow [4–6]. Due to the limited proliferative capacity of adult neurons, exploration of the underlying mechanisms is of particular importance to prevent neuronal death [7]. Various types of neuronal death have been reported, including apoptosis, necroptosis, and ferroptosis [5, 7, 8]. We

previously identified which types of cell death are involved in a specific type of spinal cord IR injury and found that blocking apoptosis effectively preserved hind-limb motor function in rodent models [5, 9]. Some recent studies have shown that phenomena disturbing ionic homeostasis, such as excessive intracellular calcium ion concentrations ($[Ca^{2+}]$) in neurons induced by ischemic or mechanical injury, could eventually trigger neuronal apoptosis by influencing vital biological functions and metabolism [10–12]. Thus, preserving intracellular calcium homeostasis may represent a promising strategy for attenuating neuronal apoptosis after IR insult.

Increased intracellular Ca^{2+} levels can activate a variety of proteases [13]. Belonging to a family of calcium-dependent neutral proteases, calcium-activated neutral proteinases (CAPNs, also called calpains) are the most well-known effectors that react to intracellular Ca^{2+} dysregulation through calcium-binding subunits [14, 15]. Eleven types of calpain isoforms have been identified in humans thus far, of which calpain-1 (μ -calpain (CAPN-1)) and calpain-2 (m-calpain (CAPN-2)) are the most widely ubiquitous isoforms in the central nervous system (CNS) [13]. Exhibiting the same subcellular localization (cytoplasm) and sharing a common small subunit (known as CAPN-4), CAPN-1 and CAPN-2 appear to have similar biochemical properties [13, 16], although they require micromolar and millimolar calcium levels for activation, respectively [13–16]. However, in contrast to traditional views, some studies have recently suggested that CAPN-1 activation plays a prosurvival role while CAPN-2 plays neurodegenerative roles based on their opposite functions in regulating neuronal plasticity following CNS injury [17–19]. Commonly, the proteolytic cleavage products of CAPN-mediated truncation substrates are bioactive [13, 20, 21]. For example, the membrane-bound protein p35 has been demonstrated to be a major substrate exclusively regulated by CAPNs and can further amplify neurotoxic insults or oxidative stress by activating cyclin-dependent kinase-5 (Cdk5) in the pathogenesis of neurodegenerative disease [13, 19, 20]. *In vivo* (rodent) and *in vitro* experiments revealed that overexpressed CAPN-2 precisely cleaved the normally membrane-bound p35 into the more stable p25 form, which finally led to inappropriate increases in p25/Cdk5 activation and protein levels of caspase-3, a final executioner of neuronal apoptosis [19, 22, 23]. Previous structural experiments further identified the N terminus of p35 as the major element necessary to preserve the intact covalent bond within the p35-caspase-8 crystal structure [25]. Consistently, the p35 protein from baculovirus effectively blocked the apoptosis cascade by forming a p35-caspase-8 complex via a thioester bond [24, 25]. Thus, in addition to modulating caspase-3, the final executioner of apoptosis, p35 might mediate the activation of all caspases by regulating caspase-8 proteolysis [26, 27]. Based on this evidence, it is reasonable to infer that increased CAPN-2-mediated p35 cleavage may lead to conformational changes in p35 and subsequently initiate caspase-8 and downstream caspase activation during IR injury.

MicroRNAs (miRs) are a group of small, endogenous, noncoding RNAs [28] that are widely expressed in the CNS and are able to negatively regulate target genes by either deg-

radation or posttranscriptional repression [5, 6, 28]. In our previous studies, we identified hundreds of aberrant miRs in injured spinal cords by microarray analysis [5, 6, 29]. Intrathecal pretreatment with a synthetic miR mimic significantly improved neurological deficits by recovering the altered miR expression [5, 6, 29]. These findings suggest promising miR-based gene therapy targeting CAPN-2. In this context, we first searched bioinformatical databases and identified potential miRs that may bind CAPN-2 among all dysregulated miRs detected by microarray analysis. Our present study results suggested that miR-137-3p and miR-124-3p have target interactions with CAPN-2, which is supported by another study that explored the roles of miR-137-3p in rescuing motor neuron degeneration after brachial plexus root avulsion injury [30]. Then, we studied the functions and mechanisms by which the miR-137-3p/CAPN-2 interaction regulates neuronal apoptosis by pretreatment of *in vivo* and *in vitro* models with synthetic miRs, a selective CAPN-2 inhibitor, recombinant rat calpain-2 (rr-CALP2), or a specific caspase-8 inhibitor.

2. Materials and Methods

2.1. Experimental Animals. Sprague-Dawley rats weighing 200 to 250 g were obtained from the Animal Center of China Medical University (Shenyang, China). All rats were preacclimatized 7 days before surgery and housed in standard cages under a 12 h light/dark cycle with a temperature of 23–24°C and humidity of 40–50%. The experiments were performed in accordance with the Guide for the Care and Use of Laboratory Animals (United States National Institutes of Health publication number 85-23, National Academy Press, Washington DC, revised 1996).

2.2. Rat IR Model Establishment and Experimental Groups. The rat IR model was established by occluding the aortic arch for 14 min [4, 29]. Briefly, after being anesthetized, the rats were catheterized at the left carotid artery and the tail artery to measure proximal and distal blood pressure (BP), respectively. Following exposure of the aortic arch, the clamp was placed between the left common carotid artery and the left subclavian artery for 14 min to induce ischemia, which was confirmed as a 90% decrease in distal BP. Then, the clamp was removed to induce reperfusion for 12 h. The sham-operated rats were subjected to the same procedures except for the induction of ischemia.

2.3. miR Microarray Analysis. As we previously reported, rat miRNA microarray analysis was performed with the miRCURY™ LNA Array (version 11.0; Exiqon, Vedbaek, Denmark) [29, 31]. The L_{4–6} segments of the spinal cord were collected at 4 h after reperfusion. According to the manufacturer's instructions, 2.5 μ g of total RNA was first labeled with the miRCURY™ Hy3™/Hy5™ Power labeling kit and then hybridized on a miRCURY™ LNA Array (version 18.0; Exiqon, Vedbaek, Denmark).

After removing nonspecifically bound proteins, the microarray slides were scanned by an Axon GenePix 4000B Microarray Scanner (Axon Instruments, CA, USA) for

fluorescence detection, and the fluorescence intensities of the scanned images were loaded into the GenePix Pro 6.0 program (Axon Instruments) for feature extraction. The averages of the replicated miRs with intensities of 50 or more were used to calculate a normalization factor. After normalization by the median normalization method, the significantly different miRs were identified by volcano plot filtering. Finally, hierarchical clustering was performed to determine the differences in miR expression by MEV software (version 4.6, TIGR).

2.4. Intrathecal Injection and Drug Delivery. All treatments *in vivo*, including synthetic miRs (Dharmacon, Chicago, IL, USA) and recombinant rat calpain-2 (rr-CALP2, B71107, 150 U/L, Calbiochem, China), were diluted to 20 μ L in total volume and intrathecally injected, as we previously described [5, 6]. Briefly, the needle of a 25 μ m microsyringe was inserted into the L₅₋₆ spinal cord segment by the sign of a tail flick. Then, 100 μ mol/L miR-137-3p mimic, 125 μ mol/L miR-137-3p inhibitor, or 100 μ mol/L negative control (NC) was coadministered with Lipofectamine 3000 (Invitrogen, USA) at 24 h intervals for five consecutive days before surgery. Likewise, rr-CALP was dissolved to a final concentration of 75 U/L immediately before injection. The overall effects of the number of treatment days and the dosage used in this study were evaluated by PCR and Western blotting in preliminary experiments. Only the rats that displayed normal motor function were included for further study.

2.5. Motor Function Assessment. After being fully preacclimated to the testing environment, the hind-limb motor functions were scored by the Tarlov system by two observers who were double-blinded to the method [5].

2.6. Luciferase Reporter Assay. The target interaction between miR-137-3p and CAPN-2 was verified by a luciferase reporter assay [5]. Briefly, 293T cells were seeded in a 96-well plate at 4×10^4 cells/well and then cotransfected with 100 nM miR-137-3p mimic or 100 nM NC and 180 ng of a luciferase reporter vector containing the wild-type (WT) 3' untranslated region (3'-UTR) (5'-ACATCGTCTCTCAT-AGCAATAT-3') or mutant (MT) 3'-UTR (5'-ACATCGTCTCTCATCAUGGCAT-3') using Lipofectamine 3000. At 48 h after transfection, the relative activity was determined with a Dual-Luciferase Reporter Assay Kit (Promega Corp., WI, USA).

2.7. Oxygen-Glucose Deprivation and Reperfusion (OGD/R) Model. As we previously described, the OGD/R model was established in 70–80% confluent VSC4.1 neurons to mimic IR insult *in vivo* [5]. After two washes and replacement of the medium with glucose-free Hank's balanced salt solution (HBSS), the neurons were kept in an anaerobic chamber (95% N₂ and 5% CO₂) at 37°C for 6 h. Then, the initial medium and air conditions were reapplied for another 18 h to induce reoxygenation. The control neurons were cultured in normal and atmosphere conditions for 24 h without deprivation of oxygen or glucose.

2.8. VSC4.1 Motor Neuron Culture and Treatments. VSC4.1 motor neurons were purchased from Huatuo Biotechnology Co., Ltd. (Shanghai, China). According to the manufacturer's instructions, the cells were grown in 75 cm² flasks containing 6 mL of culture medium (89% Eagle's minimum essential medium (EMEM) supplemented with 10% fetal bovine serum (FBS) and 1% penicillin/streptomycin) at 37°C with 5% CO₂ in humidified air. The culture medium was replaced twice weekly.

For the *in vitro* experiment, the neurons were pretreated with synthetic miR and specific inhibitors 24 h before OGD/R insult [5]. As we previously described, after seeding at a concentration of 4×10^5 cells per well, the miR-137-3p mimic (50 nmol/L) or NC (50 nmol/L) was cotransfected with 5 μ L of Lipofectamine 3000; for the inhibitor experiments, roscovitine (10 μ M, Cdk5 inhibitor, Sigma-Aldrich Co., China) or Z-IETD-FMK (50 μ M, caspase-8 inhibitor, R&D Systems, United States) was added to the culture medium alone. The concentration of each treatment agent and the *in vitro* effects were determined by PCR in preliminary experiments.

2.9. Detection of CAPN-2 Activity. The tensin homolog (PTEN), a selective CAPN-2 substrate, is degraded by CAPN-2 activation and is widely used for the quantitative analysis of neuronal CAPN-2 activity *in vivo* and *in vitro* [19, 32]. As previously described, CAPN-2 enzymatic activity was assessed by the fold change in the mean fluorescence intensity (MFI) of PTEN (Santa Cruz Biotechnology, CA, USA). The increase in CAPN-2 activity was defined as the MFI in the treated group subtracted from that in the control group. Total CAPN-2 activity was defined as the sum of the MFI in the treated and control groups.

2.10. Detection of Cytosolic [Ca²⁺]. The intracellular [Ca²⁺] in VSC4.1 neurons was measured with the Ca²⁺-sensitive indicator Fura-2/acetoxymethyl ester (AM) (Molecular Probes, CA, USA) [14]. After each treatment, the neurons were loaded with 5 μ M Fura-2-AM for 30 min at 37°C in the dark. After dilution to 1×10^6 cells/mL with the same Ca²⁺ buffer solution, Fura-2-AM was excited at wavelengths of 340 and 380 nm. The relative changes in intracellular [Ca²⁺] were determined by the fluorescence ratio (*R*) at 340/380 with the following formula: $[Ca^{2+}] = Kd \times \beta \times (R - R_{min}) / (R_{max} - R)$ [14]. The Calcium Calibration Buffer Kit with Magnesium (Molecular Probes, CA, USA) was used to determine that the *Kd*, a cell-specific constant, for VSC4.1 neurons was 0.264 μ M.

2.11. TUNEL Assay. To determine apoptosis in VSC4.1 neurons following OGD/R injury, a TUNEL assay was performed with the Apoptosis Detection Kit (Boster, Wuhan, China). The assay was carried out completely according to the manufacturer's protocol. TUNEL was visualized with DAB staining. The apoptotic neurons were those with either tightly clustered brown staining or more diffuse brown TUNEL staining confined within the cell. With the microscope under a 20x objective, at least 1000 neurons from six

random fields in each group were chosen to quantify the total of the TUNEL-positive cells.

2.12. Detection of Caspase-8 Activity. Caspase-8 activity was detected by a caspase-8 assay kit (Abcam, CA, USA), which is based on the spectrophotometric detection of the p-nitroaniline (pNA) moiety after it is cleaved from the labeled substrate Ac-IETD by caspase-8. The samples were measured in triplicate at an absorbance of 405 nm.

2.13. Detection of p25/Cdk5 and p35/Cdk5 Activities by ELISA. Commercialized ELISA kits (Runyu Biological Technology Co., Shanghai, China) were used to measure p25/Cdk5 and p35/Cdk5 activities in VSC4.1 neurons. According to the manufacturer's instructions, the activities in supernatants after each treatment were measured at 450 nm. Each sample was analyzed in triplicate, and the average is presented as ng/L.

2.14. Detection of Neuronal Apoptosis by Flow Cytometry. Apoptotic neurons were detected by a BD FACSCalibur flow cytometer (BD Biosciences, MA, USA) at excitation and emission wavelengths of 488 nm and 530 nm, respectively [5]. Briefly, 1×10^5 neurons were first stained with 10 μ L of Annexin V-fluorescein isothiocyanate (FITC) at 37°C for 15 min and then counterstained with 5 μ L of propidium iodide (PI) for 30 min in the dark. The fluorescence was excited at 488 nm and emitted at 530 nm. Each sample was prepared in triplicate.

2.15. Quantitative RT-PCR. Total RNA was extracted from L₄₋₆ segments of spinal cords or VSC4.1 neurons by the TRIzol/chloroform method or the miRNeasy FFPE kit (Qiagen, Hilden, Germany) [5]. RNA (500 ng) was reverse transcribed into cDNA by using cDNA SuperMix (TaKaRa, China) or a MicroRNA Reverse Transcription Kit (Applied Biosystems, USA). The levels of miR-137-3p and CAPN-2 were quantified with a TaqMan MicroRNA Assay Kit or a Power SYBR Green PCR Master Mix (TaKaRa, China) on an Applied Biosystems 7500 RT-PCR system (Applied Biosystems, CA, USA). β -Actin or U6 was used as an internal control, and each sample was measured in triplicate by the $2^{-\Delta\Delta CT}$ method. The primers used in this study were as follows: miR-137-3p (forward: 5'-ACACTCATTATTGCTTA-3'; reverse: 5'-CTACGCGTATTGAGAGTAC-3'); CAPN-1 (forward: 5'-CTCCGGGGCAGGAGTAGGCA-3'; reverse: 5'-CTCCGGGGCAGGAGTAGGCA-3'); CAPN-2 (forward: 5'-CTCCGGGGCAGGAGTAGGCA-3'; reverse: 5'-AACTGGCTGTGGGGCTCCCA-3'); U6 (forward: 5'-CTCGCTTCGGCAGCACA-3'; reverse: 5'-AACGCTTCCGAATTTGCGT-3'); and β -actin (forward: 5'-GGAGAT TACTGCCCTGGCTCCTA-3'; reverse: 5'-GACTCATCG TACTCCTGCTTGCTG-3').

2.16. Double Immunofluorescence (IF). As previously described [4, 5], for *in vivo* samples, the 20 μ m thick spinal cord sections were blocked with 10% bovine serum albumin (BSA) for 1 h and then incubated with the primary mouse anti-calpain-2 antibody (Santa Cruz Biotechnology, sc-

373967, 1:300, Dallas, USA) and the antibodies specific for neurons (rabbit anti-NeuN, Abcam, ab177487, 1:500), astrocytes (rabbit anti-glial fibrillary acidic protein (GFAP), Abcam, ab7260, 1:500), and microglial cells (rabbit anti-Iba-1, Abcam, ab178847, 1:400) overnight at 4°C. Then, the sections were incubated with Alexa 594-conjugated donkey anti-mouse IgG (1:500, Life Technologies, CA, USA) and Alexa 488-conjugated donkey anti-rabbit IgG (1:500, Life Technologies, CA, USA) for 2 h at room temperature.

For *in vitro* samples, after being fixed with 4% formaldehyde for 20 min at 4°C, the neurons were permeabilized with 0.1% Triton X-100 for 10 min and blocked with 3% donkey serum for 1 h at room temperature. Then, the neurons were incubated with a primary rabbit anti-p35 antibody (Abcam, ab64960, 1:300, CA, USA), primary rabbit anti-TPPP/p25 antibody (Abcam, ab92305, 1:300, CA, USA), mouse anti-calpain-2 antibody, or mouse anti-caspase-8 p18 antibody (Santa Cruz Biotechnology, sc-393776, 1:400, Dallas, USA) overnight at 4°C and then with Alexa-conjugated secondary antibodies (1:500, Life Technologies, CA, USA) for 1 h at room temperature in the dark. For cell counting, the nuclei were counterstained with 4,6-diamidino-2-phenylindole (DAPI, Beyotime Biotechnology, China) for 10 min at room temperature. The images were captured with a Leica TCS SP2 fluorescence microscope (Leica Microsystems, IL, USA), and the integrated fluorescence densities were measured with Leica IM50 software (Nussloch, Germany).

2.17. Western Blotting. The total proteins from L₄₋₆ spinal cords or VSC4.1 neurons were extracted and purified with a protein extraction kit (KangChen, China) [4, 6]. After determination by a BCA protein assay kit (Beyotime Biotechnology, China), equal protein concentrations were loaded onto a 10% SDS-PAGE gel and transferred to PVDF membranes. The membranes were incubated with 5% skim milk for 1 h to avoid nonspecific binding and probed with an anti-calpain-1 antibody (Santa Cruz Biotechnology, sc-271313, 1:400, Dallas, USA), anti-calpain-2 antibody (1:500), anti-p35 (1:400), anti-TPPP/p25 antibody (1:500), anti-PTEN antibody (Santa Cruz Biotechnology, sc-7974, 1:400, Dallas, USA), anti-Cdk5 antibody (Santa Cruz Biotechnology, sc-6247, 1:300, Dallas, USA), anti-caspase-8 p18 antibody, anti-caspase-3 antibody (Abcam, ab184787, 1:500, CA, USA), or β -actin (Santa Cruz Biotechnology, sc-47778, 1:2000, Dallas, USA) overnight at 4°C. After washing, the membranes were incubated with peroxidase-conjugated secondary antibodies (Beyotime Biotechnology, A0192, 1:10,000, China) for 2 h at room temperature. The blots were detected by an ECL kit (Beyotime Biotechnology, China) and quantified by Quantity One software (Bio-Rad Laboratories, Italy).

2.18. Statistical Analysis. The data are expressed as the mean \pm standard deviation (SD) and were analyzed using SPSS 19.0 software (SPSS, Chicago, USA). Statistical comparisons between two groups were assessed by *t*-tests or the Mann-Whitney tests, whereas comparisons among three or more groups were determined by one- or two-way ANOVA

followed by the Tukey-Kramer test. A P value < 0.05 was considered statistically significant.

3. Results

3.1. Temporal Changes in Motor Dysfunction and Spinal CAPN Subtype Expression Post IR. All rats exhibited normal motor function before undergoing IR surgery. As shown in Figure 1(a), compared with sham-operated rats, the rats in the IR groups displayed obvious hind-limb motor dysfunction, indicated by significant decreases in the average Tarlov score throughout the reperfusion period ($P < 0.05$). Likewise, the protein levels of spinal CAPN-1 and CAPN-2 were measured at 4 h intervals. In contrast to the decrease in CAPN-1 protein expression over time, CAPN-2 protein expression increased unimodally, peaking at 4 h post surgery (Figures 1(b) and 1(c), $P < 0.05$). Notably, there were no significant differences in CAPN-1 protein expression among the IR groups ($P > 0.05$). Thus, the specific cellular localization of CAPN-2 in injured spinal cords was further identified by double immunofluorescence at the time point with the highest CAPN-2 expression. Colocalization was indicated by a yellow fluorescent signal, revealing that the majority of CAPN-2 fluorescent signals overlapped with neurons, not astrocytes or microglia, at 4 h post surgery (Figure 1(d)). Similarly, the quantification of the number of CAPN-2- and NeuN-double-positive cells confirmed that the IR insult-induced increase in CAPN-2 expression was primarily localized in neurons (Figures 1(e) and 1(f), $P < 0.05$).

3.2. IR Altered Spinal miR-137-3p Expression and Negatively Regulated CAPN-2 Expression In Vivo. Microarray analysis showed that several aberrant miRs were substantially dysregulated in injured spinal cords at 4 h post IR (Figure 2(a)). Among these miRs, miR-137-3p has been indicated to be closely associated with neurodevelopment and CNS diseases and to be highly expressed in the brain [30, 33]. Thus, we hypothesized that miR-137-3p was also widely expressed in spinal cord tissues and confirmed that it showed abnormally decreased expression at 4 h post IR by RT-PCR (Figure 2(b), $P < 0.05$). Moreover, analysis with TargetScan (Release 7.2, http://www.targetscan.org/vert_72/) showed that the miR-137-3p binding site has 7 base pairs that matched the 3'-UTR of the CAPN-2 mRNA. This negative target interaction was further confirmed by a luciferase reporter assay, in which the miR-137-3p mimic significantly decreased the luciferase activity in cells containing the WT 3'-UTR but not the MT 3'-UTR (Figure 2(c), $P < 0.05$), and there were no obvious changes in the luciferase activities of the WT and MT 3'-UTRs of the reporter vector upon cotransfection with the miR-137-3p NC ($P > 0.05$). As we previously reported, the potential *in vivo* interactions were assessed by intrathecal pretreatment with synthetic miRs [5, 6]. Consistently, compared with the IR group, the group intrathecally administered with the miR-137-3p mimic had significantly lower CAPN-2 protein and mRNA expression levels, whereas the group pretreated with miR-137-3p inhibitor injection had significantly higher CAPN-2 expression (Figures 2(d) and 2(e), $P < 0.05$). As expected, the synergistic

upregulation in CAPN-2 expression post IR that occurred after injection of rr-CALP2, a recombinant CAPN-2 that specifically upregulates CAPN-2 expression, was partially reversed by miR-137-3p mimic injection ($P < 0.05$). No significant changes were detected after injection of the miR-137-3p NC, which had no significant effects on IR-induced CAPN-2 expression ($P > 0.05$).

3.3. Effects of the miR-137-3p/CAPN-2 Interaction on IR-Induced Hind-Limb Motor Dysfunction. To further clarify the regulatory roles of the miR-137-3p/CAPN-2 interaction *in vivo*, hind-limb motor function was assessed (Figure 2(f)). As expected, compared with baseline and sham-operated rats, all IR-injured rats showed obvious hind-limb motor dysfunction during the reperfusion period ($P < 0.05$). Compared with the time-matched injured rats in the IR group, the rats injected with the miR-137-3p mimic exhibited higher average Tarlov's scores, whereas those injected with the miR-137-3p inhibitor showed lower Tarlov's scores ($P < 0.05$). Likewise, in conjunction with the mRNA and protein levels of CAPN-2, rr-CALP2 injection reversed the improvement in motor function, indicated by the comparable Tarlov scores in the IR groups at all observed timepoints ($P > 0.05$). There were no detectable differences between the IR-injured rats treated with or without miR-137-3p NC at any of the observed time points ($P > 0.05$).

3.4. Modulation of CAPN-2 Expression and Activity by miR-137-3p in VSC4.1 Neurons after OGD/R. Given that increased intracellular Ca^{2+} levels can activate CAPN-2 [13], we measured the free intracellular $[Ca^{2+}]$ in each treatment group at 24 h post OGD/R. As expected, compared to control cells, VSC4.1 neurons exposed to OGD/R for 24 h exhibited significantly increased intracellular free $[Ca^{2+}]$ (Figure 3(a), $P < 0.05$). In addition, miR-137 mimic pretreatment effectively prevented the OGD/R-induced $[Ca^{2+}]$ increase, whereas the miR-137 inhibitor aggravated the $[Ca^{2+}]$ increase ($P < 0.05$). No differences were detected between cells treated with or without miR-137 NC ($P > 0.05$).

Because PTEN is a selective substrate for CAPN-2 [32], the OGD/R-induced changes in CAPN-2 expression and activity were further confirmed by assessment of PTEN at the same observed time points. As shown by representative images of double fluorescent staining, both PTEN and p35 fluorescent labels were predominantly localized in the cytoplasm and nuclei of VSC4.1 neurons (Figure 3(b)). Consistent with previous studies [19, 32], the mean PTEN and CAPN-2 immunoreactivities exhibited opposite changes in all treatment groups, confirming that the net and total CAPN-2 activities were changed in accordance with the intracellular $[Ca^{2+}]$ (Figures 3(c) and 3(d), $P < 0.05$). Similar to the Western blot results *in vivo* and fluorescence quantification shown in Figure 3(c), the CAPN-2 protein levels were significantly decreased by miR-137 mimic treatment but increased by miR-137 inhibitor treatment (Figure 3(e), $P < 0.05$). Conversely, PTEN protein levels were increased in miR-137 mimic-transfected cells and decreased in miR-137 inhibitor-transfected cells ($P < 0.05$). No such changes were detected upon pretreatment with miR-137 NC ($P > 0.05$).

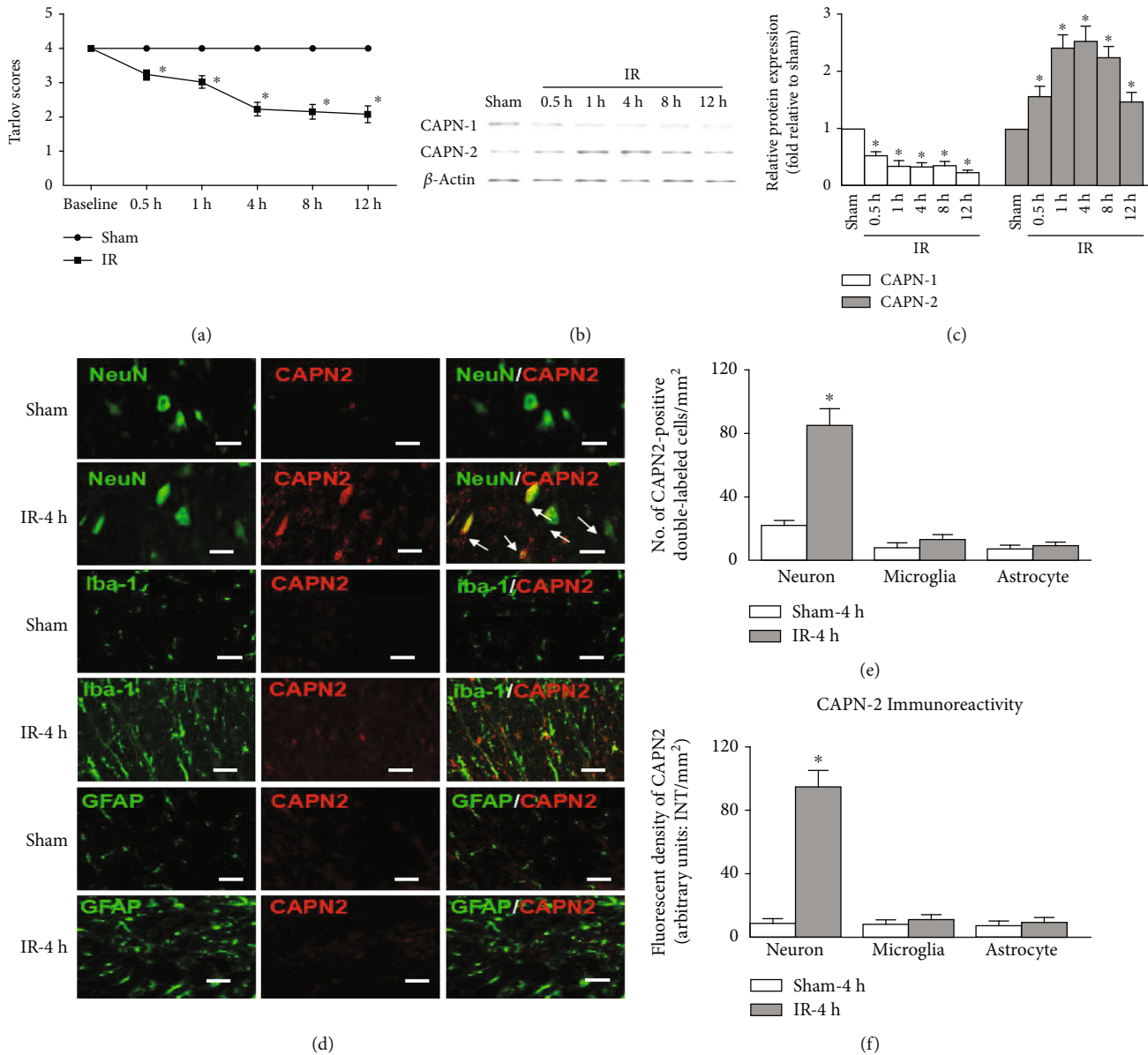


FIGURE 1: Temporal changes in motor dysfunction and spinal CAPN subtype expression post IR. (a) Temporal changes in hind-limb motor function were evaluated using Tarlov's scores at 0.5, 1, 4, 8, and 12 h after IR. $n = 6$ per group. (b) Representative Western blots of CAPN-1 and CAPN-2 in injured spinal cord samples after IR. (c) Protein quantification of CAPN-1 and CAPN-2 levels after IR. The relative protein levels were normalized to those in the sham group. The data are expressed as the mean \pm standard deviation (SD). $n = 6$ per group. * $P < 0.05$ versus the sham group. (d) Representative double immunofluorescence staining of CAPN-2 with spinal neurons (NeuN), microglia (Iba-1), and astrocytes (glial fibrillary acidic protein (GFAP)) in the anterior horns of spinal cords at 4 h after IR. The yellow labels with white arrows indicate colocalization. Scale bars = 50 μ m. $n = 6$ per group. (e, f) Quantification of cells double-labeled with CAPN-2 immunoreactivity and markers of specific cell types. The data are presented as the average of three independent images of laminae II and III in the gray matter and expressed as the mean \pm SD. * $P < 0.05$ versus the sham group.

3.5. Modulation of p35 Cleavage and p25/Cdk5 Activation by the miR-137-3p/CAPN-2 Interaction after OGD/IR. Then, we tested whether p35 cleavage and subsequent p25/Cdk5 activation were regulated by the miR-137-3p/CAPN-2 interaction in VSC4.1 neurons by double immunofluorescence staining and Western blot, as previously published [5, 19]. As shown in Figure 4(a), representative fluorescence images showed CAPN-2, p35, and p25, and all were predominantly localized in the cytoplasm and nuclei of VSC4.1 neurons.

OGD/R injury induced significant increases in CAPN-2 and p25 immunoreactivity but decreased p35 immunoreactivity in neurons at 24 h post injury, consistent with the Western blot results shown in Figures 4(d) and 4(e) ($P < 0.05$). Furthermore, the ELISA and Western blot results showed that, in contrast to the decrease in CAPN-2 expression caused by mimic transfection, transfection with the miR-137-3p mimic significantly reversed the OGD/R-induced decrease in p35 activity and protein expression (Figures 4(b)–4(e), $P < 0.05$), whereas

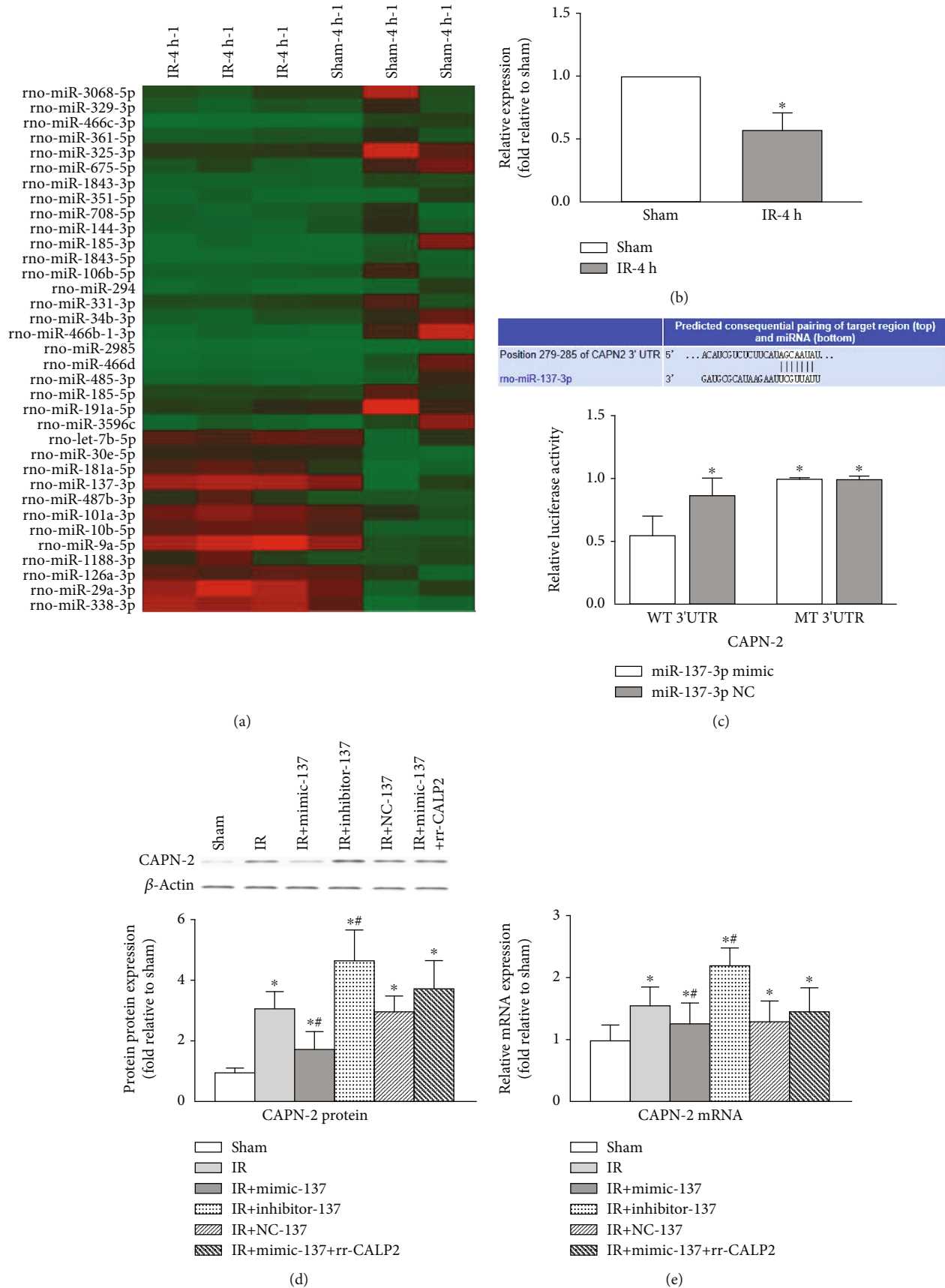


FIGURE 2: Continued.

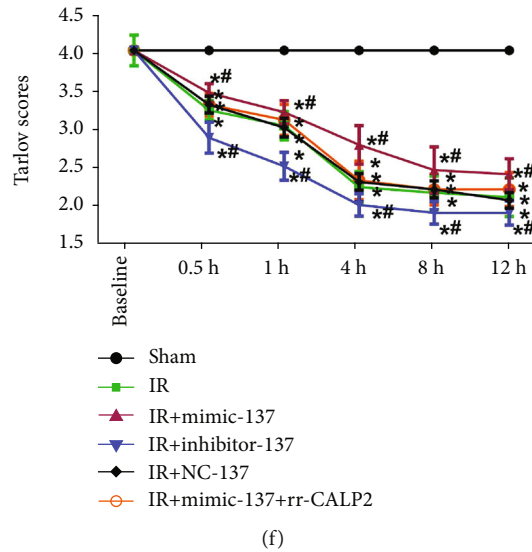


FIGURE 2: IR induced aberrant spinal miR-137-3p expression and negatively regulated CAPN-2 expression *in vivo*. (a) A heat map representation of miRs differentially expressed in spinal cord samples at 4 h post IR. Three independent replicates were performed. The red signals indicate the upregulated miRs, and the green signals indicate the downregulated miRs. (b) Quantification of miR-137-3p expression post IR. $n = 4$ per group. The data are expressed as the mean \pm SD. $*P < 0.05$ versus the sham group. (c) The putative target binding site of miR-137-3p in the rat 3'-UTR of CAPN-2 was predicted by the TargetScan database and confirmed by a luciferase reporter assay. $*P < 0.05$ versus the WT 3'-UTR cells transfected with the miR-137-3p mimic. (d) Representative Western blots and protein quantification of CAPN-2 in the spinal cord after different treatments. β -Actin was used as a loading control. (e) Quantification of CAPN-2 mRNA expression after different treatments. (f) Hind-limb motor function was assessed by Tarlov's scores after different treatments. $*P < 0.05$ versus the sham group; $^{\#}P < 0.05$ versus the IR group.

no differences were detected in the presence of miR-137 NC ($P > 0.05$). As expected, following p35 cleavage, the activity and protein expression profiles of p25 and Cdk5 were changed in parallel to the CAPN-2 protein level detected in each treated group ($P < 0.05$).

Additionally, transfection with roscovitine, a specific Cdk5 inhibitor, regulated p35, p25, and Cdk5 protein levels and activity in a manner similar to that of miR-137-3p mimic transfection, just as roscovitine and the mimic had comparable effects on CAPN-2 expression (Figures 4(b)–4(e), $P > 0.05$).

3.6. Modulation of Caspase-8 Activation by the miR-137-3p/CAPN-2 Interaction after OGD/R. Likewise, we also assessed the regulatory effects of the miR-137-3p/CAPN-2 interaction on the caspase-8-mediated apoptotic network. As shown in representative fluorescent images, p35 and caspase-8 were identically localized in the cytoplasm of VSC4.1 neurons. OGD/R injury induced opposite changes in p35 and caspase-8, as it decreased the immunoreactivity and protein expression of p35 but increase the immunoreactivity and protein expression of caspase-8 at 24 h post injury (Figures 5(a), 5(c), and 5(d), $P < 0.05$). In contrast to the effects of mimic transfection on p35 expression, miR-137-3p mimic transfection significantly decreased the caspase-8 activity and protein levels (Figures 5(b)–5(d), $P < 0.05$), whereas miR-137 NC had no effect ($P > 0.05$). However, compared with that of the miR-137-3p mimic, transfection with Z-IETD-FMK, a specific caspase-8 inhibitor, had greater inhibitory effects on caspase-8 activity and protein levels at 24 h post transfection (Figures 5(b)–5(d), $P < 0.05$).

Additionally, the protein expression of caspase-3, the final executor of the apoptotic network, was measured in each treatment group at the same time point. The Western blot results showed that the change in caspase-3 protein expression was in accordance with that in caspase-8 protein expression (Figures 5(c) and 5(d)).

3.7. Modulation of VSC4.1 Neuronal Apoptosis by the miR-137-3p/CAPN-2 Interaction after OGD/R. Finally, the effects of the miR-137-3p/CAPN-2 interaction on neuronal apoptosis were assessed by flow cytometry *in vitro*. Consistent with the assessment of motor function *in vivo*, OGD/R insult obviously increased the percentage of apoptotic neurons (A2 + A4 quadrant) at 24 h after reperfusion (Figures 6(a) and 6(b), $P < 0.05$). Treatment with the miR-137-3p mimic, roscovitine, or Z-IETD-FMK had comparable and significant inhibitory effects on OGD/R-induced neuronal apoptosis ($P < 0.05$), whereas treatment with miR-137 NC had no such inhibitory effects ($P > 0.05$).

In addition, a TUNEL assay was performed to further validate and visualize the neuronal apoptosis. Consistent with the manufacturer's instructions, the representative apoptosis were neurons with tightly clustered brown staining (Figure 6(c)). And the quantification of the TUNEL-positive cells were changed in the same pattern as those in flow cytometry among the treatment groups, suggesting an important role of the miR-137-3p/CAPN-2 interaction in regulating subsequent Cdk5 and caspase-8 overactivation and neuronal apoptosis (Figure 6(d), $P < 0.05$). No

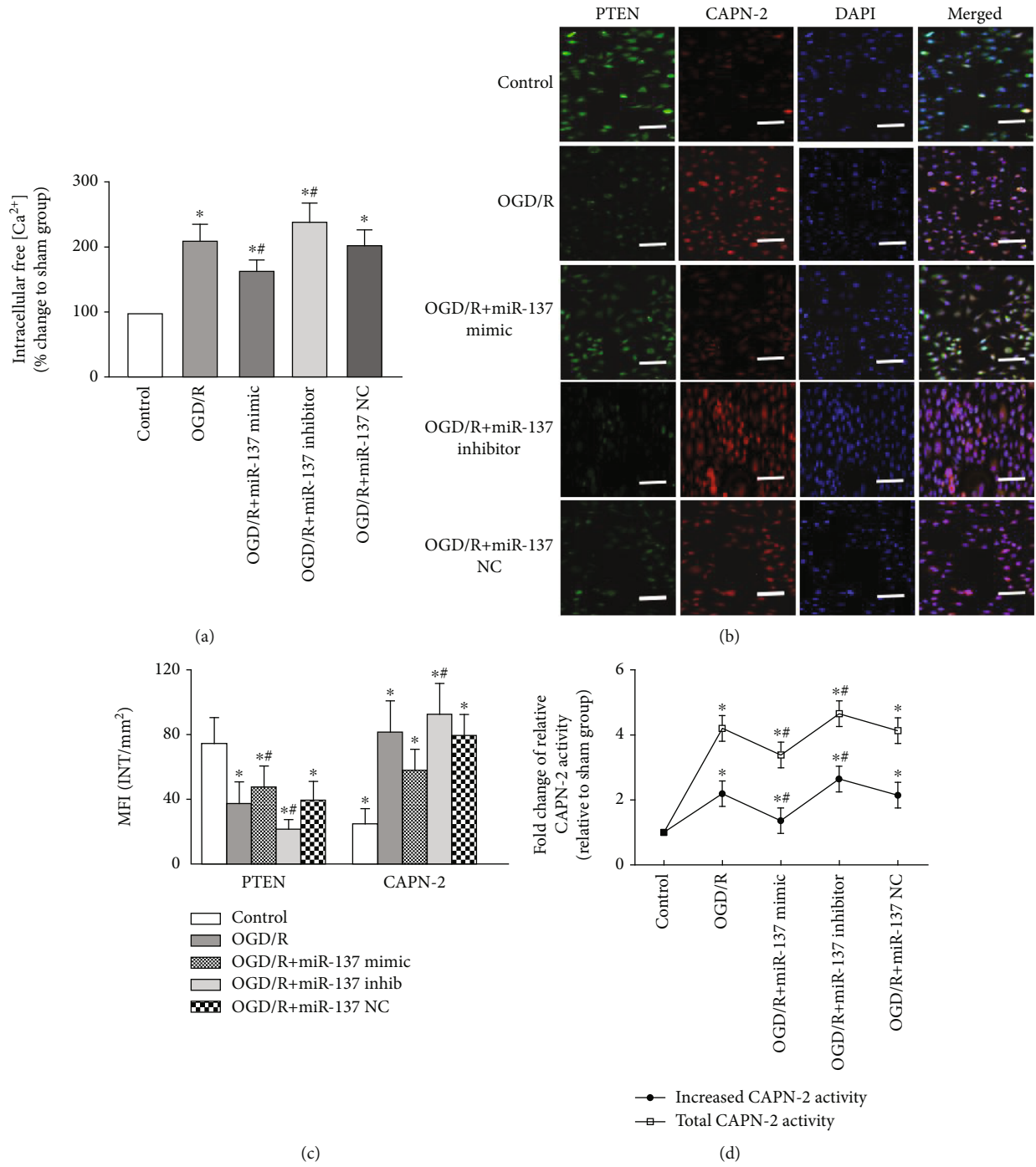


FIGURE 3: Continued.

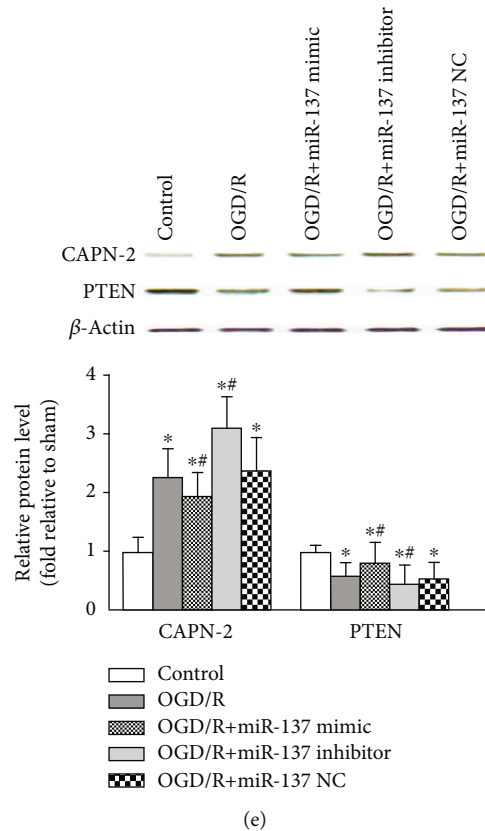


FIGURE 3: Modulation of CAPN-2 expression and activity by miR-137-3p in VSC4.1 neurons after OGD/R. (a) Percentage of intracellular free $[Ca^{2+}]$ in each condition after OGD/R. (b) Representative double immunofluorescence staining showing that PTEN (green) and CAPN-2 (red) are predominantly localized in the cytoplasm of VSC4.1 neurons. Scale bar = 50 μ m. (c) Quantification of the MFIs of PTEN and CAPN-2 in neurons of each treatment group. (d) Statistical analysis of total CAPN-2 and increased CAPN-2 activities at 24 h post OGD/R. (e) Representative Western blots and protein quantification of CAPN-2 and PTEN in neurons. All samples were analyzed in triplicate, and the data are expressed as the mean \pm SD. * $P < 0.05$ versus the control group; # $P < 0.05$ versus the OGD/R group.

significant differences were observed between the injured neurons treated with or without miR-137 NC ($P > 0.05$).

4. Discussion

Our previous studies revealed that IR-induced dysregulation of miR expression in spinal cords played important roles in driving pathogenesis during the reperfusion period and finally caused severe motor and sensory dysfunction [5, 6, 29]. Recently, an increasing number of studies have suggested that miR-based gene therapy is a promising treatment for neurological recovery by effectively preventing neuronal apoptosis. In the present study, we investigated the function and mechanisms of miR-137-3p and its target CAPN-2 in both *in vivo* and *in vitro* IR models to better understand the pathophysiological mechanisms and find better treatments in the clinic.

Previous studies have suggested prosurvival roles for CAPN-1 activation but destructive roles for CAPN-2 activation in retinal ganglion cell degeneration [17, 19]. However, none of the studies addressed the definite roles of calpain isoforms during the development of IR-induced pain hypersensitivity. In this context, we examined CAPN-1 and CAPN-2

protein expression and assessed motor function using the Tarlov scores at several time points post IR. Our results showed that only the temporal expression patterns of CAPN-2 were negatively correlated with IR-induced motor dysfunction, with initial significant differences being detected at 0.5 h post IR and peaking at 4 h post IR (Figure 1). This finding was consistent with that of a previous study on spinal cord injury, in which the progressively increased calpain content in the lesion was first detected as early as 30 min after trauma and increased by 91% at 4 h after trauma [36]. We further explored the cellular localization of CAPN-2 in major spinal cord cell types by double immunofluorescence at 4 h post IR when CAPN-2 expression reached its peak. Representative images and quantification showed that CAPN-2 was primarily expressed in spinal neurons, indicating that neuronal CAPN-2 might be the major effector during the reperfusion period.

MiRs are small RNA molecules that negatively regulate gene expression by binding with the 3'-UTRs of targets via complementary base pairs [28, 34]. MiRs are widely expressed in the CNS and have been implicated in multiple pathological processes, including IR [29]. We have suggested that some miRs, including miR-187-3p, miR-27, and miR-

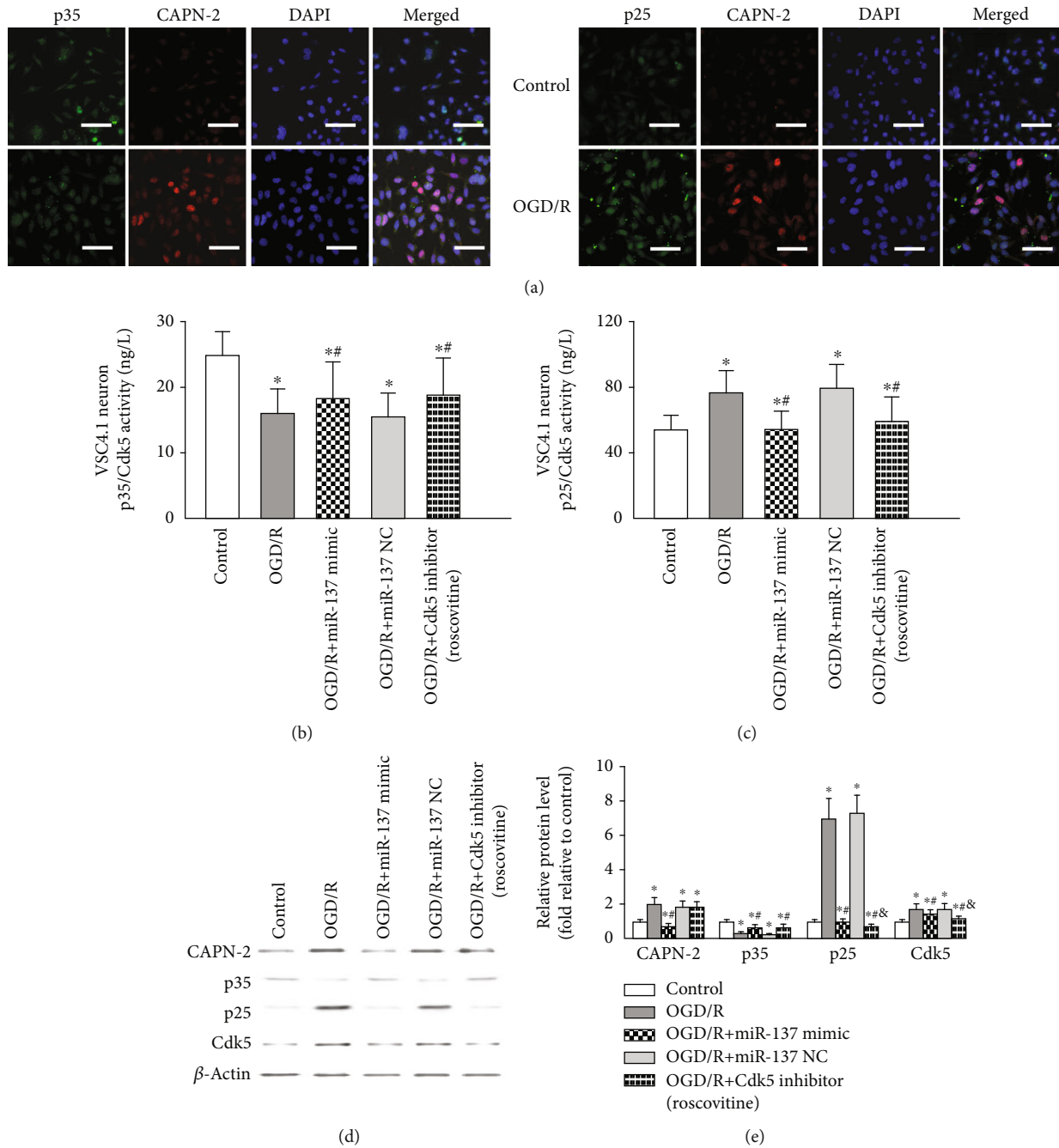


FIGURE 4: Modulation of p35 cleavage and p25/Cdk5 activation by the miR-137-3p/CAPN-2 interaction after OGD/R. (a) Representative double immunofluorescence staining showing that p35 (green) and CAPN-2 (red) (left panel) and p25 (green) and CAPN-2 (red) (right panel) are predominantly localized in the cytoplasm of VSC4.1 neurons. Scale bar = 50 μm. (b, c) Quantification of p35/Cdk5 and p25/Cdk5 activities in VSC4.1 neurons of each treatment group by ELISA. (d) Representative Western blots and protein quantification of CAPN-2, p35, p25, and Cdk5 in neurons. All samples were analyzed in triplicate, and the data are expressed as the mean ± SD. **P* < 0.05 versus the control group; #*P* < 0.05 versus the OGD/R group; &*P* < 0.05 versus the OGD/R+miR-137 mimic group.

125b that are highly expressed in spinal cords, may provide new insights for research and clinical treatment [5, 6, 29]. Likewise, using miR microarray and luciferase assays, we herein found that miR-137-3p expression was substantially changed at 4 h post IR, and miR-137-3p exhibited a targeted interaction with CAPN-2 (Figure 2). Continuous intrathecal injection of synthetic miRs before IR was previously reported

to effectively regulate miR expression and that of corresponding target genes *in vivo* [5, 6, 29]. Given the complicated cellular crosstalk *in vivo*, we defined the overall effects of the miR-137-3p/CAPN-2 interaction by assessing motor function in a rat model. As expected, in contrast to the decreased CAPN-2 protein expression, intrathecal injection of the miR-137-3p mimic substantially increased Tarlov's scores,

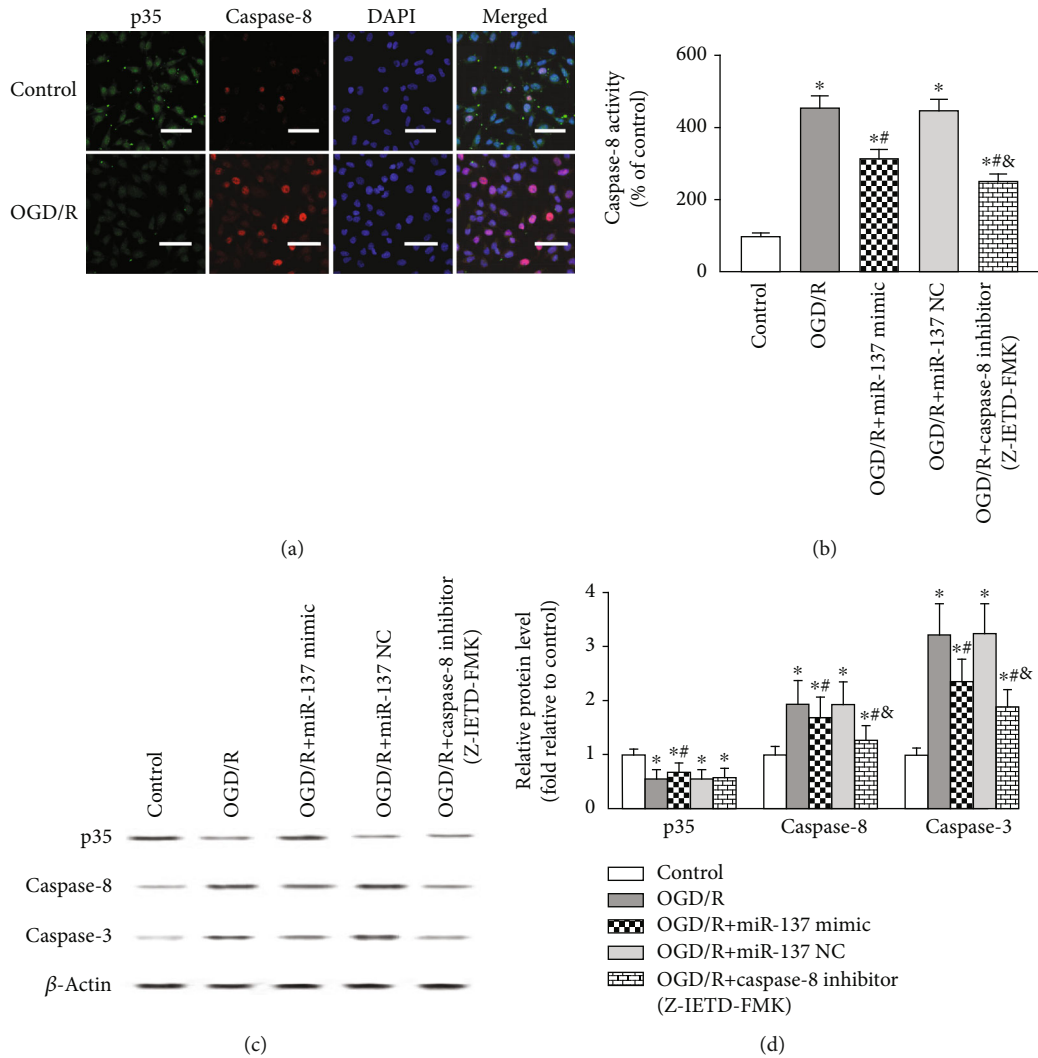
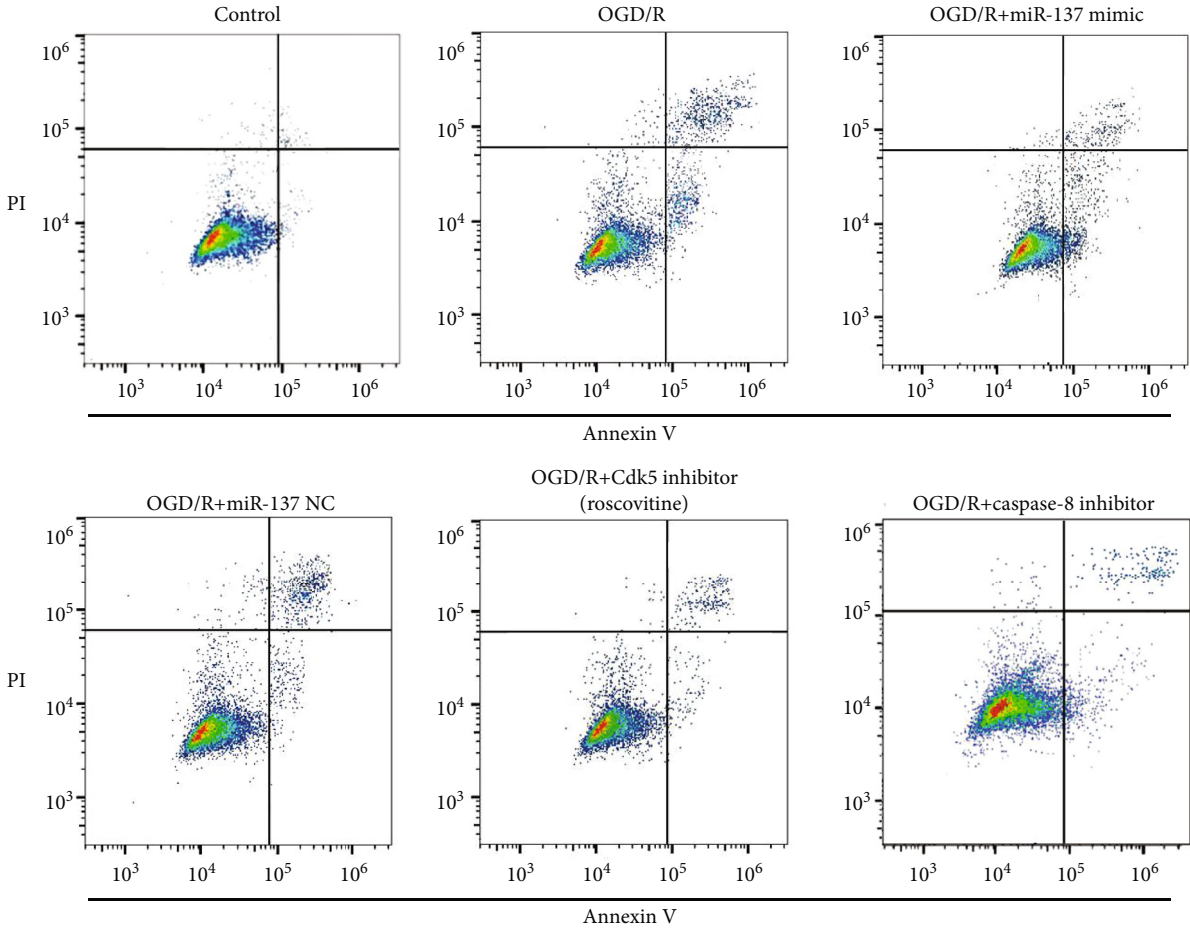


FIGURE 5: Modulation of caspase-8 activation by the miR-137-3p/CAPN-2 interaction after OGD/R. (a) Representative double immunofluorescence staining showing that p35 (green) and caspase-8 are predominantly localized in the cytoplasm of VSC4.1 neurons. Scale bar = 50 μ m. (b) Quantitative analysis of caspase-8 activity in VSC4.1 neurons of each treatment group. (c, d) Representative Western blots and protein quantification of p35, caspase-8, and caspase-3 in neurons. All samples were analyzed in triplicate, and the data are expressed as the mean \pm SD. * P < 0.05 versus the control group; # P < 0.05 versus the OGD/R group; & P < 0.05 versus the OGD/R + miR-137 mimic group.

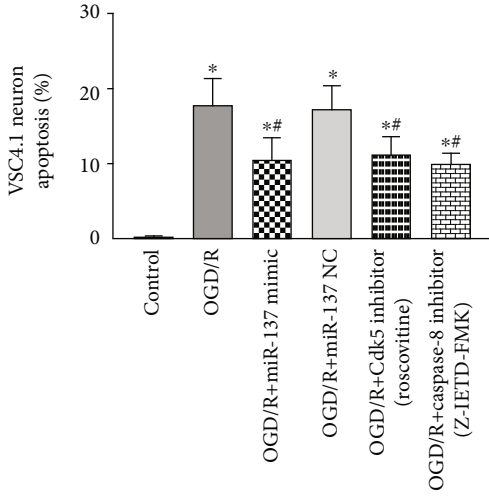
indicating decreased motor dysfunction, whereas treatment with the miR-137-3p inhibitor or NC did not have these effects. Moreover, to further confirm the above interaction, exogenous CAPN-2 (rr-CALP2) was delivered directly via the intrathecal route. Consistent with the ability of exogenous CAPN-2 to activate intrinsic CAPN-2 in uninjured nerves [35, 37], the synergistic increase in CAPN-2 expression caused by exogenous rr-CALP2 injection was significantly prevented by the miR-137-3p mimic, as comparable CAPN-2 protein levels and similar behavioral assessments were observed throughout the reperfusion period in injured rats treated with or without combined injection with rr-CALP2 (Figure 2). These findings suggested that miR-137-3p acted as a functional regulator of CAPN-2 in the spinal cord.

As a trigger, CAPN-2 requires millimolar (0.250–0.750 mM) calcium concentrations for its activation [13]. Thus, parallel *in vitro* experiments were performed to better

define the possible mechanisms by which the miR-137-3p/CAPN-2 interaction is implicated in VSC4.1 neuronal apoptosis. Consistent with the *in vivo* results and VSC4.1 neuron glutamate-related neurotoxicity [14], overactivation of CAPN-2 was accompanied by an increase in the intracellular free $[Ca^{2+}]$ in OGD/R-stressed VSC4.1 neurons; both the MFI of CAPN-2 and total and net CAPN-2 activities were significantly increased by OGD/R treatment (Figure 3). Previous reports have indicated that both peptide and nonpeptide CAPN inhibitors downregulate CAPN expression by preventing increases in intracellular free $[Ca^{2+}]$ [14, 38]. Consistently, our current data showed that the synthetic miR-137 mimic also prevented the increase in intracellular $[Ca^{2+}]$ and decreased CAPN-2 expression and activity in stressed neurons. In addition, PTEN is a selective substrate for CAPN-2 [32] and is thus widely used to quantitatively measure neuronal CAPN-2 activity *in vivo* and *in vitro* [19,



(a)



(b)

FIGURE 6: Continued.

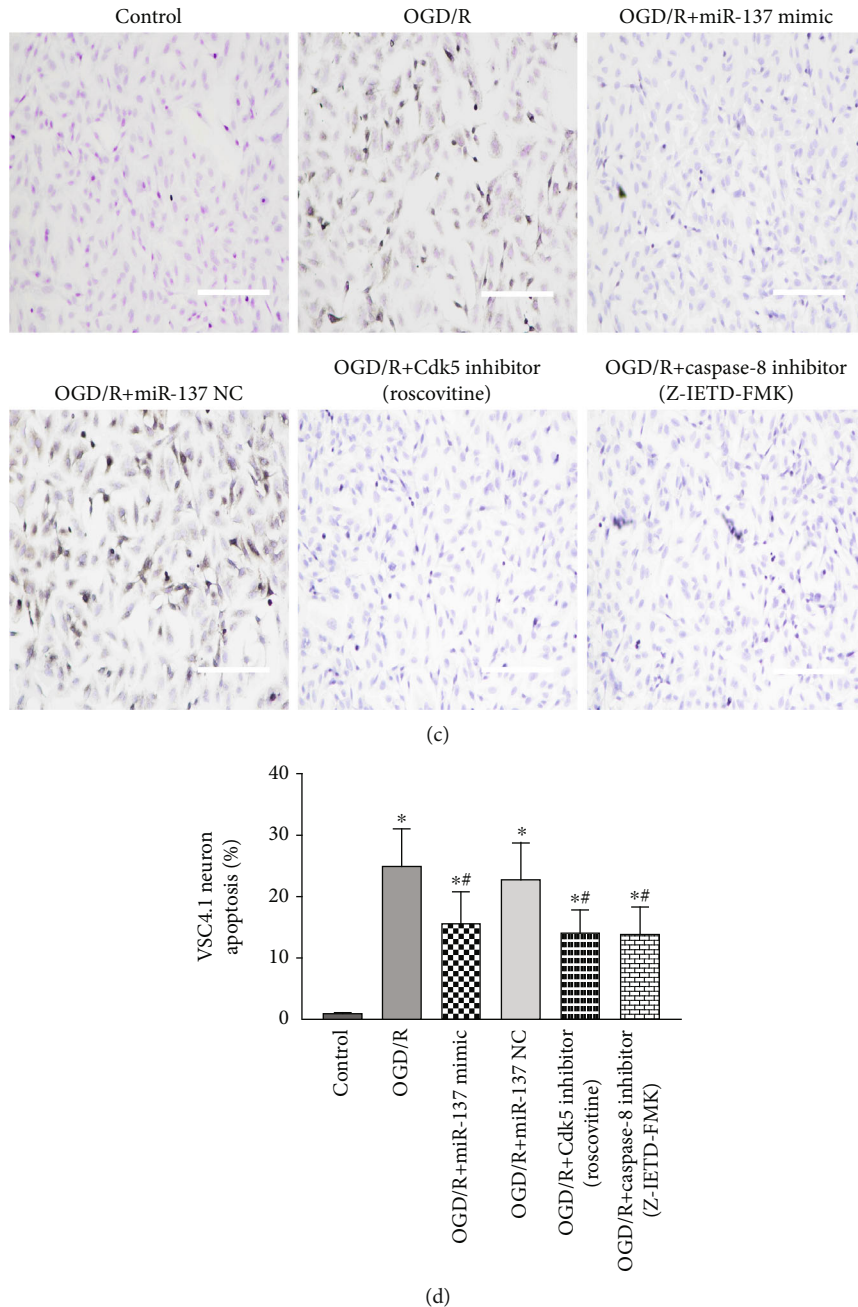


FIGURE 6: Modulation of VSC4.1 neuronal apoptosis by the miR-137-3p/CAPN-2 interaction after OGD/R. (a) The percentage of OGD/R-induced neuronal apoptosis in each treatment group as determined by flow cytometry. (b) Quantification of the percentage of apoptotic neurons. (c) Representative images of OGD/R-induced neuronal apoptosis in each treatment group as determined by the TUNEL assay. (d) Quantification of the percentage of apoptotic neurons. The cells detected with the brown color were regarded as positive, and the quantity was determined from six random fields. Scale bar = 50 μ m. All samples were analyzed in triplicate, and the data are expressed as the mean \pm SD. * P < 0.05 versus the control group; # P < 0.05 versus the OGD/R group.

32]. As expected, PTEN and CAPN-2 were identically localized in the cytoplasm of neurons, but their protein levels and immunoreactivities changed in opposite directions in response to transfection with the different treatments. Decreased PTEN expression indicates an increase in CAPN-2 activation; therefore, these results suggest that OGD/R-induced CAPN-2 overactivation was regulated by synthetic miR.

Previous *in vitro* and *in vivo* studies have shown that CAPN-2 upregulation triggers neuronal apoptosis [20, 39]. These studies found that activated CAPN-2 directly and precisely cleaved its substrate, membrane-bound protein p35, into p25, which consequently resulted in Cdk5 activation in cultured primary neurons and retinal ganglion cells [13, 20, 39]. Similarly, our *in vitro* immunofluorescence staining (Figure 4) revealed that the cytoplasmic and nuclear labels

for p35 and p25 fluorescence completely overlapped with the CAPN-2 labels in VSC4.1 neurons. In a previous study, during polybrominated diphenyl ether-153-induced neuronal apoptosis, p35 was found to accumulate in the perinuclear region and plasma membrane, and p25 was localized in both the cytoplasm and nucleus [20]. Given that the p35/Cdk5 complex mainly functions in the nucleus, these mislocalizations of p35 and p25 might signify the formation of the p25/Cdk5 complex [20, 40, 41]. Additionally, our Western blot results showed that the pattern of Cdk5 protein expression in each group changed in agreement with the protein levels of p25 and CAPN-2 and oppositely with the protein levels of p35 (Figure 4). On the other hand, the changes in p35 and p25 activities in being accordance with the protein level of CAPN-2 in neurons transfected with the miR-137-3p mimic or NC also demonstrated that the conversion of p35 into p25 requires CAPN-2. Additionally, selective inhibition of CAPN-2 expression has been shown to preserve both the structure and function of vulnerable neurons [14, 17, 19]. In this study, pretreatment with the miR-137-3p and Cdk5 inhibitors comparably inhibited the numbers of neurons located in the A4 and A2 quadrants of the flow cytometry dot-plot graphs and also the neurons with tightly clustered brown staining (referred as the TUNEL-positive cells) in the TUNEL assay after OGD/R insult (Figure 6). These findings all support the hypothesis that the dynamic localization of p35 and p25 is a marker of p25/Cdk5 activation-induced apoptosis.

Caspase cascade activation has been suggested to be central to neuronal apoptosis during IR injury [5, 9]. Acting as the apical member of the caspase family, caspase-8 overactivation has been shown to be especially important for controlling a series of broad caspase cascade networks by initiating the activation of downstream caspases, such as caspase-3 [24, 42]. Furthermore, as a cysteine protease, caspase-8 requires proteolytic cleavage before activation. Under normal conditions, caspase-8 forms the p35-caspase-8 complex via the formation of a covalent bond with the N terminus of p35 [26], which is known to be a major element necessary for preserving the p35-caspase-8 complex, and the baculovirus p35 protein has been demonstrated to effectively block the apoptosis cascade by preventing caspase-8 proteolysis and activation [24, 26]. In contrast, CAPN-2 overexpression-mediated p35 cleavage may cause conformational changes in p35 and consequently initiate aberrant caspase-8 activation. In agreement with the above hypothesis, a previous study showed that CAPN-2 was required to initiate endoplasmic reticulum stress-induced apoptosis mediated by a caspase-8-dependent pathway [25]. Similar to our *in vitro* immunofluorescence and Western blotting results, the fluorescent labels for p35 in the cytoplasm were identical to those for caspase-8 in neurons, and the protein expression levels of p35 and caspase-8 were changed in opposite directions when CAPN-2 expression was downregulated by pretreatment with the miR-137-3p mimic (Figure 5). In addition, our hypothesis that CAPN-2 initiates caspase-8-mediated apoptosis was additionally supported by similar results observed in neurons transfected with the miR-137-3p mimic and those transfected with the caspase-8-specific inhibitor Z-IETD-FMK. Both

treatments exerted comparable inhibitory effects on the protein level and activity of caspase-8, the numbers of injured neurons in the A4 and A2 quadrants of the dot-plot graphs, and the amount of the TUNEL-positive cells (Figures 5 and 6). Acting as the final executor of the caspase family, caspase-3 expression was equally decreased in neurons transfected with the miR-137-3p mimic and Z-IETD-FMK, supporting the assumption that CAPN-2-induced caspase-8 activation may simultaneously lead to caspase-3 activation. Indeed, similar observations were made in a study of hydrogen peroxide-induced apoptotic pathways [25].

Of note, the CALP2-mediated mechanisms of pain hypersensitivity are somewhat divergent. First, CALP2 activity is not absolutely associated with reciprocal modulation of the CALP2 protein level. Interestingly, the addition of rr-CALP2 at 50 U/L induced significant decreases in the withdrawal thresholds of bilateral hind paws, but the differences in CALP2 expression increases on either side failed to reach significance at 3 d post drug administration [35]. Given the complicated *in vivo* crosstalk and signaling pathway network, CALP2-mediated cascade responses might be amplified by other factors in a positive feedback loop, such as the activation of nuclear factor-kappa B (NF- κ B) and the proinflammatory cytokine IL-6 [35]. Thus, it cannot be concluded from these data whether the increased CALP2 expression *in vivo* resulted from the activation of CALP2, NF- κ B-mediated inflammatory responses, or both or even by other signaling pathways, such as oxidative stress [43]. In addition, transfection with the Cdk5 inhibitor roscovitine had no significant effects on the expression of CAPN-2 or p35, possibly due to the eventual modulation of the CAPN-2/p35-p25/Cdk5 pathway [20]. Roscovitine is known to be highly specific for Cdk5 and is therefore unlikely to influence the activities of apical members of the signaling pathway [20]. Undoubtedly, whether caspase-8 directly activates caspase-3 by proteolytic cleavage or by the activation of caspase-3 activators needs to be elucidated in future studies.

5. Conclusions

This study highlights the roles of CAPN-2 in triggering motor dysfunction after spinal cord IR injury and investigates the target interactions with miR-137-3p both *in vivo* and *in vitro*. The effects of the miR-137-3p/CAPN-2 interaction on neuronal apoptosis may be attributed to CAPN-2 inhibition, which consequentially results in substrate p35 cleavage inhibition and thus prevents the overactivation of p25/Cdk5 and the initiation of the caspase-8-mediated caspase cascade.

Abbreviations

BP:	Blood pressure
BSA:	Bovine serum albumin
Ca ²⁺ :	Calcium ion
[Ca ²⁺]:	Ca ²⁺ concentration
CAPNs:	Calcium-activated neutral proteinases
Cdk5:	Cyclin-dependent kinase-5
CNS:	Central nervous system

EMEM: Eagle's minimum essential medium
 FBS: Fetal bovine serum
 HBSS: Hank's balanced salt solution
 IF: Immunofluorescence
 IR: Ischemia-reperfusion
 miR: MicroRNA
 MFI: Mean fluorescence intensity
 MT: Mutant
 NC: Negative control
 pNA: P-Nitroaniline
 PTEN: Tensin homolog
 R: Ratio
 SD: Standard deviation
 VSC: Ventral spinal cord
 UTR: Untranslated region
 WT: Wild type.

Data Availability

The materials supporting the conclusions of this article are included within the article.

Conflicts of Interest

All authors in this study declare that they have no conflicts of interest.

Authors' Contributions

H.W. and Z.-L.Z. participated in animal care and made the animal models; H.W. and Q.Y. established the cell models and prepared samples for RT-PCR and immunohistochemistry assays; H.W., Q.Y., and Z.-L.Z. performed the experiments and statistical analysis; X.-Q.L. conducted the luciferase assays; and H.M. guided the study design and provided important suggestions for writing the manuscript.

Acknowledgments

This work was supported by the National Natural Science Foundation of China (nos. 81601053 and 81771342), the Scientific Research Project of Liaoning Educational Department (no. LK201636), and the Key Project of Liaoning Natural Science Foundation (no. 20180530087).

Supplementary Materials

Supplementary Figure: OGD/R-induced CAPN-2 upregulation and apoptosis in VSC4.1 neurons. (A) Representative double immunofluorescence staining shows that DAPI (blue), CAPN-2 (green), and Annexin V (red) are colocalized in the same neurons. Scale bar = 50 μm . (B) Quantification of the number of CAPN-2-positive neurons with Annexin V. (C) Representative double immunofluorescence staining shows that DAPI (blue), CAPN-2 (green), and cleaved caspase-3 (red) are colocalized in the same neurons. Scale bar = 50 μm . (D) Quantification of the number of CAPN-2-positive neurons with cleaved caspase-3. The data are expressed as the mean \pm SD. * $P < 0.05$ versus the control group. (*Supplementary Materials*)

References

- [1] H. Awad, M. E. Ramadan, H. F. El Sayed, D. A. Tolpin, E. Tili, and C. D. Collard, "Spinal cord injury after thoracic endovascular aortic aneurysm repair," *Canadian Journal of Anesthesia/Journal Canadien D'anesthésie*, vol. 64, no. 12, pp. 1218–1235, 2017.
- [2] M. M. Wynn and C. W. Acher, "A modern theory of spinal cord ischemia/injury in thoracoabdominal aortic surgery and its implications for prevention of paralysis," *Journal of Cardiothoracic and Vascular Anesthesia*, vol. 28, no. 4, pp. 1088–1099, 2014.
- [3] R. B. Borgens and P. Liu-Snyder, "Understanding secondary injury," *The Quarterly Review of Biology*, vol. 87, no. 2, pp. 89–127, 2012.
- [4] X. Q. Li, H. W. Lv, W. F. Tan, B. Fang, H. Wang, and H. Ma, "Role of the TLR4 pathway in blood-spinal cord barrier dysfunction during the bimodal stage after ischemia/reperfusion injury in rats," *Journal of Neuroinflammation*, vol. 11, no. 1, p. 62, 2014.
- [5] X. Q. Li, Q. Yu, W. F. Tan, Z. L. Zhang, and H. Ma, "MicroRNA-125b mimic inhibits ischemia reperfusion-induced neuroinflammation and aberrant p53 apoptotic signalling activation through targeting TP53INP1," *Brain, Behavior, and Immunity*, vol. 74, pp. 154–165, 2018.
- [6] X. Q. Li, Q. Yu, Z. L. Zhang, X. J. Sun, and H. Ma, "MiR-187-3p mimic alleviates ischemia-reperfusion-induced pain hypersensitivity through inhibiting spinal P2X7R and subsequent mature IL-1 β release in mice," *Brain, Behavior, and Immunity*, vol. 79, pp. 91–101, 2019.
- [7] M. Fricker, A. M. Tolkovsky, V. Borutaite, M. Coleman, and G. C. Brown, "Neuronal cell death," *Physiological Reviews*, vol. 98, no. 2, pp. 813–880, 2018.
- [8] X. Teng, W. Chen, Z. Liu et al., "NLRP3 inflammasome is involved in Q-VD-OPH induced necroptosis following cerebral ischemia-reperfusion injury," *Neurochemical Research*, vol. 43, no. 6, pp. 1200–1209, 2018.
- [9] X. Q. Li, X. Z. CAO, J. Wang, B. Fang, W. F. Tan, and H. Ma, "Sevoflurane preconditioning ameliorates neuronal deficits by inhibiting microglial MMP-9 expression after spinal cord ischemia/reperfusion in rats," *Molecular Brain*, vol. 7, no. 1, p. 69, 2014.
- [10] E. Garcia, J. Aguilar-Cevallos, R. Silva-Garcia, and A. Ibarra, "Cytokine and growth factor activation in vivo and in vitro after spinal cord injury," *Mediators of Inflammation*, vol. 2016, Article ID 9476020, 21 pages, 2016.
- [11] L. Jiang, J. Zhong, X. Dou, C. Cheng, Z. Huang, and X. Sun, "Effects of ApoE on intracellular calcium levels and apoptosis of neurons after mechanical injury," *Neuroscience*, vol. 301, pp. 375–383, 2015.
- [12] D. Radak, N. Katsiki, I. Resanovic et al., "Apoptosis and acute brain ischemia in ischemic stroke," *Current Vascular Pharmacology*, vol. 15, no. 2, pp. 115–122, 2017.
- [13] M. Siklos, M. BenAissa, and G. R. Thatcher, "Cysteine proteases as therapeutic targets: does selectivity matter? A systematic review of calpain and cathepsin inhibitors," *Acta Pharmaceutica Sinica B*, vol. 5, no. 6, pp. 506–519, 2015.
- [14] A. Das, E. A. Sribnick, J. M. Wingrave et al., "Calpain activation in apoptosis of ventral spinal cord 4.1 (VSC4.1) motoneurons exposed to glutamate: calpain inhibition provides functional neuroprotection," *Journal of Neuroscience Research*, vol. 81, no. 4, pp. 551–562, 2005.

- [15] S. Y. Cheng, S. C. Wang, M. Lei, Z. Wang, and K. Xiong, "Regulatory role of calpain in neuronal death," *Neural Regeneration Research*, vol. 13, no. 3, pp. 556–562, 2018.
- [16] C. G. Yu, Y. Li, K. Raza, X. X. Yu, S. Ghoshal, and J. W. Geddes, "Calpain 1 knockdown improves tissue sparing and functional outcomes after spinal cord injury in rats," *Journal of Neurotrauma*, vol. 30, no. 6, pp. 427–433, 2013.
- [17] Y. Wang, D. Lopez, P. G. Davey et al., "Calpain-1 and calpain-2 play opposite roles in retinal ganglion cell degeneration induced by retinal ischemia/reperfusion injury," *Neurobiology of Disease*, vol. 93, pp. 121–128, 2016.
- [18] M. Baudry, "Calpain-1 and calpain-2 in the brain: Dr. Jekyll and Mr Hyde?," *Neuropharmacology*, vol. 17, no. 9, pp. 823–829, 2019.
- [19] S. Wang, Y. Huang, Y. Yan et al., "Calpain2 but not calpain1 mediated by calpastatin following glutamate-induced regulated necrosis in rat retinal neurons," *Annals of Anatomy*, vol. 221, pp. 57–67, 2019.
- [20] H. Zhang, L. Chang, H. Zhang et al., "Calpain-2/p35-p25/Cdk5 pathway is involved in the neuronal apoptosis induced by polybrominated diphenyl ether-153," *Toxicology Letters*, vol. 277, pp. 41–53, 2017.
- [21] M. Amini, C. L. Ma, R. Farazifard et al., "Conditional disruption of calpain in the CNS alters dendrite morphology, impairs LTP, and promotes neuronal survival following injury," *The Journal of Neuroscience*, vol. 33, no. 13, pp. 5773–5784, 2013.
- [22] Y. L. Zheng, X. Zhang, H. X. Fu et al., "Knockdown of expression of Cdk5 or p35 (a Cdk5 activator) results in podocyte apoptosis," *PLoS One*, vol. 11, no. 8, article e0160252, 2016.
- [23] X. Tan, Y. Chen, J. Li et al., "The inhibition of Cdk5 activity after hypoxia/ischemia injury reduces infarct size and promotes functional recovery in neonatal rats," *Neuroscience*, vol. 290, pp. 552–560, 2015.
- [24] Y. Shi, "Mechanisms of caspase activation and inhibition during apoptosis," *Molecular Cell*, vol. 9, no. 3, pp. 459–470, 2002.
- [25] G. Xu, R. L. Rich, C. Steegborn et al., "Mutational analyses of the p35-caspase interaction. A bowstring kinetic model of caspase inhibition by p35," *The Journal of Biological Chemistry*, vol. 278, no. 7, pp. 5455–5461, 2003.
- [26] H. Weber, L. Müller, L. Jonas, C. Schult, G. Sparmann, and P. Schuff-Werner, "Calpain mediates caspase-dependent apoptosis initiated by hydrogen peroxide in pancreatic acinar AR42J cells," *Free Radical Research*, vol. 47, no. 5, pp. 432–446, 2013.
- [27] Y. Wang, X. Bi, and M. Baudry, "Calpain-2 as a therapeutic target for acute neuronal injury," *Expert Opinion on Therapeutic Targets*, vol. 22, no. 1, pp. 19–29, 2017.
- [28] R. Chandran, S. L. Mehta, and R. Vemuganti, "Non-coding RNAs and neuroprotection after acute CNS injuries," *Neurochemistry International*, vol. 111, pp. 12–22, 2017.
- [29] X. Q. Li, H. W. Lv, W. F. Tan, Z. L. Wang, B. Fang, and H. Ma, "MiR-27a ameliorates inflammatory damage to the blood-spinal cord barrier after spinal cord ischemia-reperfusion injury in rats by down-regulating TICAM-2 of the TLR4 signaling pathway," *Journal of Neuroinflammation*, vol. 12, no. 1, p. 25, 2015.
- [30] Y. Tang, R. Fu, Z. M. Ling et al., "MiR-137-3p rescue motoneuron death by targeting calpain-2," *Nitric Oxide*, vol. 74, pp. 74–85, 2018.
- [31] Y. Tang, Z. M. Ling, R. Fu et al., "Time-specific microRNA changes during spinal motoneuron degeneration in adult rats following unilateral brachial plexus root avulsion: ipsilateral vs. contralateral changes," *BMC Neurosci.*, vol. 15, no. 1, p. 92, 2014.
- [32] Y. Wang, Y. Liu, D. Lopez et al., "Protection against TBI-induced neuronal death with post-treatment with a selective calpain-2 inhibitor in mice," *Journal of Neurotrauma*, vol. 35, no. 1, pp. 105–117, 2018.
- [33] J. Liu, C. Xiang, W. Huang et al., "Neurotoxicological effects induced by up-regulation of miR-137 following triclosan exposure to zebrafish (*Danio rerio*)," *Aquatic Toxicology*, vol. 206, pp. 176–185, 2019.
- [34] D. Zhao, S. C. Deng, Y. Ma, Y. H. Hao, and Z. H. Jia, "miR-221 alleviates the inflammatory response and cell apoptosis of neuronal cell through targeting TNFAIP2 in spinal cord ischemia-reperfusion," *Neuroreport*, vol. 29, no. 8, pp. 655–660, 2018.
- [35] Y. Zang, S. X. Chen, G. J. Liao et al., "Calpain-2 contributes to neuropathic pain following motor nerve injury via up-regulating interleukin-6 in DRG neurons," *Brain, Behavior, and Immunity*, vol. 44, pp. 37–47, 2015.
- [36] N. L. Banik, D. C. Matzelle, G. Gantt-Wilford, A. Osborne, and E. L. Hogan, "Increased calpain content and progressive degradation of neurofilament protein in spinal cord injury," *Brain Research*, vol. 752, no. 1-2, pp. 301–306, 1997.
- [37] M. S. Castejon, D. G. Culver, and J. D. Glass, "Generation of spectrin breakdown products in peripheral nerves by addition of M-calpain," *Muscle & Nerve*, vol. 22, no. 7, pp. 905–909, 1999.
- [38] X. Liu, J. F. Harriman, and R. G. Schnellmann, "Cytoprotective properties of novel nonpeptide calpain inhibitors in renal cells," *The Journal of Pharmacology and Experimental Therapeutics*, vol. 302, no. 1, pp. 88–94, 2002.
- [39] Y. Miao, L. D. Dong, J. Chen, X. C. Hu, X. L. Yang, and Z. Wang, "Involvement of calpain/p35-p25/Cdk5/NMDAR signaling pathway in glutamate-induced neurotoxicity in cultured rat retinal neurons," *PLoS One*, vol. 7, no. 8, article e42318, 2012.
- [40] X. Fu, Y. K. Choi, D. Qu, Y. Yu, N. S. Cheung, and R. Z. Qi, "Identification of nuclear import mechanisms for the neuronal Cdk5 activator," *The Journal of Biological Chemistry*, vol. 281, no. 51, pp. 39014–39021, 2006.
- [41] A. Asada, N. Yamamoto, M. Gohda, T. Saito, N. Hayashi, and S. Hisanaga, "Myristoylation of p39 and p35 is a determinant of cytoplasmic or nuclear localization of active cyclin-dependent kinase 5 complexes," *Journal of Neurochemistry*, vol. 106, no. 3, pp. 1325–1336, 2008.
- [42] P. P. Monnier, P. M. D'Onofrio, M. Magharious et al., "Involvement of caspase-6 and caspase-8 in neuronal apoptosis and the regenerative failure of injured retinal ganglion cells," *The Journal of Neuroscience*, vol. 31, no. 29, pp. 10494–10505, 2011.
- [43] A. A. Mohsin, J. Thompson, Y. Hu, J. Hollander, E. J. Lesnfsky, and Q. Chen, "Endoplasmic reticulum stress-induced complex I defect: central role of calcium overload," *Archives of Biochemistry and Biophysics*, vol. 683, p. 108299, 2020.

Research Article

A Preclinical Systematic Review of Curcumin for Protecting the Kidney with Ischemia Reperfusion Injury

Zi-Hao Wang, Li-Hui Deng, Chang-Wei Chi, Hong Wang , Yue-Yue Huang ,
and Qun Zheng 

Department of Nephrology and Rheumatism Immunity, The Second Affiliated Hospital and Yuying Children's Hospital of Wenzhou Medical University, Wenzhou, China

Correspondence should be addressed to Hong Wang; 202020@wzhealth.com, Yue-Yue Huang; 1019264345@qq.com, and Qun Zheng; 344457512@qq.com

Received 16 May 2020; Revised 1 October 2020; Accepted 11 October 2020; Published 12 November 2020

Academic Editor: Hong Zheng

Copyright © 2020 Zi-Hao Wang et al. This is an open access article distributed under the Creative Commons Attribution License, which permits unrestricted use, distribution, and reproduction in any medium, provided the original work is properly cited.

Renal ischemia-reperfusion injury (RIRI) refers to a phenomenon associated with dysfunction of the kidney and tissue damage. Unfortunately, no specific drugs have been found that effectively prevent and treat RIRI. Curcumin (Cur), a polyphenol extracted from turmeric, possesses a variety of biological activities involving antioxidation, inhibition of apoptosis, inhibition of inflammation, and reduction of lipid peroxidation. Eight frequently used databases were searched using prespecified search strategies. The CAMARADES 10-item quality checklist was used to evaluate the risk of bias of included studies, and the RevMan 5.3 software was used to analyze the data. The risk of bias score of included studies ranged from 3 to 6 with an average score of 5.22. Compared with the control group, Cur significantly alleviated renal pathology, reduced blood urea nitrogen and serum creatinine levels, and improved inflammatory indexes, oxidant, and apoptosis in RIRI animal models. Despite the heterogeneity of the response to Cur in terms of serum creatinine, BUN, TNF- α , and SOD, its effectiveness for improving the injury of RIRI was remarkable. In the mouse model subgroup of serum creatinine, the effect size of the method of unilateral renal artery ligation with contralateral nephrectomy and shorter ischemic time showed a greater effect than that of the control group. No difference was seen in the methods of model establishment, mode administration, or medication times. The preclinical systematic review provided preliminary evidence that Cur partially improved RIRI in animal models, probably via anti-inflammatory, antioxidant, antiapoptosis, and antifibrosis activities and via improving microperfusion. ARRIVE guidelines are recommended; blinding and sample size calculation should be focused on in future studies. These data suggest that Cur is a potential renoprotective candidate for further clinical trials of RIRI.

1. Introduction

Renal ischemia-reperfusion injury (RIRI) refers to a phenomenon of aggravation of kidney dysfunction and tissue damage caused by reflow of blood to the kidneys [1, 2]. RIRI is one of the main causes of acute kidney injury (AKI) and acute renal failure (ARF) [1, 2] and is a common adverse pathophysiological change in patients with organ transplantation, shock, sepsis, burns, cardiovascular disease, and trauma [3]. Among patients with kidney transplantation, it is a major cause of delayed graft function in as many as 80% [4]. The incidence of in-hospital death is high for patients with RIRI in the intensive care unit who have a high probability of AKI. Patients who

survive remain at high risk of developing chronic renal disorder that may evolve into end-stage renal disorder (ESRD), which also carries high economic, societal, and personal burdens [5]. Unfortunately, the possible mechanism of RIRI is still unclear and no specific drugs have been found to effectively prevent and treat RIRI. Therefore, it is imperative to seek a new treatment strategy to alleviate kidney damage in patients with RIRI.

Turmeric, obtained from the rhizome of *Curcuma longa* L. (Zingiberaceae), is widely used as a spice, flavor, and colorant worldwide. Since ancient times in Asia, it has been used to prevent and treat conditions such as pain, digestive diseases, ischemic disease wounds, and gynecological problems [6]. Curcumin (Cur, $C_{21}H_{20}O_6$, Figure 1), a polyphenol extracted

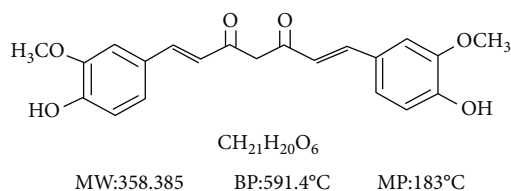


FIGURE 1: The chemical structure of Cur.

from turmeric, was first isolated in 1870. Recent evidence suggests that Cur protects against ischemia injury (IR) of organs by antioxidation mechanisms, inhibiting apoptosis, inhibiting inflammatory reaction, and reducing lipid peroxidation [7]. Several studies have investigated whether supplementation with Cur improves renal pathology and renal function indexes in animal models of RIRI [4, 8, 9]. Nevertheless, scattered evidence and insufficient mechanisms have impeded the translation of laboratory results to the clinic. Systematic reviews and meta-analyses of animal studies play a pivotal role in drug development, and the clarification of physiological and pathological mechanisms could contribute to this transformation [10]. The present systematic review and meta-analysis were performed to determine the effectiveness and the mechanisms of Cur in RIRI animal models.

2. Materials and Methods

2.1. Search Strategies. Eight frequently used databases including PubMed, Cochrane Library, Embase, Wanfang database, China National Knowledge Infrastructure (CNKI), VIP database (VIP), and China Biology Medicine disc (CBM) were searched using the term “Curcumin” AND “Renal ischemia” for Cur in treatment of animal model of RIRI. The time of publication ranges from its inception to February 2020. In addition, the reference list of related studies was also searched for eligible studies.

2.2. Eligibility Criteria. The inclusion criteria were prespecified as follows: (1) the animal model of RIRI established by any way; (2) the treatment group accepted Cur as monotherapy at any dose and mode administration, while the control group accepted nonfunctional liquid or blank by the same dose and mode administration; (3) the primary outcome was renal pathology and/or glomerular filtration rate (GFR) and/or creatinine clearance (CCr) and/or serum creatinine (SCr) and/or blood urea nitrogen (BUN) and/or 24-hour urine protein, while the secondary outcome was the mechanisms of Cur for RIRI. The exclusion criteria were as follows: (1) not RIRI model, (2) not monotherapy, (3) no control group, and (4) duplicate publication.

2.3. Data Extraction. Two authors were appointed to extract the following data from included studies: (1) the surname of the first author and publication year; (2) the feature of animals including age, weight, sex, male/female, and number; (3) the method of RIRI model establishment and anesthesia; (4) the dose, mode administration, and duration time of the trial group and the same information of the control group; (5) the outcome index. The data of the highest dose and the result of the peak time point were extracted for analysis when multiple-dose and measurement time groups existed.

2.4. Quality Assessment. The CAMARADES 10-item quality checklist [2] with minor change was adopted to assess the quality of included studies. The change point is listed as follows: (F) use of anesthetic without significant intrinsic renoprotection and nephrotoxicity. Two authors independently assessed eligible studies, and the difference was settled by correspondence authors.

2.5. Statistical Analysis. The RevMan 5.3 software was used for statistical analysis. If meta-analysis is not applicable, the performing comparisons between groups for individual studies will be used. All data were considered as continuous data, and the combined effect size utilizes standard mean difference (SMD) or mean difference (MD) to estimate. The heterogeneity was assessed by I^2 statistic. According to I^2 statistic, a fixed effects model ($I^2 < 50\%$) or a random-effects model ($I^2 > 50\%$) was selected. The P value was considered statistically significant when the score < 0.05 .

3. Results

3.1. Study Selection. Eighteen eligible comparison groups [4, 8, 9, 11–25] were included in the present study. The search process according to prespecified search strategies is shown in Figure 2.

3.2. Characteristics of Included Studies. Eleven English studies [4, 8, 9, 11–16, 24, 25] and seven Chinese studies [17–23] published from 2008 to 2019 were identified. One of the studies [22] was a non-peer-reviewed dissertation, and the remaining studies were peer-reviewed journal studies. As for animal species, SD rats were used in six studies [12, 16, 18, 20–22, 24], Wistar rats in five [4, 9, 17, 19, 23, 25], BALB/C mice in one [8], and C57/B6 mice in one [11]. Occluding renal vessel was adopted by sixteen studies [4, 8, 9, 11–19, 21, 22, 24, 25] to establish the RIRI model and sports training by two studies [20, 23] to simulate renal ischemia. Detailed information regarding the source, mode, and quality of Cur is displayed in Table 1. Five studies [4, 9, 19, 20, 23] used a dose gradient of Cur by oral administration ranging from 10 mg/kg/d to 200 mg/kg/d; seven studies [11, 12, 17, 19, 21, 24, 25] used intravenous administration ranging from 4 mg/kg/d to 100 mg/kg/d; three studies [8, 18, 22] used intraperitoneal injection ranging from 100 mg/kg/d to 200 mg/kg/d. Regarding primary outcome, renal pathology was measured in twelve studies [4, 8, 9, 11–13, 15, 18, 19, 22–25], BUN in fourteen studies [8, 9, 12, 13, 16–25], SCr in fifteen studies [4, 8, 9, 11, 16–25], and CCr in one study [13]. Mechanistic indicators and other details of the eighteen studies are summarized in Table 2.

3.3. Study Quality. The scores of all studies ranged from 3 to 6 with a mean score of 5.22. The methodological quality is shown in Table 3.

3.4. Effectiveness

3.4.1. Renal Pathology. Compared with the control group, four studies showed [13, 18, 23, 24] that the Cur group had lesser degrees of macroscopic congestion, edema, and

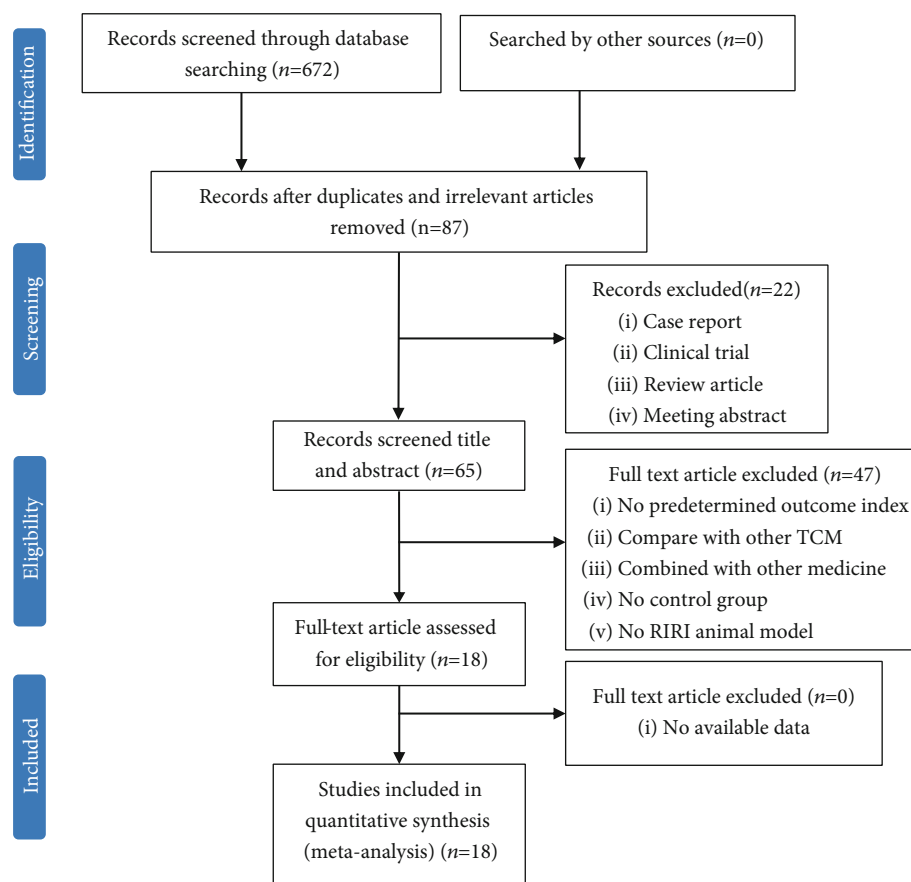


FIGURE 2: Summary of the process for identifying candidate studies.

detachment of the basement membrane from glomeruli. In eleven studies [4, 8, 11–13, 15, 18, 19, 22–24], Cur mitigated turbidity and swelling and water and vacuole degeneration; the brush-like edges disappeared, and some tubular epithelial cells appeared coagulated, with necrosis of renal tubular epithelial cells. Of these, four studies [4, 8, 15, 22] utilized various renal tubular pathological scores [26, 27] to assess the renal tubular injury and found by quantification that Cur could reduce the renal tubular pathological injury.

3.4.2. Renal Function Index. Meta-analysis of 14 studies [4, 8, 9, 11, 12, 16–21, 23–25] indicated that the SCr level of the Cur groups is significantly below than that of the control groups ($n = 301$, SMD -2.08 , 95% CI $(-2.43-1.73)$, $P < 0.00001$; heterogeneity: $\chi^2 = 144.42$, $I^2 = 91\%$, Figure 3). This result was also showed in the dissertation [22] ($P < 0.05$). The funnel plot of the fourteen studies showed an approximately equal number of articles; however, there may have been asymmetric distribution on the central axis, indicating publication bias (Figure 4). Meta-analysis of 13 studies [8, 9, 12, 13, 16–23, 25] indicated that the serum level of BUN of the Cur groups is significantly below than that of the control groups ($n = 281$, SMD -1.35 , 95% CI $(-1.68, -1.01)$, $P < 0.00001$; heterogeneity: $\chi^2 = 170.20$, $I^2 = 93\%$, Figure 5). This result of BUN in the dissertation [22] showed similar conclusion ($P < 0.05$). One study [13] indicates that CCr could be increased by Cur ($P < 0.05$).

3.4.3. Important Mechanism Indicator. In terms of anti-inflammatory mechanism, meta-analysis of five studies [12, 15, 17, 20, 21] and four studies [12, 14, 17, 20] manifested that Cur could significantly reduce the serum level of tumor necrosis factor (TNF- α) ($n = 130$, SMD -2.10 , 95% CI $(-2.58, -1.62)$, $P < 0.00001$; heterogeneity: $\chi^2 = 28.86$, $I^2 = 86\%$, Figure 6(a)) as well as the level of TNF- α in renal tissue ($n = 108$, SMD -0.95 , 95% CI $(-1.46, -0.43)$, $P = 0.0003$; heterogeneity: $\chi^2 = 67.91$, $I^2 = 96\%$, Figure 6(b)). In addition, Cur was reported to reduce the level of Interleukin-6 (IL) in renal tissue [12, 17] as well as the serum level of IL-1 β [14, 20] and Interferon- γ (IFN- γ) [14, 20] ($P < 0.05$). In terms of antioxidant mechanism, meta-analysis of four studies showed that Cur significantly increased the serum level of superoxide dismutase (SOD) [4, 23] ($n = 37$, SMD 0.49 , 95% CI $(0.04, 0.93)$, $P = 0.03$; heterogeneity: $\chi^2 = 6.11$, $I^2 = 84\%$, Figure 7) as well as the level of SOD in renal tissue [4, 22] ($P < 0.05$). Serum level of Malondialdehyde (MAD) [4, 9, 23] ($n = 49$, SMD -1.22 , 95% CI $(-1.86, -0.58)$, $P = 0.0002$; heterogeneity: $\chi^2 = 2.21$, $I^2 = 10\%$, Figure 8(a)) was significantly reduced by Cur. Although MAD in renal tissue of dissertation [22] showed the same conclusion, it showed no difference by meta-analysis of two studies [4, 25] ($n = 26$, SMD -0.53 , 95% CI $(-1.52, -0.46)$, $P = 0.3$; heterogeneity: $\chi^2 = 1.50$, $I^2 = 33\%$, Figure 8(b)). In terms of antiapoptosis, two studies [22, 23] showed that Bcl-2-associated X protein/B cell lymphoma 2 (Bacl-2/Bax) was

TABLE 1: Information of curcumin of each study.

Study (year)	Specifications (purity)	Source	Quality control reported
Ni (2019) [24]	Dry powder	Shanghai Yuanye Biotechnology Co., Ltd.	Batch number: MO307RF
Chen (2018) [8]	NM	NM	NM
Zhang (2018) [12]	Dry powder	Sigma, St. Louis, MO	HPLC
Hu (2018) [23]	Dry powder (>99%)	Shaanxi Yuantai Biotechnology Company	Batch number: 17012571
Kaur (2016) [13]	Dry powder	Central Drug House Pvt. Ltd., India	NM
Liu (2016) [9]	Dry powder	Sigma, St. Louis, MO	HPLC
Xu (2016) [21]	Dry powder	Sigma, St. Louis, MO	HPLC
Najafi (2015) [25]	Dry powder	Sigma, St. Louis, MO	HPLC
Chen (2013) [16]	NM	NM	NM
Wang (2013) [19]	Dry powder (>90%)	Wuhan Zhongxi Instrument Daquan Company	HPLC
Hammad (2012) [15]	Dry powder	Sigma, St. Louis, MO	HPLC
Niu (2012) [20]	Dry powder (>95%)	Shanghai Ronghe Pharmaceutical Technology Development Co., Ltd.	Batch number: 110107
Nian (2012) [18]	Dry powder	Sigma, St. Louis, MO	HPLC
Tao (2012) [22]	Dry powder	Biobasic Canada Inc.	HPLC
Awad (2011) [14]	Dry powder	Sigma, St. Louis, MO	HPLC
Li (2011) [17]	Dry powder ($\geq 90\%$)	Wuhan Zhongxi Instrument Daquan Company	Batch number: HB108YHSY
Rogers (2011) [11]	Dry powder	Sigma, St. Louis, MO	HPLC
Bayrak (2008) [4]	NM	NM	NM

HPLC: high-performance liquid chromatography; NM: not mentioned.

greater in the Cur group than in the control group ($P < 0.05$). Two studies [9, 14] reported that Cur could reduce the serum level of caspase-3 ($P < 0.5$).

3.4.4. Subgroup Analysis. In fourteen peer-reviewed studies, we explored potential confounding factors (including animals chosen, methods of model establishment, modes of administration, medication times, and ischemic times) that may increase the heterogeneity of outcome measures using subgroup analysis of SCr. The subgroup analysis of animal species showed that the effect size of the mouse group was better than that of rats ($SMD_m -3.92$ vs. $SMD_r -1.89$, $P = 0.0008$, Figure 9(a)) without a significant decline in heterogeneity between subgroups. No difference was seen among modeling methods (i.e., occlusion of renal vessels vs. sport training) ($SMD_o -2.01$ vs. $SMD_s -2.49$, $P = 0.29$, Figure 9(b)), diverse mode administration (including oral gavage, intravenous injection, and intraperitoneal injection) ($SMD_{ip} -2.13$ vs. $SMD_{iv} -1.82$ vs. $SMD_{po} -2.07$, $P = 0.35$, Figure 9(c)), and diverse medication times (including repeated administration and single administration) ($SMD_r -2.11$ vs. $SMD_s -1.84$, $P = 0.46$, Figure 10(a)). However, the effect size displayed substantial discrepancy in terms of methods of blocking blood vessels. Unilateral renal artery ligation with contralateral nephrectomy (uIRIx) with 4.7% weight showed a higher effect than did unilateral renal artery ligation (uIRI) or bilateral renal artery ligation RIRI (bIRI) ($SMD_{uIRIx} -14.52$ vs. $SMD_{bIRI} -2.19$ vs. $SMD_{uIRI} -1.74$, $P < 0.00001$, Figure 10(b)). Finally, we analyzed the effects of various ischemic times on the effect size of SCr and the result indicated that longer ischemia times were associated with

effect size ($SMD_{30min} -2.42$ vs. $SMD_{45min} -3.44$ vs. $SMD_{60min} -1.29$, $P = 0.009$, Figure 10(c)).

4. Discussion

4.1. Summary of Evidence. This is the first preclinical systematic review to estimate the efficacy and possible mechanism of Cur for the RIRI animal model. The 18 moderate quality studies including 396 animals manifested that Cur alleviated renal pathological injury via multiple signaling pathways.

4.2. Limitations. Some limitations that may affect the accuracy of the study should be considered. First, the source of studies was only from Chinese and English databases, and this may produce selection bias. Second, the calculation of sample size and blinding outcome measurements would be pivotal for quality control of research, and this was not shown in included studies. Third, only one study [13] reported CCr, which is the most valuable clinical index for renal function. Fourth, given the fact that RIRI could not be predicted in the clinic, the preventive effect of Cur alone is insufficient. Fifth, though the sensitivity analysis and subgroup analysis were done, the high heterogeneity of curcumin for serum creatinine, BUN, TNF-alpha, and SOD cannot be ignored. Sixth, using funnel plots, there was publication bias that should be managed by expanding the sample size.

4.3. Implications. High-quality methodologies of studies are the cornerstones of translating animal research into clinical drug treatments for human disease [28]. Although the score

TABLE 2: Characteristics of the included studies.

Study (year)	Species (sex, <i>n</i> = experimental/control group)	Weight	Model (method)	Anesthetic	Treatment group (method to astragal sides)	Control group	Outcome index (time)	Intergroup differences
Ni (2019) [24]	SD rats (male, 10/10)	230-260 g	Block the right renal pedicle vessels for 45 minutes and then reflow for 24 hours	3.5% chloral hydrate (10 mL/kg)	By intravenous injection of 1 mL of 0.1% DMSO containing 100 mg/kg curcumin at 2 hours before establishing the model	By intravenous injection of 1 mL of 0.1% DMSO at 2 hours before establishing the model	(1) Renal pathology (2) The serum levels of β_2 -MG, UAER, BUN, and Cr (3) The expression and the transcriptional efficiency of miR-146a, nNOS, eNOS, and iNOS (4) The serum levels of NO and cGMP	(1) $P < 0.05$ (2) $P < 0.05$ (3) $P < 0.05$ (4) $P < 0.05$
Chen (2018) [8]	BALB/c mice (male, 12/12)	NM	Block the bilateral renal arteries for 30 minutes and then reflow for 24 hours	Ketamine (80 mg/kg) and xylazine (10 mg/kg)	By intraperitoneal injection of curcumin before establishing the model	By intraperitoneal injection of isovolumic NS before establishing the model	(1) The serum level of BUN and Cr (2) Kidney fibrosis (3) The expression of (ECM) protein expression (4) Western blot of APPL1 and phosphorylated Akt	(1) $P < 0.05$ (2) $P < 0.05$ (3) $P < 0.05$ (4) $P < 0.05$
Zhang (2018) [12]	SD rats (male, 10/10)	280-320 g	Block the left renal pedicle vessels for 45 minutes and then reflow for 24 hours	Pentobarbital sodium (50 mg/kg)	By intravenous injection of 60 mg/kg curcumin at 45 minutes before establishing the model	By intravenous injection of isovolumic NS before establishing the model	(1) Renal pathology (2) The serum levels of BUN and Cr (3) The serum level of TNF- α , IL-6, and IL-8 (4) The TNF- α , IL-6, and IL-8 content in renal tissue (5) Western blot of JAK2, p-JAK2, STAT3, p-STAT3, p65, and p-p65	(1) $P < 0.01$ (2) $P < 0.05$ (3) $P < 0.05$ (4) $P < 0.05$ (5) $P < 0.05$
Hu (2018) [23]	Wistar rats (male, 24/24)	218.4 \pm 10.7 g	8-week incremental load swimming training ⁽¹⁾	Ethyl ether	By oral gavage of 200 mg/kg/d curcumin during the swimming training	By oral gavage of isovolumic CMC-Na during the swimming training	(1) Renal pathology (2) The serum levels of BUN and Cr (3) The serum levels of testosterone and corticosterone (4) The serum levels	(1) $P < 0.05$ (2) $P < 0.05$ (3) $P < 0.05$ (4) $P < 0.01$

TABLE 2: Continued.

Study (year)	Species (sex, <i>n</i>) = experimental/control group)	Weight	Model (method)	Anesthetic	Treatment group (method to astragal sides)	Control group	Outcome index (time)	Intergroup differences
Kaur (2016) [13]	Wistar rats (female, 6/6)	175–225 g	Block the bilateral renal arteries for 40 minutes and then reflow for 24 hours	Ethyl ether	By oral gavage of 60 mg/kg curcumin at 60 minutes before establishing the model	By oral gavage of nothing at 60 minutes before establishing the model	of T-AOC, SOD, and MDA (5) Effect of apoptosis and Bcl-2/Bax expression in rat renal tissue (6) The expression of Nrf-2 and HO-1 in renal tissue (1) Renal pathology (2) CCL (3) The serum levels of BUN and UA (4) Estimation of sodium/potassium levels and macroproteinuria (5) The MPO, GSH TBARS, and SAG content in renal tissue	0.05 (5) <i>P</i> < 0.05 (6) <i>P</i> < 0.05 (1) <i>P</i> < 0.05 (2) <i>P</i> < 0.05 (3) <i>P</i> < 0.05 (4) <i>P</i> < 0.05 (5) <i>P</i> < 0.05
Liu (2016) [9]	Wistar rats (NM, 6/6)	150–200 g	Block the bilateral renal arteries for 45 minutes and then reflow for 6 hours	Pentobarbital sodium	By oral gavage of 10 mg/kg/d curcumin for 2 weeks before establishing the model	By oral gavage of isovolumic corn oil for 2 weeks before establishing the model	(1) The serum levels of BUN, Cr, and LDH (2) The serum level of MPO (3) The serum level of MDA and GSH (4) The caspase-3 and KIM-1 content in renal tissue (5) The serum levels of IL-10 and IFN- γ	(1) <i>P</i> < 0.001 (2) <i>P</i> < 0.001 (3) <i>P</i> < 0.001 (4) <i>P</i> < 0.001 (5) <i>P</i> < 0.001
Xu (2016) [21]	SD rats (male, 15/15)	200–250 g	Block the bilateral renal arteries for 60 minutes and then reflow for 24 hours	3% chloral hydrate (300 mg/kg)	By intravenous injection of 100 mg/kg curcumin for 5 days before establishing the model	By intravenous injection of isovolumic NS for 5 days before establishing the model	(1) The serum levels of BUN and Cr (2) The serum level of TNF- α , HO-1, and ICAM-1 (3) The content of MPO in renal tissue	(1) <i>P</i> < 0.01 (2) <i>P</i> < 0.01 (3) <i>P</i> < 0.01

TABLE 2: Continued.

Study (year)	Species (sex, <i>n</i> = experimental/control group)	Weight	Model (method)	Anesthetic	Treatment group (method to astragal sides)	Control group	Outcome index (time)	Intergroup differences
Najafi (2015) [25]	Wistar rats (male, 7/7)	200–250 g	Block the bilateral renal arteries and veins for 30 minutes and then reflow for 72 hours	Ethyl ether	By intravenous injection of 20 mg/kg curcumin every 24 hours during 72 h reperfusion period	By intravenous injection of isovolumic NS every 24 hours during 72 h reperfusion period	(1) Renal pathology (2) The serum levels of BUN and Cr (3) The MDA and FRAP content in renal tissue (4) Leukocyte infiltration in renal tissue	(1) <i>P</i> < 0.05 (2) <i>P</i> > 0.05 (3) <i>P</i> < 0.05 (4) <i>P</i> < 0.01
Chen (2013) [16]	SD rats (NM, 10/10)	250–300 g	Block the bilateral renal arteries and veins for 45 minutes and then reflow for 3 hours	Pentobarbital sodium (35 mg/kg)	By oral gavage of 12.5 mg/kg/d curcumin for 2 days before establishing the model	By oral gavage of nothing for 2 days before establishing the model	(1) The serum levels of BUN and Cr (2) EF, LV, SV, SP, and ESPVR (3) The serum levels of CK-MB and cTnI (4) The content of MDA and TNF- α in heart tissue	(1) <i>P</i> < 0.05 (2) <i>P</i> < 0.05 (3) <i>P</i> < 0.05 (4) <i>P</i> < 0.05
Wang (2013) [19]	Wistar rats (male, 8/8)	220–280 g	Resect right kidney and block the left renal pedicle vessels for 45 minutes and then reflow for 24 hours	2% pentobarbital sodium (45 mg/kg)	By intravenous injection of 20 mg/kg curcumin at 30 minutes before establishing the model	By intravenous injection of nothing at 30 minutes before establishing the model	(1) Renal pathology (2) The serum levels of BUN and Cr (3) The NF- κ B content in renal tissue	(1) <i>P</i> < 0.05 (2) <i>P</i> < 0.05 (3) <i>P</i> < 0.05
Hammad (2012) [15]	Wistar rats (male, 8/8)	280–321 g	Block the left renal pedicle vessels for 45 minutes and then reflow for 24 hours	Ketamine hydrochloride (70 mg/kg) and pentobarbital sodium (20 mg/kg)	By oral gavage of 200 mg/kg/d curcumin for 5 days before establishing the model until the day after modeling	By oral gavage of isovolumic CMC-Na for 5 days before establishing the model until the day after modeling	(1) Renal pathology (2) GFR (3) RBF (4) UV (5) UNaV (6) FENa (7) The serum levels of TNF- α	(1) <i>P</i> < 0.05 (2) <i>P</i> < 0.0001 (3) <i>P</i> < 0.0001 (4) <i>P</i> > 0.05 (5) <i>P</i> > 0.05 (6) <i>P</i> > 0.05 (7) <i>P</i> < 0.05

TABLE 2: Continued.

Study (year)	Species (sex, <i>n</i> = experimental/control group)	Weight	Model (method)	Anesthetic	Treatment group (method to astragal sides)	Control group	Outcome index (time)	Intergroup differences
Niu (2012) [20]	SD rats (male, 8/8)	200–280 g	Treadmill training 6 days and rest 1 day a week, circularly for 5 weeks	NM	By oral gavage of 200 mg/kg/d curcumin during the treadmill training	By oral gavage of isovolumic NS during the treadmill training	(1) The serum level of BUN and Cr (2) Renal coefficient (3) The serum level of TNF- α , IL-1 β (IL-18) (4) The TNF- α content in renal tissue	(1) $P < 0.05$ (2) $P < 0.01$ (3) $P < 0.05$ (4) $P < 0.01$
Nian (2012) [18]	SD rats (female/male, 10/10)	200–250 g	Resect right kidney and block the right renal pedicle vessels for 45 minutes and then reflow for 2 hours	7% chloral hydrate	By intraperitoneal injection of 200 mg/kg/d curcumin for 3 days before establishing the model	By intraperitoneal injection of isovolumic NS for 3 days before establishing the model	(1) Renal pathology (2) The serum level of BUN and Cr (3) The HIF-1 α content in renal tissue	(1) $P < 0.05$ (2) $P < 0.05$ (3) $P < 0.05$ (3) $P < 0.05$
Tao (2012) [22]	SD rats (male, 12/12)	220–260 g	Block the right renal pedicle vessels for 45 minutes and then reflow for 24 hours	10% chloral hydrate (350 mg/kg)	By intraperitoneal injection of 1 mL of 0.1% DMSO containing 100 mg/kg curcumin at 2 hours before establishing the model	By intraperitoneal injection of isovolumic 0.1% DMSO at 2 hours before establishing the model	(1) Renal pathology (2) The serum level of BUN and Cr (3) The level of MDA and SOD in renal tissue (4) The expression of Bax and Fas (5) Effect of apoptosis Bcl-2/Bax and Fas expression in rat renal	(1) $P < 0.05$ (2) $P < 0.05$ (3) $P < 0.05$ (4) $P < 0.05$ (5) $P > 0.05$
Awad (2011) [14]	SD rats (male, 12/12)	200–250 g	Block the bilateral renal content in renal tissue, arteries, and veins for 40 minutes and then reflow for 24 hours	Chloral hydrate (400 mg/kg)	By oral gavage of 100 mg/kg/d curcumin for 5 days before establishing the model	By oral gavage of isovolumic NS for 5 days before establishing the model	(1) The serum level of IL-1 β , TGF- β , IL-18, IL-12, and IFN- γ (2) TNF- α , IL-1 β , TGF- β , IL-18, IL-12, and IFN- γ (3) The TGF- β content in lung tissue (4) The caspase-3 content in lung tissue	(1) $P < 0.05$ (2) $P < 0.05$ (3) $P > 0.05$ (4) $P < 0.05$

TABLE 2: Continued.

Study (year)	Species (sex, <i>n</i> = experimental/control group)	Weight	Model (method)	Anesthetic	Treatment group (method to astragal sides)	Control group	Outcome index (time)	Intergroup differences
Li (2011) [17]	Wistar rats (male, 24/24)	200–280 g	Block the right renal pedicle vessels for 60 minutes and then reflow for 24 hours	3% pentobarbital sodium (30 mg/kg)	By intravenous injection of 20 mg/kg curcumin at 30 minutes before establishing the model	By intravenous injection of isovolumic of NS at 30 min before establishing the model	(1) The serum level of BUN and Cr (2) Renal coefficient (3) The TNF- α and IL-6 content in renal tissue and serum (1) Renal pathology (2) The serum level of urea and Cr (3) NF- κ B-p50 subunit in renal APC (4) Phosphorylated NF- κ B-p65 in renal TEC (5) IEC apoptosis (6) The gene expression of TLR4, HSP70, and TNF- α (7) The mRNA expression of CCL5, CCL2, and CXCL2 (8) Neutrophil infiltration in renal tissue (9) SOD mRNA expression (10) The protein expression of tyrosine nitration in renal tissue (11) The gene expression of iNOS (12) The expression of TXNIP	(1) $P < 0.05$ (2) $P < 0.01$ (3) $P < 0.05$ (1) $P < 0.05$ (2) $P < 0.01$ (3) $P < 0.05$ (4) $P < 0.05$ (5) $P < 0.05$ (6) $P < 0.05$ (7) $P < 0.05$ (8) $P < 0.05$ (9) $P < 0.05$ (10) $P < 0.05$ (11) $P < 0.05$ (12) $P < 0.05$
Rogers (2011) [11]	C57/B6 mice (male, 10/10)	NM	Block the bilateral renal arteries for 30 minutes and then reflow for 24 hours	Isoflurane	By intravenous injection of 4 mg/kg/d curcumin at 12 hours before establishing the model	By intravenous injection of 150 mL empty liposome at 12 hours before establishing the model		

TABLE 2: Continued.

Study (year)	Species (sex, <i>n</i> = experimental/control group)	Weight	Model (method)	Anesthetic	Treatment group (method to astragal sides)	Control group	Outcome index (time)	Intergroup differences
Bayrak (2008) [4]	Wistar rats (male, 6/6)	150–200 g	Block the bilateral renal arteries for 45 minutes and then reflow for 24 hours	Xylazine (10 mg kg ⁻¹) and ketamine (70 mg kg ⁻¹)	By oral gavage of 200 mg/kg/d curcumin for 7 days before establishing the model	By oral gavage of nothing for 7 days before establishing the model	(1) Renal pathology (2) The serum level of Cr (3) The serum level of urea and cystatin C (4) The serum level of SOD (5) The serum level of GSH-Px, MDA, NO, and PC (6) The CAT, SOD, GSH-Px, MDA, NO, and PC content in renal tissue (7) The serum level of TAC and TOS	(1) <i>P</i> < 0.05 (2) <i>P</i> < 0.05 (3) <i>P</i> > 0.05 (4) <i>P</i> > 0.05 (5) <i>P</i> < 0.05 (6) <i>P</i> < 0.01 (7) <i>P</i> < 0.001

TABLE 3: Risk of bias of the included studies.

Study	A	B	C	D	E	F	G	H	I	J	Total
Ni (2019) [24]	√	√	√			√				√	5
Chen (2018) [8]	√	√	√		√	√				√	6
Zhang (2018) [12]	√	√	√			√			√	√	6
Hu (2018) [23]	√	√	√			√			√	√	6
Kaur (2016) [13]	√	√	√			√			√	√	6
Liu (2016) [9]	√	√	√			√			√	√	6
Xu (2016) [21]	√	√	√			√				√	5
Najafi (2015) [25]	√	√	√			√			√	√	6
Chen (2013) [16]	√	√				√			√	√	5
Wang (2013) [19]	√	√	√			√				√	5
Hammad (2012) [15]	√	√	√			√			√	√	6
Niu (2012) [20]	√	√							√		3
Nian (2012) [18]	√	√	√			√			√		5
Tao (2012) [22]		√	√			√					3
Awad (2011) [14]	√	√	√			√			√	√	6
Li (2011) [17]	√	√	√			√					4
Rogers (2011) [11]	√	√	√			√				√	5
Bayrak (2008) [4]	√	√	√			√			√	√	6

Note: studies fulfilling the criteria of the following: A: peer-reviewed publication; B: control of temperature; C: random allocation to treatment or control; D: blinded induction of model (group randomly after modeling); E: blinded assessment of outcome; F: use of anesthetic without significant renoprotective activity or nephrotoxicity; G: appropriate animal model (aged, hyperlipemia or hypertensive); H: sample size calculation; I: compliance with animal welfare regulations (including three or more of the following points: preoperative anesthesia, postoperative analgesia, nutrition, disinfection, environment temperature, environment humidity, circadian rhythm, and euthanasia); J: statement of potential conflict of interest.

(mean 5.22) by prudent assessment of included studies was better than that of most studies of traditional Chinese medicine (TCM) [29], there were limitations in terms of blinding and sample size calculation. The blinding methods in animal model establishment and outcome assessment were usually seen as technical difficulties for most studies. Group randomization after modeling, as in Guo et al. [30] and Lei et al. [31], and selecting animals randomly for outcome assessment, as in Chen et al. [8], were regarded as a good solution to overcome this problem and raise the quality of the study. A sample size calculation could avoid the waste of resources caused by oversize and the imprecision of study result by undersizing, and the specific steps could be referred to the literature [32]. In addition, the animal research reporting in vivo experiments (ARRIVE) guidelines are aimed at improving the quality of research reports by guiding complete and transparent reporting of in vivo animal research. These should be adopted in the future study management of Cur for RIRI.

Three main molding methods based on blocking blood vessels were widely utilized in the present study: uIRI in 4 studies [12, 17, 20, 22, 24], bIRI in 7 studies [4, 8, 9, 11, 16, 21, 25], and uIRIx in 2 studies [18, 19]. Subgroup analysis found that the method of uIRIx gave a higher effect size than did uIRI or bIRI ($SMD_{uIRIx} -4.87$ vs. SMD_{bIRI}

-2.19 vs. $SMD_{uIRI} -1.36$, $P < 0.00001$, Figure 10(b)), suggesting that different modeling methods may be the source of high heterogeneity. Therefore, we carefully analyzed the strengths and weaknesses of these three methods and the results are summarized as follows. (1) Regarding the uIRI model, although it is easy to operate and highly repeatable, renal function as an indication of the progression of kidney injury and deterioration is difficult to estimate due to powerful compensation function of the contralateral kidney. (2) Regarding the bIRI model, it is also easy to operate and can perfectly imitate the hemodynamic changes in RIRI patients with shock, sepsis, and burns. However, the degree of renal injury is difficult to control due to the bilateral renal artery ligation. If RIRI is too severe, mice may die in the acute injury phase, and if too mild, the kidneys may fully recover and do not progress to chronic pathologies or chronic kidney disease (CKD) [33, 34]. (3) Regarding the uIRIx model, the study of Finn et al. [35] found that, if the contralateral kidney was removed prior to ischemia, the reflow of blood to the postischemic kidney would be better and conducive to recovery to preserve renal tubular structure and function. Thus, compared to the bIRI model, the uIRIx model allows for longer ischemic time to induce consistent RIRI for studying its progression to chronic pathologies with less variability and it is closer to the clinical characteristics of renal transplant patients. Compared to the uIRI model, the process of the uIRIx model is complex and changeable. The 30% death rate after 2 weeks of uIRIx by Fu et al. cannot be ignored [36]. The good news is that it allows a more accurate functional evaluation of the IRI-injured kidney at several points in time to indicate kidney injury and repair. In summary, the bIRI and uIRIx models are instrumental in monitoring renal indexes at multiple time points, but with bigger variations and significant animal loss, especially in long-term studies. The uIRI model is suitable for experiments that require a long time to observe changes of renal indexes because it can achieve the target of long-term animal survival [37]. Reviewing the included studies according to this theory, we found that the one study [18] which used the uIRI model to assess the effect of Cur for RIRI at various time points (1, 4, and 24 hours) may cause inaccurate prediction in consideration of the compensation by the contralateral kidney. We suggest that future studies need to choose the modeling method according to the specific purpose of the experimental design.

The subgroup analysis of animal species indicated that the effect size in the mouse group was better than that in the rat group ($SMD_m -2.03$ vs. $SMD_r -1.85$, $P = 0.0006$, Figure 9(a)), suggesting that diverse animals may be one of the sources of high heterogeneity. Considering high cost and low efficiency of large size for experimenters to test the initial efficacy and mechanism of the drug, rodents have become the mainstream experimental animals since the 1960s [38]. Because of the availability of transgenic models and reduced drug consumption for experimental testing, there have been more studies using mice to establish the RIRI model in the past decade [34]. Despite the advantages it possesses, it cannot be ignored that the mouse model entails

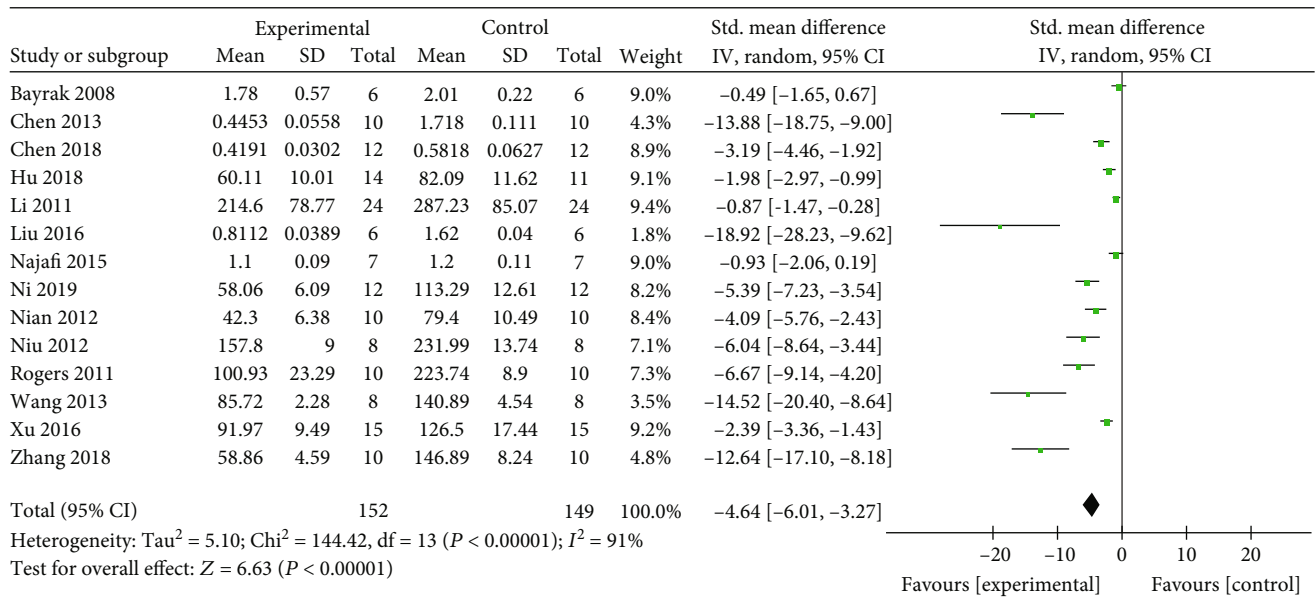


FIGURE 3: The forest plot: effects of Cur for decreasing SCr compared with the control group.

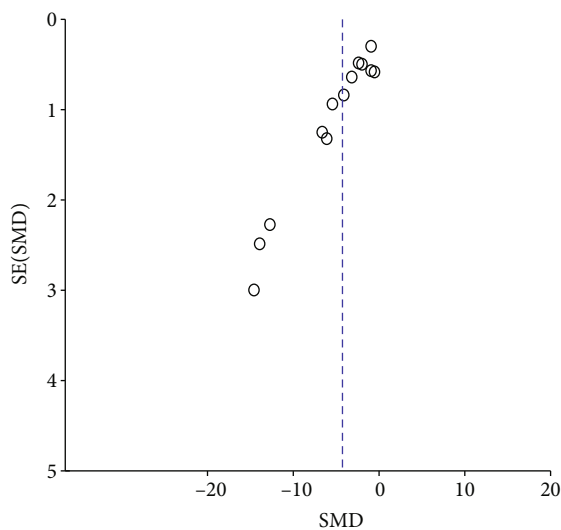


FIGURE 4: The funnel plot of SCr.

greater variations, causing inconsistency in results. Thus, higher technical requirements are necessary if mice are selected as experimental animals, and the experience of mouse modeling summarized by Wei et al. [34] could be referred to in future experiments of RIRI. In addition, RIRI is a common complication for patients with infection, shock, postoperative hypoperfusion, bleeding, and dehydration; these are difficult to predict and prevent in clinical practice. However, all included studies were designed to determine whether the animals pretreated with Cur could have reduced damage of RIRI. Although the outcome was positive, it remains unknown if the effect of Cur on animals post-RIRI is similar to clinical cases of RIRI, and this may limit its clinical application. Therefore, further research designed to

assess the effect of Cur for animals with post-RIRI and comparisons of the differences between pretreatment and post-treatment of Cur for RIRI are to be encouraged.

RIRI involves several mechanisms, including mitochondrial damage, oxidative stress, calcium overload, and tissue inflammation responses [39]. (1) In the early stage of renal ischemia, neutrophils and monocytes in circulating blood are recruited by various cytokines, initiating the host's defenses. This process activates the nuclear factor kappa-B (NF- κ B) and further increases the release of inflammatory factors to break the proinflammatory/anti-inflammatory balance [40]. Cur was reported to alleviate renal inflammation caused by RIRI by activating the JAK2/STAT3 signaling pathway to reduce the expression of NF- κ B [12] by directly reducing the crucial inflammation factor TNF- α [9, 17, 20, 21]; it then reduces inflammatory factors including IL-1 β , IL-8, IL-18, and intercellular cell adhesion molecule-1. (2) Oxidative stress damage is the main cause of RIRI. After vascular recanalization, vascular endothelial cells activated by reperfusion trigger the production of reactive oxygen species (ROS) and oxygen free radicals, causing oxidative stress. These processes downregulate the antioxidant enzyme system including catalase (CAT), SOD, and glutathione peroxidase (GSH-Px) [40, 41]. Cur was reported to reduce renal oxidative damage via reducing expression of N-methyl-D-aspartic acid (NMDA) receptor and increasing the expression of nuclear factor erythroid 2-related factor/heme oxygenase-1 (Nrf2/HO-1) to increase antioxidants including glutathione (GSH), SOD, and CAT and then by decreasing activity of oxidases such as MDA, nitric oxide (NO), and protein carbonyl (PC) [4, 9, 21–23]. (3) Apoptosis is a mechanism of tubular cell death in RIRI [40]. The upregulation of proapoptotic protein Bax and the downregulation of antiapoptotic protein Bcl-2 apoptosis are important processes during apoptosis when encountering ischemia [42]. Under the influence of oxidation factors, glycogen synthase

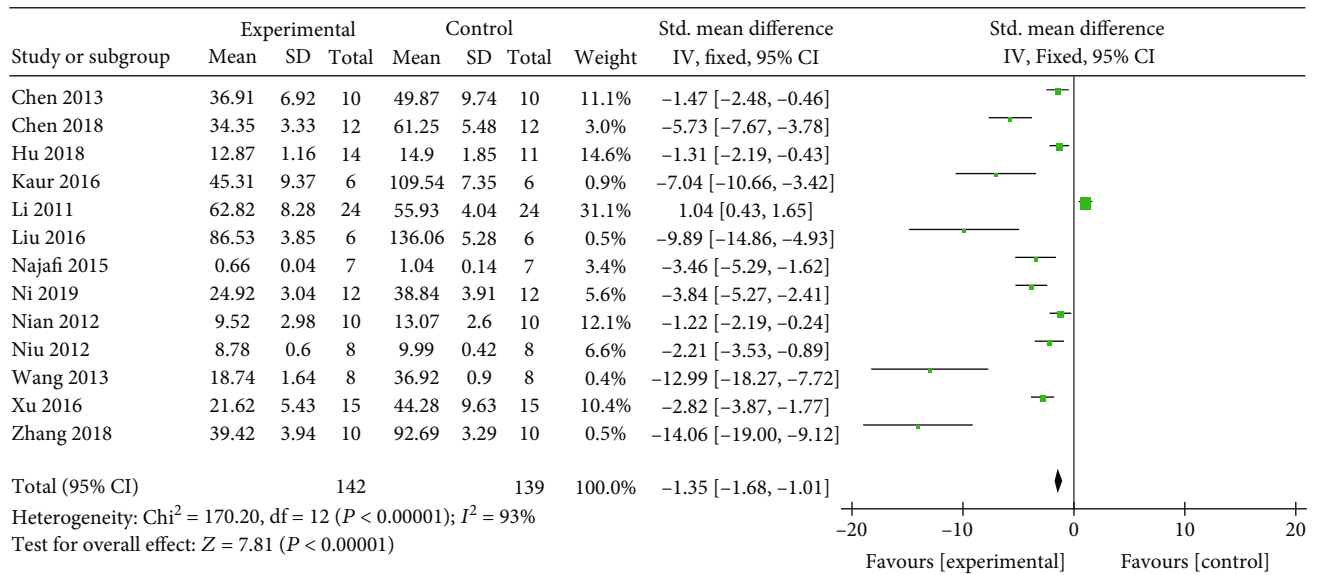


FIGURE 5: The forest plot: effects of Cur for increasing BUN compared with the control group.

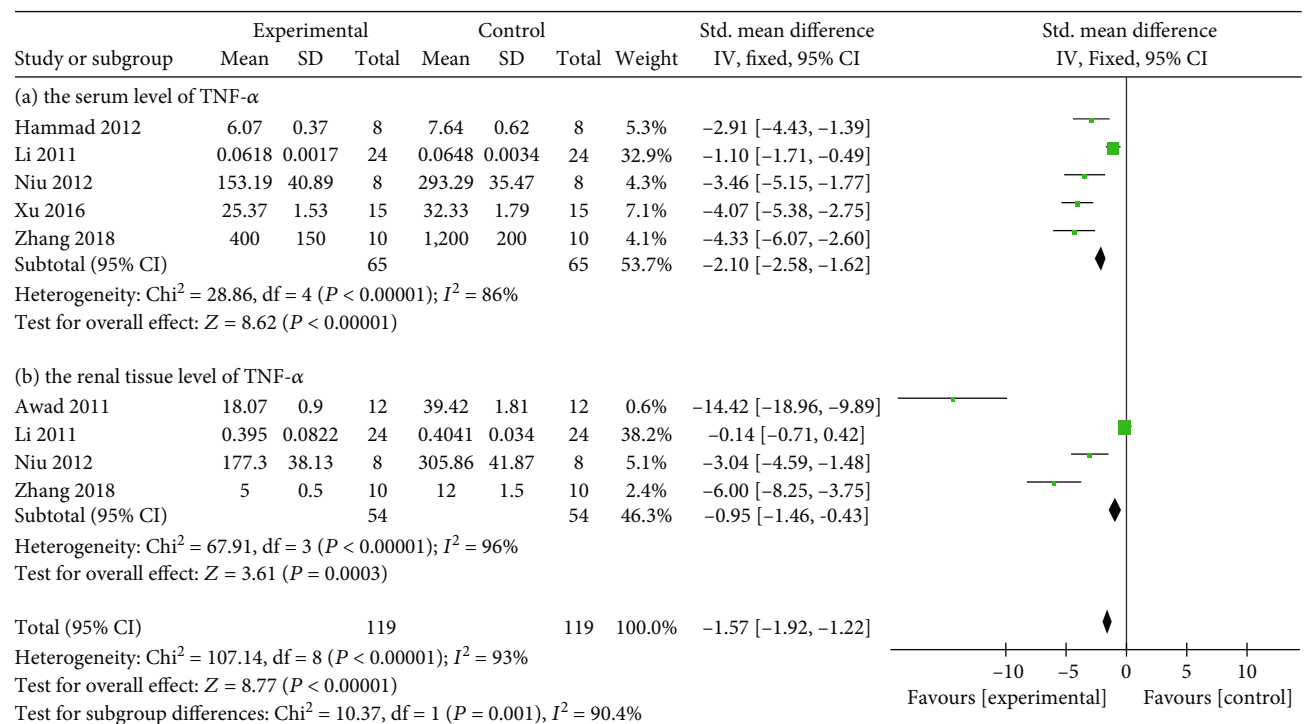


FIGURE 6: (a) The forest plot: effects of Cur for decreasing the serum level of TNF- α compared with the control group. (b) The forest plot: effects of Cur for decreasing the level of TNF- α in renal tissue compared with the control group.

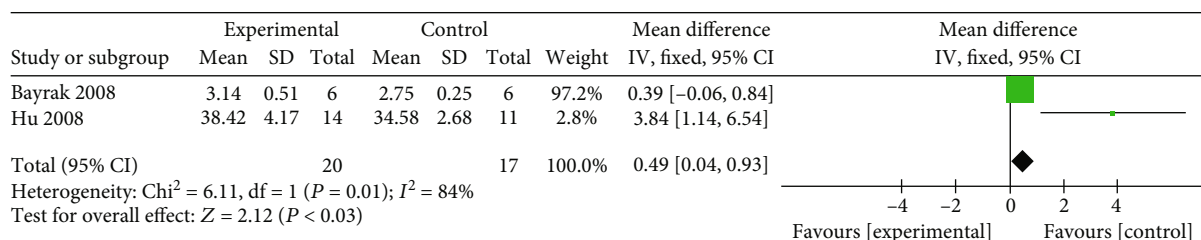


FIGURE 7: The forest plot: effects of Cur for increasing the serum level of SOD compared with the control group.

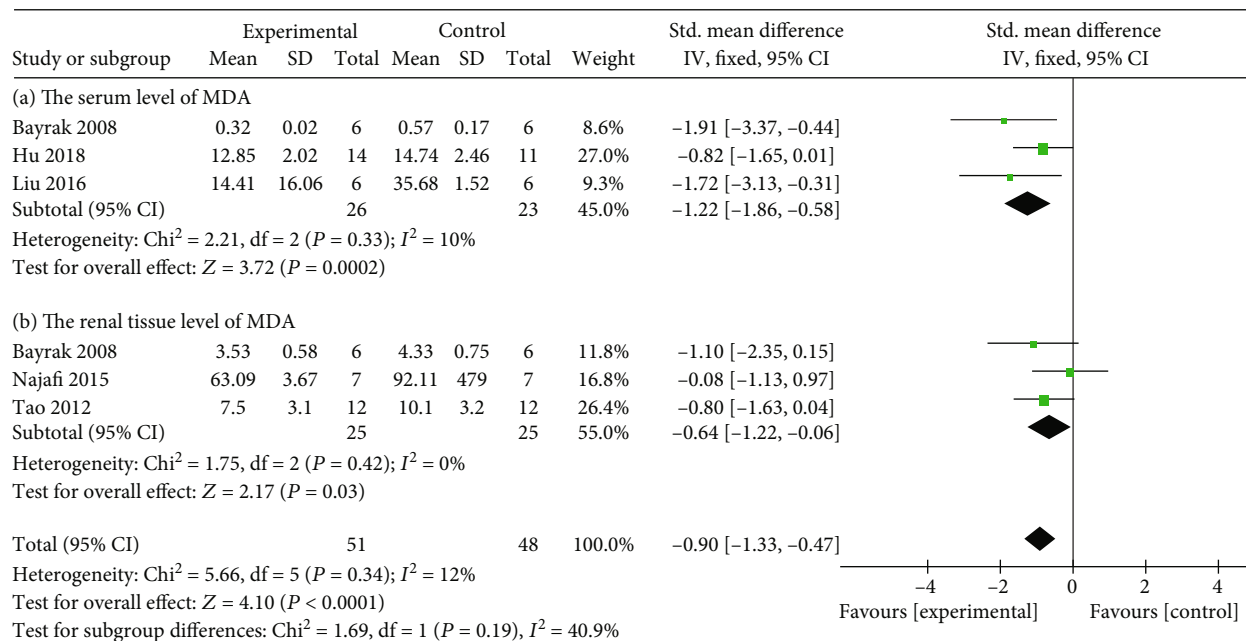


FIGURE 8: (a) The forest plot: effects of Cur for decreasing the serum level of MDA compared with the control group. (b) The forest plot: effects of Cur for decreasing the level of MDA in renal tissue compared with the control group.

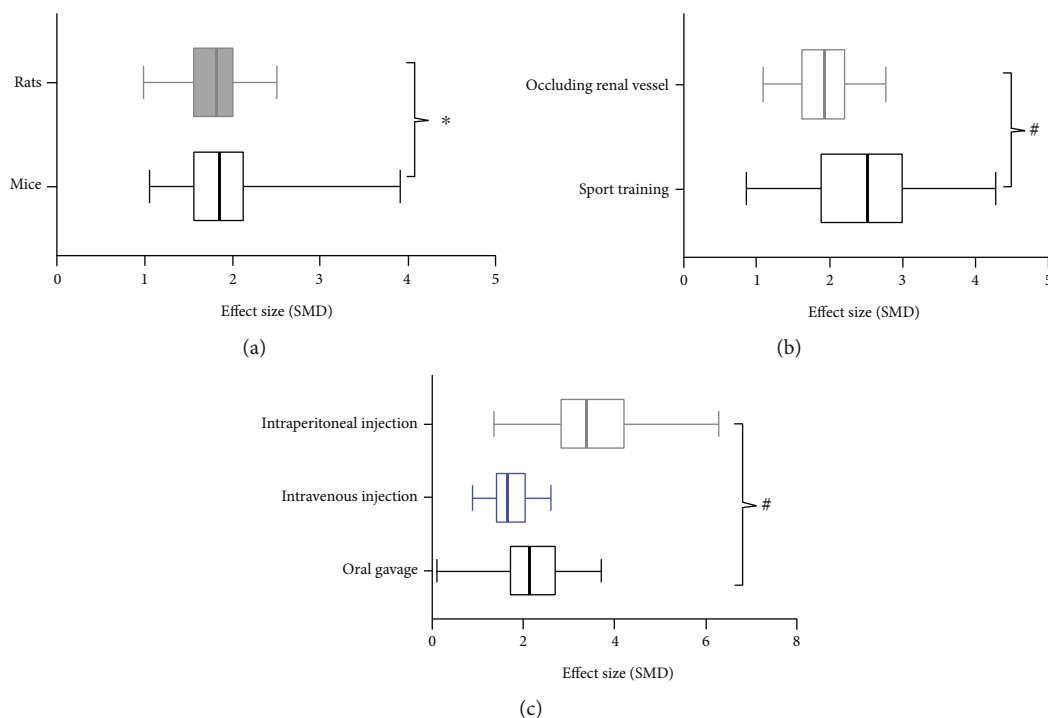


FIGURE 9: Subgroup analyses of the SCR. (a) The different effect sizes between mice and rats; (b) the different effect sizes between occluding renal vessel model group and sport training model group; (c) the different effect sizes between different mode administrations. * $P < 0.05$ between subgroups; # $P > 0.05$ between subgroups.

kinase 3- β (GSK3 β) is activated to mediate apoptosis [43]. Cur was reported to alleviate renal cell apoptosis by inhibiting activation of the PKG/cGMP/NO signaling pathway [9, 14, 22, 24] to enhance the expression of miR-146a, thereby attenuating the expression of caspase-3. It can also upregu-

late Bax and downregulate Bcl-2 by increasing the expression Nrf-2 [23]. (4) There were antifibrotic effects mediated by increasing the expression of adaptor protein phosphotyrosine interacting with PH domain and leucine zipper 1 (APPL1) to inhibit the AKT/MAPK signaling pathway [16] as well as a

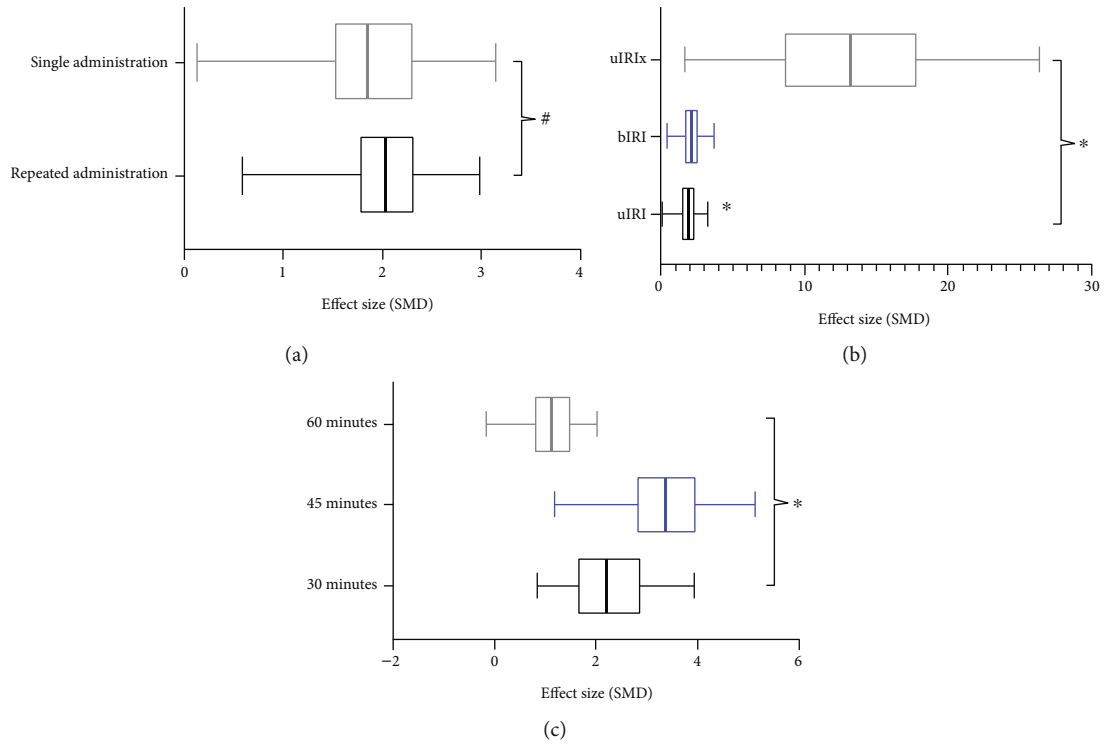


FIGURE 10: Subgroup analyses of the SCR. (a) The different effect sizes between single administration and repeated administration; (b) the different effect sizes between different occluding renal vessel model groups; (c) the different effect sizes between different ischemic times. * $P < 0.05$ between subgroups; # $P > 0.05$ between subgroups.

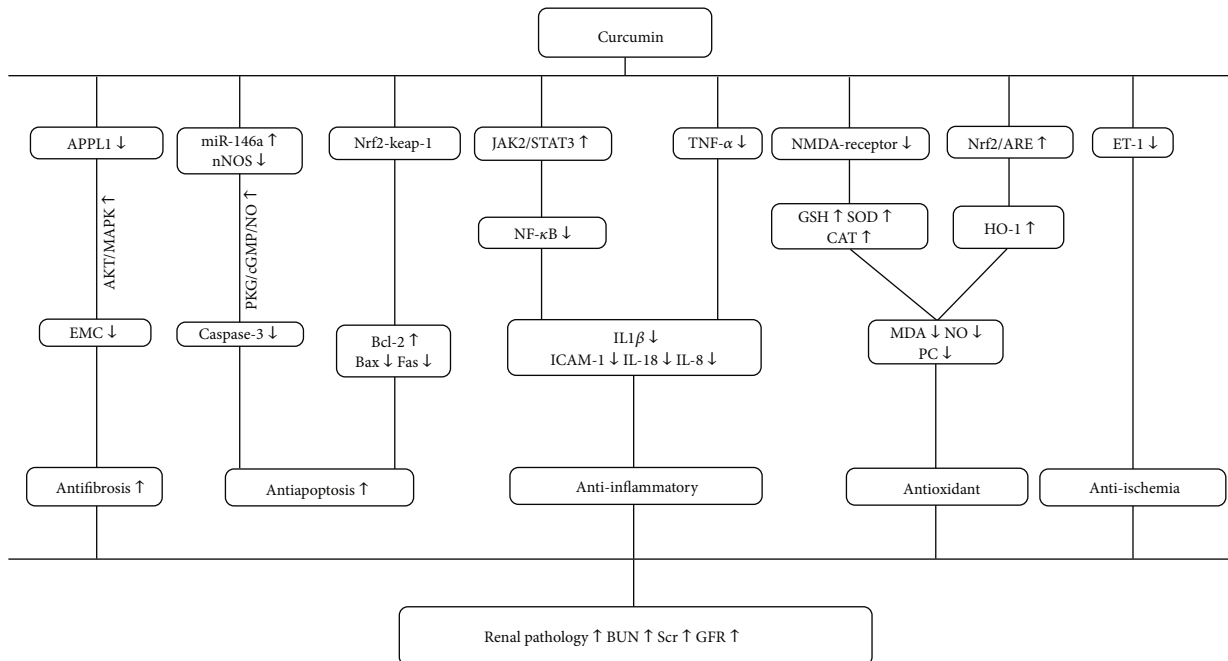


FIGURE 11: A schematic representation of osteoprotective mechanisms of Cur for RIRI.

vasodilative effect by decreasing the expression of endothelin-1 (ET-1) [9]. The mechanism is summarized in Figure 11.

4.4. Conclusion. This preclinical systematic review provided preliminary evidence that Cur partially improves RIRI in

animal models probably via anti-inflammatory, antioxidant, antiapoptosis, and antifibrosis mechanisms, as well as by improving microperfusion. The findings suggest the possibility of developing Cur as a drug for the clinical treatment of RIRI.

Data Availability

Previously reported data were used to support this study. These prior studies and datasets are cited at relevant places within the text as references [8–10, 12–26].

Conflicts of Interest

The authors declare that there is no conflict of interests regarding the publication of this study.

Authors' Contributions

ZHW, QZ, and HW designed the study; ZHW and LHD collected the data; ZHW, YYH, and LHD performed all analyses. All authors contributed to writing of this manuscript. All the listed authors have read and approved the submitted manuscript. Zi-Hao Wang, Li-Hui Deng, and Chang-Wei Chia contributed equally to this work.

Acknowledgments

This project was supported by the Clinical Research Foundation of the 2nd Affiliated Hospital of Wenzhou Medical University (SAHoWMU-CR2018-01-105), Lin He's New Medicine and Clinical Translation Academician Workstation Research Fund (17331208), Wenzhou Science and Technology Bureau Programs (H2015006 and Y20170322), and Programs of Zhejiang Traditional Chinese Medicine Administration (2015ZB077 and 2018ZB080).

References

- [1] G. Manoeuvrier, K. Bach-Ngohou, E. Batard, D. Masson, and D. Treweek, "Diagnostic performance of serum blood urea nitrogen to creatinine ratio for distinguishing prerenal from intrinsic acute kidney injury in the emergency department," *BMC Nephrology*, vol. 18, no. 1, p. 173, 2017.
- [2] M. R. Macleod, T. O'Collins, D. W. Howells, and G. A. Donnan, "Pooling of animal experimental data reveals influence of study design and publication bias," *Stroke*, vol. 35, no. 5, pp. 1203–1208, 2004.
- [3] S. Sandal, P. Bansal, and M. Cantarovich, "The evidence and rationale for the perioperative use of loop diuretics during kidney transplantation: a comprehensive review," *Transplantation Reviews*, vol. 32, no. 2, pp. 92–101, 2018.
- [4] O. Bayrak, E. Uz, R. Bayrak et al., "Curcumin protects against ischemia/reperfusion injury in rat kidneys," *World Journal of Urology*, vol. 26, no. 3, pp. 285–291, 2008.
- [5] S. G. Coca, B. Yusuf, M. G. Shlipak, A. X. Garg, and C. R. Parikh, "Long-term risk of mortality and other adverse outcomes after acute kidney injury: a systematic review and meta-analysis," *American Journal of Kidney Diseases*, vol. 53, no. 6, pp. 961–973, 2009.
- [6] S. C. Gupta, B. Sung, J. H. Kim, S. Prasad, S. Li, and B. B. Aggarwal, "Multitargeting by turmeric, the golden spice: from kitchen to clinic," *Molecular Nutrition & Food Research*, vol. 57, no. 9, pp. 1510–1528, 2013.
- [7] H. Liu, C. Wang, Z. Qiao, and Y. Xu, "Protective effect of curcumin against myocardium injury in ischemia reperfusion rats," *Pharmaceutical Biology*, vol. 55, no. 1, pp. 1144–1148, 2017.
- [8] H. Chen, Y. Fan, F. Huang, H. Peng, J. Zhong, and J. Zhou, "Curcumin alleviates ischemia reperfusion-induced late kidney fibrosis through the Appl1/Akt signaling pathway," *Journal of Cellular Physiology*, vol. 233, no. 11, pp. 8588–8596, 2018.
- [9] F. H. Liu, W.-J. Ni, G.-K. Wang, and J.-J. Zhang, "Protective role of curcumin on renal ischemia reperfusion injury via attenuating the inflammatory mediators and caspase-3," *Cellular and Molecular Biology (Noisy-le-Grand, France)*, vol. 62, no. 11, pp. 95–99, 2016.
- [10] J. van Luijk, M. Leenaars, C. Hooijmans, K. Wever, R. de Vries, and M. Ritskes-Hoitinga, "Towards evidence-based translational research: the pros and cons of conducting systematic reviews of animal studies," *ALTEX*, vol. 30, no. 2, pp. 256–257, 2013.
- [11] N. M. Rogers, M. D. Stephenson, A. R. Kitching, J. D. Horowitz, and P. T. H. Coates, "Amelioration of renal ischaemia-reperfusion injury by liposomal delivery of curcumin to renal tubular epithelial and antigen-presenting cells," *British Journal of Pharmacology*, vol. 166, no. 1, pp. 194–209, 2012.
- [12] J. Zhang, L. Tang, G. S. Li, and J. Wang, "The anti-inflammatory effects of curcumin on renal ischemia-reperfusion injury in rats," *Renal Failure*, vol. 40, no. 1, pp. 680–686, 2018.
- [13] A. Kaur, T. Kaur, B. Singh, D. Pathak, H. Singh Buttar, and A. Pal Singh, "Curcumin alleviates ischemia reperfusion-induced acute kidney injury through Nmda receptor antagonism in rats," *Renal Failure*, vol. 38, no. 9, pp. 1462–1467, 2016.
- [14] A. S. Awad and A. A. El-Sharif, "Curcumin immune-mediated and anti-apoptotic mechanisms protect against renal ischemia/reperfusion and distant organ induced injuries," *International Immunopharmacology*, vol. 11, no. 8, pp. 992–996, 2011.
- [15] F. Hammad, S. Al-Salam, and L. Lubbad, "Curcumin provides incomplete protection of the kidney in ischemia reperfusion injury," *Physiological Research*, vol. 61, no. 5, pp. 503–511, 2012.
- [16] T. H. Chen, Y. C. Yang, J. C. Wang, and J. J. Wang, "Curcumin treatment protects against renal ischemia and reperfusion injury-induced cardiac dysfunction and myocardial injury," *Transplantation Proceedings*, vol. 45, no. 10, pp. 3546–3549, 2013.
- [17] C. Z. Li, T. P. Wu, Y. Y. Xia et al., "Effect and mechanism of curcumin pretreatment on renal ischemia-reperfusion injury in rats," *Journal of Wuhan University*, vol. 32, no. 3, pp. 320–323, 2011.
- [18] J. H. Nian, Y. T. Lu, H. P. Huang, W. G. Zhou, and X. Y. Zhu, "Effect of curcumin on renal ischemia-reperfusion injury and Hif-1 A expression in rats," *Zhejiang Journal of Integrated Traditional and Western Medicine*, vol. 22, no. 12, pp. 943–945, 2012.
- [19] L. Wang, X. H. Liu, H. Chen, X. D. Weng, T. Qiu, and L. Liu, "Effect of curcumin on the expression of nuclear factor - K B after renal ischemia-reperfusion injury in rats," *China Medical Herald*, vol. 10, no. 19, pp. 31–33, 2013.
- [20] A. L. Niu, Q. Liao, S. Zhang, Y. S. Chen, and S. L. Qu, "Protective effect and mechanism of curcumin on renal injury in rats with high intensity exercise," *Journal of Hunan Normal University*, vol. 9, no. 1, pp. 36–39, 2012.

- [21] G. Q. Xu, Y. Y. Guo, C. Guan, W. G. Fang, and Z. Y. Cha, "Protective effect of curcumin on renal ischemia-reperfusion injury in rats," *Journal of Bengbu Medical College*, vol. 41, no. 1, pp. 16–19, 2016.
- [22] J. Y. Tao, *Protective Effect of Curcumin Pretreatment and Post Ischemic Treatment on Renal Ischemia-Reperfusion Injury in Rats and Its Mechanism* 硕士, Guangxi Medical University, 2012.
- [23] Y. Hu, H. Cao, H. T. Zhou et al., "Regulatory effect and mechanism of curcumin on renal cell apoptosis in overtraining rats," *Chinese Journal of Applied Physiology*, vol. 34, no. 6, pp. 513–518+583–584, 2018.
- [24] W. Ni, S. Yu, F. Li et al., "Renoprotective effect of curcumin labelled on mesoscale nanoparticles (Mnps) on renal ischemia-reperfusion injury (Riri) via the Mir-146a/Nnos-No/Cgmp/Pkg signaling pathway," *Curr Pharm Biotechnol*, vol. 20, 2019.
- [25] H. Najafi, S. C. Ashtiyani, S. A. Sayedzadeh, Z. M. Yarijani, and S. Fakhri, "Therapeutic effects of curcumin on the functional disturbances and oxidative stress induced by renal ischemia/reperfusion in rats," *Avicenna Journal of Phytomedicine*, vol. 5, no. 6, pp. 576–586, 2015.
- [26] G. Chen, S. C. Lin, J. Chen et al., "Cxcl16 recruits bone marrow-derived fibroblast precursors in renal fibrosis," *Journal of the American Society of Nephrology*, vol. 22, no. 10, pp. 1876–1886, 2011.
- [27] M. S. Paller, J. R. Hoidal, and T. F. Ferris, "Oxygen free radicals in ischemic acute renal failure in the rat," *The Journal of Clinical Investigation*, vol. 74, no. 4, pp. 1156–1164, 1984.
- [28] L. García-Bonilla, M. Campos, D. Giralt et al., "Evidence for the efficacy of statins in animal stroke models: a meta-analysis," *Journal of Neurochemistry*, vol. 122, no. 2, pp. 233–243, 2012.
- [29] D. Moher, M. Avey, G. Antes, and D. G. Altman, "Erratum: the National Institutes of Health and guidance for reporting pre-clinical research," *BMC Medicine*, vol. 13, no. 1, p. 80, 2015.
- [30] H. Guo, Y. Wang, X. Zhang et al., "Astragaloside Iv protects against podocyte injury via Serca2-dependent Er stress reduction and Ampka-regulated autophagy induction in streptozotocin-induced diabetic nephropathy," *Scientific Reports*, vol. 7, no. 1, article 6852, 2017.
- [31] X. Lei, L. Zhang, Z. Li, and J. Ren, "Astragaloside iv/Lncrna-Tug1/Traf5 signaling pathway participates in podocyte apoptosis of diabetic nephropathy rats," *Drug Design, Development and Therapy*, vol. 12, pp. 2785–2793, 2018.
- [32] K. Gupta, J. Attri, A. Singh, H. Kaur, and G. Kaur, "Basic concepts for sample size calculation: critical step for any clinical trials!," *Saudi Journal of Anaesthesia*, vol. 10, no. 3, pp. 328–331, 2016.
- [33] N. I. Skrypnyk, R. C. Harris, and M. P. de Caestecker, "Ischemia-reperfusion model of acute kidney injury and post injury fibrosis in mice," *Journal of Visualized Experiments*, vol. 9, no. 78, 2013.
- [34] Q. Wei and Z. Dong, "Mouse model of ischemic acute kidney injury: technical notes and tricks," *American Journal of Physiology-Renal Physiology*, vol. 303, no. 11, pp. F1487–F1494, 2012.
- [35] W. Finn, E. Fernandez-Repollet, D. Goldfarb, A. Iaina, and H. E. Eliahou, "Attenuation of injury due to unilateral renal ischemia: delayed effects of contralateral nephrectomy," *The Journal of Laboratory and Clinical Medicine*, vol. 103, no. 2, pp. 193–203, 1984.
- [36] Y. Fu, C. Tang, J. Cai, G. Chen, D. Zhang, and Z. Dong, "Rodent models of Aki-Ckd transition," *American Journal of Physiology-Renal Physiology*, vol. 315, no. 4, pp. F1098–F1106, 2018.
- [37] R. A. Zager, A. C. M. Johnson, and K. Becker, "Acute unilateral ischemic renal injury induces progressive renal inflammation, lipid accumulation, histone modification, and "end-stage" kidney disease," *American Journal of Physiology-Renal Physiology*, vol. 301, no. 6, pp. F1334–F1345, 2011.
- [38] D. A. Shoskes, N. A. Parfrey, and P. F. Halloran, "Increased major histocompatibility complex antigen expression in unilateral ischemic acute tubular necrosis in the mouse," *Transplantation*, vol. 49, no. 1, pp. 201–207, 1990.
- [39] H. Zhou and S. Toan, "Pathological roles of mitochondrial oxidative stress and mitochondrial dynamics in cardiac microvascular ischemia/reperfusion injury," *Biomolecules*, vol. 10, no. 1, p. 85, 2020.
- [40] K. H. Lee, W. C. Tseng, C. Y. Yang, and D. C. Tarnag, "The anti-inflammatory, anti-oxidative, and anti-apoptotic benefits of stem cells in acute ischemic kidney injury," *International Journal of Molecular Sciences*, vol. 20, no. 14, article 3529, 2019.
- [41] M. Malek and M. Nematbakhsh, "Renal ischemia/reperfusion injury; from pathophysiology to treatment," *Journal of Renal Injury Prevention*, vol. 4, no. 2, pp. 20–27, 2015.
- [42] S. Borkan, "The role of Bcl-2 family members in acute kidney injury," *Seminars in Nephrology*, vol. 36, no. 3, pp. 237–250, 2016.
- [43] E. Y. Plotnikov, A. V. Kazachenko, M. Y. Vysokikh et al., "The role of mitochondria in oxidative and nitrosative stress during ischemia/reperfusion in the rat kidney," *Kidney International*, vol. 72, no. 12, pp. 1493–1502, 2007.

Review Article

Implication of Gut Microbiota in Cardiovascular Diseases

Wenyi Zhou ^{1,2}, Yiyu Cheng,¹ Ping Zhu ², M. I. Nasser ², Xueyan Zhang ¹,
and Mingyi Zhao ¹

¹Department of Pediatrics, The Third Xiangya Hospital, Central South University, Changsha, Hunan 410013, China

²Guangdong Cardiovascular Institute, Guangdong Provincial People's Hospital, Guangdong Academy of Medical Sciences, Guangzhou, Guangdong 510100, China

Correspondence should be addressed to Mingyi Zhao; 36163773@qq.com

Received 3 May 2020; Revised 13 July 2020; Accepted 16 July 2020; Published 26 September 2020

Guest Editor: Wai Lydia Tai

Copyright © 2020 Wenyi Zhou et al. This is an open access article distributed under the Creative Commons Attribution License, which permits unrestricted use, distribution, and reproduction in any medium, provided the original work is properly cited.

Emerging evidence has identified the association between gut microbiota and various diseases, including cardiovascular diseases (CVDs). Altered intestinal flora composition has been described in detail in CVDs, such as hypertension, atherosclerosis, myocardial infarction, heart failure, and arrhythmia. In contrast, the importance of fermentation metabolites, such as trimethylamine N-oxide (TMAO), short-chain fatty acids (SCFAs), and secondary bile acid (BA), has also been implicated in CVD development, prevention, treatment, and prognosis. The potential mechanisms are conventionally thought to involve immune regulation, host energy metabolism, and oxidative stress. However, numerous types of programmed cell death, including apoptosis, autophagy, pyroptosis, ferroptosis, and clockophagy, also serve as a key link in microbiome-host cross talk. In this review, we introduced and summarized the results from recent studies dealing with the relationship between gut microbiota and cardiac disorders, highlighting the role of programmed cell death. We hope to shed light on microbiota-targeted therapeutic strategies in CVD management.

1. Introduction

Cardiovascular disease (CVD), with its rising prevalence rate and mortality, entails both health threats and economic burdens to our society. As a chronic progressive condition, the development of CVDs often begins with risk factors like obesity, type 2 diabetes, and hypertension, most of which would irreversibly damage vascular structure and eventually lead to detrimental clinical outcomes like arterial thrombosis and ischemic stroke. While heredity can only be blamed for less than 20% occurrence of CVDs, dietary and nutritional statuses are two stimuli with more profound and lasting impacts [1]. Therefore, increasing evidence has suggested a close relationship between gut microbiota and CVD development [2].

The gut microbiota refers to trillions of commensal microorganisms located in the intestine in a certain proportion, whose balance is easily disturbed by food intake, lifestyle, and environment [3]. Considered a complex organ, the microbial community is required in the committed step

through which food would be converted into small compounds and metabolites, thus modulating intestine structure, gut barrier integrity, inflammatory status, and host metabolism both directly and indirectly [4]. Since Hippocrates claimed that “all diseases begin in the gut” centuries ago, a great body of research has demonstrated the interplay between intestinal microbiota and diseases, including colorectal cancer [5], cerebral ischemia-reperfusion injury [6], liver fibrosis [7], and CVDs [8]. The gut microbiota accounts for 0.2–2.0 kg of the weight of an adult and approximately 50% of the dry weight of adult feces. The enormous genome of microbial genes and their functions are described as the microbiome, which outnumbers the human genome tremendously [3, 9]. Although the characteristics of the gut community may be inherited in early life, the composition could also be altered by external conditions [10, 11]. Appropriate gut microbiota structure and metabolite functions are essential in homeostasis maintenance, whereas gut dysbiosis contributes to atherosclerosis, hypertension, heart failure, arrhythmia,

cardiac tumours, and others [12]. However, its underlying mechanisms are multifactorial and yet to be determined.

In this report, we introduce the role of gut microbiota in CVDs and summarize possible mechanisms, which may provide a theoretical basis and shed light on novel therapeutic strategies in the prevention and treatment of CVDs.

2. Mechanisms Underlying the Interaction between Gut Microbiota and the Host

The community of gut microbiota consists mostly of bacteria, fungi, and viruses in which the primary component is bacteria. There are 5 major families in the intestinal flora: *Bacteroidetes*, *Firmicutes*, *Actinobacteria*, *Proteobacteria*, and *Verrucomicrobia* [13]. Although the variety of species is abundant, the architecture of gut microbiota is comparatively fixed in different sites. However, the differences in gut microorganism quantities between locations are significant, with the ascending colon containing the largest number [13]. Under physiological conditions, more than 90% of the bacteria comprise *Bacteroidetes* and *Firmicutes*, while an elevated *Firmicutes/Bacteroidetes* (F/B) proportion is associated with CVDs [14]. Koliada et al. found that with the body mass index (BMI) in Ukraine adult population increasing, their F/B ratio raised likewise after removing other confounders such as age or smoking [15]. Subsequently, evaluation of children's gut microbiota composition and BMI had confirmed F/B ratio as a key risk indicator for childhood obesity [16]. Additionally, the F/B ratio is related to low-grade inflammation leading diabetes mellitus [17]. These diseases serve as both risk factors and stimulatives for CVDs. In addition to intestinal integrity maintenance, gut metabolites serve as essential messengers in the communication between gut microbiota and the host. Here, we review the mechanisms underlying the interaction between gut microbiota and the host, especially in CVDs.

2.1. Immunoregulation. Generated by fiber fermentation in the colon, short-chain fatty acids (SCFAs) include three major products, namely, acetate, propionate, and butyrate, all of which contain less than six carbons [18]. Apart from being nutrients and energy sources for intestinal epithelial cells, these small-molecule metabolites could enter the blood circulation, participate in immune regulation and inflammation modulation either by binding to G protein-coupled receptors (GPCRs) or by inhibiting histone deacetylases (HDACs) [18], and thereby influence gut homeostasis and host diseases. Laurence et al. found that SCFAs induce NLRP3 inflammasome activation and subsequent abundant IL-18 secretion in a GPR43- and GPR109A-dependent manner, thus eliciting favourable effects on intestinal integrity maintenance [19]. Of note, GPR43 and GPR109A are two receptors that are expressed on intestinal epithelial cells and some immune cells, where GPR43 mainly binds to acetate and propionate, while GPR109A is specifically activated by butyrate [20]. Studies have demonstrated that SCFAs beneficially upregulate not only the proliferation and differentiation of regulatory T cells (Tregs) but also the anti-inflammatory IL-10 secreted from Foxp3+ Tregs, which are mediated through GPR43 (also

known as *Ffar2*) activation and HDAC inhibition [21]. Additionally, butyrate was shown to suppress proinflammatory factors, including IL-6, IL-12, and NO, from intestinal macrophages by HDAC inhibition [18]. Likewise, Bartolomeus et al. recently proved that the anti-inflammatory role of SCFAs such as propionate significantly reduced the number of effector memory T cells and T helper 17 cells, thus mitigating cardiovascular damage [22]. However, the proinflammatory functions mediated by GPR41 (also known as *Ffar3*) and GPR43 were reported elsewhere [23], indicating that SCFA-induced immunoregulatory effects are dependent on the distinct cell types.

Additionally, trimethylamine N-oxide (TMAO) is generally investigated as a risk indicator for cardiovascular diseases, diabetes mellitus, nonalcoholic fatty liver disease, and other metabolic events [24–26]. As the end-product of dietary choline and L-carnitine, TMAO is converted from trimethylamine (TMA) in the liver by flavin-containing monooxygenases (FMOs), especially FMO3 [24]. However, how exactly TMAO functions to regulate homeostasis is seldom discussed. According to Sun et al., TMAO induces inflammation by activating the ROS-TXNIP-NLRP3 inflammasome, thereby contributing to endothelial dysfunction in human umbilical vein endothelial cells [27]. Similarly, Yue et al. showed that TMAO promotes the release of the inflammatory cytokines IL-1 β and IL-18 via activation of the NLRP3 inflammasome from foetal human colon cells in a time- and dose-dependent manner [28]. Moreover, injection of TMAO was shown to significantly increase inflammatory markers, including cyclooxygenase 2, IL-6, E-selectin, and ICAM1, through the MAPK and NF- κ B signalling pathways, which then recruit leukocytes and induce vascular inflammation [29]. In these fine experiments in which treatments against TMAO were adopted, inflammatory damage was prevented. Taken together, the proinflammatory role of TMAO is established.

Plasma cholesterol, the key cellular membranes constituent and precursor of steroid hormones, vitamin D, and bile acids, is positively correlative with cardiovascular diseases. There are two main sources of cholesterol, with one-third being exogenous from daily dietary and the other two-third synthesized inside the body [30]. Confirmed with various models, microbial regulation is believed to be critically involved in cholesterol balance modulation [31]. To begin with, gut microbiome is reported to convert cholesterol into poorly absorbed coprostanol, reducing the risk of cardiovascular diseases [30, 32]. Further elucidation reveals that the presence of intestinal sterol metabolism A genes is responsible for such metabolism mediation [32]. Another key aspect the gut microbiota enrolled is bile acids metabolism. Bile acids deconjugation yields free bile acids as well as free glycine or taurine residues, which requires the participation of bile salt hydrolase enzymes (BSHs) [30]. The presence of BSHs was found within *Clostridium*, *Bifidobacterium*, *Lactobacillus*, and others. With higher degree of bile salts deconjugation, more free BAs were excreted into feces [30]. Primary bile acids refer to steroid molecules that result from the decomposition of cholesterol in the liver. Most of them are recycled back to the liver, while the rest enter the intestine,

where they are converted into secondary bile acids by gut microbiota [33]. The most well-studied secondary bile acids are deoxycholic acid (DCA), lithocholic acid (LCA), and ursodeoxycholic acid (UDCA), which often function through their receptors, including G protein-coupled BA receptor 1 (TGR5), farnesoid X receptor (FXR), and vitamin D receptor (VDR) [33]. When bound to the TGR5 receptor, secondary bile acids cause the activation of macrophages and then the production of inflammatory cytokines [34]. Interestingly, researchers found that low concentrations of secondary bile acids bring anti-inflammatory effects, while high concentrations would instead cause damage. For example, Wang et al. demonstrated that low-dose DCA mitigates the inflammatory response in birds [35].

Additionally, these products from commensal microbiota would trigger innate immune signalling, thereby communicating with the host. Microbial-associated molecular patterns (MAMPs) including LPS or peptidoglycan are recognized by receptors like Toll-like receptors (TLRs), NOD-like receptors (NLRs), and others [4]. The strong connection between TLRs and atherosclerosis was confirmed in genetic mice researches. In the TLR4^{-/-} apoE^{-/-} mice model fed with cholesterol-rich diet, the size of aortic plaque was significantly reduced [36]. Interestingly, deficiency of TLR2 in myeloid cells had no influence in the development of atherosclerosis, suggesting the role of endothelial TLR2 in atherogenesis [37]. Furthermore, the development of arterial thrombosis was relative to NOD2, TLR2, and TLR9 signalling in platelets as well as TLR2 and TLR4 pathways in endothelial cells [4].

2.2. Energy Metabolism and Homeostasis. Among the numerous risk factors contributing to CVD, abnormal immune regulation and metabolic disorders represent two major elements. Metabolic syndromes such as obesity, dyslipidosis, hyperglycaemia, and insulin resistance are closely related to the occurrence and development of CVD. In recent years, the link between gut microbiota, metabolism, and CVD has gained much attention. For instance, Den and his coworkers considered SCFAs to carry metabolic benefits for those with a high-fat diet through inhibition of peroxisome proliferator-activated receptor gamma (PPAR γ), converting lipid synthesis to lipid oxidation [38]. Moreover, a fiber-rich diet upregulates the levels of SCFAs in the gut, which then promotes intestinal gluconeogenesis [39]. SCFAs accelerate the production of GLP-1 by binding to GPR41 and GPR43, therefore facilitating insulin secretion [39]. In contrast, TMAO aggravates triglyceride accumulation and lipogenesis in the livers of high-fat diet-fed mice [40]. Propionate was found to induce glycogenolysis and hyperglycaemia via the upregulation of glucagon and fatty acid-binding protein 4 (FABP4), thereby hindering the effects of insulin [41]. In mice with obesity, bile acid promotes GLP-1 secretion via the TGR5 pathway, thereby modulating blood sugar [42]. Notably, there is multiplicity in the associations between gut microbiota and their microbiome. For instance, TMAO could alter the bile acid profile and metabolism, thus contributing to liver steatosis and atherosclerosis [40, 43], whereas bile acid stimulates FMO3 expression via FXR, eventually resulting in TMAO production (Bennett et al., 2013).

Moreover, butyrate was found to restore bile acid dysregulation and counteract hepatic inflammation [44].

To sum up, the gut microbiota communicates with the host through diverse manners. To begin with, SCFAs and secondary bile acids are two of the main products by gut microbiota. They play their immune-regulatory role either by directly affecting the proliferation of immune cells or by stimulating the production of cytokines. Moreover, SCFAs are involved in both lipid and sugar metabolism. Second, TMAO that primarily comes from L-carnitine and choline consumption participates in inflammatory modulation by promoting IL-18 and IL-1 β release or activating MAPK/NF- κ B signalling pathway, thus upregulating the levels of COX2, IL-6, and ICAM1. Moreover, MAMPs including LPS and peptidoglycan serve as another vital contributor in the development of atherosclerosis and arterial thrombosis, mainly through TLRs and NLRs (Figure 1).

2.3. Programmed Cell Death. Apart from the well-known immune and inflammation modulation properties of gut microbiota, accumulating evidence has revealed its potential in the determination of diverse manners of cell death (Figure 2).

2.3.1. Apoptosis. Characterized by the formation of a distinctive apoptotic body, apoptosis is one of the most widely investigated programmed cell deaths. It is often observed in myocardial infarction, heart failure, and other vascular damage. Saito et al. found that *Bacteroides fragilis* (*B. fragilis*) is able to protect HT29 cells from apoptosis resulting from Shiga toxin [45]. Butyrate promotes vascular smooth muscle cell growth via proliferation arrest as well as apoptosis inhibition [46]. Notably, there are proapoptotic effects as well. Sodium propionate was reported to induce apoptosis in H1299 and H1703 lung cancer cells, as evidenced by increased protein expression of p21, Bad, and Bax as well as apoptosis markers, including cleaved PARP and cleaved caspase 3 [47]. According to Nie et al., *Bifidobacterium* (BIF) ameliorates TNF- α -induced cell apoptosis in Caco-2 cells [48]. Likewise, butyrate causes apoptosis and cell cycle arrest in kidney epithelial cells [49].

2.3.2. Autophagy. Nie et al. discovered that BIF ameliorates TNF- α -induced autophagy in Caco-2 cells by suppressing the level of p62 and inhibiting the expression of autophagy-related markers such as Beclin1 and LC3II [48]. According to their research, BIF may provide a therapeutic target aimed at the Kawasaki disease, which is highly related to acquired heart disease in children. Lannucci and his coworkers proved that SCFAs induce autophagy in hepatic cells by uncoupling protein 2 (UCP2) [50]. Accordingly, Qiao et al. demonstrated that sodium butyrate contributes to the reduction in α -synuclein both via the inhibition of the PI3K/Akt/mTOR autophagy pathway and enhancement of Atg5-mediated autophagy, manifested as elevated LC3II and reduced p62 expression [51].

2.3.3. Pyroptosis. As a type of proinflammatory cell death, pyroptosis is characterized by swollen cells, subcellular organelle damage, and the release of cytokines, including the NLRP3 inflammasome, NLRP6, an apoptosis-associated speck-like protein containing CARD (ASC), cysteinyl-

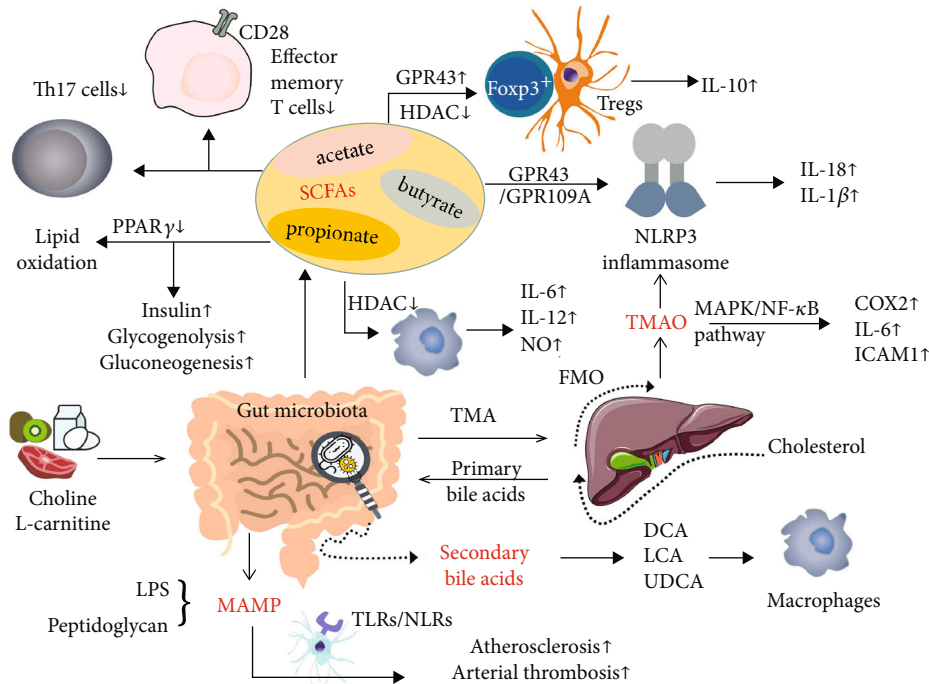


FIGURE 1: Mechanisms involved in gut microbiota-host communication. Short-chain fatty acids (SCFAs), mainly propionate, acetate, and butyrate, stimulate Foxp3⁺ Tregs and macrophages via GPR43 activation and HDAC inhibition. Foxp3⁺ Tregs subsequently produce the anti-inflammatory cytokine IL-10, while proinflammatory cytokines such as IL-6 and IL-12 are secreted by macrophages. Moreover, Th17 cells and effector memory T cells were downregulated by SCFAs. By suppressing PPAR γ , SCFAs promote lipid oxidation. Although insulin production was enhanced by SCFAs, glycogenolysis and gluconeogenesis were both observed to occur even with SCFA treatment. L-carnitine and choline consumption contribute to the release of trimethylamine (TMA), which is then converted by FMO into trimethylamine N-oxide (TMAO). Both SCFAs and TMAO activate the NLRP3 inflammasome, leading to IL-18 and IL-1 β release. Through the MAPK/NF- κ B signalling pathway, TMAO increases the levels of COX2, IL-6, and ICAM1. Secondary bile acids such as deoxycholic acid (DCA), lithocholic acid (LCA), and ursodeoxycholic acid (UDCA) are produced in the intestine by gut microbiota and then participate in inflammatory modulation and blood sugar regulation.

aspartate-specific proteinase 1 (caspase-1), and gasdermin D. Data have shown that sodium butyrate is capable of breaking down the gingival epithelial barrier by inducing pyroptosis [52]. Similarly, TMAO promotes vascular endothelial cell pyroptosis via ROS production, thus resulting in the development of atherosclerosis [53]. However, Gu et al. proved the antipyroptosis effects of sodium butyrate on renal glomerular endothelial cells, protecting them from damage caused by high glucose [54]. From the perspective of the mechanism, the classic caspase-1-gasdermin D pathway and NF- κ B/I κ B- α signalling may both be involved [54]. Moreover, Cohen et al. confirmed that *Vibrio proteolyticus* (VPRH), a Gram-negative bacterium from the gut of a wood borer, induces pyroptosis by activating the NLRP3 inflammasome and caspase-1, thereby resulting in IL-1 β secretion, suggesting that the NLRP3 inflammasome pyroptotic pathway can benefit the host during infection [55].

2.3.4. Ferroptosis. Induced by lipid reactive oxygen species accumulation, ferroptosis refers to another distinct kind of cell death mediated by mitochondria. Studies concerning whether gut microbiota are implicated in ferroptosis are rather rare. Until recently, Robert et al. proposed that supplementation of omega-3 polyunsaturated fatty acids (n-3

PUFAs) and butyrate may both facilitate mitochondrial Ca²⁺- and Gpx4-dependent ferroptosis [56]. Hopefully, this hypothesis may shed light on the link between gut microbiota and ferroptosis as well as accelerate related research.

2.3.5. Clockophagy. The circadian rhythm, namely, clockophagy, is controlled by a complex circadian clock gene network including the ARNTL, CLOCK, CRY2, and PER2 genes [57]. The interaction between circadian rhythms and diverse gut microbiota has been well studied, where the acute sleep-wake cycle shift alters the functional profiles of gut microbes. Together, the clock-microbial communities affect host homeostasis [58]. The circadian rhythm of SCFA production was observed by Segers et al. to cause rhythmicity in intestinal movement [59]. However, such effects were abolished by the deletion of Bmal1 [59]. Besides, Marques et al. found that in hypertensive mice, a high-fiber diet changes the composition of the gut microbiota and restores gut dysbiosis, which may be partially due to increased levels of clock genes in the heart and kidney [60]. Additionally, a negative correlation between the phylum *Firmicutes* and Bmal1 as well as a positive correlation between *Bacteroidetes* and Bmal1 was observed in mice [61].

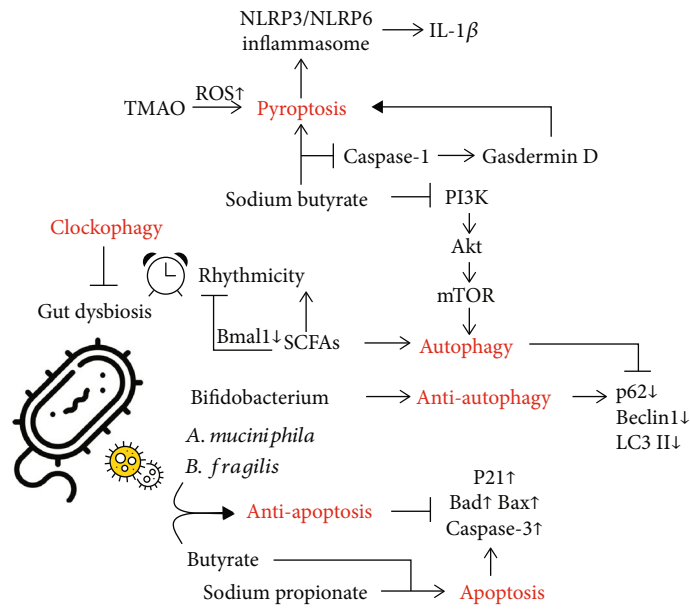


FIGURE 2: Manners of cell death induced by gut microbiota. A variety of gut flora have been demonstrated to be effective in regulating cell death. (a) Muciniphila and (b) fragilis were shown to counteract apoptosis. In contrast, sodium propionate has the ability to induce apoptosis. Interestingly, the effects of butyrate on apoptosis are controversial, manifesting elevated biomarkers such as P21, Bad, Bax, and caspase-3. In addition, SCFAs stimulate autophagy, while *Bifidobacterium* is autophagy-protective, with decreased expression of P62, Beclin1, and LC3II. Sodium butyrate promotes autophagy by inhibiting the PI3K/Akt/mTOR pathway. Additionally, it is involved in pyroptosis via regulation of the caspase-1/gasdermin D pathway. In addition, TMAO stimulates ROS activation and thus induces pyroptosis. Along with pyroptosis, the NLRP3/NLRP6 inflammasome and IL-1 β are produced. Moreover, clockophagy can reverse gut dysbiosis. For instance, SCFAs are capable of controlling rhythmicity via clock genes such as Bmal1.

3. Implications of Gut Microbiota in CVDs

To concisely describe the role of gut microbiota in cardiovascular disease, the positive or negative effects of gut microbiota on CVDs are listed in Table 1.

3.1. Hypertension. Hypertension (HTN) has been a key link in the occurrence and development of cardiovascular diseases. Although HTN is currently beyond cure, it is preventable and controllable. According to the mosaic theory advanced by Irvin Page, HTN is induced by multiple factors, including inheritance, diet, and environment [62]. HTN also has extensive impacts on various tissues and organs, such as endothelial cells, the kidneys, and brain. Moreover, in recent years, the value of gut microbiota in HTN has been widely investigated.

In the work conducted by Li et al., fecal transplantation was performed from hypertensive individuals to germ-free mice. Along with microbiota shift, blood pressure was also elevated in those mice, indicating the contributing role of gut microbiota in hypertension [63]. It has been demonstrated that butyrate-producing bacteria and butyrate levels are relatively low in patients with HTN, indicating that imbalanced host-microbiome cross talk is relevant to systolic blood pressure [64]. Accordingly, in mice pretreated with angiotensin II, supplementation with butyrate effectively lowered blood pressure [65]. Interestingly, the same team found that gut barrier dysfunction is another contributor to HTN, as evidenced by elevated levels of zonulin, a gut epithelial

tight junction protein regulator [65]. However, the same metabolite may yield contradictory biological effects through different receptors. For instance, Jennifer et al. found that propionate may upregulate blood pressure via olfactory receptor 78 (Olf78) while exerting hypotensive effects through activation of Gpr41 [66]. In-depth knowledge reveals that vascular inflammation and endothelial dysfunction are two key processes in the development of hypertension [67]. In mice fed with Western diet, endothelial dysfunction was associated with decreased proportion of *Bifidobacterium* spp., whereas antibiotic administration helped mitigate such vascular damage [68]. As compared with germ-free mice, the conventionally raised mice pretreated with Ang II presented with a higher level of IL-4 and IL-10, indicating a vascular inflammation-prone role of enteric flora [68]. In a meta-analysis of 8 studies, a higher circulating TMAO level was positively associated with hypertension risk, which was dose-dependent [69]. Liu and coworkers identified that administration of the *Lactobacillus rhamnosus* GG strain is an effective approach to prevent exacerbation of HTN, which is in part mediated by reducing TMAO levels [70]. However, it is worth noting that the application of TMAO alone would not alter blood pressure in normotensive rats but prolonged the hypertensive-prone effects of angiotensin II [71]. More recently, a novel mechanism different from inflammation or immunity regulation has been presented. In high salt-induced hypertensive mice, elevated blood pressure is closely related to increased levels of intestinal-derived corticosterone [72].

TABLE 1: The exact role of different gut microbiota in CVDs.

CVDs Species	Atherosclerosis	Myocardial infarction	Heart failure	Arrhythmia
<i>Enterobacteriaceae</i>	Negative			
<i>Ruminococcus gnavus</i>	Negative			
<i>Eggerthella lenta</i>	Negative			
<i>Roseburia intestinalis</i>	Positive			
<i>Faecalibacterium cf. prausnitzii</i>	Positive			
<i>Synergistetes phylum</i>		Negative		
<i>Lachnospiraceae</i> family		Negative		
<i>Spirochaetes</i> phylum		Negative		
<i>Syntrophomonadaceae</i> family		Negative		
<i>Tissierella</i> and <i>Soehngenia</i> genera		Negative		
<i>Lactobacillus plantarum</i> 299v		Positive		
<i>Faecalibacterium prausnitzii</i>			Positive	
<i>Bacteroides fragilis</i>			Positive	
<i>Ruminococcus</i>				Negative
<i>Streptococcus</i>				Negative
<i>Enterococcus</i>				Negative
<i>Faecalibacterium</i>				Positive
<i>Alistipes</i>				Positive
<i>Oscillibacter</i>				Positive
<i>Bilophila</i>				Positive

Taken together, these results established that the gut microbiota is involved in blood pressure regulation. However, the underlying mechanisms still await further validation.

3.2. Atherosclerosis and Arterial Thrombosis. Initially related to dyslipidaemia, abnormal accumulation of macrophages, and massive production of inflammatory cytokines, atherosclerosis is considered a chronic inflammatory disease that underlies end-stage CVDs such as myocardial infarction or heart failure. In recent years, people have started to consider gut microbiota potent regulators during the development of atherosclerotic lesions. Koren et al. first identified bacterial DNA in atherosclerotic plaques, and the amount of DNA was associated with the infiltration of leukocytes in the plaques [73]. Moreover, the altered composition of the gut microbiome was confirmed in a metagenome-wide association study encompassing 218 individuals with atherosclerosis and 187 healthy controls. Specifically, the abundances of *Enterobacteriaceae*, *Ruminococcus gnavus*, and *Eggerthella lenta* were significantly increased in those with atherosclerosis, whereas *Roseburia intestinalis* and *Faecalibacterium cf. prausnitzii*, both butyrate-yielding bacteria, were reduced [74]. The above findings strongly suggest correlations between gut microbiota and atherosclerosis.

With the use of atherosclerosis-prone germ-free mice and antibiotic treatments, the role of gut microbiota in atherosclerosis development was further elucidated (Table 2). First people suggested that bacterial or viral infection is necessary for the initiation of atherosclerosis. However, such hypothesis was overturned by Samuel and his colleagues' work [75].

Apolipoprotein (apo) E^{-/-} murine model was often adopted for atherosclerosis research given the self-driven ability of atherosclerotic plaque formation. Samuel et al. compared the atherosclerosis lesion in germ-free apoE^{-/-} animals with those raised in conventional environment, and they found no evident difference [75]. Alternatively, with the help of antibiotics to suppress gut microflora, choline-enhanced atherosclerosis in aorta was off-set along with reduced macrophage and scavenger receptor CD36 [76]. However, given the complexity of enteric flora, the pro- or antiatherosclerosis role of gut microbiota depends. Kasahara and his colleagues demonstrated that *Roseburia intestinalis* is capable of ameliorating atherosclerosis by shaping gene expression, enhancing fatty acid metabolism, and reducing the inflammatory response [77]. However, treatment with butyrate markedly mitigates the formation of atherosclerotic plaques via the upregulation of ABCA1 and subsequent cholesterol efflux [78]. In contrast, the production of TMAO by gut microbiota yields negative effects on atherosclerosis [79].

Rupture of the atherosclerotic plaque would likely cause arterial thrombus elsewhere, resulting in detrimental consequences. For one, the LPS-TLR pathway is a major contributor in thrombosis formation. Both TLR2 and TLR4 were found expressed on endothelial cells and platelets. Activation of TLR2 and TLR4 pathway would facilitate the release of VWF and factor VIII expression, contributing to platelet-proinflammatory cell aggregation [80]. For another, gut microbiota metabolites take part in arterial thrombosis as well. Feces transplantation of TMAO-rich gut microbiota into germ-free mice would promote platelet function and

TABLE 2: Researches of gut microbiota in CVDs.

Diseases	Sample	Observations	Mechanism	Ref.
Hypertension	HTN patients	Decreased butyrate-producing bacteria and butyrate level	SCFA-dependent	[62]
	Ang-II pretreated mice	Reduced BP after butyrate administration; increased zonulin level	SCFA-dependent; gut barrier dysfunction	[65]
	Mice	Increased BP after propionate treatment	Olf78-dependent	[66]
	Mice	Decreased BP after propionate treatment	Gpr41-dependent	[66]
		<i>Lactobacillus rhamnosus</i> GG prevents HTN development	Reduced TMAO levels	[70]
	Mice	High salt-induced HTN	Increased intestinal-derived corticosterone	[72]
	Patients	Bacterial DNA observed in atherosclerotic plaques	/	[73]
Atherosclerosis		<i>Roseburia intestinalis</i> ameliorates atherosclerosis	Alter gene expression, induce fatty acid metabolism, and reduce inflammation response	[77]
	apoE ^{-/-} mice	Comparable atherosclerosis lesion in germ-free apoE ^{-/-} animals and their conventionally raised counterparts	/	[75]
		Choline-enhanced atherosclerosis in aorta was off-set by antibiotics	Reduced macrophage and scavenger receptor CD36	[76]
	apoE ^{-/-} mice with HFD	Butyrate mitigates atherosclerotic plaque formation	Upregulation of ABCA1 and subsequent cholesterol efflux	[78]
AMI rat model	Increased <i>Synergistetes phylum</i> , <i>Lachnospiraceae family</i> , <i>Spirochaetes phylum</i> , <i>Syntrophomonadaceae family</i> , and <i>Tissierella</i> and <i>Soehngenia</i> genera	In parallel with gut barrier impairment	[83]	
Myocardial infarction	STEMI patients	Over 12% plasma bacteria originated from the gut	Partially associated with an inflammatory response	[84]
	Patients presenting with chest pain	Predictive value of plasma TMAO levels for incident cardiovascular events	TMAO-related proinflammatory monocytes augment	[85]
	Mice	Improve cardiac repair and post-MI outcome through modulation of immune composition	Gut microbiota-derived SCFAs modulate immune composition	[86]
		<i>Lactobacillus plantarum</i> 299v improved ischemia tolerance and acute cardiac injury after MI	Reduce leptin level	[87]
Heart failure	Mice	<i>Bacteroides fragilis</i> reduces ventricular remodelling	Increased Foxp3+ Treg cells and anti-inflammatory cytokine	[92]
		Depletion of SCFAs finally leads to HF	Intestinal barrier destruction, with endotoxin translocation	[93, 94]
	Mice	TMAO alters cardiac muscle cells contractility	Promotion of calcium ions release	[95, 96]
		TMAO confers detrimental effects on adult cardiomyocytes	T-tubule network damage; Ca handling dysfunction	[97]
	Mice	Pulmonary edema, cardiac enlargement, and decreased ejection fraction	TMAO-dependent	[98]
	Patients	TMAO increases susceptibility to HF	Induction of myocardial fibrosis	[99]
	Overload-induced HF mice	DMB ameliorates adverse cardiac structural remodelling	Downregulating TMAO levels	[100]
Arrhythmia	Patients	Shared common features of gut microbiota dysbiosis	Alike ratio of <i>Firmicutes</i> and <i>Bacteroidetes</i>	[104, 105]
	Patients	Thrombus formation; platelet hyperreactivity	Elevated TMAO level	[107]
		TMAO stimulates ischemia-induced VA	Release of proinflammatory markers such as IL-1 β and TNF- α	[109]
	Canine AF model	Gut microbes counteracts AF progression	TMAO production and CANS activation	[110]
	Mice	Reduced susceptibility to cardiac ventricular arrhythmias	SCFA-dependent	[22]

arterial thrombosis [81]. Recently, another gut microbial metabolite, Phenylacetylglutamine (PAGln), was shown to induce hyperreactivity of platelet via adrenergic receptors [82].

3.3. Myocardial Infarction. The connection between intestinal flora and myocardial infarction (MI) has been supported by a growing body of literature. In a rat model of acute myocardial infarction (AMI), enrichment of the *Synergistetes* phylum, *Lachnospiraceae* family, *Spirochaetes* phylum, *Syntrophomonadaceae* family, and *Tissierella and Soehngenia* genera was observed compared with the sham group, which is in parallel with gut barrier impairment [83]. In patients with ST-elevation myocardial infarction (STEMI), systemic microbiome alteration was also observed. Over 12% of plasma bacteria were identified to originate from the gut after STEMI, which is partially associated with the inflammatory response [84]. Accordingly, reduced cardiac damage and decreased inflammation were noticed following the abrogation of bacterial translocation [84]. Of clinical value, plasma TMAO levels may be potential markers to predict the risks of incident cardiovascular events in patients presenting with chest pain [85]. Such potency may in part be explained by TMAO-related proinflammatory monocyte augmentation [85]. Moreover, Tang et al. demonstrated that gut microbiota-derived SCFAs would benefit cardiac repair and improve post-MI outcome through modulation of immune composition [86]. With the administration of the probiotic *Lactobacillus plantarum* 299v, the leptin level in blood was reduced, leading to enhancement of ischemic tolerance in the myocardium and alleviation of acute cardiac injury after MI [87].

3.4. Heart Failure. As an irreversible end-stage disease, heart failure (HF) is characterized by oedema and dyspnoea, with a five-year mortality rate of over 50% [88]. At present, a growing body of research has confirmed the “gut hypothesis of heart failure” [89, 90]. That is, decreased cardiac output in HF leads to intestinal mucosa barrier damage and dysbacteriosis, with elevated levels of pathogenic bacteria such as *Candida* [91] and reduced levels of anti-inflammatory bacteria such as *Faecalibacterium prausnitzii* [3]. Reciprocally, intestinal flora promotes HF development by participating in mucosal immunity modulation [3]. Segmented filamentous bacteria can stimulate the secretion of IL-6 and IL-23 and then promote the differentiation of Th17 cells. *Bacteroides fragilis* increases the abundance of Foxp3+ Treg cells and induces the secretion of anti-inflammatory cytokines, which have been found to reduce ventricular remodelling in MI mice [92].

Not surprisingly, metabolites of intestinal flora are also important for HF. Although studies concerning SCFAs and HF are limited, it has been proven that SCFAs are beneficial for the intestinal mucosa [3]. The depletion of SCFAs would result in intestinal barrier destruction, which then facilitates the translocation of endotoxin into blood circulation and finally leads to HF [93, 94].

However, the level of TMAO has long been recognized as a risk factor. Savi et al. found that TMAO promotes the release of calcium ions in cardiac muscle cells of healthy mice and thus alters their contractility [95, 96]. Recently, the in-

depth work carried out by Jin et al. showed that TMAO confers detrimental effects on adult cardiomyocytes by inducing T-tubule network damage and Ca handling dysfunction [97]. When TMAO was administered to HF mice, Organ et al. found that mouse cardiac function deteriorated significantly, characterized by pulmonary oedema, cardiac enlargement, and decreased ejection fraction [98]. Schuett et al. proved that TMAO could enhance patient susceptibility to HF by increasing myocardial fibrosis [99]. Likewise, Wang and his team proved that 3,3-dimethyl-1-butanol (DMB) ameliorates adverse cardiac structural remodelling in overload-induced HF mice by downregulating TMAO levels [100]. Given the critical role of TMAO in HF, it may serve as a potential therapeutic target.

3.5. Arrhythmia. Arrhythmia, including atrial fibrillation (AF), ventricular arrhythmia (VA), and atrioventricular block, is emerging as intractable CVD that contributes to heart failure or sudden cardiac death. Up-to-date studies have shown that anticancer therapies may induce cardiotoxicities, such as corrected QT interval prolongation and arrhythmia [101]. Additionally, Vahdatpour et al. found that atrial arrhythmia can be secondary to chronic lung disease-associated pulmonary hypertension [102]. Due to its prevalence and accompanying adverse events, investigation about arrhythmia has deepened, and we are now looking at the implications between gut microbiota and arrhythmia.

Zuo et al. previously identified variable metabolic patterns as well as imbalanced gut microbiota composition in patients with AF in which *Ruminococcus*, *Streptococcus*, and *Enterococcus* significantly increased while *Faecalibacterium*, *Alistipes*, *Oscillibacter*, and *Bilophila* obviously reduced [103]. Later, they found that patients with persistent AF (psAF) shared a great proportion of common features of gut microbiota dysbiosis [104]. In their latest study, the fecal microbiota from patients with psAF and those with paroxysmal AF were investigated, verifying a similar pattern of gut microbiota, with similar ratios of *Firmicutes* to *Bacteroidetes* [105].

Svingen et al. conducted a study in thousands of patients with suspected stable angina and proposed that plasma TMAO levels are definitely related to AF [106]. It is well known that thrombi can easily take place in the left atrial appendage of patients with AF, which then leads to embolism. Gong et al. found that in patients with AF, elevated TMAO levels are related to thrombus formation, manifested as platelet hyperreactivity [107]. It has been confirmed that the cardiac autonomic nervous system (CANS) can regulate the pathophysiology of AF or VA [108]. Meng et al. first proposed that preserving dysbacteriosis or modulating metabolites such as TMAO may be a target to treat arrhythmia due to the ability of TMAO to stimulate CANS and deteriorate ischaemia-induced VA by releasing proinflammatory markers such as IL-1 β and TNF- α [109]. Similarly, according to the experiment of Yu et al., gut microbes have the ability to counteract AF progression by producing TMAO and can thus activate CANS in a rapid atrial pacing-induced canine AF model [110]. Likewise, in a propionate-treated hypertensive mouse model, the susceptibility to cardiac ventricular arrhythmias was significantly reduced, indicating

possible links between SCFAs and arrhythmia development [22]. Although the connection between gut microbiota and arrhythmia has been established, the precise underlying mechanisms still await further investigation (Table 2).

4. Microorganism-Targeted Therapies

4.1. Fecal Microbiota Transplantation. As an effective approach to directly introduce intestinal flora, fecal microbiota transplantation (FMT) has gained much attention. The therapeutic value of FMT in gastrointestinal diseases, neurological and psychiatric disorders, and immunology regulation has been extensively examined [22, 111, 112]. However, studies concerning its application in CVDs are limited. Although oral supplementation of resveratrol has been proven to improve glucose homeostasis by altering gut microbiota, in the work of Kim and his colleagues [113], FMT from resveratrol-fed mice to obese mice was found to yield better results than oral administration of resveratrol alone, indicating that FMT is more straightforward and direct. Moreover, Hu et al. showed that FMT could abolish the increased proportion of *Firmicutes/Bacteroidetes*, diminish inflammatory infiltration in cardiomyocytes, and thereby attenuate myocarditis in mice [5]. However, in a double-blind trial involving 20 patients, the composition of intestinal flora was altered in the recipients after FMT from vegetarians, whereas the vasculitis indicators presented no improvement [114]. There are also disadvantages to FMT. For instance, endotoxins are transferred along with the donor microbiome. How to weigh the pros and cons of actual practice is still an issue to be addressed. To guarantee the reliable and smooth application of FMT in clinical use, the establishment of stool banks is on its way.

4.2. Probiotic Administration. Among the numerous bacteria residing in the host intestine, some are beneficial. An extra boost of these bacteria would probably bring positive results, thus leading to the application of probiotics. In a meta-analysis involving 846 individuals with hypertension, mild reductions in blood pressure, body mass index (BMI), and blood glucose levels were observed after probiotic administration, supporting the beneficial role of probiotics in blood pressure control [115]. Similarly, in other studies with spontaneously hypertensive rats, the probiotics *Bifidobacterium breve* and *Lactobacillus fermentum* were found to elicit antihypertensive effects by restoring gut microbiota balance and preventing endothelial dysfunction [116], whereas long-term supplementation with kefir ameliorated high blood pressure via improvement in intestinal integrity [117]. Moreover, in apoE^{-/-} mice fed with HFD, supplementation with *Lactobacillus rhamnosus* GR-1 markedly reduced atherosclerotic lesion size by alleviating oxidative stress and inflammation [118]. Likewise, *Lactobacillus plantarum* ZDY04 has been shown to downregulate serum TMAO levels, which is a critical factor contributing to atherosclerosis development [119].

4.3. Herbal Medicine. Traditional Chinese medicine (TCM), which mainly utilizes herbs and their extracts, has recently been demonstrated to treat CVDs via intestinal microbial modulation. Ou et al. reviewed and summarized the mecha-

nisms of gut flora in TCM's theory of "stasis of intermingled phlegm and blood stasis" [120]. For example, the fact that TMAO promotes thrombosis might be one of the major causes of CVDs [121]. Anlu et al. showed that berberine originating from the Chinese herb *Coptis chinensis* has the ability to regulate the "microbiota-metabolism-immunity" axis [122]. Moreover, resveratrol derived from *Polygonum cuspidatum* was demonstrated to attenuate TMAO-induced atherosclerosis in apoE^{-/-} mice by remodelling microbiota as well as decreasing TMAO and BA levels [123]. In addition, Ghosh et al. found that curcumin, a phytochemical component of *Curcuma longa*, attenuates atherosclerosis in LDLR^{-/-} mice by regulating intestinal barrier function [124]. Anwar et al. showed that Trigonelline, which is purified from the seeds of *Trigonella foenum-graecum*, can inhibit the growth of *Citrobacter freundii* and subsequently decrease the production of TMAO in mice [125].

5. Conclusion

Evidence from a compilation of studies of animals and humans indicates that the implications of gut microbiota and their metabolites in CVDs are well established. With high-throughput technologies, verification of the intestinal flora composition and in-depth mechanistic exploration are accessible. However, the links between gut microbiota and disease development are so complex that they involve immune regulation, the inflammatory response, gut barrier integrity, metabolic homeostasis, etc. Further investigations into the specific mechanisms are needed, which then share the possibility of being transferred into clinical practice.

Conflicts of Interest

The authors declare no conflicts of interest, financial or otherwise.

Authors' Contributions

MZ conceived of and designed the study and revised the manuscript for important intellectual content; XZ performed the literature search. YC generated the figures and tables; MN performed the background research. MZ and PZ edited the manuscript. WZ and YC drafted the manuscript. All authors have read and approved the content of the manuscript. Wenyi Zhou, Yiyu Cheng, and Ping Zhu contributed equally to this work.

Acknowledgments

This research was funded by the National Key Research and Development Program of China (2018YFA0108700), the NSFC Projects of International Cooperation and Exchanges (81720102004), the National Natural Science Foundation of China (81974019, 81970248), and the National Training Program of Innovation and Entrepreneurship for Undergraduates (2020105330125). AJE edited the manuscript for grammar, punctuation and spelling.

References

- [1] J. M. Brown and S. L. Hazen, "Microbial modulation of cardiovascular disease," *Nature Reviews Microbiology*, vol. 16, no. 3, pp. 171–181, 2018.
- [2] W. H. Tang, T. Kitai, and S. L. Hazen, "Gut microbiota in cardiovascular health and disease," *Circulation Research*, vol. 120, no. 7, pp. 1183–1196, 2017.
- [3] W. Tang, D. Y. Li, and S. L. Hazen, "Dietary metabolism, the gut microbiome, and heart failure," *Nature Reviews Cardiology*, vol. 16, no. 3, pp. 137–154, 2019.
- [4] K. Kiouptsi and C. Reinhardt, "Contribution of the commensal microbiota to atherosclerosis and arterial thrombosis," *British journal of pharmacology*, vol. 175, no. 24, pp. 4439–4449, 2018.
- [5] T. T. Kim, N. Parajuli, M. M. Sung et al., "Fecal transplant from resveratrol-fed donors improves glycaemia and cardiovascular features of the metabolic syndrome in mice," *American Journal of Physiology-Endocrinology and Metabolism*, vol. 315, no. 4, pp. E511–E519, 2018.
- [6] J. Liu, T. Zhang, Y. Wang et al., "Baicalin ameliorates neuropathology in repeated cerebral ischemia-reperfusion injury model mice by remodeling the gut microbiota," *Aging (Albany NY)*, vol. 12, no. 4, pp. 3791–3806, 2020.
- [7] S. Wan, Y. Nie, Y. Zhang, C. Huang, and X. Zhu, "Gut microbial dysbiosis is associated with profibrotic factors in liver fibrosis mice," *Frontiers in cellular and infection microbiology*, vol. 10, p. 18, 2020.
- [8] M. Jin, Z. Qian, J. Yin, W. Xu, and X. Zhou, "The role of intestinal microbiota in cardiovascular disease," *Journal of Cellular and Molecular Medicine*, vol. 23, no. 4, pp. 2343–2350, 2019.
- [9] F. Z. Marques, C. R. Mackay, and D. M. Kaye, "Beyond gut feelings: how the gut microbiota regulates blood pressure," *Nature Reviews Cardiology*, vol. 15, no. 1, pp. 20–32, 2018.
- [10] Y. Li, H. S. Faden, and L. Zhu, "The response of the gut microbiota to dietary changes in the first two years of life," *Frontiers in Pharmacology*, vol. 11, p. 334, 2020.
- [11] F. Fava, L. Rizzetto, and K. M. Tuohy, "Gut microbiota and health: connecting actors across the metabolic system," *Proceedings of the Nutrition Society*, vol. 78, no. 2, pp. 177–188, 2019.
- [12] W. H. W. Tang, F. Bäckhed, U. Landmesser, and S. L. Hazen, "Intestinal microbiota in cardiovascular health and disease: JACC State-of-the-Art Review," *Journal of the American College of Cardiology*, vol. 73, no. 16, pp. 2089–2105, 2019.
- [13] P. B. Eckburg, E. M. Bik, C. N. Bernstein et al., "Diversity of the human intestinal microbial flora," *Science*, vol. 308, no. 5728, pp. 1635–1638, 2005.
- [14] S. R. Gill, M. Pop, R. T. DeBoy et al., "Metagenomic analysis of the human distal gut microbiome," *Science*, vol. 312, no. 5778, pp. 1355–1359, 2006.
- [15] A. Koliada, G. Syzenko, V. Moseiko et al., "Association between body mass index and Firmicutes/Bacteroidetes ratio in an adult Ukrainian population," *BMC Microbiology*, vol. 17, no. 1, pp. 1–6, 2017.
- [16] C. Indiani, K. F. Rizzardi, P. M. Castelo, L. F. C. Ferraz, M. Darrieux, and T. M. Parisotto, "Childhood obesity and Firmicutes/Bacteroidetes ratio in the gut microbiota: a systematic review," *Childhood Obesity*, vol. 14, no. 8, pp. 501–509, 2018.
- [17] A. Pascale, N. Marchesi, S. Govoni, A. Coppola, and C. Gazzaruso, "The role of gut microbiota in obesity, diabetes mellitus, and effect of metformin: new insights into old diseases," *Current Opinion in Pharmacology*, vol. 49, pp. 1–5, 2019.
- [18] P. V. Chang, L. Hao, S. Offermanns, and R. Medzhitov, "The microbial metabolite butyrate regulates intestinal macrophage function via histone deacetylase inhibition," *Proceedings of the National Academy of Sciences*, vol. 111, no. 6, pp. 2247–2252, 2014.
- [19] L. Macia, J. Tan, A. T. Vieira et al., "Metabolite-sensing receptors GPR43 and GPR109A facilitate dietary fibre-induced gut homeostasis through regulation of the inflammasome," *Nature communications*, vol. 6, no. 1, p. 6734, 2015.
- [20] J. Tan, C. McKenzie, M. Potamitis, A. N. Thorburn, C. R. Mackay, and L. Macia, "The role of short-chain fatty acids in health and disease," *Advances in Immunology*, vol. 121, pp. 91–119, 2014.
- [21] P. M. Smith, M. R. Howitt, N. Panikov et al., "The microbial metabolites, short-chain fatty acids, regulate colonic Treg cell homeostasis," *Science*, vol. 341, no. 6145, pp. 569–573, 2013.
- [22] H. Bartolomeaus, A. Balogh, M. Yakoub et al., "Short-chain fatty acid propionate protects from hypertensive cardiovascular damage," *Circulation*, vol. 139, no. 11, pp. 1407–1421, 2019.
- [23] M. H. Kim, S. G. Kang, J. H. Park, M. Yanagisawa, and C. H. Kim, "Short-chain fatty acids activate GPR41 and GPR43 on intestinal epithelial cells to promote inflammatory responses in mice," *Gastroenterology*, vol. 145, no. 2, pp. 396–406.e10, 2013.
- [24] G. G. Schiattarella, A. Sannino, E. Toscano et al., "Gut microbe-generated metabolite trimethylamine-N-oxide as cardiovascular risk biomarker: a systematic review and dose-response meta-analysis," *European Heart Journal*, vol. 38, no. 39, pp. 2948–2956, 2017.
- [25] R. Zhuang, X. Ge, L. Han et al., "Gut microbe-generated metabolite trimethylamine-N-oxide and the risk of diabetes: a systematic review and dose-response meta-analysis," *Obesity Reviews*, vol. 20, no. 6, pp. 883–894, 2019.
- [26] O. Manor, N. Zubair, M. P. Conomos et al., "A multi-omic association study of trimethylamine N-oxide," *Cell Reports*, vol. 24, no. 4, pp. 935–946, 2018.
- [27] X. Sun, X. Jiao, Y. Ma et al., "Trimethylamine N-oxide induces inflammation and endothelial dysfunction in human umbilical vein endothelial cells via activating ROS-TXNIP-NLRP3 inflammasome," *Biochemical and Biophysical Research Communications*, vol. 481, no. 1-2, pp. 63–70, 2016.
- [28] C. Yue, X. Yang, J. Li et al., "Trimethylamine N-oxide prime NLRP3 inflammasome via inhibiting ATG16L1-induced autophagy in colonic epithelial cells," *Biochemical and Biophysical Research Communications*, vol. 490, no. 2, pp. 541–551, 2017.
- [29] M. M. Seldin, Y. Meng, H. Qi et al., "Trimethylamine N-oxide promotes vascular inflammation through signaling of mitogen-activated protein kinase and nuclear Factor- κ B," *Journal of the American Heart Association*, vol. 5, no. 2, 2016.
- [30] A. Kriaa, M. Bourgin, A. Potiron et al., "Microbial impact on cholesterol and bile acid metabolism: current status and future prospects," *Journal of Lipid Research*, vol. 60, no. 2, pp. 323–332, 2019.
- [31] R. Villette, P. Kc, S. Beliard et al., "Unraveling host-gut microbiota dialogue and its impact on cholesterol levels," *Frontiers in Pharmacology*, vol. 11, 2020.

- [32] D. J. Kenny, D. R. Plichta, D. Shungin et al., "Cholesterol metabolism by uncultured human gut bacteria influences host cholesterol level," *Cell Host & Microbe*, vol. 28, no. 2, pp. 245–257.e6, 2020.
- [33] J. M. Ridlon, S. C. Harris, S. Bhowmik, D. J. Kang, and P. B. Hylemon, "Consequences of bile salt biotransformations by intestinal bacteria," *Gut Microbes*, vol. 7, no. 1, pp. 22–39, 2016.
- [34] S. A. Joyce and C. G. Gahan, "Disease-associated changes in bile acid profiles and links to altered gut microbiota," *Digestive Diseases*, vol. 35, no. 3, pp. 169–177, 2017.
- [35] H. Wang, J. D. Latorre, M. Bansal et al., "Microbial metabolite deoxycholic acid controls *Clostridium perfringens*-induced chicken necrotic enteritis through attenuating inflammatory cyclooxygenase signaling," *Scientific Reports*, vol. 9, no. 1, article 14541, 2019.
- [36] K. S. Michelsen, M. H. Wong, P. K. Shah et al., "Lack of Toll-like receptor 4 or myeloid differentiation factor 88 reduces atherosclerosis and alters plaque phenotype in mice deficient in apolipoprotein E," *Proceedings of the National Academy of Sciences*, vol. 101, no. 29, pp. 10679–10684, 2004.
- [37] A. E. Mullick, P. S. Tobias, and L. K. Curtiss, "Modulation of atherosclerosis in mice by Toll-like receptor 2," *The Journal of Clinical Investigation*, vol. 115, no. 11, pp. 3149–3156, 2005.
- [38] G. den Besten, A. Bleeker, A. Gerding et al., "Short-chain fatty acids protect against high-fat diet-induced obesity via a PPAR γ -Dependent switch from lipogenesis to fat oxidation," *Diabetes*, vol. 64, no. 7, pp. 2398–2408, 2015.
- [39] M. Hernandez, E. E. Canfora, J. Jocken, and E. E. Blaak, "The short-chain fatty acid acetate in body weight control and insulin sensitivity," *Nutrients*, vol. 11, no. 8, p. 1943, 2019.
- [40] X. Tan, Y. Liu, J. Long et al., "Trimethylamine N-oxide aggravates liver steatosis through modulation of bile acid metabolism and inhibition of farnesoid X receptor signaling in nonalcoholic fatty liver disease," *Molecular Nutrition & Food Research*, vol. 63, no. 17, article e1900257, 2019.
- [41] A. Tirosh, E. S. Calay, G. Tuncman et al., "The short-chain fatty acid propionate increases glucagon and FABP4 production, impairing insulin action in mice and humans," *Science Translational Medicine*, vol. 11, no. 489, p. eaav0120, 2019.
- [42] A. Bronden and F. K. Knop, "Glucose-metabolic effects of pharmacotherapy-induced modulation of bile acid physiology," *The Journal of Clinical Endocrinology & Metabolism*, vol. 105, no. 1, pp. 362–373, 2020.
- [43] L. Ding, M. Chang, Y. Guo et al., "Trimethylamine-N-oxide (TMAO)-induced atherosclerosis is associated with bile acid metabolism," *Lipids in Health and Disease*, vol. 17, no. 1, p. 286, 2018.
- [44] L. Sheng, P. K. Jena, Y. Hu et al., "Hepatic inflammation caused by dysregulated bile acid synthesis is reversible by butyrate supplementation," *The Journal of pathology*, vol. 243, no. 4, pp. 431–441, 2017.
- [45] K. Saito, R. Suzuki, Y. Koyanagi, H. Isogai, H. Yoneyama, and E. Isogai, "Inhibition of enterohemorrhagic *Escherichia coli* O157:H7 infection in a gnotobiotic mouse model with pre-colonization by *Bacteroides* strains," *Biomedical Reports*, vol. 10, no. 3, pp. 175–182, 2019.
- [46] O. P. Mathew, K. Ranganna, J. Mathew et al., "Cellular effects of butyrate on vascular smooth muscle cells are mediated through disparate actions on dual targets, histone deacetylase (HDAC) Activity and PI3K/Akt Signaling Network," *International Journal of Molecular Sciences*, vol. 20, no. 12, p. 2902, 2019.
- [47] K. Kim, O. Kwon, T. Y. Ryu et al., "Propionate of a microbiota metabolite induces cell apoptosis and cell cycle arrest in lung cancer," *Molecular Medicine Reports*, vol. 20, no. 2, pp. 1569–1574, 2019.
- [48] N. Nie, C. Bai, S. Song, Y. Zhang, B. Wang, and Z. Li, "Bifidobacterium plays a protective role in TNF- α -induced inflammatory response in Caco-2 cell through NF- κ B and p38MAPK pathways," *Molecular and Cellular Biochemistry*, vol. 464, no. 1-2, pp. 83–91, 2020.
- [49] C. J. Li and T. H. Elsasser, "Butyrate-induced apoptosis and cell cycle arrest in bovine kidney epithelial cells: involvement of caspase and proteasome pathways1," *Journal of Animal Science*, vol. 83, no. 1, pp. 89–97, 2005.
- [50] L. F. Iannucci, J. Sun, B. K. Singh et al., "Short chain fatty acids induce UCP2-mediated autophagy in hepatic cells," *Biochemical and biophysical research communications*, vol. 480, no. 3, pp. 461–467, 2016.
- [51] C. M. Qiao, M. F. Sun, X. B. Jia et al., "Sodium butyrate causes α -synuclein degradation by an Atg5-dependent and PI3K/Akt/mTOR-related autophagy pathway," *Experimental Cell Research*, vol. 387, no. 1, article 111772, p. 111772, 2020.
- [52] J. Liu, Y. Wang, H. Meng et al., "Butyrate rather than LPS subverts gingival epithelial homeostasis by downregulation of intercellular junctions and triggering pyroptosis," *Journal of Clinical Periodontology*, vol. 46, no. 9, pp. 894–907, 2019.
- [53] P. Wu, J. Chen, J. Chen et al., "Trimethylamine N-oxide promotes apoE(-/-) mice atherosclerosis by inducing vascular endothelial cell pyroptosis via the SDHB/ROS pathway," *Journal of Cellular Physiology*, vol. 235, no. 10, pp. 6582–6591, 2020.
- [54] J. Gu, W. Huang, W. Zhang et al., "Sodium butyrate alleviates high-glucose-induced renal glomerular endothelial cells damage via inhibiting pyroptosis," *International Immunopharmacology*, vol. 75, article 105832, 2019.
- [55] H. Cohen, N. Baram, L. Edry-Botzer, A. Munitz, D. Salomon, and M. Gerlic, "Vibriopore-forming leukocidin activates pyroptotic cell death via the NLRP3 inflammasome," *Emerging Microbes & Infections*, vol. 9, no. 1, pp. 278–290, 2020.
- [56] R. S. Chapkin, S. L. Navarro, M. Hullar, and J. W. Lampe, "Diet and gut microbes act coordinately to enhance programmed cell death and reduce colorectal cancer risk," *Digestive Diseases and Sciences*, vol. 65, no. 3, pp. 840–851, 2020.
- [57] P. Lavtar, G. Rudolf, A. Maver et al., "Association of circadian rhythm genes ARNTL/BMAL1 and CLOCK with multiple sclerosis," *PloS One*, vol. 13, no. 1, article e0190601, 2018.
- [58] Z. Liu, Z. Y. Wei, J. Chen et al., "Acute sleep-wake cycle shift results in community alteration of human gut microbiome," *Msphere*, vol. 5, no. 1, 2020.
- [59] A. Segers, L. Desmet, T. Thijs, K. Verbeke, J. Tack, and I. Depoortere, "The circadian clock regulates the diurnal levels of microbial short-chain fatty acids and their rhythmic effects on colon contractility in mice," *Acta Physiologica*, vol. 225, no. 3, article e13193, 2019.
- [60] F. Z. Marques, E. Nelson, P. Y. Chu et al., "High-fiber diet and acetate supplementation change the gut microbiota and prevent the development of hypertension and heart failure in hypertensive mice," *Circulation*, vol. 135, no. 10, pp. 964–977, 2017.

- [61] X. Wu, L. Chen, F. Zeb et al., “Clock-Bmal1 mediates MMP9 induction in acrolein-promoted atherosclerosis associated with gut microbiota regulation,” *Environmental Pollution*, vol. 252, no. Part B, pp. 1455–1463, 2019.
- [62] I. H. Page, “The mosaic theory of arterial hypertension—its interpretation,” *Perspectives in Biology and Medicine*, vol. 10, no. 3, pp. 325–333, 1967.
- [63] J. Li, F. Zhao, Y. Wang et al., “Gut microbiota dysbiosis contributes to the development of hypertension,” *Microbiome*, vol. 5, no. 1, p. 14, 2017.
- [64] J. Huart, J. Leenders, B. Taminiau et al., “Gut microbiota and fecal levels of short-chain fatty acids differ upon 24-hour blood pressure levels in men,” *Hypertension*, vol. 74, no. 4, pp. 1005–1013, 2019.
- [65] S. Kim, R. Goel, A. Kumar et al., “Imbalance of gut microbiome and intestinal epithelial barrier dysfunction in patients with high blood pressure,” *Clinical Science*, vol. 132, no. 6, pp. 701–718, 2018.
- [66] J. L. Pluznick, R. J. Protzko, H. Gevorgyan et al., “Olfactory receptor responding to gut microbiota-derived signals plays a role in renin secretion and blood pressure regulation,” *Proceedings of the National Academy of Sciences*, vol. 110, no. 11, pp. 4410–4415, 2013.
- [67] I. R. Barrows, A. Ramezani, and D. S. Raj, “Inflammation, immunity, and oxidative stress in hypertension—partners in crime?,” *Advances in Chronic Kidney Disease*, vol. 26, no. 2, pp. 122–130, 2019.
- [68] A. W. C. Man, H. Li, and N. Xia, “Resveratrol and the interaction between gut microbiota and arterial remodelling,” *Nutrients*, vol. 12, no. 1, p. 119, 2020.
- [69] X. Ge, L. Zheng, R. Zhuang et al., “The gut microbial metabolite trimethylamine N-oxide and hypertension risk: a systematic review and dose-response meta-analysis,” *Advances in Nutrition*, vol. 11, no. 1, pp. 66–76, 2020.
- [70] J. Liu, T. Li, H. Wu et al., “Lactobacillus rhamnosus GG strain mitigated the development of obstructive sleep apnea-induced hypertension in a high salt diet via regulating TMAO level and CD4(+) T cell induced-type I inflammation,” *Biomedicine & Pharmacotherapy*, vol. 112, article 108580, 2019.
- [71] M. Ufnal, R. Jazwiec, M. Dadlez, A. Drapala, M. Sikora, and J. Skrzypecki, “Trimethylamine-N-oxide: a carnitine-derived metabolite that prolongs the hypertensive effect of angiotensin II in rats,” *Canadian Journal of Cardiology*, vol. 30, no. 12, pp. 1700–1705, 2014.
- [72] X. Yan, J. Jin, X. Su et al., “Intestinal flora modulates blood pressure by regulating the synthesis of intestinal-derived corticosterone in high salt-induced hypertension,” *Circulation Research*, vol. 126, no. 7, pp. 839–853, 2020.
- [73] O. Koren, A. Spor, J. Felin et al., “Human oral, gut, and plaque microbiota in patients with atherosclerosis,” *Proceedings of the National Academy of Sciences*, vol. 108, Supplement_1, pp. 4592–4598, 2011.
- [74] Z. Jie, H. Xia, S. L. Zhong et al., “The gut microbiome in atherosclerotic cardiovascular disease,” *Nature Communications*, vol. 8, no. 1, p. 845, 2017.
- [75] S. D. Wright, C. Burton, M. Hernandez et al., “Infectious agents are not necessary for murine atherogenesis,” *The Journal of Experimental Medicine*, vol. 191, no. 8, pp. 1437–1442, 2000.
- [76] Z. Wang, E. Klipfell, B. J. Bennett et al., “Gut flora metabolism of phosphatidylcholine promotes cardiovascular disease,” *Nature*, vol. 472, no. 7341, pp. 57–63, 2011.
- [77] K. Kasahara, K. A. Krautkramer, E. Org et al., “Interactions between Roseburia intestinalis and diet modulate atherogenesis in a murine model,” *Nature Microbiology*, vol. 3, no. 12, pp. 1461–1471, 2018.
- [78] Y. Du, X. Li, C. Su et al., “Butyrate protects against high-fat diet-induced atherosclerosis via up-regulating ABCA1 expression in apolipoprotein E-deficiency mice,” *British Journal of Pharmacology*, vol. 177, no. 8, pp. 1754–1772, 2020.
- [79] Z. He, W. Hao, E. Kwek et al., “Fish oil is more potent than flaxseed oil in modulating gut microbiota and reducing trimethylamine-N-oxide-exacerbated atherogenesis,” *Journal of Agricultural and Food Chemistry*, vol. 67, no. 49, pp. 13635–13647, 2019.
- [80] R. A. Hasan, A. Y. Koh, and A. Zia, “The gut microbiome and thromboembolism,” *Thrombosis Research*, vol. 189, pp. 77–87, 2020.
- [81] K. Huynh, “Novel gut microbiota-derived metabolite promotes platelet thrombosis via adrenergic receptor signalling,” *Nature Reviews Cardiology*, vol. 17, no. 5, p. 265, 2020.
- [82] A. Lassiger-Herfurth, G. Pontarollo, A. Grill, and C. Reinhardt, “The gut microbiota in cardiovascular disease and arterial thrombosis,” *Microorganisms*, vol. 7, no. 12, p. 691, 2019.
- [83] Z. X. Wu, S. F. Li, H. Chen et al., “The changes of gut microbiota after acute myocardial infarction in rats,” *PLoS One*, vol. 12, no. 7, article e0180717, 2017.
- [84] X. Zhou, J. Li, J. Guo et al., “Gut-dependent microbial translocation induces inflammation and cardiovascular events after ST-elevation myocardial infarction,” *Microbiome*, vol. 6, no. 1, p. 66, 2018.
- [85] A. Haghikia, X. S. Li, T. G. Liman et al., “Gut microbiota-dependent trimethylamine N-oxide predicts risk of cardiovascular events in patients with stroke and is related to proinflammatory monocytes,” *Arteriosclerosis, Thrombosis, and Vascular Biology*, vol. 38, no. 9, pp. 2225–2235, 2018.
- [86] T. Tang, H. C. Chen, C. Y. Chen et al., “Loss of gut microbiota alters immune system composition and cripples postinfarction cardiac repair,” *Circulation*, vol. 139, no. 5, pp. 647–659, 2019.
- [87] V. Lam, J. Su, S. Koprowski et al., “Intestinal microbiota determine severity of myocardial infarction in rats,” *The FASEB Journal*, vol. 26, no. 4, pp. 1727–1735, 2011.
- [88] P. Ponikowski, A. A. Voors, S. D. Anker et al., “016 ESC Guidelines for the diagnosis and treatment of acute and chronic heart failure: The Task Force for the diagnosis and treatment of acute and chronic heart failure of the European Society of Cardiology (ESC) Developed with the special contribution of the Heart Failure Association (HFA) of the ESC,” *European Heart Journal*, vol. 18, no. 8, pp. 891–975, 2016.
- [89] Y. Heianza, W. Ma, J. E. Manson, K. M. Rexrode, and L. Qi, “Gut microbiota metabolites and risk of major adverse cardiovascular disease events and death: a systematic review and meta-analysis of prospective studies,” *Journal of the American Heart Association*, vol. 6, no. 7, 2017.
- [90] J. Peng, X. Xiao, M. Hu, and X. Zhang, “Interaction between gut microbiome and cardiovascular disease,” *Life Sciences*, vol. 214, pp. 153–157, 2018.

- [91] E. Pasini, R. Aquilani, C. Testa et al., "Pathogenic gut flora in patients with chronic heart failure," *JACC: Heart Failure*, vol. 4, no. 3, pp. 220–227, 2016.
- [92] Q. Jia, H. Li, H. Zhou et al., "Role and effective therapeutic target of gut microbiota in heart failure," *Cardiovascular Therapeutics*, vol. 2019, Article ID 5164298, 10 pages, 2019.
- [93] T. T. Tang, J. Yuan, Z. F. Zhu et al., "Regulatory T cells ameliorate cardiac remodeling after myocardial infarction," *Basic Research in Cardiology*, vol. 107, no. 1, pp. 232–232, 2012.
- [94] Y. Nagatomo and W. H. Tang, "Intersections between microbiome and heart failure: revisiting the gut hypothesis," *Journal of Cardiac Failure*, vol. 21, no. 12, pp. 973–980, 2015.
- [95] A. Zabell and W. H. Tang, "Targeting the microbiome in heart failure," *Current Treatment Options in Cardiovascular Medicine*, vol. 19, no. 4, p. 27, 2017.
- [96] M. Savi, L. Bocchi, L. Bresciani et al., "Trimethylamine-N-oxide (TMAO)-induced impairment of cardiomyocyte function and the protective role of urolithin B-glucuronide," *Molecules*, vol. 23, no. 3, p. 549, 2018.
- [97] B. Jin, F. Ji, A. Zuo et al., "Destructive role of TMAO in T-tubule and excitation-contraction coupling in the adult cardiomyocytes," *International Heart Journal*, vol. 61, no. 2, pp. 355–363, 2020.
- [98] C. L. Organ, H. Otsuka, S. Bhushan et al., "Choline diet and its gut microbe-derived metabolite, trimethylamine N-oxide, exacerbate pressure overload-induced heart failure," *Circulation: Heart Failure*, vol. 9, no. 1, article e002314, 2016.
- [99] K. Schuett, M. E. Kleber, H. Scharnagl et al., "Trimethylamine-N-oxide and heart failure with reduced versus preserved ejection fraction," *Journal of the American College of Cardiology*, vol. 70, no. 25, pp. 3202–3204, 2017.
- [100] G. Wang, B. Kong, W. Shuai, H. Fu, X. Jiang, and H. Huang, "3,3-Dimethyl-1-butanol attenuates cardiac remodeling in pressure-overload-induced heart failure mice," *The Journal of Nutritional Biochemistry*, vol. 78, p. 108341, 2020.
- [101] J. Herrmann, "Adverse cardiac effects of cancer therapies: cardiotoxicity and arrhythmia," *Nature Reviews Cardiology*, vol. 17, no. 8, pp. 474–502, 2020.
- [102] C. A. Vahdatpour, J. J. Luebbert, and H. I. Palevsky, "Atrial arrhythmias in chronic lung disease-associated pulmonary hypertension," *Pulmonary Circulation*, vol. 10, no. 1, article 204589402091068, 2020.
- [103] K. Zuo, J. Li, K. Li et al., "Disordered gut microbiota and alterations in metabolic patterns are associated with atrial fibrillation," *GigaScience*, vol. 8, no. 6, 2019.
- [104] K. Zuo, J. Li, P. Wang et al., "Duration of persistent atrial fibrillation is associated with alterations in human gut microbiota and metabolic phenotypes," *Msystems*, vol. 4, no. 6, 2019.
- [105] K. Zuo, X. Yin, K. Li et al., "Different types of atrial fibrillation share patterns of gut microbiota dysbiosis," *Msphere*, vol. 5, no. 2, 2020.
- [106] G. Svingen, H. Zuo, P. M. Ueland et al., "Increased plasma trimethylamine-N-oxide is associated with incident atrial fibrillation," *International Journal of Cardiology*, vol. 267, pp. 100–106, 2018.
- [107] D. Gong, L. Zhang, Y. Zhang, F. Wang, Z. Zhao, and X. Zhou, "Gut microbial metabolite trimethylamine N-oxide is related to thrombus formation in atrial fibrillation patients," *The American Journal of the Medical Sciences*, vol. 358, no. 6, pp. 422–428, 2019.
- [108] K. Shivkumar, O. A. Ajijola, I. Anand et al., "Clinical neurocardiology defining the value of neuroscience-based cardiovascular therapeutics," *The Journal of Physiology*, vol. 594, no. 14, pp. 3911–3954, 2016.
- [109] G. Meng, X. Zhou, M. Wang et al., "Gut microbe-derived metabolite trimethylamine N-oxide activates the cardiac autonomic nervous system and facilitates ischemia-induced ventricular arrhythmia via two different pathways," *EBioMedicine*, vol. 44, pp. 656–664, 2019.
- [110] L. Yu, G. Meng, B. Huang et al., "A potential relationship between gut microbes and atrial fibrillation: trimethylamine N-oxide, a gut microbe-derived metabolite, facilitates the progression of atrial fibrillation," *International Journal of Cardiology*, vol. 255, pp. 92–98, 2018.
- [111] H. Antushevich, "Fecal microbiota transplantation in disease therapy," *Clinica Chimica Acta*, vol. 503, pp. 90–98, 2020.
- [112] F. Zhang, T. Zhang, H. Zhu, and T. J. Borody, "Evolution of fecal microbiota transplantation in methodology and ethical issues," *Current Opinion in Pharmacology*, vol. 49, pp. 11–16, 2019.
- [113] P. F. de Groot, M. N. Frissen, N. C. de Clercq, and M. Nieuwdorp, "Fecal microbiota transplantation in metabolic syndrome: History, present and future," *Gut Microbes*, vol. 8, no. 3, pp. 253–267, 2017.
- [114] X. F. Hu, W. Y. Zhang, Q. Wen et al., "Fecal microbiota transplantation alleviates myocardial damage in myocarditis by restoring the microbiota composition," *Pharmacological Research*, vol. 139, pp. 412–421, 2019.
- [115] L. P. Smits, R. S. Kootte, E. Levin et al., "Effect of vegan fecal microbiota transplantation on carnitine- and choline-derived trimethylamine-N-oxide production and vascular inflammation in patients with metabolic syndrome," *Journal of the American Heart Association*, vol. 7, no. 7, 2018.
- [116] C. Chi, C. Li, D. Wu et al., "Effects of probiotics on patients with hypertension: a systematic review and meta-analysis," *Current Hypertension Reports*, vol. 22, no. 5, 2020.
- [117] I. Robles-Vera, M. Toral, N. la Visitación et al., "Probiotics prevent dysbiosis and the rise in blood pressure in genetic hypertension: role of short-chain fatty acids," *Molecular Nutrition & Food Research*, vol. 64, no. 6, article 1900616, 2020.
- [118] S. M. de Almeida, F. E. Mowry, S. C. Peaden, T. U. Andrade, and V. C. Biancardi, "Kefir ameliorates hypertension via gut-brain mechanisms in spontaneously hypertensive rats," *The Journal of Nutritional Biochemistry*, vol. 77, 2020.
- [119] Y. Fang, H. Q. Chen, X. Zhang et al., "Probiotic administration of lactobacillus rhamnosus GR-1 attenuates atherosclerotic plaque formation in ApoE^{-/-} mice fed with a high-fat diet," *European Review for Medical and Pharmacological Sciences*, vol. 23, no. 8, pp. 3533–3541, 2019.
- [120] L. Qiu, X. Tao, H. Xiong, J. Yu, and H. Wei, "Lactobacillus plantarum ZDY04 exhibits a strain-specific property of lowering TMAO via the modulation of gut microbiota in mice," *Food & Function*, vol. 9, no. 8, pp. 4299–4309, 2018.
- [121] Y. Ou, C. Zhang, M. Yao, and L. Wang, "Gut Flora: Novel therapeutic target of Chinese medicine for the treatment of cardiovascular diseases," *Evidence-Based Complementary and Alternative Medicine*, vol. 2019, Article ID 3719596, 7 pages, 2019.
- [122] W. Anlu, C. Dongcheng, Z. He et al., "Using herbal medicine to target the "microbiota-metabolism-immunity" axis as possible therapy for cardiovascular disease," *Pharmacological Research*, vol. 142, pp. 205–222, 2019.

- [123] M. L. Chen, L. Yi, Y. Zhang et al., “Resveratrol attenuates trimethylamine-N-oxide (TMAO)-induced atherosclerosis by regulating TMAO synthesis and bile acid metabolism via remodeling of the gut microbiota,” *MBio*, vol. 7, no. 2, pp. e02210–e02215, 2016.
- [124] S. S. Ghosh, J. Bie, J. Wang, and S. Ghosh, “Oral supplementation with non-absorbable antibiotics or curcumin attenuates western diet-induced atherosclerosis and glucose intolerance in LDLR^{-/-} mice—role of intestinal permeability and macrophage activation,” *PloS One*, vol. 9, no. 9, article e108577, 2014.
- [125] S. Anwar, U. Bhandari, B. P. Panda, K. Dubey, W. Khan, and S. Ahmad, “Trigonelline inhibits intestinal microbial metabolism of choline and its associated cardiovascular risk,” *Journal of Pharmaceutical and Biomedical Analysis*, vol. 159, pp. 100–112, 2018.

Research Article

Dexmedetomidine Improves Lung Function by Promoting Inflammation Resolution in Patients Undergoing Totally Thoracoscopic Cardiac Surgery

Junji Cui,^{1,2} Mintai Gao,^{1,2} Hongqian Huang,^{1,2} Xiaoyan Huang,³ and Qingshi Zeng^{1,2} 

¹Department of Anesthesiology, Guangdong Cardiovascular Institute, Guangdong Provincial People's Hospital, Guangdong Academy of Medical Sciences, Guangzhou 510080, China

²Department of Anesthesiology, Guangdong Provincial People's Hospital Zhuhai Hospital (Zhuhai Golden Bay Center Hospital), Zhuhai 519040, China

³Department of Clinical Laboratory, Guangdong Provincial People's Hospital Zhuhai Hospital (Zhuhai Golden Bay Center Hospital), Zhuhai 519040, China

Correspondence should be addressed to Qingshi Zeng; 1963088488@qq.com

Received 11 May 2020; Revised 12 August 2020; Accepted 19 August 2020; Published 8 September 2020

Academic Editor: Ziqing Hei

Copyright © 2020 Junji Cui et al. This is an open access article distributed under the Creative Commons Attribution License, which permits unrestricted use, distribution, and reproduction in any medium, provided the original work is properly cited.

Objective. Totally thoracoscopic cardiac surgery under cardiopulmonary bypass combined with one-lung ventilation has been identified as the trend in cardiac surgery. The aim of this study was to examine the effects of the selective α_2 adrenergic receptor agonist dexmedetomidine on the pulmonary function of patients who underwent mitral valve surgery using the totally thoracoscopic technique. **Methods.** Fifty-seven patients who underwent thoracoscopic mitral valve surgery between July 2019 and December 2019 were selected. The patients were randomly divided into the control (Con) group ($n = 28$) and the dexmedetomidine (DEX) group ($n = 29$) using the random number table method. Arterial blood gas analyses were performed, and the oxygenation ($\text{PaO}_2/\text{FiO}_2$) and respiratory indexes ($\text{P(A-a)O}/\text{PaO}_2$) were calculated 5 min after tracheal intubation (T1), 2 h after operation (T2), 6 h after operation (T3), and 24 h after operation (T4). Moreover, the serum cytokines interleukin-6 (IL-6), tumor necrosis factor- α (TNF- α), and intercellular adhesion molecule-1 (ICAM-1) were detected using the enzyme-linked immunosorbent method at all time points. Chest radiography was performed 24 h after surgery. Peripheral blood samples were collected before and after the operation for a complete hemogram. Additionally, the procalcitonin concentration was measured and recorded when the patients were transported to the intensive care unit (ICU). The postoperative extubation time, length of ICU stay, and pulmonary infection rate were also recorded. **Results.** Inflammatory reaction after surgery was evident. However, the inflammatory cytokines IL-6, TNF- α , and ICAM-1 in the DEX group were lower than those in the Con group after surgery (T2 to T4; $P < 0.05$). Neutrophil counts and procalcitonin concentration were higher in the Con group than in the DEX group ($P < 0.05$). In addition, in the DEX group, pulmonary exudation on chest radiography was lower, and pulmonary function, as shown by an increase in oxidation index and decrease in the respiratory index, improved after surgery ($P < 0.05$). Moreover, the duration of mechanical ventilation in the Con group was 3.4 h longer than that in the DEX group. **Conclusion.** Dexmedetomidine has a protective effect on pulmonary function in patients undergoing mitral valve surgery using a totally video-assisted thoracoscopic technique, which may be related to a reduction in the concentration of inflammatory cytokines in the early perioperative period.

1. Introduction

Totally thoracoscopic cardiac surgery has developed rapidly in clinical practice due to its minimally invasive technique and rapid recovery [1]. Thoracoscopic cardiac surgery requires cardiopulmonary bypass (CPB) and the one-lung

ventilation (OLV) technique. Both CPB and OLV can result in acute lung injury associated with the systemic inflammatory response syndrome (SIRS) and pulmonary ischemia-reperfusion injury, which can lead to pulmonary dysfunction and seriously affect a patient's prognosis [2–4]. SIRS caused by CPB has been one of the main factors that lead to

postoperative lung injury after CPB. Activation of the complement system is considered the initiating factor of postoperative lung injury from CPB [5]. Both the classic and alternative pathways of the complement system are activated during the CPB process, with the intensity of the inflammatory response enhanced through interaction with inflammatory factors such as tumor necrosis factor- α (TNF- α), procalcitonin (PCT), interleukin-1 (IL-1), IL-2, IL-6, and IL-8. Neutrophils adhere to pulmonary vascular endothelial cells under the influence of inflammatory factors such as IL-1, IL-6, IL-8, and TNF- α ; platelet-activating factors; and leukotriene B, which causes an increase in pulmonary capillary permeability and edema. The interaction and cascade of cytokines during OLV are the primary mechanisms that cause lung injury [6].

Dexmedetomidine (DEX) is a highly selective α_2 adrenergic receptor (α_2 AR) that is widely used in perioperative cardiovascular surgeries. Specifically, DEX activates α_2 adrenergic receptors and acts as a sedative agent by blocking signal transduction in the nucleus coeruleus near the fourth ventricle [7]. In recent years, clinical and basic research has confirmed that DEX has a protective effect against lung injury [8]. One study has shown that DEX can reduce lung inflammation in septic rats by inhibiting the TLR4/NF- κ B pathway [9]. DEX also increases the expression level of heme oxygenase-1 and the activity of superoxide dismutase in the lung during OLV, reducing oxidative stress and inflammation caused by OLV in patients with lung cancer during surgery, thereby improving intrapulmonary shunting and hypoxemia [10, 11]. In addition, DEX may reduce IL-6 levels and high-mobility group box-1 generation by inhibiting the activation of NF- κ B, which leads to a suppression of SIRS after CPB [12].

This study is aimed at examining the effects of DEX on inflammatory factors and respiratory indicators during thoracoscopic mitral valve surgery to provide clinical evidence for organ protection during cardiac surgery.

2. Materials and Methods

2.1. Study Design. The experimental methods of this study were designed in accordance with the Declaration of Helsinki. The clinical trial was registered under No. ChiCTR2000032652 in the Chinese Clinical Trial Registry, and patients provided informed consent after the study was approved by the Institute of Medical Ethics Committee at Guangdong Provincial People's Hospital (No. GDREC2020001H).

2.2. Study Patients and Protocol. The present study was conducted at Guangdong Provincial People's Hospital. Fifty-seven consecutive patients who underwent totally thoracoscopic valvular cardiac surgery between July 2019 and September 2019 were included after they were assessed for the following criteria: (1) patients aged between 18 and 65 years, (2) American Society of Anesthesiology score II or III and New York Heart Association class II or III, (3) an estimated extracorporeal circulation of ≤ 180 min, (4) no active infective endocarditis, and (5) a rheumatic factor (RF) level of < 20 IU/mL.

The following patients were excluded: (1) elderly patients ≥ 70 years old; (2) patients without sick sinus syndrome and atrioventricular block (bradycardia, heart rate < 60 beats per minute, atrioventricular block above the first degree, or indoor conduction block); (3) patients accompanied with coronary heart disease or cerebrocardiac syndrome; (4) patients with Gold grade of $> \text{level } 2$; (5) patients with severe pulmonary hypertension, with a pulmonary artery systolic pressure of > 60 mmHg; (6) patients with immune system diseases; (7) patients with abnormal renal function with a blood creatinine level of > 110 $\mu\text{mol/L}$; and (8) patients in whom CPB or the prevention of all-cause mortality from reoperation was difficult.

Patients were randomly divided into 2 groups according to the random number table method (Figure 1). In the DEX group, after successful tracheal intubation, the patients received an infusion of 0.5 $\mu\text{g/kg}$ DEX within 10 min using a microinfusion pump. DEX was then continuously infused at 0.5 $\mu\text{g/kg/h}$ until the operation was completed. In the control (Con) group, the patients were administered normal saline instead of DEX, but at the same rate and dose as in the experimental group.

2.3. Sample Size. Based on the main outcome measures (various points of pulmonary function) in our preliminary experiment, to achieve acceptable results, the sample allocation ratio of the two groups was 1.0, the test effect ($1 - \beta$) of the study was 0.9, and the significance level was $\alpha = 0.05$. The PASS 11.0 software was used for calculating the sample size and the T2 time point oxygenation index (Con group 322 ± 45 and DEX group 370 ± 60). The maximum of the minimum sample size was 27 patients. Based on a potential dropout rate of 20%, each group needed 33 patients, and 72 patients were included in the actual study.

2.4. Anesthesia and Surgical Procedure. The patients, monitored using electrocardiography, underwent radial artery puncture and catheterization after entering the operating room. Intravenous injections of midazolam 0.05 mg/kg (Jiangsu Nhwa Pharmaceutical Co., Ltd., Jiangsu, China), sufentanil 1 $\mu\text{g/kg}$ (Yichang Humanwell Pharmaceutical Co., Ltd., Yichang, China), etomidate 0.3 mg/kg (Jiangsu Nhwa Pharmaceutical Co., Ltd., Jiangsu, China), and cisatracurium 0.3 mg/kg (Hengrui Medicine, Jiangsu, China) were used for the induction of anesthesia. Tracheal intubation was performed 5 min after induction using the Shiley Endobronchial Tube (Covidien, Medtronic, Inc., USA), and tracheal catheterization was performed using bronchoscopy. Next, a superior vena cava drainage tube and central venous catheters (B Braun, Ltd., Germany) were inserted through the right internal jugular vein.

During the maintenance of anesthesia, remifentanyl (Yichang Humanwell Pharmaceutical Co., Ltd., Yichang, China) was infused with a micropump at a rate of 0.3 $\mu\text{g/kg/min}$, propofol (Jiangsu Nhwa Pharmaceutical Co., Ltd., Jiangsu, China) at a rate of $2-3$ mg/kg/h, and cisatracurium (Hengrui Medicine, Jiangsu, China) at a rate of 2 $\mu\text{g/kg/min}$, with intermittent inhalation of sevoflurane (Hengrui Medicine). The Narcotrend Index was kept at $25-35$, and the protective pulmonary

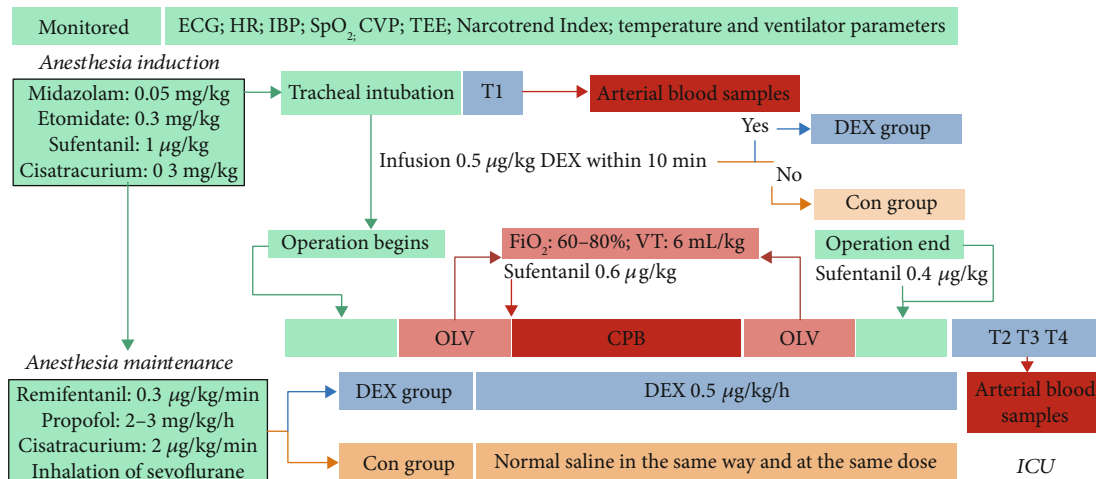


FIGURE 1: Flow diagram of the study protocol. (1) Dexmedetomidine (DEX) group. The patients in the DEX group received an infusion of 0.5 µg/kg DEX within 10 min via a microinfusion pump after successful tracheal intubation. DEX at a dose of 0.5 µg/kg/h was then continuously infused until the operation was completed. (2) The control (Con) group. The patients in the Con group were administered normal saline in the same way and at the same dose. Arterial blood samples (3 mL) were collected in the Con and DEX groups at 5 min (T1) after tracheal intubation and 2 h (T2), 6 h (T3), and 24 h (T4) after surgery. ECG: electrocardiography; HR: heart rate; HR: heart rate; CPB: cardiopulmonary bypass; OLV: one-lung ventilation; IBP: invasive blood pressure; VT: tidal volume; TEE: transesophageal echocardiography.

ventilation strategy was adopted during OLV with the anesthesia system Aisys CS2 (GE Medical System Trade Development-Shanghai Co., Ltd.). The fraction of inspiration O₂ (FiO₂) was 50%–80%, the tidal volume was controlled at approximately 6 mL/kg, the respiratory rate was 16–22 times per minute, an inspiratory-to-expiratory ratio of 1:2 was performed, the transcutaneous oxygen saturation (SpO₂) was maintained at >90%, and an end-expiratory pressure of 3–5 cmH₂O (0.29–0.49 kPa) was used.

After anesthesia induction, for achieving a good operation position, the CPB was established through the superior vena cava and femoral vein-to-artery cannulation. A right anterior external fourth thoracotomy of approximately 3.5 cm was performed. At the level of the axillary midline, an endoscope was inserted through the fifth intercostal space, inserting Chitwood aortic occlusive forceps through the fourth intercostal and parallel atrial sulcus incision of the left atrium. During the operation, the CPB was operated with Stockert S5 (Solin Medical-Shanghai, Co., Ltd.), an artificial cardiopulmonary system, and a CPB perfusion flow of 1.8–2.4 L/m²/min was maintained. The intraoperative hematocrit level was controlled at 25%–30%, and the internal environment was stable. Vacuum-assisted venous drainage technology (negative pressure controlled at –50 to –35 mmHg, 1 mmHg = 0.133 kPa) with whole-body cooling (moderate degrees of systemic hypothermia at 28°C) was used intraoperatively. After the completion of the intracardiac operation, rewarming to a rectal temperature of 36°C was initiated. Once the results of the qualitative and quantitative analyses of cardiac structure and function using the esophageal echocardiography technique were found to be satisfactory, CPB was stopped. Before chest closure, sputum aspiration and atelectasis were performed. In both patient groups, the basic balance between liquid intake and output was maintained during operation.

2.5. Inflammatory Cytokine Detection and Outcome Parameter Measurements. In both groups, arterial blood samples (3 mL) were collected at all time points (T1–T4). RapidPoint 500 (R) (Siemens Healthcare Diagnostics) blood gas analysis system was used to calculate the oxidation index (OI) and respiratory index (RI). The remaining arterial blood was stored in a tube containing coagulant ethylenediaminetetraacetic acid (Zhejiang Huafu Medical Equipment Co., Ltd., China), allowed to stand for 1 h, and then centrifuged at room temperature at 3500 r/min in a BY-600A centrifuge (Bai yang Medical, Guangdong, China) for 10 min. The supernatant was then collected for the detection of TNF-α, IL-6, and intercellular adhesion molecule-1 (ICAM-1).

Peripheral venous blood samples were collected before and after the operation for a complete hemogram (white blood cell (WBC) counts, neutrophil counts, hemoglobin (Hb) levels, and platelet counts) and for assessing the levels of creatinine, blood urea nitrogen, alanine aminotransferase (ALT), aspartate aminotransferase (AST), activated partial thromboplastin time (APTT), and prothrombin time (PT). In addition, procalcitonin (PCT) activity was measured using the ELISA method in accordance with the manufacturer's instructions (KeyGen Biotech. Co., Ltd., Nanjing, China).

In addition, the postoperative extubation time, length of intensive care unit (ICU) stay, and the incidence of pulmonary infections were recorded.

2.6. Statistical Analyses. The SPSS 25.0 statistical software was used for the data analysis. Numerical data are described as numbers or rates. The Pearson χ^2 test was used for intergroup comparisons. The measurement data are described as mean \pm standard deviation. The *t*-test was used for intergroup comparisons. Repeated-measures data were analyzed using repeated-measures analysis of variance. Differences

were considered significant when the two-tailed P values were <0.05 .

3. Results

3.1. No Significant Difference in Basic Patient Characteristics Was Found between the Con and DEX Groups. In accordance with the inclusion and exclusion criteria, 57 patients were included in the present study (Figure 2). As shown in Table 1, no statistically significant differences were found between the Con and DEX groups in terms of sex, age, body mass index, cardiac function grade, left ventricular ejection fraction, pulmonary artery systolic pressure, aortic occlusion time, extracorporeal circulation time, surgical type, or comorbidities such as diabetes, grade 3 hypertension, and atrial fibrillation ($P > 0.05$). As shown in Table 2, there were no significant differences found between the two groups in terms of preoperative and postoperative hemoglobin levels, liver function, coagulation parameters, or renal function ($P > 0.05$). The mean postoperative creatinine level in the Con group was $11 \mu\text{mol/L}$ higher than that in the DEX group, but this did not affect normal renal function. As shown in Table 3, no significant difference in postoperative 24 h left ventricular ejection fraction was found between the two groups ($P > 0.05$). All patients in both groups successfully underwent the operation and were discharged after recovery.

3.2. DEX Effectively Reduced the Inflammatory Response after Thoracoscopic Cardiac Surgery. As shown in Figure 3, in the Con group, the serum IL-6 and ICAM-1 levels after thoracoscopic cardiac surgery were significantly higher at T2–T4 ($P < 0.05$ vs. T1; Figures 3(a) and 3(c)). The serum TNF- α level was also significantly higher at T2–T3 than at T1 ($P < 0.05$ vs. T1) but gradually decreased by T4 (Figure 3(b)). In the DEX group, the serum IL-6, ICAM-1, and TNF- α levels were higher at T2–T3 ($P < 0.05$ vs. T1), but these levels were significantly lower at T4 than at T1 ($P > 0.05$ vs. T1; Figures 3(a)–3(c)). The serum IL-6 and ICAM-1 levels in the DEX group were significantly lower at T2, T3, and T4 ($P < 0.05$ vs. the Con group; Figures 3(a) and 3(c)). In addition, the decrease in the serum TNF- α level at T2 was significantly greater in the DEX group ($P < 0.05$ vs. Con group; Figure 3(b)).

3.3. DEX Reduced the Serum PCT Concentration and Neutrophil Count in Peripheral Blood. As shown in Table 2, the postoperative complete blood cell count (white blood cell and neutrophil counts) was lower in the DEX group than in the Con group ($P < 0.05$). Moreover, the serum PCT concentration was lower in the DEX group than in the Con group ($P < 0.05$), suggesting that the risks of inflammation and infection were lower in the DEX group.

3.4. DEX Attenuated Postoperative Pulmonary Exudation after Thoracoscopic Cardiac Surgery. As shown in the digital radiography image in Figure 4, the two groups showed clear lung texture before surgery with no obvious parenchymal lesions and normal brightness of the lung field. Postoperative changes in lung texture were observed in both groups; however, lung exudation was more obvious in the Con group

than in the DEX group. These results show that DEX could alleviate postoperative pulmonary exudation after thoracoscopic cardiac surgery.

3.5. DEX Improved Pulmonary Dispersion, Ventilation, and Oxygenation after Thoracoscopic Cardiac Surgery. The RI reflects lung diffusion and ventilation function, while the oxygenation index (OI) reflects pulmonary oxygenation function.

After thoracoscopic cardiac surgery, the OI of the patients in the Con group was lower at T2–T4 ($P < 0.05$ vs. T1; Figure 5(a)), reaching its lowest value at T3. The OI at T3 showed a 21% decrease compared to that at baseline. In addition, the RI was higher at T2–T3 ($P < 0.05$ vs. T1; Figure 5(b)), reaching its highest level at T2, when the RI was three times the baseline value.

In the DEX group, the OI was lower at T2–T3 than at T1 ($P < 0.05$ vs. T1; Figure 5(a)) and reached its lowest value at T3, but the OI decreased by only 15% compared to the baseline value. The RI was also higher at T2–T3 ($P < 0.05$ vs. T1) and showed the highest value at T2; however, at T2, the RI was only 1.95-times the baseline value (Figure 5(b)). The OI levels at T2, T3, and T4 in the DEX group were significantly higher than those in the Con group ($P < 0.05$ vs. the Con group; Figure 5(a)). In addition, the RI levels at T2 were significantly lower in the DEX group ($P < 0.05$ vs. the Con group; Figure 5(b)).

3.6. DEX Reduced the Mechanical Ventilation Time in the ICU. As shown in Table 4, the extubation time in the Con group was 3.4 h longer than that in the DEX group ($P < 0.05$). However, no significant differences were found between the groups in terms of postoperative ICU stay and pulmonary infection incidence.

4. Discussion

This large-sample retrospective study demonstrated that administering DEX to manage perioperative anesthesia can reduce the impact of CPB, surgery, and anesthesia on various organs of the body, reducing the occurrence of postoperative complications and improving prognosis [13]. While DEX has a high potential of benefit in this context, no uniform dose standard has been established for DEX in cardiovascular surgery. To avoid transient hypertension and excessive inhibition of the cardiovascular system, $0.5 \mu\text{g/kg}$ [14] administered over <10 min was selected as the loading dose, followed by a continuous infusion rate of $0.5 \mu\text{g/kg/h}$ until the end of surgery.

With the development of new technology in cardiac surgery, the associated mortality rate has noticeably decreased. However, postoperative pulmonary insufficiency remains as one of the main causes of postoperative mortality [15]. The systemic inflammatory response associated with CPB, such as the activation of the complement system; cytokines TNF- α , IL-6, and other inflammatory mediators; and the aggregation and activation of neutrophils in the lung, is involved in the process of lung injury. In addition, lung ischemia-reperfusion injury, which includes ischemia and cell damage caused by reperfusion and subsequent oxygen free radical

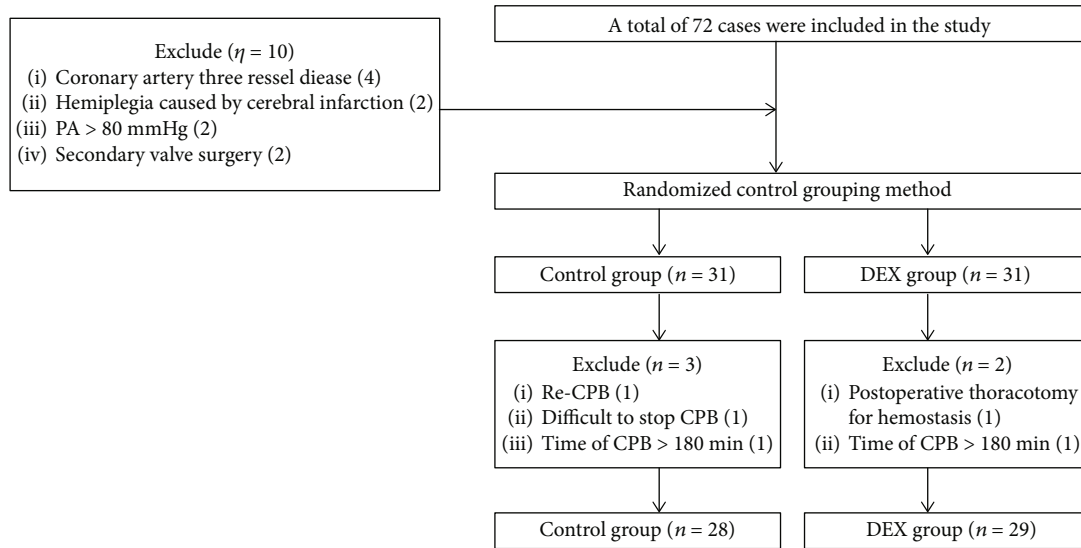


FIGURE 2: Flow chart of patient selection. In total, 76 patients were enrolled, of whom 16 dropped out of the study after randomization (shorter CPB than planned in 6 patients, surgical complications of thoracotomy and secondary chest closure in 5, irregular randomization in 1, heavily calcified large blood vessels that made cannulation impossible for CPB in 1, and loss of follow-up in 3).

TABLE 1: Demographic characteristics of participants in the two groups.

	Con group (n = 28)	DEX group (n = 29)	P value
Age (y)	49.89 ± 13.89	48.04 ± 14.40	0.625
Sex (male/female)	16/12	18/11	0.705
Body mass index (kg/m ²)	22.10 ± 3.02	22.40 ± 3.40	0.722
NYHA classification, n (%)			0.669
II	26 (92.9)	26 (89.7)	
III	2 (7.7)	3 (10.3)	
LVEF (%)	63.89 ± 6.31	62.28 ± 4.97	0.286
PASP (mmHg)	39.39 ± 14.11	34.31 ± 11.96	0.148
Duration of CPB (min)	135.86 ± 33.75	134.71 ± 25.97	0.888
Aortic cross-clamping (min)	92.46 ± 27.53	85.32 ± 19.14	0.265
Operation type, n (%)			0.760
MVR	4 (14.3)	5 (82.8)	
MVP	24 (85.7)	24 (17.2)	
Comorbidities, n (%)			
Grade 3 hypertension	2 (7.7)	3 (10.3)	0.669
Diabetes mellitus	2 (7.1)	1 (3.4)	0.532
Atrial fibrillation	7 (25.0)	5 (17.2)	0.473

Quantitative data are presented as means ± standard deviations or numbers (percentages). NYHA: New York Heart Association; PASP: pulmonary artery systolic pressure; LVEF: left ventricular ejection fraction; MVR: mitral valve replacement; MVP: mitral valvuloplasty.

release, various inflammatory mediators, and factor secretion, eventually leads to lung dysfunction, which is characterized by an increase in pulmonary vascular permeability, pulmonary edema, elevated pulmonary vascular resistance, and leukocyte infiltration [16]. In addition, OLV is accompanied by a large increase in plasma levels of inflammatory factors, resulting in systemic and pulmonary inflammatory responses, which may lead to a relatively high tidal volume

and airway pressure and to overexpansion and collapse of the alveoli [17, 18]. Compared with the traditional techniques, totally thoracoscopic cardiac surgery requires more time for CPB and OLV [19], which may lead to an increase in the risk of lung injury. Moreover, owing to pulmonary ischemia-reperfusion and swelling mechanical injury, 8.0% of patients undergoing totally thoracoscopic cardiac surgery develop unilateral pulmonary edema after the operation

TABLE 2: Perioperative blood biochemistry results of the patients in the two groups.

	Con group (<i>n</i> = 28)	DEX group (<i>n</i> = 29)	<i>P</i> value
Hemoglobin (g/L)			
Preoperative	12.48 ± 1.42	12.62 ± 1.53	0.725
Postoperative	11.11 ± 1.47	10.81 ± 1.38	0.425
Aspartate aminotransferase (U/L)			
Preoperative	27.44 ± 9.17	25.57 ± 7.09	0.392
Postoperative	88.43 ± 21.86	82.19 ± 23.21	0.302
Alanine aminotransferase (U/L)			
Preoperative	22.68 ± 11.36	20.50 ± 10.14	0.266
Postoperative	34.01 ± 12.70	30.39 ± 11.57	0.392
Urea nitrogen (mmol/L)			
Preoperative	5.54 ± 1.71	5.38 ± 1.29	0.623
Postoperative	7.57 ± 2.63	7.15 ± 2.45	0.536
Creatinine (μmol/L)			
Preoperative	71.36 ± 20.68	71.03 ± 18.92	0.951
Postoperative	92.07 ± 25.37	81.66 ± 19.75	0.089
Platelet (10 ⁹ /L)			
Preoperative	189.46 ± 36.40	194.38 ± 38.39	0.622
Postoperative	153.25 ± 43.10	151.17 ± 41.58	0.854
APTT (sec)			
Preoperative	31.36 ± 3.96	31.83 ± 3.94	0.659
Postoperative	42.49 ± 12.07	42.98 ± 6.99	0.852
PT (sec)			
Preoperative	14.89 ± 4.99	15.43 ± 4.96	0.679
Postoperative	14.29 ± 2.68	13.70 ± 2.32	0.376
WBC (10 ⁹ /L)			
Preoperative	5.45 ± 1.12	5.38 ± 0.94	0.789
Postoperative	16.69 ± 5.71	13.93 ± 3.50	0.031
Neutrophil (10 ⁹ /L)			
Preoperative	3.64 ± 0.79	3.48 ± 1.03	0.506
Postoperative	14.26 ± 5.31	11.46 ± 3.42	0.021
Procalcitonin (ng/mL)			
Postoperative	7.55 ± 6.82	3.14 ± 2.27	0.020

Quantitative data are presented as means ± standard deviations. WBC: white blood cell; APTT: activated partial thromboplastin time; PT: prothrombin time.

TABLE 3: Postoperative vasoactive-inotropic score (VIS) and left ventricular ejection fraction (LVEF) of the patients in the two groups.

	Con group (<i>n</i> = 28)	DEX group (<i>n</i> = 29)	<i>P</i> value
VIS (μg/kg/min)			
Postoperative 2 h	6.18 ± 3.57	4.88 ± 3.28	0.158
Postoperative 6 h	5.20 ± 3.24	3.34 ± 1.20	0.006
LVEF (%)			
Postoperative 24 h	58.18 ± 5.81	57.00 ± 5.10	0.419

Quantitative data are presented as means ± standard deviations. VIS: vasoactive-inotropic drug score = dopamine (μg/kg/min) * 1 + dobutamine (μg/kg/min) * 1 + milrinone (μg/kg/min) * 10 + adrenaline (μg/kg/min) * 100 + norepinephrine (μg/kg/min) * 100 + pituitrin (units/kg/min) * 1000; h: hour.

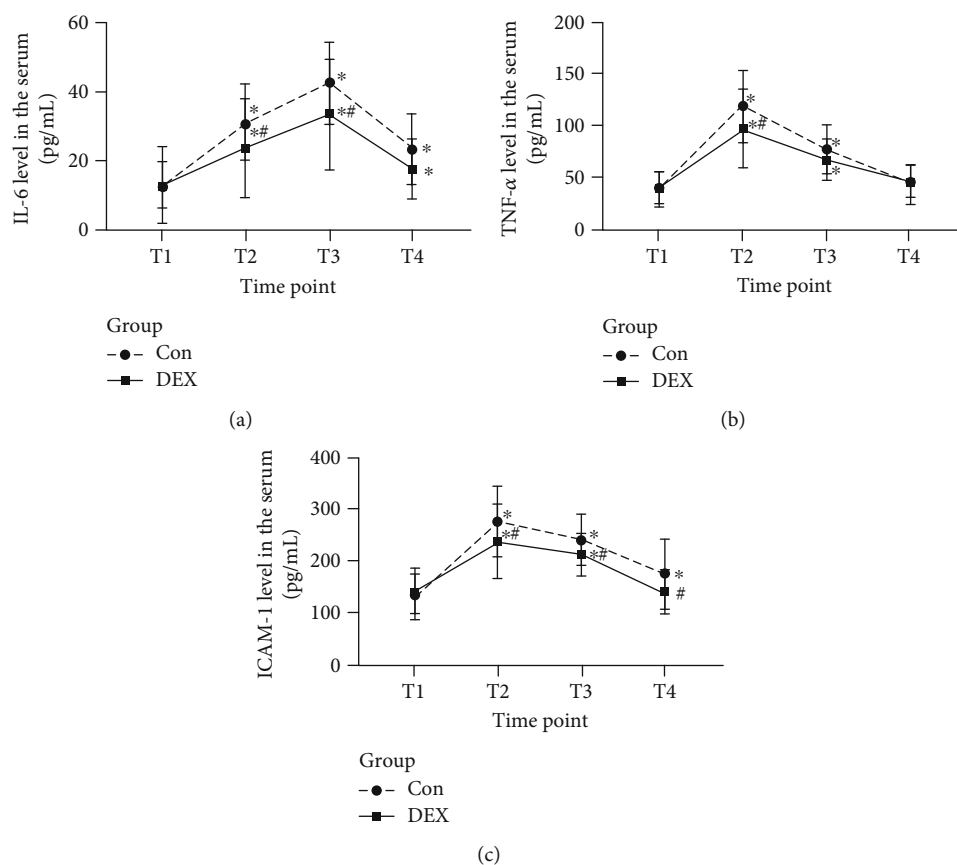


FIGURE 3: Changes in the perioperative serum levels of inflammatory factors. (a) Serum IL-6 level. (b) Serum TNF- α level. (c) Serum ICAM-1 level. *A higher level with a P value of <0.05 for a within-group comparison at the time point T1. #A higher level with a P value of <0.05 in comparison with the Con group at the same time point.

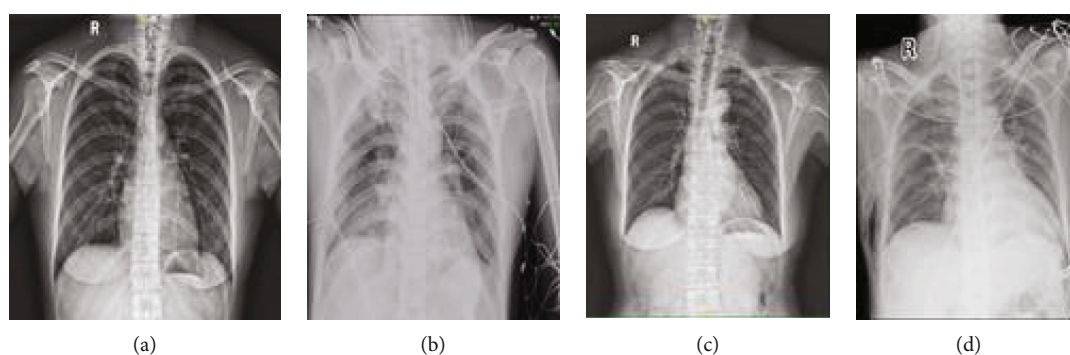


FIGURE 4: Digital radiography. Representative digital radiograph of a patient in the Con group taken (a) before surgery and (b) 1 d after surgery. Representative digital radiograph of a patient in the DEX group taken (c) before surgery and (d) 1 d after surgery.

and have a higher risk of death [20, 21]. Therefore, lung protection is of great importance to the prognosis of totally thoracoscopic cardiac surgery.

A number of inflammatory factors are involved in the damage to the lungs and other important organs after CPB [22, 23]. Evidence shows that neutrophils are closely related to the degree of lung injury and the levels of inflammatory factors [24]. IL-6 has proinflammatory effects on various cells during the acute inflammatory response. It can induce

multiple-organ involvement, mainly including the respiratory system and central nervous systems [25]. TNF- α is considered an early inflammatory responder and can increase the permeability of microcirculatory vessels and affect the RI of patients after CPB and is closely related to multiple-organ dysfunction after CPB [26]. Plasma ICAM-1 is considered a key molecule in mediating the inflammatory process and plays an important role in all phases of an inflammatory reaction. In the inflammatory microenvironment, ICAM-1 can be activated

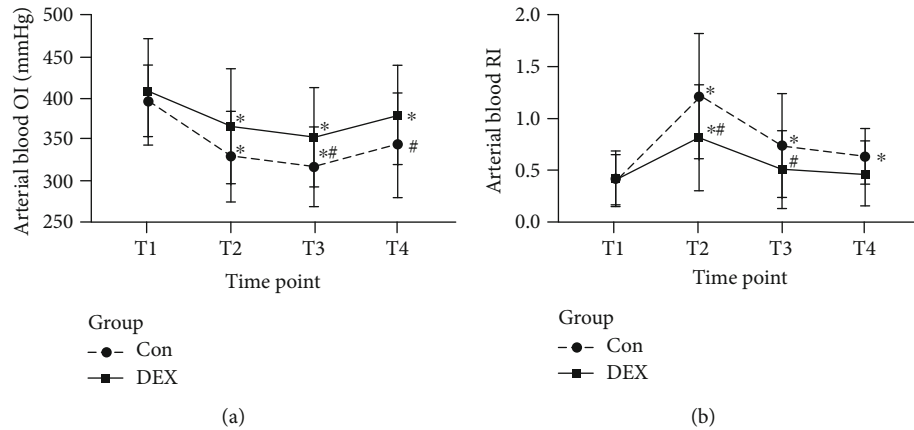


FIGURE 5: Changes in perioperative pulmonary function in both groups. (a) Arterial oxygenation index. (b) Respiratory index based on the assessment of arterial blood. *A higher level with a P value of <0.05 for a within-group comparison at the time point T1. #A higher level with a P value of <0.05 in comparison with the Con group at the same time point.

TABLE 4: Postoperative duration of extubation and ICU stay in the two groups.

	Con group ($n = 28$)	DEX group ($n = 29$)	P value
Duration of extubation (h)	8.782 ± 7.18	5.310 ± 4.37	0.031
Duration of ICU stay (h)	59.89 ± 37.74	49.41 ± 24.01	0.220
Pulmonary infection rate, n (%)	8 (28.5)	4 (13.8)	0.171

Quantitative data are presented as means \pm standard deviations or numbers (percentages). ICU: intensive care unit.

in various cells. ICAM-1 binds to lymphocyte function-related antigen 1, the macrophage-1 molecule, and CD43 on the leukocyte surface, promoting the adhesion of the leukocyte to vascular endothelial cells, with an increased expression as the degree of lung injury increases [27]. *In vivo* and *in vitro* studies have revealed that CPB causes the cascade release of TNF- α , IL-6, IL-8, IL-10, and other proinflammatory and anti-inflammatory mediators and promotes the generation of PCT, which more sensitively reflects the severity of the inflammatory response in the early postoperative stage [28]. The risk of various postoperative complications such as cardiopulmonary insufficiency and SIRS increases in patients after coronary bypass or valve replacement cardiac surgery when the PCT concentration exceeds the threshold of 2 ng/mL after surgery [29]. Therefore, IL-6, TNF- α , and ICAM-1 were used as inflammatory indicators in this study. PCT can reflect the response state of intraoperative inflammation in patients and is a good indicator of postoperative infections. After thoracoscopic cardiac surgery, when the patient is still under anesthesia, a blood gas analysis can objectively reflect the patient's ventilation and ventilatory function, as it is not affected by the environment and patient's cooperation. The RI refers to the ratio of the difference in alveolar-arterial oxygen tension to the partial pressure of arterial oxygen, which means that an increase in RI indicates a decrease in lung dispersion and ventilation. A decrease in OI, which indicates pulmonary ventilatory function, indicates a decrease in pulmonary oxygenation function [30]. In the present study, the levels of IL-6, TNF- α , and ICAM-1 significantly increased at T2 and T3, accompanied by higher RI and lower OI than those before the operation, indicating that the inflammation

after thoracoscopic cardiac surgery is noticeably enhanced and pulmonary function was impaired.

Preventing and reducing inflammation during thoracoscopic heart surgery are important methods for preserving lung function. The development of strategies to optimize the anesthesia scheme so as to reduce perioperative traumatic stress experienced by patients, reduce the production of inflammatory mediators, further improve the pulmonary function of patients, and promote the rapid recovery of patients is an important topic for anesthesiologists. DEX selectively activates the α_2 adrenaline receptors to reduce sympathetic tone and indirectly improves vagal tone, thereby activating the cholinergic anti-inflammatory pathway and reducing the systemic inflammatory response [31]. In addition, DEX can inhibit the production of inflammatory factors such as TNF- α and IL-6 during CPB [32], alleviate the infiltration of inflammatory cells into the alveolar cavity, and reduce the levels of TNF- α and IL-1 levels in plasma and alveolar fluid by inhibiting the activation of NF- κ B, finally reducing the inflammatory response of rat lung tissues and playing a role in lung protection in rats with lung injury [33]. In the present study, we found that neutrophil counts and the levels of IL-6, TNF- α , and ICAM-1 after surgery were lower in the DEX group than in the Con group. The PCT concentration was higher in the Con group than in the DEX group. Pulmonary exudation was reduced in the DEX group based on the basis of radiography, and pulmonary function had improved in the DEX group, as evidenced by the increase in the OI and decrease in the RI at T2 to T4 as compared with T1. Moreover, the duration of mechanical ventilation in the Con group was

3.4 h longer than that in the DEX. These results suggest that DEX can reduce postoperative exudation and protect lung function, which may be related to a reduction in inflammatory factors. However, no significant difference was found between the groups in terms of postoperative ICU time and pulmonary infection rate. Therefore, whether increasing the dose of DEX or whether extending the duration of its action affects postoperative ICU time and pulmonary infection rates must be further verified.

In summary, the clinical use of dexmedetomidine is safe and feasible and has a certain value in improving pulmonary function after totally video-assisted thoracoscopic mitral valve surgery under CPB combined with OLV, further improving the effect of minimally invasive cardiac surgery.

Data Availability

The datasets generated and/or analyzed during the present study are available from the corresponding author on reasonable request.

Conflicts of Interest

The authors report no conflict of interest.

Authors' Contributions

Junji Cui, Mintai Gao, and Hongqian Huang contributed equally to this work. Qingshi Zeng is responsible for the study design. Junji Cui is responsible for the study registration. Junji Cui, Xiaoyan Huang, and Mintai Gao contributed to patient recruitment. Junji Cui, Mintai Gao, and Hongqian Huang revised the manuscript. All authors wrote and approved the manuscript. Junji Cui, Xiaoyan Huang, and Mintai Gao collected and interpreted the data. Junji Cui contributed to the statistical analysis.

References

- [1] M. R. Dehghani, M. Kasianzadeh, Y. Rezaei, and N. Sephehrvand, "Atorvastatin reduces the incidence of postoperative atrial fibrillation in statin-naïve patients undergoing isolated heart valve surgery," *Journal of Cardiovascular Pharmacology and Therapeutics*, vol. 20, no. 5, pp. 465–472, 2015.
- [2] S. S. C. Wong and M. G. Irwin, "Anaesthesia and minimally invasive surgery," *Anaesthesia & Intensive Care Medicine*, vol. 19, no. 1, pp. 11–15, 2018.
- [3] Z. Xing, J. Han, X. Hao et al., "Immature monocytes contribute to cardiopulmonary bypass-induced acute lung injury by generating inflammatory descendants," *Thorax*, vol. 72, no. 3, pp. 245–255, 2017.
- [4] M. Ranucci, A. Ballotta, M. T. la Rovere, S. Castelvechio, and for the Surgical and Clinical Outcome Research (SCORE) Group, "Postoperative hypoxia and length of intensive care unit stay after cardiac surgery: the underweight paradox?," *PLoS One*, vol. 9, no. 4, article e93992, 2014.
- [5] H. Chen, Z. B. Cheng, and R. G. Yu, "Procalcitonin as a predictor of moderate to severe acute respiratory distress syndrome after cardiac surgery with cardiopulmonary bypass: a study protocol for a prospective cohort study," *BMJ Open*, vol. 4, no. 10, article e006344, 2014.
- [6] U. J. Sachs, "Recent insights into the mechanism of transfusion-related acute lung injury," *Current Opinion in Hematology*, vol. 18, no. 6, pp. 436–442, 2011.
- [7] J. Afonso and F. Reis, "Dexmedetomidine: current role in anesthesia and intensive care," *Revista Brasileira de Anestesiologia*, vol. 62, no. 1, pp. 118–133, 2012.
- [8] N. Bao and B. Tang, "Organ-protective effects and the underlying mechanism of dexmedetomidine," *Mediators of Inflammation*, vol. 2020, Article ID 6136105, 11 pages, 2020.
- [9] Y. Wu, Y. Liu, H. Huang et al., "Dexmedetomidine inhibits inflammatory reaction in lung tissues of septic rats by suppressing TLR4/NF- κ B pathway," *Mediators of Inflammation*, vol. 2013, Article ID 562154, 9 pages, 2013.
- [10] S. Gao, Y. Wang, J. Zhao, and A. Su, "Effects of dexmedetomidine pretreatment on heme oxygenase-1 expression and oxidative stress during one-lung ventilation," *International Journal of Clinical and Experimental Pathology*, vol. 8, no. 3, pp. 3144–3149, 2015.
- [11] C. Y. Wu, Y. F. Lu, M. L. Wang et al., "Effects of dexmedetomidine infusion on inflammatory responses and injury of lung tidal volume changes during one-lung ventilation in thoracoscopic surgery: a randomized controlled trial," *Mediators of Inflammation*, vol. 2018, Article ID 2575910, 8 pages, 2018.
- [12] M. Ueki, T. Kawasaki, K. Habe, K. Hamada, C. Kawasaki, and T. Sata, "The effects of dexmedetomidine on inflammatory mediators after cardiopulmonary bypass," *Anaesthesia*, vol. 69, no. 7, pp. 693–700, 2014.
- [13] F. Ji, Z. Li, H. Nguyen et al., "Perioperative dexmedetomidine improves outcomes of cardiac surgery," *Circulation*, vol. 127, no. 15, pp. 1576–1584, 2013.
- [14] F. Lam, C. Ransom, J. M. Gossett et al., "Safety and efficacy of dexmedetomidine in children with heart failure," *Pediatric Cardiology*, vol. 34, no. 4, pp. 835–841, 2013.
- [15] M. L. Bailey, S. M. Richter, D. V. Mullany, P. J. Tesar, and J. F. Fraser, "Risk factors and survival in patients with respiratory failure after cardiac operations," *The Annals of Thoracic Surgery*, vol. 92, no. 5, pp. 1573–1579, 2011.
- [16] C. Schlensak, T. Doenst, S. Preusser, M. Wunderlich, M. Kleinschmidt, and F. Beyersdorf, "Cardiopulmonary bypass reduction of bronchial blood flow: a potential mechanism for lung injury in a neonatal pig model," *The Journal of Thoracic and Cardiovascular Surgery*, vol. 123, no. 6, pp. 1199–1205, 2002.
- [17] J. Lohser and P. Slinger, "Lung injury after one-lung ventilation: a review of the pathophysiologic mechanisms affecting the ventilated and the collapsed lung," *Anesthesia and Analgesia*, vol. 121, no. 2, pp. 302–318, 2015.
- [18] T. Schilling, A. Kozian, C. Huth et al., "The pulmonary immune effects of mechanical ventilation in patients undergoing thoracic surgery," *Anesthesia & Analgesia*, vol. 101, no. 4, pp. 957–965, 2005.
- [19] G. Dieberg, N. A. Smart, and N. King, "Minimally invasive cardiac surgery: a systematic review and meta-analysis," *International Journal of Cardiology*, vol. 223, pp. 554–560, 2016.
- [20] K. Inoue, A. Hiraoka, G. Chikazawa et al., "Preventive strategy for re-expansion pulmonary edema after minimally invasive cardiac surgery," *The Annals of Thoracic Surgery*, vol. 109, no. 5, pp. e375–e377, 2020.
- [21] M. P. Tutschka, D. Bainbridge, M. W. A. Chu, B. Kiaii, and P. M. Jones, "Unilateral postoperative pulmonary edema after minimally invasive cardiac surgical procedures: a case-control

- study,” *The Annals of Thoracic Surgery*, vol. 99, no. 1, pp. 115–122, 2015.
- [22] S. Yamashiro, R. Arakaki, Y. Kise, and Y. Kuniyoshi, “Prevention of pulmonary edema after minimally invasive cardiac surgery with mini-thoracotomy using neutrophil elastase inhibitor,” *Annals of Thoracic and Cardiovascular Surgery*, vol. 24, no. 1, pp. 32–39, 2018.
- [23] E. Apostolakis, K. S. Filos, E. Koletsis, and D. Dougenis, “Lung dysfunction following cardiopulmonary bypass,” *Journal of Cardiac Surgery*, vol. 25, no. 1, pp. 47–55, 2010.
- [24] N. Inoue, N. Oka, T. Kitamura et al., “Neutrophil elastase inhibitor sivelestat attenuates perioperative inflammatory response in pediatric heart surgery with cardiopulmonary bypass,” *International Heart Journal*, vol. 54, no. 3, pp. 149–153, 2013.
- [25] M. C. Kapoor and T. R. Ramachandran, “Inflammatory response to cardiac surgery and strategies to overcome it,” *Annals of Cardiac Anaesthesia*, vol. 7, no. 2, pp. 113–128, 2004.
- [26] S. Chen, H. Luan, L. Li et al., “Relationship of HLA – B * 51 and HLA – B * 52 alleles and TNF- α -308A/G polymorphism with susceptibility to Takayasu arteritis: a meta-analysis,” *Clinical Rheumatology*, vol. 36, no. 1, pp. 173–181, 2017.
- [27] J. Reutershan and K. Ley, “Bench-to-bedside review: acute respiratory distress syndrome - how neutrophils migrate into the lung,” *Critical Care*, vol. 8, no. 6, pp. 453–461, 2004.
- [28] M. W. N. Nijsten, P. Olinga, H. T. The et al., “Procalcitonin behaves as a fast responding acute phase protein in vivo and in vitro,” *Critical Care Medicine*, vol. 28, no. 2, pp. 458–461, 2000.
- [29] J. Pasnik, “Participation of procalcitonin in inflammatory response after cardiovascular surgery,” *Postępy Higieny i Medycyny Doświadczalnej (Online)*, vol. 58, pp. 522–529, 2004.
- [30] J. M. Michalski, G. Golden, J. Ikari, and S. I. Rennard, “PDE4: a novel target in the treatment of chronic obstructive pulmonary disease,” *Clinical Pharmacology and Therapeutics*, vol. 91, no. 1, pp. 134–142, 2011.
- [31] A. Rhodes, L. E. Evans, W. Alhazzani et al., “Surviving sepsis campaign: international guidelines for management of sepsis and septic shock: 2016,” *Intensive Care Medicine*, vol. 43, no. 3, pp. 304–377, 2017.
- [32] S. Chen, F. Hua, J. Lu et al., “Effect of dexmedetomidine on myocardial ischemia-reperfusion injury,” *International Journal of Clinical and Experimental Medicine*, vol. 8, no. 11, pp. 21166–21172, 2015.
- [33] X. Wu, X. Song, N. Li, L. Zhan, Q. Meng, and Z. Xia, “Protective effects of dexmedetomidine on blunt chest trauma-induced pulmonary contusion in rats,” *Journal of Trauma and Acute Care Surgery*, vol. 74, no. 2, pp. 524–530, 2013.

Research Article

MG53 Protects against Sepsis-Induced Myocardial Dysfunction by Upregulating Peroxisome Proliferator-Activated Receptor- α

Xue Han,¹ Daili Chen,² Ning Liufu,¹ Fengtao Ji,¹ Qingshi Zeng,³ Weifeng Yao ,⁴ and Minghui Cao ¹

¹Department of Anesthesiology, Sun Yat-sen Memorial Hospital, Sun Yat-sen University, Guangzhou 510120, China

²Department of Anesthesiology, Affiliated Shenzhen Maternity & Child Healthcare Hospital, Southern Medical University, Shenzhen, 518028 Guangdong, China

³Department of Anesthesiology, Cardiovascular Institute of Guangdong Province, Guangdong Provincial People's Hospital, Guangzhou, Guangdong 510030, China

⁴Department of Anesthesiology, The Third Affiliated Hospital of Sun Yat-sen University, Guangzhou 510630, China

Correspondence should be addressed to Weifeng Yao; yaowf3@mail.sysu.edu.cn and Minghui Cao; caomh@mail.sysu.edu.cn

Received 5 April 2020; Revised 2 July 2020; Accepted 10 July 2020; Published 27 August 2020

Academic Editor: Daniel Lopez-Malo

Copyright © 2020 Xue Han et al. This is an open access article distributed under the Creative Commons Attribution License, which permits unrestricted use, distribution, and reproduction in any medium, provided the original work is properly cited.

Background. The heart is one of the most commonly affected organs during sepsis. Mitsugumin-53 (MG53) has attracted attention in research due to its cardioprotective function. However, the role of MG53 in sepsis-induced myocardial dysfunction (SIMD) remains unknown. The purpose of this study was to explore the underlying mechanism of MG53 in SIMD and investigate its potential relationship with peroxisome proliferator-activated receptor- α (PPAR α). **Methods.** The cecal ligation and puncture (CLP) model was created to induce SIMD in rats. Protein levels of MG53 and PPAR α , cardiac function, cardiomyocyte injury, myocardial oxidative stress and inflammatory indicators, and cardiomyocyte apoptosis were measured at 18 h after CLP. The effects of MG53 on PPAR α in SIMD were investigated via preconditioning recombinant human MG53 (rhMG53) and PPAR α antagonist GW6471. **Results.** The expression of MG53 and PPAR α sharply decreased in the myocardium at 18 h after CLP. Compared with the sham group, cardiac function was significantly depressed, which was associated with the destructed myocardium, upregulated oxidative stress indicators and proinflammatory cytokines, and excessive cardiomyocyte apoptosis in the CLP group. Supplementation with rhMG53 enhanced myocardial MG53, increased the survival rate with improved cardiac function, and reduced oxidative stress, inflammation, and myocardial apoptosis, which were associated with PPAR α upregulation. Pretreatment with GW6471 abolished the abovementioned protective effects induced by MG53. **Conclusions.** Both MG53 and PPAR α were downregulated after sepsis shock. MG53 supplement protects the heart against SIMD by upregulating PPAR α expression. Our results provide a new treatment strategy for SIMD.

1. Introduction

Sepsis is a life-threatening organ dysfunction caused by the uncontrolled response of a host's anti-infective immunity [1]. According to the US Centers for Disease Control's (CDC) estimation in 2019, sepsis contributes to the death of approximately 270,000 Americans annually [2], and this figure is at least 6 million per year globally [1]. Evans [3] simplified this complex pathophysiological process into four

main features: endothelial dysfunction, coagulopathy, cellular dysfunction, and cardiovascular dysfunction. This demonstrates that the cardiovascular system acts as a pivotal area in the pathogenesis of sepsis, and the heart is the most vulnerable organ. Approximately 40~60% of patients with sepsis exhibit signs of myocardial dysfunction, and mortality rates are remarkably increased in these patients compared to those without myocardial dysfunction (70% vs. 20%) [4]. Sepsis-induced myocardial dysfunction (SIMD) is defined

as the intrinsic myocardial systolic and diastolic dysfunction of both the left and right sides of the heart, induced by sepsis [5].

It is generally accepted that SIMD is a result of the interaction of uncontrolled inflammation, autonomic malfunction, intracellular Ca^{2+} transporter dysfunction, energetic starvation, mitochondrial dysfunction, oxidant/antioxidant imbalance, and excessive cardiomyocyte apoptosis [6]. The pathophysiologic process of SIMD is complicated; thus, there is no expert consensus guideline for its diagnosis and treatment at present [4]. Although the Surviving Sepsis Campaign (SSC) guidelines [7, 8] propose a therapeutic schedule for sepsis and its complications, mortality remains high [9]. Currently, SIMD therapies are restricted to symptomatic support, such as anti-infection, fluid resuscitation, and oxygen delivery amelioration [7, 8]. Attempts to develop molecular-targeted therapy have failed clinically [10]. Therefore, the personalized treatment of SIMD is still lacking.

Mitsugumin-53 (MG53) is a member of the muscle-specific tripartite motif (TRIM) family that plays an essential role in plasma membrane damage repair [11]. It is rapidly recruited when cell membranes are attacked, following which it facilitates the movement of membrane-repair vesicles toward the damage site and binds exposed phosphatidylserine at the damaged lipid bilayer [12]. Pathogenic factors, such as Ca^{2+} influx and oxidant entry into the cytoplasm, are prevented when membrane disruption is ended. Both in vivo and in vitro, MG53 has demonstrated a protective effect against membrane disruption associated with muscular dystrophy [13], acute kidney [14] and lung [15] injury, ischemic [16] and traumatic [17] brain injury, and myocardial infarction (MI) [18]. We found that MG53 is anchored by dysferlin, which reduces oxidative stress and hepatocyte apoptosis in a hepatic ischemic/reperfusion injury (HIRI) model [19]. MG53 interacts with p85 and caveolin 3 (CaV3) and activates the prosurvival reperfusion injury salvage kinase (RISK) pathway (PI3K/Akt/GSK-3 β cascade and ERK_{1/2} pathway) in cardiac ischemic preconditioning (IPC) or post-conditioning (IPO) [20, 21]. Genetic deletion of MG53 results in damage to cell membrane integrity and impaired myocardial regeneration [20–22].

However, Liu et al. [23], using transgenic mice, showed that the cardiac-specific upregulation of MG53 induced diabetic cardiomyopathy (DCM) via transcriptional activation of peroxisome proliferator-activated receptor- α (PPAR α). Interestingly, PPAR α has been proven to support heart function during SIMD [24]. However, the relationship between MG53 and PPAR α in SIMD is an enigma. Therefore, we designed the current study to investigate the role of MG53 on SIMD and the underlying mechanisms of action.

2. Materials and Methods

2.1. Animals and Operative Procedure. This study was approved by the Animal Care Committee, Sun Yat-Sen University, China. In total, 172 adult Sprague-Dawley rats (240–270 g) were purchased from the Laboratory Animal Center of Sun Yat-Sen University and housed in individual cages in the specific pathogen-free (SPF) experimental room for acclimatization one week before the study. Rats were given

ad libitum access to a standard diet and water under a controlled temperature (21–23°C), humidity (20–30%), and alternating light cycle (12 h light/dark) environment. Food was removed 8 h before the study, but free access to water remained. All the experimental procedures were strictly performed in accordance with the *Guide for the Care and Use of Laboratory Animals* (1996). All possible efforts were made to minimize the number of animals used and their suffering. Cecal ligation and puncture (CLP) operation was performed as described in previous studies [25]. Rats were positioned on a homeothermic heating pad to maintain a rectal temperature at $37 \pm 1^\circ\text{C}$ and inhaled a gas mixture containing 3% isoflurane and 40% oxygen for general anesthesia during the surgery. A midline laparotomy (approximately 3 cm long incision) was performed on the anterior abdomen after disinfection with 10% povidone iodine. The cecum was exposed and ligated by a 3-0 silk suture just below the ileocecal valve to maintain bowel continuity. The cecum was punctured twice with an 18-gauge needle, and a small amount of bowel content was expelled from the punctures by manual application of sufficient pressure. Then, the cecum was returned to the peritoneal cavity, and the abdominal incision was closed with 4-0 silk suture in two layers. At the end of surgery, each rat received a subcutaneous injection of physiological saline solution (5 ml/kg), then returned to ambient air. For the sham-operated animals, the cecum was mobilized but neither ligated nor punctured.

2.2. Experimental Protocol and Drug Administration. As the schematic diagram is shown in Figure 1, two experiments were performed. In experiment 1, a total of 80 rats were randomly assigned to receive sham or CLP operation. At 3 h, 6 h, 12 h, 18 h, and 24 h after the operation, the myocardial tissues from the left ventricle (LV) were collected to measure the expression trend of MG53 and PPAR α by western blotting ($n = 8$).

In experiment 2, a total of 32 rats were randomly allocated to four groups ($n = 8$), consisting of a sham group, CLP group, CLP+recombinant human MG53 (rhMG53) group, and CLP+rhMG53+GW6471 group. Animals received a sham operation in the sham group and CLP operation in the other three groups. rhMG53 protein was administered (5 mg/kg, i.v.) in the CLP+rhMG53 and CLP+rhMG53+GW6471 groups 120 min before CLP surgery [16] while the sham and CLP groups were administered isopycnic vehicle (0.9% sterile saline). Rats in the CLP+rhMG53+GW6471 group also received 1 mg/kg/day i.p. GW6471 (Sigma, St. Louis, MO, USA), a PPAR α antagonist, for 10 consecutive days before surgery [26]. The preparation, separation, and purification of rhMG53 protein have been described in our previous study [19].

2.3. Cardiac Function Evaluation. Then, 18 h after the operation, a hypodynamic stage of sepsis [27], the cardiac function of rats was assayed. After anesthesia by 3% isoflurane inhalation, the LVs were intubated via the right common carotid artery by a catheter filled with heparin saline (500 U/ml) to measure mean arterial blood pressure (MABP) and LV pressure. Left ventricular systolic pressure (LVSP), left ventricular

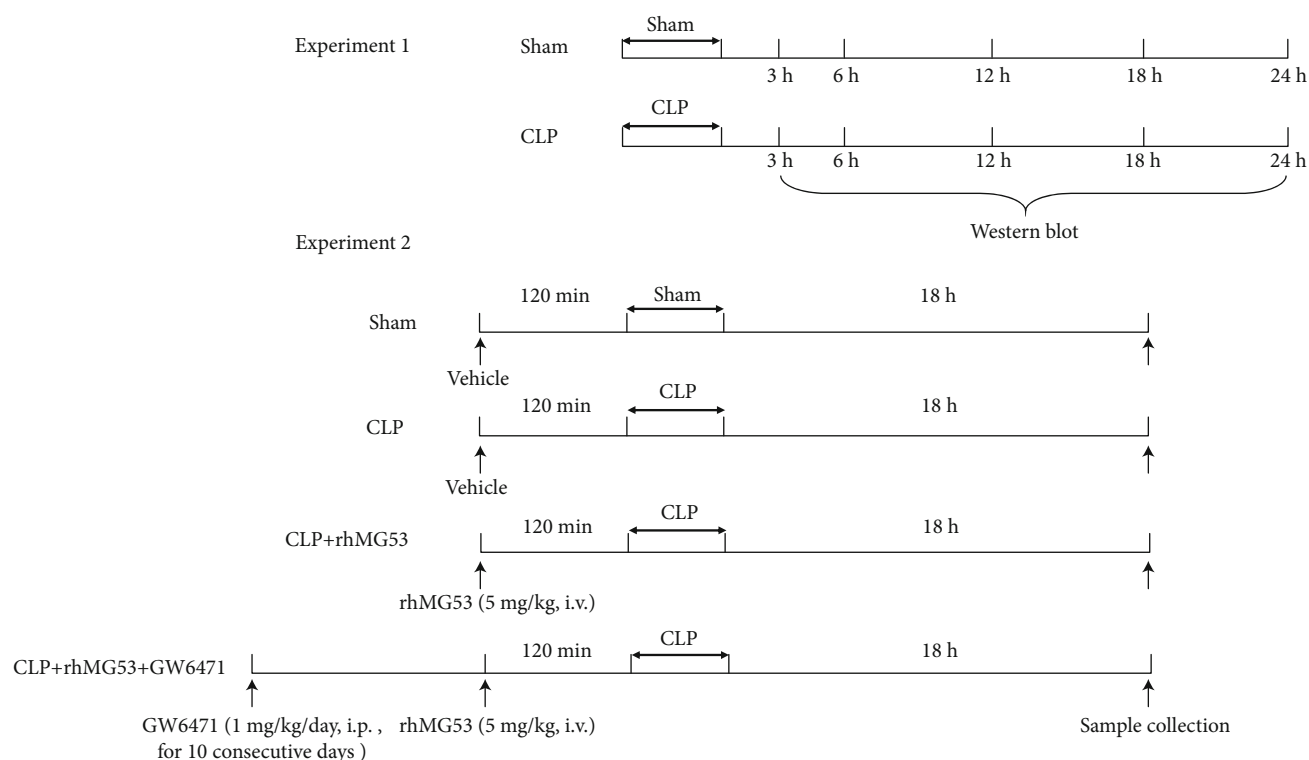


FIGURE 1: Protocol for experiments. CLP = cecal ligation and puncture; rhMG53 = recombinant human MG53.

end-diastolic pressure (LVEDP), and maximum rise/fall rate of LV pressure ($\pm dp/dt_{\max}$) were recorded by the PowerLab Data Acquisition and Analysis System (ADInstruments, Australia).

2.4. Sample Collection. In experiment 1, the LVs were snap-frozen in liquid nitrogen, then stored at -80°C for western blotting at 3 h, 6 h, 12 h, 18 h, and 24 h after the CLP.

In experiment 2, immediately after cardiac function evaluation, the common carotid artery was punctured by a disposable needle for blood collection (5 ml). Blood samples were layered at room temperature (26°C) and centrifuged at 4°C $3000 \times \text{rpm}$ for 10 min to collect the serum for subsequent detections. Then, the rats were euthanized by excessive anesthesia administration. Myocardial tissues from the lower third apex of the LV were selected. One-third of these tissues was postfixed by 10% paraformaldehyde at 4°C for 48 h, paraffin-embedded, and sectioned to a thickness of $5 \mu\text{m}$. Another third was collected for H-FABP and oxidative stress biomarker detection. The final third was snap-frozen in liquid nitrogen, then stored at -80°C for western blotting.

2.5. Hematoxylin and Eosin (H&E) Staining. Sections were stained using a H&E Staining Kit (Abcam, Cambridge, MA, USA), according to the manufacturer's instructions. Morphological changes were evaluated by light microscopy (Nikon Corporation, Japan) at $200\times$ magnification.

2.6. Myocardial Injury Marker Detection in Serum. An enzyme-linked immunosorbent assay (ELISA) was performed to measure the levels of cardiac troponin I (cTnI) (Abcam,

Cambridge, UK) and creatine kinase isoenzyme MB (CK-MB) (MyBioSource, Inc., San Diego, CA, USA) in serum. The lactate dehydrogenase (LDH) activity in serum was determined by chemical colorimetry using an LDH Cytotoxicity Assay Kit (Cayman Chemical Company, Ann Arbor, Michigan, USA).

2.7. Myocardial Heart-Type Fatty Acid Binding Protein (H-FABP) Detection. Myocardial tissues (approximately 0.2 g) were cut with ophthalmic scissors, dissolved in 4x RIPA lysate, and homogenized using an electric homogenizer to obtain the supernatant. Quantitative analysis of H-FABP levels was performed using an ELISA kit (MyBioSource, Inc., San Diego, CA, USA) with a sensitivity of 45–1200 pg/ml.

2.8. Detection of Superoxide Production in Heart Tissues. Fresh LVs were embedded in Tissue-Tek[®] O.C.T. Compound (VWR, Atlanta, GA, USA) and sectioned ($5 \mu\text{m}$) onto slides for fluorescent staining with dihydroethidium (DHE, $10 \mu\text{M}$; Beyotime, China). Images of LVs were immediately acquired and assessed at $400\times$ using Image-Pro Plus software (Version 6.0, Media Cybernetics, USA) linked to a Ti-S inverted fluorescence microscope (Nikon, Japan). DHE fluorescent intensity was quantified as folds of the sham group.

2.9. Assay of Oxidative Stress Biomarkers in Myocardium. LVs were homogenized and centrifuged to determine the concentrations of the antioxidative and oxidative indicators. The level of superoxide dismutase (SOD) was determined via a colorimetric method using a SOD assay kit with WST-1 (BioVision, Inc., Milpitas, California, USA). The

concentration of glutathione (GSH) was detected via the DTNB colorimetric method using the detection kit (Geno Technology, Inc., MO, USA). The level of malondialdehyde (MDA) was detected via the thiobarbituric acid colorimetric method using a Lipid Peroxidation (MDA) Assay Kit (Abcam, Cambridge, MA, USA). The activity of free 15-F2t-isoprostane was measured using a 15-Isoprostane F2t ELISA Kit (Neogen Co., Lexington, KY, USA). All procedures were conducted in strict accordance with the manufacturer's instructions. All samples were measured in triplicate, and the results were averaged.

2.10. Masson's Trichrome Staining. Slides were stained with Masson's trichrome stain (Masson) kit (Sigma-Aldrich, Saint Louis, MO, USA), as per the manufacturer's instructions. Figures were captured at 400x magnification with a light microscope (Nikon, Tokyo, Japan) and analyzed with Image-Pro Plus software (Version 6.0, Media Cybernetics, USA) for semiquantitative analysis by two persons blinded to the experimental design. Five different fields for each section were randomly selected for analysis, and the average value was taken as the final value for the samples.

2.11. Cytokine Measurement by ELISA. Inflammatory cytokines, interleukin-1 β (IL- β), IL-6, and tumor necrosis factor- α (TNF- α) in serum were measured using ELISA kits, according to the manufacturer's instructions (R&D Systems Inc., Minneapolis, USA). The concentrations of the cytokines were quantified by referring to standard curves.

2.12. TdT-Mediated dUTP Nick-End Labeling (TUNEL) for DNA Fragmentation. Extensive DNA degradation is the signature of the late stage of apoptosis. TUNEL staining (horseradish peroxidase method) was conducted to detect apoptotic myocardial cells. All procedures were conducted in strict accordance with the manufacturer's instructions of the TACS[®] TdT In Situ Apoptosis Detection Kit-DAB (R&D Systems Inc., Minneapolis, USA). Figures were immediately acquired at 400x magnification by a light microscope (Nikon, Tokyo, Japan). The proportion of TUNEL-positive cells was counted using Image-Pro Plus software (Version 6.0, Media Cybernetics, USA) by two persons blinded to the experimental design. Five different fields of each section were randomly selected for analysis, and the average value was taken as the final value of the sample.

2.13. Western Blot Analysis. Myocardial tissues were homogenized, and protein concentrations were determined using the BCA protein assay (Bio-Rad, Hemel Hempstead, Herts, UK). In total, 60 μ g of each sample was subjected to western blotting using the following primary antibodies incubated overnight at 4°C: anti-MG53 at 1:1000 dilution, anti-PPAR α at 1:2000 dilution, anti-cyclooxygenase-2 (COX-2) at 1:2000 dilution, anti-caspase-3 (proform and the p17 cleaved form) (#9662, Cell Signaling Technology, Danvers, MA, USA) at 1:1500 dilution, anti-Bax at 1:1000 dilution, anti-Bcl-2 at 1:1000 dilution, and anti- β -actin at 1:2000 dilution. The secondary antibodies were goat-anti-rabbit IgG at 1:5000 dilution. All antibodies except anti-caspase-3 were purchased from Abcam Inc., Cambridge, MA, USA.

Immunoreactive proteins were visualized using the ECL Western Blot System (Pierce Biotechnology, Rockford, IL, USA) and detected by a Tanon 5500 imaging system (Tanon, Shanghai). Images were analyzed using ImageQuant TL software v2003.03 (GE Healthcare, Milwaukee, WI, USA). The band density of the target proteins was normalized to those of the corresponding β -actin and expressed as fractions of the control sample from the same gels.

2.14. Survival Analysis. Rats ($n = 15$) under the same treatments in experiment 2 (Figure 1) were used to evaluate the survival rate. Animals in each group were kept under SPF conditions and monitored via video. All rats had free access to food and water. From the onset of operations, animals were monitored via a video camera. The survivors were transferred to their individual cages and had free access to food and water. The survival rate was evaluated within 72 h.

2.15. Statistical Analysis. The data were expressed as mean \pm standard deviation (SD) and analyzed by one-way ANOVA after a homogeneity test for variance, followed by Tukey's test. Statistical analyses were conducted using GraphPad Prism 8.0 software, and $P < 0.05$ in two-tailed testing was considered statistically significant.

3. Results

3.1. Myocardial MG53 and PPAR α Decreased in SIMD Rats: Supplementation of MG53 Improved PPAR α Expression. MG53 is abundantly expressed in rodent cardiac muscle tissues under normal circumstances [28]. However, the expression of MG53 and PPAR α in SIMD is unknown.

As shown in Figures 2(a)–2(c), we identified a decreasing trend of MG53 and PPAR α in rat myocardial tissue after CLP surgery via western blotting. The protein levels of MG53 and PPAR α reached to the lowest point at 18 h after CLP (both $P < 0.05$ vs. sham group) and improved slightly at 24 h after CLP (both $P < 0.05$ vs. sham group). So, we chose the point-in-time, 18 h after CLP, to investigate the relationship between MG53 and PPAR α in SIMD. Then, we supplemented myocardial MG53 via intravenous injection of rhMG53 and selected the GW6471 precondition group as a control. MG53 administration significantly increased myocardial PPAR α protein levels ($P < 0.01$ vs. CLP group) in SIMD rats. These results suggest that MG53 may be effective in enhancing PPAR α expression in the myocardium of septic rats.

3.2. MG53 Improved the Cardiac Function and Survival Rate in SIMD Rats, Which Was Exacerbated by GW6471. SIMD is characterized by cardiovascular disturbances and high mortality rates [29]. As shown in Figures 3(b)–3(e), rat cardiac functions were impaired after septic shock. In the CLP group, MABP ($P < 0.01$ vs. sham group), LVSP ($P < 0.01$ vs. sham group), and $+dp/dt_{\max}$ ($P < 0.05$ vs. sham group) significantly decreased while LVEDP ($P < 0.05$ vs. sham group) and $-dp/ds_{\max}$ ($P < 0.05$ vs. sham group) significantly increased, indicating a decline in myocardial systolic and diastolic functions. MG53 relieved the cardiac function damage demonstrated by the amelioration of MABP, LVSP, and $+dp/dt_{\max}$ (all $P < 0.05$ vs. CLP group) and the reduction of

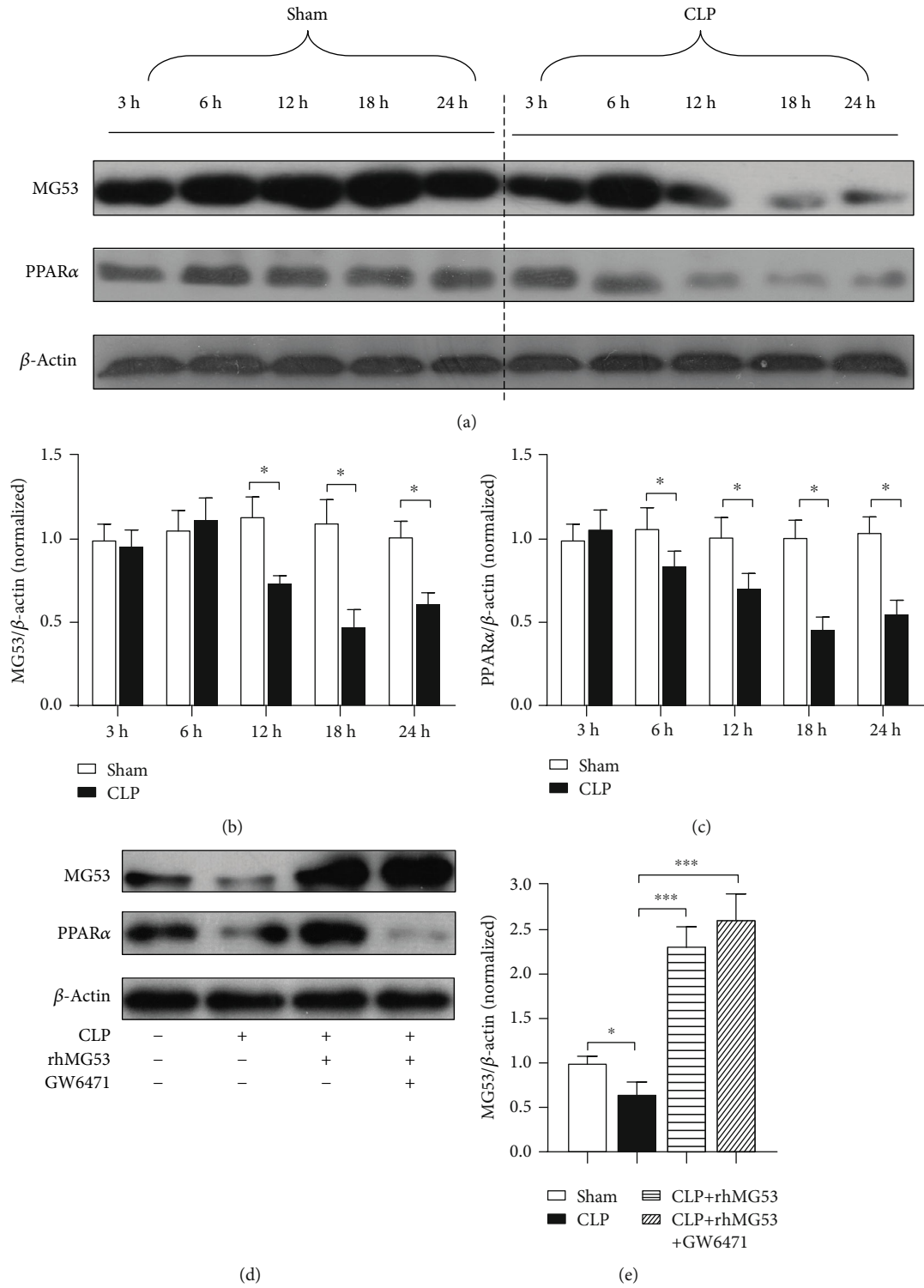


FIGURE 2: Continued.

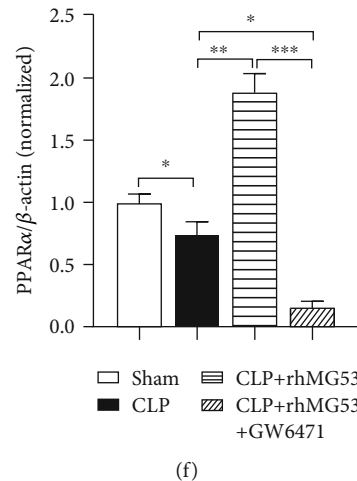


FIGURE 2: Myocardial MG53 and PPAR α decreased in SIMD rats. Supplementation of MG53 improved PPAR α expression. (a) Representative western blot bands of MG53 and PPAR α at 3 h, 6 h, 12 h, 18 h, and 24 h after CLP in experiment 1. Densitometric analysis of the (b) MG53 and (c) PPAR α protein levels in experiment 1. (d) Representative western blot bands of MG53 and PPAR α at 18 h after CLP in experiment 2. Densitometric analysis of the (e) MG53 and (f) PPAR α protein levels in experiment 2. Data are presented as mean \pm SD, $n = 8$. * $P < 0.05$, ** $P < 0.01$, and *** $P < 0.001$. CLP = cecal ligation and puncture; rhMG53 = recombinant human MG53.

LVEDP ($P < 0.01$ vs. CLP group). On the contrary, GW6471 abolished the protective effects of rhMG53, which manifested as a deterioration of MABP ($P < 0.05$ vs. CLP+rhMG53 group), LVSP ($P < 0.01$ vs. CLP+rhMG53 group), and $+dp/dt_{max}$ ($P < 0.01$ vs. CLP+rhMG53 group) and increased LVEDP and $-dp/ds_{max}$ (both $P < 0.01$ vs. CLP+rhMG53 group). There was no significant difference in HR among the four groups (Figure 3(a)).

As shown in Figure 3(f), the survival rate dropped by approximately 8.3% in both the CLP and CLP+rhMG53+GW6471 groups in 24h after septic shock and continued to decline sharply. The mortality rates at 72h were 0%, 75.0%, 41.7%, and 66.7% in the sham, CLP, CLP+rhMG53, and CLP+rhMG53+GW6471 groups, respectively. MG53 administration prolonged the survival time, and the first drop in survival rate was observed at 32h after CLP, and 41.7% of rats survived at 72h ($P < 0.05$ vs. CLP group). This protective effect was reversed by GW6471, wherein the first drop in survival rate was observed at 15h after CLP and only 33.3% of rats survived at 72h ($P < 0.05$ vs. CLP+rhMG53 group).

3.3. MG53 Prevented Cardiomyocyte Injury in SIMD Rats, Which Was Reversed by GW6471. The integrity of cardiomyocytes was destroyed, and the myocardial injury marker levels were elevated in serum when SIMD occurred [4]. As shown in Figure 4(a), the clear myocardial striation and neatly arranged cells demonstrate the normal architecture of the myocardium in the sham group. On the contrary, the cardiomyocytes were degenerated, myocardial fibers were disorganized, and interstitium was edematous, congested, and infiltrated with inflammatory cells in the CLP group. MG53 prevented morphological deformation in SIMD rats, which was reversed by GW6471. As shown in Figures 4(b)–4(d), serum myocardial injury and necrosis markers, cTnI ($P < 0.01$ vs. sham group), CK-MB ($P < 0.01$ vs. sham group),

and LDH ($P < 0.05$ vs. sham group), significantly increased 18h after CLP. The MG53 supplement prevented the changes (all $P < 0.05$ vs. CLP group), which were reversed by GW6471 ($P < 0.05$ in cTnI and $P < 0.01$ in CK-MB and LDH vs. CLP+rhMG53 group). H-FABP is a striated muscle abundant cytoplasmic protein that is rapidly released from cytoplasm at the very early stages of myocardial injury [30]. As shown in Figure 4(e), myocardial H-FABP was downregulated after CLP ($P < 0.01$ vs. sham group). MG53 improved the levels of H-FABP in the myocardium ($P < 0.05$ vs. CLP group), which were reversed by GW6471 ($P < 0.05$ vs. CLP+rhMG53 group).

3.4. MG53 Attenuated Myocardial Oxidative Stress in SIMD Rats, Which Was Abolished by GW6471. As shown in Figures 5(a)–5(f), myocardial antioxidative indicators, SOD activity ($P < 0.01$ vs. sham group), and GSH levels ($P < 0.05$ vs. sham group) significantly decreased accompanied by increased oxidative indicators, DHE fluorescent intensity ($P < 0.01$ vs. sham group), MDA ($P < 0.01$ vs. sham group), and 15-F2t-isoprostane ($P < 0.01$ vs. sham group), 18h after CLP. These changes were attenuated by MG53 administration ($P < 0.05$ in SOD, GSH, DHE fluorescent intensity, and 15-F2t-isoprostane vs. CLP group) and aggravated by GW6471 (all $P < 0.05$ vs. CLP+rhMG53 group).

3.5. MG53 Alleviated Myocardial Inflammation in SIMD Rats, Which Was Exacerbated by GW6471. SIMD presents inflammatory cardiomyopathy manifesting as subendocardial collagen deposition, myocardial hypertrophy, and fibrosis [31]. Several cytokines, such as IL-1, IL-6, and TNF- α , have been considered myocardium-depressing factors [4]. As shown in Figures 6(a) and 6(b), collagen volume significantly increased 18h after CLP ($P < 0.01$ vs. sham group) and was reduced by MG53 ($P < 0.05$ vs. CLP group). GW6471 reversed the effect of MG53 demonstrated by

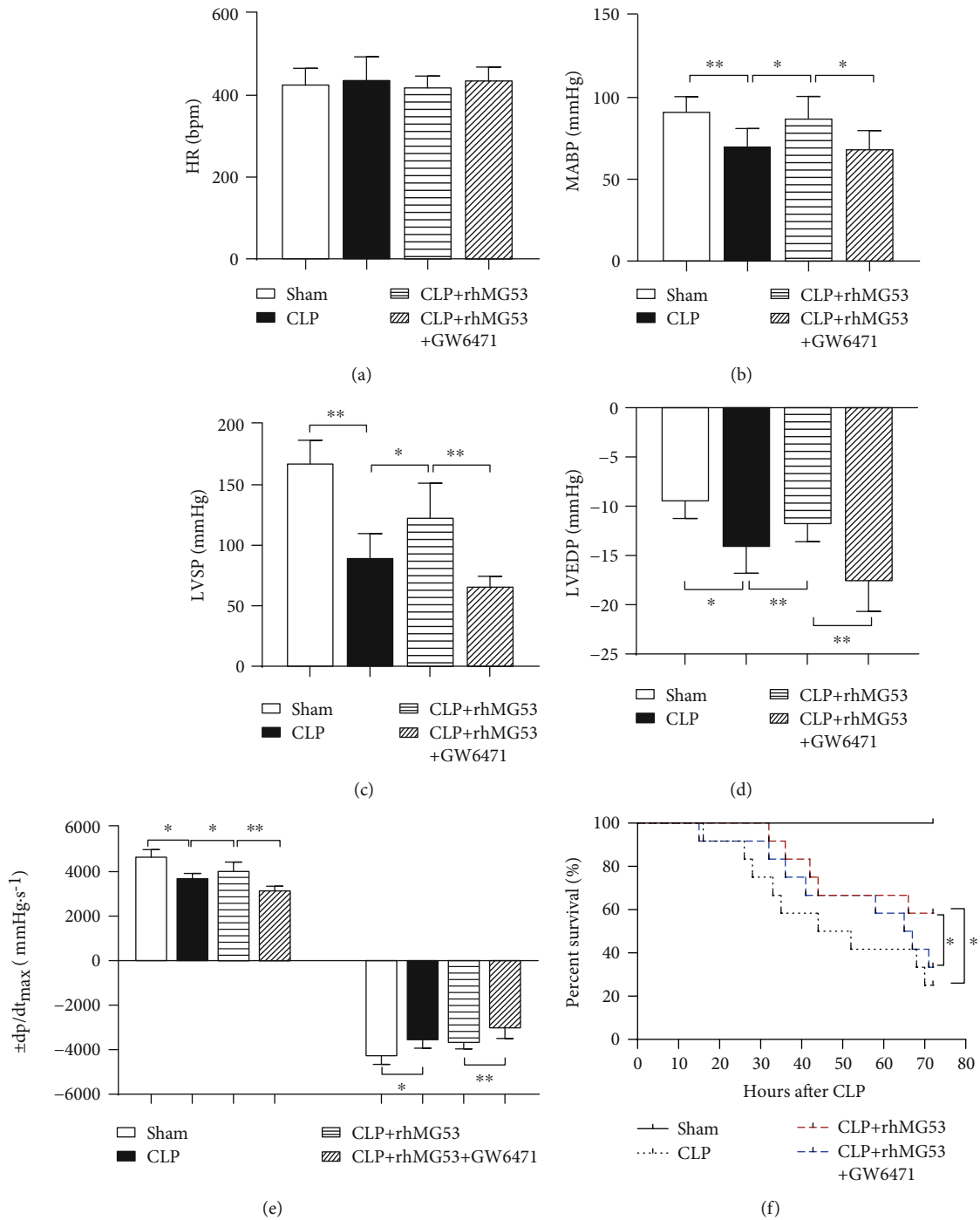


FIGURE 3: MG53 improved cardiac function and survival rate in SIM2 rats, which was exacerbated by GW6471. Cardiac function indexes were demonstrated by (a) heart rate (HR), (b) mean arterial blood pressure (MABP), (c) left ventricular systolic pressure (LVSP), (d) left ventricular end-diastolic pressure (LVEDP), and (e) maximum rate of rise/fall of left ventricle pressure ($\pm dp/dt_{max}$) in four groups. (f) Survival analysis. Data are presented as mean \pm SD, $n = 8$ in cardiac function evaluation, $n = 15$ in survival rate evaluation. * $P < 0.05$, ** $P < 0.01$, and *** $P < 0.001$. CLP = cecal ligation and puncture; rhMG53 = recombinant human mitsugumin-53.

profoundly increased cardiac collagen volume ($P < 0.05$ vs. CLP+rhMG53 group). As shown in Figures 6(c)–6(g), serum proinflammatory cytokines IL-1 β ($P < 0.01$ vs. sham group), IL-6 ($P < 0.05$ vs. sham group), and TNF- α ($P < 0.05$ vs. sham group) and myocardial COX-2 protein levels ($P < 0.01$ vs.

sham group) significantly increased 18h after CLP. This change in inflammatory biomarkers was attenuated by MG53 ($P < 0.05$ in IL-1 β , TNF- α , and COX-2 vs. CLP group) and aggravated by GW6471 ($P < 0.01$ in IL-1 β , $P < 0.05$ in IL-6, TNF- α , and COX-2 vs. CLP+rhMG53 group).

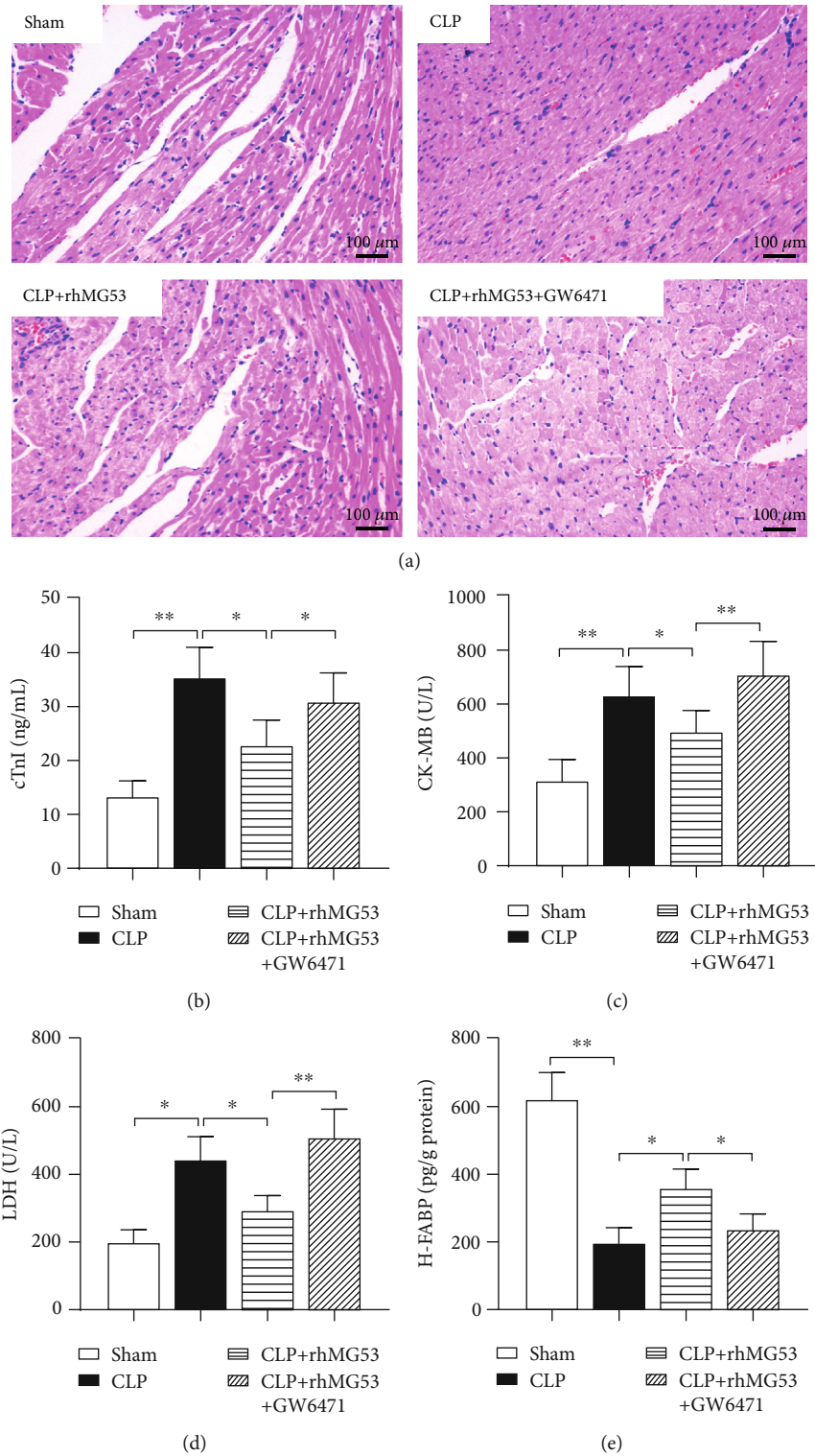
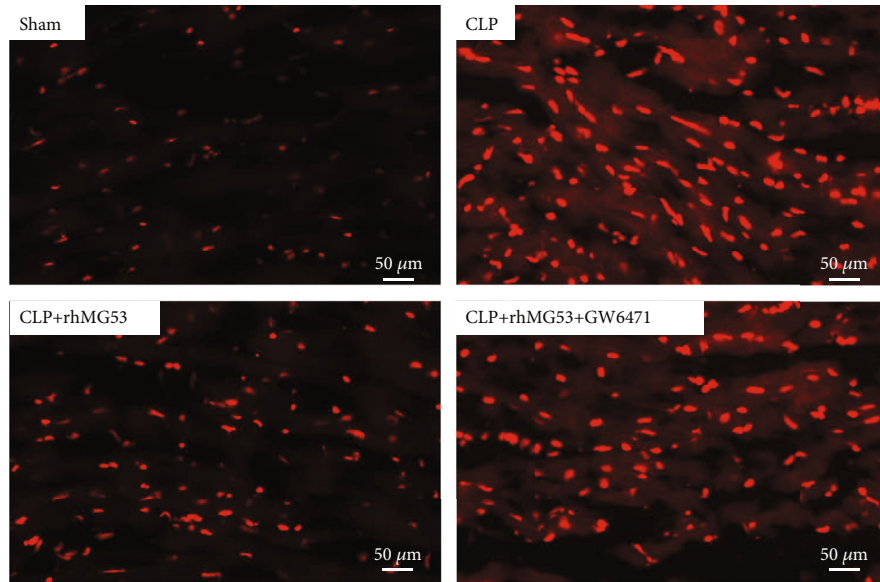
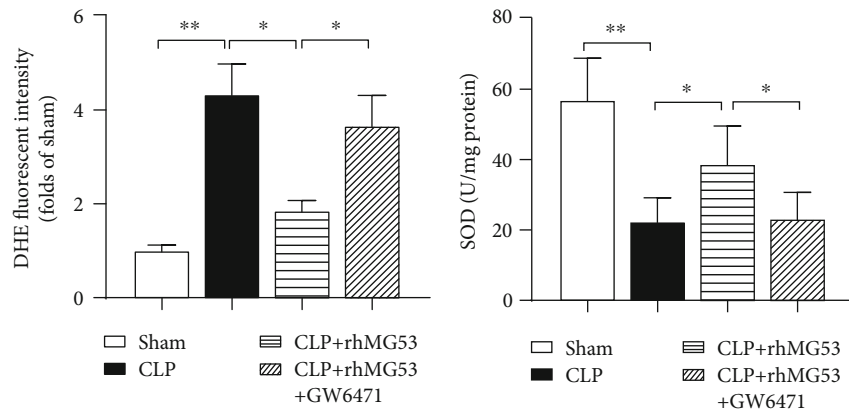


FIGURE 4: MG53 prevented cardiomyocyte injury in SIM2 rats, which was reversed by GW6471. Myocardium architecture was visualized by (a) H&E staining (200x magnification, scale bar = 100 μ m). Myocardial injury was detected through serum levels of (b) cardiac troponin I (cTnI), (c) creatine kinase isoenzyme MB (CK-MB), (d) lactate dehydrogenase (LDH), and (e) heart-type fatty acid-binding protein (H-FABP) by the ELISA method. Data are presented as mean \pm SD, $n = 8$. * $P < 0.05$, ** $P < 0.01$, and *** $P < 0.001$. CLP = cecal ligation and puncture; rhMG53 = recombinant human mitsugumin-53.

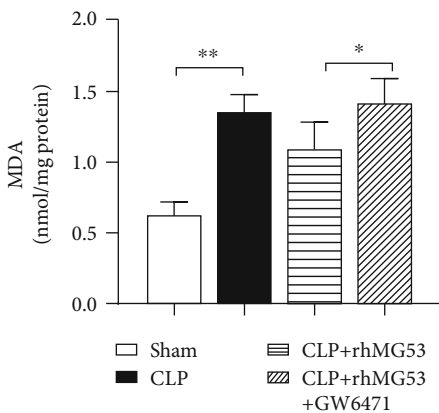


(a)

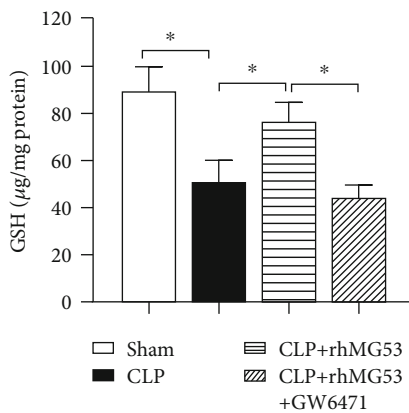


(b)

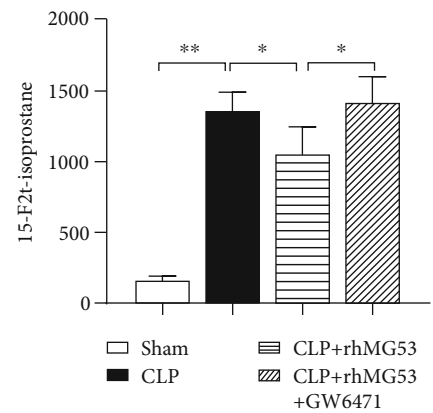
(c)



(d)



(e)



(f)

FIGURE 5: MG53 attenuated myocardial oxidative stress in SIMD rats, which was abolished by GW6471. Oxidative stress injury was detected through (a) representative DHE stained images depicting in situ superoxide production (red, 400x magnification, scale bar = 50 μm), (b) quantification of DHE-signal intensity (folds of the sham group), (c) superoxide dismutase (SOD), (d) malondialdehyde (MDA), (e) glutathione (GSH) activity, and (f) free 15-F2t-isoprostane levels in the myocardium via an ELISA. Data are presented as mean ± SD, $n = 8$. * $P < 0.05$, ** $P < 0.01$, and *** $P < 0.001$. CLP = cecal ligation and puncture; rhMG53 = recombinant human mitsugumin-53.

3.6. MG53 Prevented Cardiomyocyte Apoptosis in SIMD Rats, Which Was Abolished by GW6471. It is generally accepted that abundant inflammatory mediators and excessive oxidative stress are crucial in caspase-3 activation and cardiomyocyte apoptosis, which contributes to SIMD [6]. As shown in Figures 7(a) and 7(b), the percentage of myocardial TUNEL-positive cells (stained brown) significantly increased 18 h after CLP ($P < 0.01$ vs. sham group), which was significantly reduced by MG53 ($P < 0.01$ vs. CLP group) and augmented by GW6471 ($P < 0.05$ vs. CLP+rhMG53 group). As shown in Figures 7(c)–7(e), the expression of apoptosis-related proteins in the myocardium, the cleaved-caspase-3 to pro-caspase-3 and Bax to Bcl-2 ratio (both $P < 0.01$ vs. sham group), sharply increased in SIMD rats and was prevented by MG53 (both $P < 0.05$ vs. CLP group) and reversed by GW6471 (both $P < 0.05$ vs. CLP+rhMG53 group).

4. Discussion

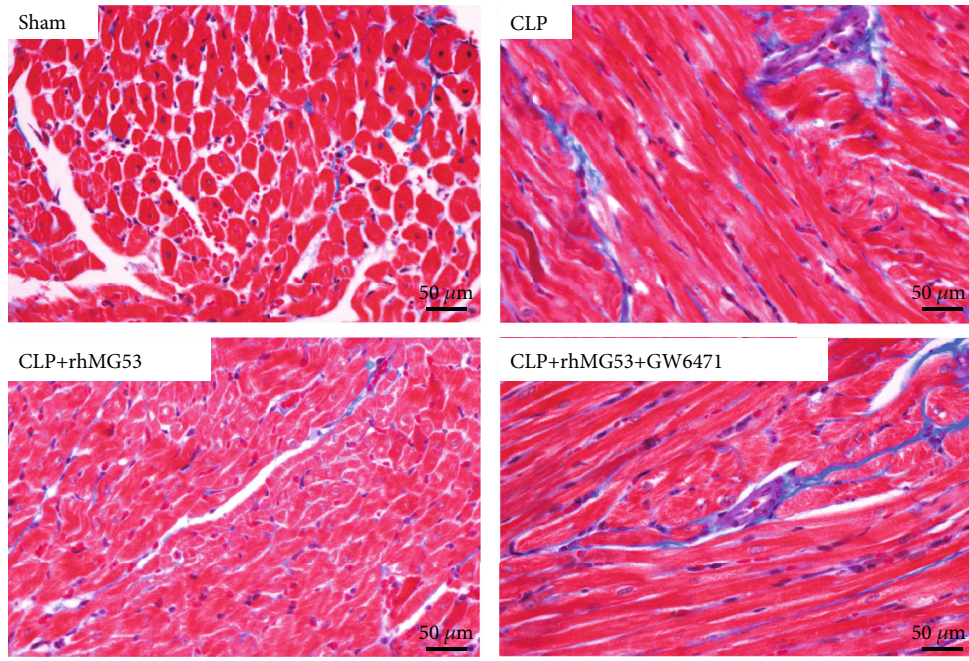
Sepsis is the leading cause of death among inpatients and is responsible for rising mortality and hospitalization rates worldwide every year [32]. It often leads to life-threatening multiple organ dysfunction, and the heart is one of the most commonly affected organs^[1]. SIMD is recognized as a major contributor to the prognosis of septic shock [33]. Previous studies [18–22, 34, 35] have demonstrated that MG53 is beneficial for treating cardiac diseases; however, studies primarily focusing on the effect of MG53 in SIMD are still relatively rare. In the present study, we established a SIMD model of rats and found a downregulation of endogenous MG53 and PPAR α , which was increased by exogenous rhMG53 in the myocardium 18 h after CLP. We further demonstrated that the supplementation of MG53 reduced myocardial oxidative stress and inflammatory injury and attenuated cardiomyocyte damage and apoptosis, which eventually improved cardiac function and survival rate in SIMD rats. To further clarify the protective mechanism of MG53, GW6471 (a PPAR α antagonist) was preprocessed. Our results suggest that the upregulation of PPAR α protein levels may be a possible mechanism for MG53 conferred myocardial protection in SIMD.

MG53 (also known as TRIM72) is a skeletal and cardiac muscle-specific TRIM-family protein that facilitates plasma membrane repair [12]. We previously reported that MG53 alleviated HIRI-induced oxidative stress and hepatocyte apoptosis by being anchored by dysferlin [19]. MG53 mediates cardiac cell membrane damage induced by MI [18], ischemia-reperfusion injury, [19, 20], or aortic valve disease [22]. It interacts with p85 and CaV3 and activates the prosurvival RISK pathway both in cardiac IPC and IPO [20, 21]. MG53 recently exhibited an anti-inflammatory function in cardiac hypertrophy by inhibiting the nuclear transfer of p65 and β -catenin, thereby downregulating their downstream target genes, including ANP, BNP, and β -MHC [22, 35]. Insufficient expression of MG53 plays a critical role in a range of myocardial pathological processes [18–22, 34, 35], and systemic delivery of exogenous recombinant MG53 protein ameliorates cardiomyocyte injury [18, 21, 35]. However, there have been few studies regarding MG53 on SIMD. Herein, we established

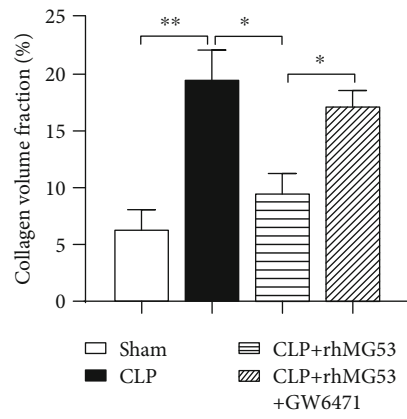
a SIMD model and confirmed that the endogenous MG53 levels were insufficient after CLP. rhMG53 promoted the expression of MG53. Our results were similar to those of our previous study regarding HIRI [19] and those of Liu et al. regarding MI [18]. Moreover, we found the PPAR α protein levels were downregulated after CLP and elevated by MG53. It was in keeping with studies regarding DCM that MG53 overexpression led to the transcriptional upregulation of PPAR α [23]. Our findings suggest that MG53 may have an effect by upregulating PPAR α in SIMD.

SIMD is defined as the intrinsic, reversible, global impairment in cardiac function induced by sepsis [5]. Decreased systolic and diastolic myocardial contractility are the clinical features of SIMD [33]. Troponins and CK-MB levels are often elevated in SIMD patients or laboratory animals [36]. In the present study, the CLP group exhibited an impaired systolic (LVSP and $+dp/dt_{max}$) and diastolic (LVEDP and $-dp/dt_{max}$) heart function accompanied by histological change and cTnI, CK-MB, and LDH elevation in serum. MG53 improved sepsis-induced cardiac function impairment and cardiomyocyte damage, which was abolished by GW6471. In this study, the myocardial H-FABP levels decreased after CLP but were increased by MG53 supplement and suppressed by GW6471. FABPs are a class of small cytoplasmic proteins that facilitate the transfer of fatty acids (FAs) between extra- and intracellular membranes. H-FABP is abundant in myocardial cells [37] and is released from cytoplasm at almost the onset of myocardial injury [30]. Chen and Li [38] reported that circulating H-FABP levels may serve as biomarkers of organ dysfunction in patients with sepsis. Fan et al. [39] identified the upregulation of serum H-FABP in a mouse model of SIMD. Nevertheless, we chose to detect H-FABP levels in the myocardium rather than serum. This was partly because H-FABP levels in the serum can be disturbed when skeletal muscles are damaged or renal clearance is impaired [40]. The most important, H-FABP selectively cooperates with PPAR α and enables it to exert biological functions [41]. Our results further indicated that PPAR α may participate in the process of MG53 improving SIMD.

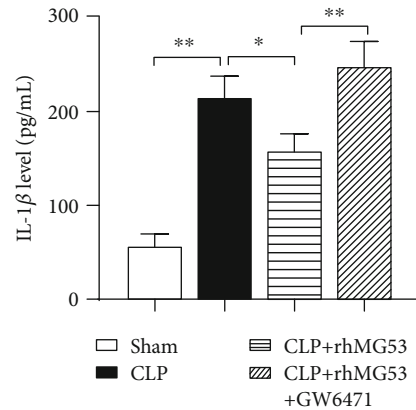
PPAR α is a nuclear receptor that regulates the expression of genes involved in FAs metabolism, lipoprotein synthesis, and metabolism [42]. When bound with endogenous or exogenous lipid/lipid metabolite ligands, PPAR α is activated, which heterodimerizes with retinoid X receptor (RXR) and binds to PPAR response elements (PPRE); the specific region of the DNA sequence is located in the promoters of target genes. Then, the transcription by recruiting RNA polymerase II (RNA Pol II) or other transcription factors was initiated; thus, PPAR α regulates gene function [43]. Under normal conditions, fatty acid oxidation (FAO) provides almost 70% of adenosine triphosphate (ATP) for energy production in cardiomyocytes [6]. Sepsis inhibits intracellular FAO, reduces cardiomyocyte ATP production, and eventually injures myocardial function [44]. It has been reported that Ppara^{-/-} mice cannot sustain the elevated heart function and energy supply necessary to compensate for sepsis pathophysiology. PPAR α expression supports the hyperdynamic cardiac response and increased FAO in SIMD [24]. However, a sequence of studies has suggested that PPAR α exerts a



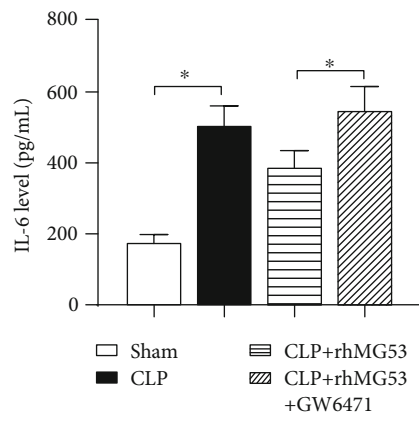
(a)



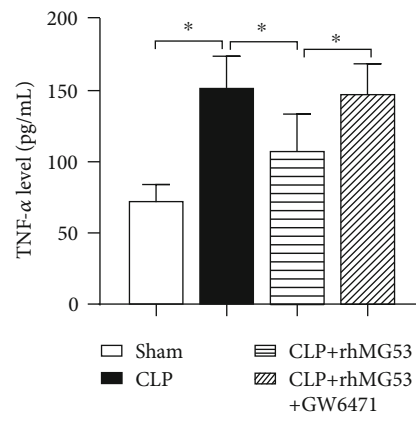
(b)



(c)



(d)



(e)

FIGURE 6: Continued.

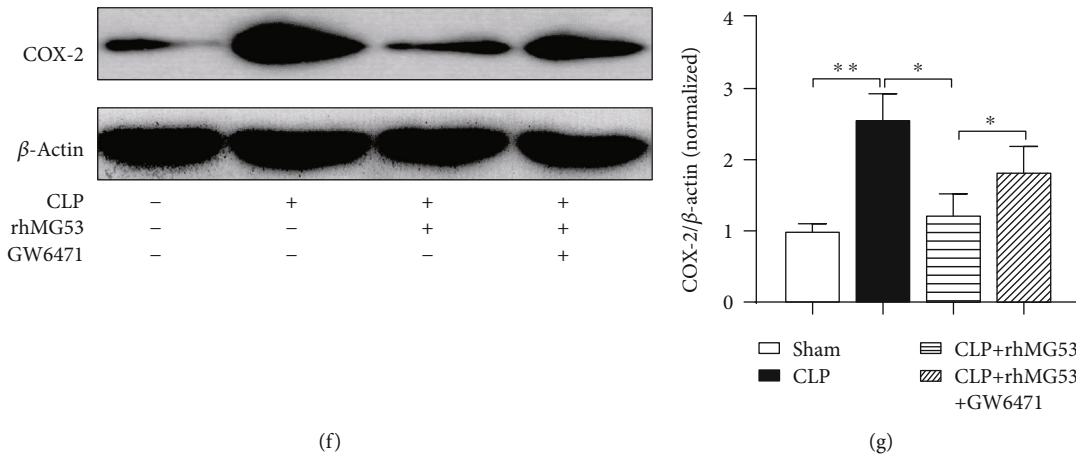


FIGURE 6: MG53 alleviated myocardial inflammation in SIMD rats, which was exacerbated by GW6471. Collagen accumulation was demonstrated by (a) Masson's trichrome staining. Collagen was stained blue in paraffin-embedded heart tissue sections (400x magnification, scale bar = 50 μ m) and (b) the quantitation of interstitial fibrosis area (%). Inflammatory cytokines (c) interleukin-1 β (IL- β), (d) IL-6, and (e) tumor necrosis factor- α (TNF- α) in serum were detected by ELISA, and (f) cyclooxygenase-2 (COX-2) expression in the myocardium was detected by western blotting. Data are presented as mean \pm SD, $n = 8$. * $P < 0.05$, ** $P < 0.01$, and *** $P < 0.001$. CLP = cecal ligation and puncture; rhMG53 = recombinant human mitsugumin-53.

protective effect in myocardial injury, not just by improving lipid utilization [45].

In the current study, we found that MG53 alleviated myocardial oxidative stress and inflammation damage in SIMD. The myocardial collagen volume stained by Masson's trichrome significantly increased 18 h after CLP operation, and MG53 could reduce the myocardial collagen volume. Additionally, we discovered that the protective function of MG53 may be connected to PPAR α upregulation. GW6471 reversed the protective effects of MG53 in SIMD. Even pre-operatively injected with rhMG53, the myocardial oxidative indicators, the DHE fluorescent intensity, and serum proinflammatory cytokine (IL-1 β , IL-6, and TNF- α) levels significantly increased in the GW6471 preconditioning group. Our results were consistent with those of Lou et al. [46], who found that PPAR α exhibited antioxidant and anti-inflammatory effects by upregulating antioxidative indicators and downregulating oxidative indicators and proinflammatory cytokine expression. PPAR α has also been implicated in potent antioxidant effects by enhancing endothelial nitric oxide synthase and the release of nitric oxide [47]. It exhibited an anti-inflammatory effect through the inhibition of proinflammatory signaling pathways, such as nuclear factor- κ B (NF- κ B) in vascular injury [48]. The PPAR α knockout mice could not maintain appropriate immune functions against sepsis shock [49]. Nonetheless, how PPAR α reduced SIMD-induced oxidative stress and inflammation damage deserves further study.

It has been proven that cardiomyocyte apoptosis and caspase-3 activation contribute to SIMD [6]. The overproduction of reactive oxygen species (ROS) and inflammatory mediators plays a critical role in this pathological process [6]. In the current study, we found that the MG53 supplement alleviated cardiomyocyte apoptosis, inhibited caspase-3 activation, and downregulated the ratio of Bax to Bcl-2 in SIMD. This finding was similar to those of our previous study

regarding MG53 in HIRI [19]. Intravenous injection of rhMG53 inhibited the toll-like receptor 4 (TLR4)/NF- κ B pathway and attenuated neurocyte apoptosis in LPS-induced neurotoxicity [50]. Furthermore, we found that GW6471 reversed the effect induced by MG53, suggesting that PPAR α may participate in the antiapoptotic effect induced by MG53 in SIMD. The activation of the sirtuin 1 (Sirt1)/PPAR α pathway participated in trimetazidine-mitigated cardiomyocyte apoptosis in SIMD [51]. Therefore, the underlying antiapoptotic mechanism of MG53/PPAR α in SIMD requires further investigation.

It has been reported that the overexpression of MG53 decreases glucose uptake and facilitates free FAs uptake in DCM and that this deleterious effect is connected to increased PPAR α expression [23]. As a nuclear receptor regulating lipid metabolism, the leading cause of the detrimental effect exerted by PPAR α is that excess lipid accumulation surpassed FAO leading to the overproduction of ROS and lipotoxicity in cardiomyocytes [23, 45]. We suspected that both MG53 and PPAR α played conflicting roles due to the different patterns of energy supply in SIMD and DCM. Therefore, energetic starvation in cardiomyocytes is a critical mechanism responsible for SIMD. Although we found MG53 protecting SIMD by upregulating PPAR α , the explicit mechanism is ambiguous. The nutrient utilization (glucose and FAs) and the underlying pathway between MG53 and PPAR α in SIMD require further investigation.

In conclusion, we discovered a previously unreported relationship between MG53 and PPAR α in SIMD (Figure 8). The supplementation of MG53 upregulated PPAR α , reduced myocardial oxidative stress and inflammatory injury, attenuated cardiomyocyte damage and apoptosis, and eventually improved cardiac function and survival rate in SIMD rats. GW6471 preprocessing abolished the protective effects of MG53. Additionally, this study provides a new treatment strategy for SIMD.

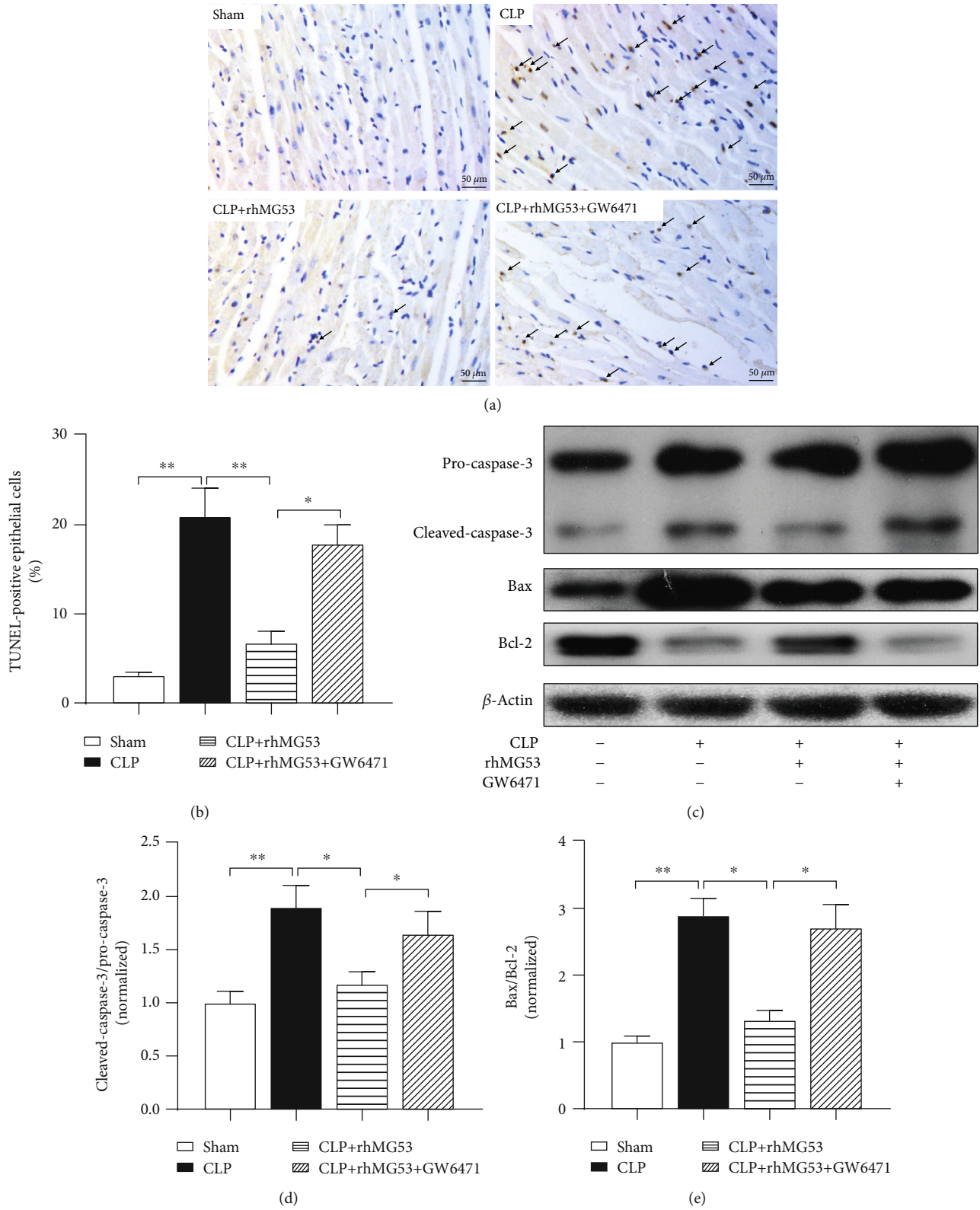


FIGURE 7: MG53 prevents cardiomyocyte apoptosis in SIMD rats, which was abolished by GW6471. Cardiomyocyte apoptosis was assessed by (a) terminal deoxynucleotidyl transferase dUTP nick-end labeling (TUNEL) (400x magnification, scale bar = 50 μ m) and (b) the quantitation of TUNEL-positive cells. TUNEL-positive cells were stained brown and are indicated by black arrows. (c) Representative western blot bands of pro-caspase-3, cleaved-caspase-3 (p17 form), Bax, and Bcl-2. Quantitative analysis of (d) the ratio of cleaved-caspase-3 (p17 form) to pro-caspase-3 and (e) the ratio of Bax to Bcl-2 in heart tissues. Data are presented as mean \pm SD, $n = 12$. * $P < 0.05$, ** $P < 0.01$, and *** $P < 0.001$. CLP = cecal ligation and puncture; rhMG53 = recombinant human mitsugumin-53.

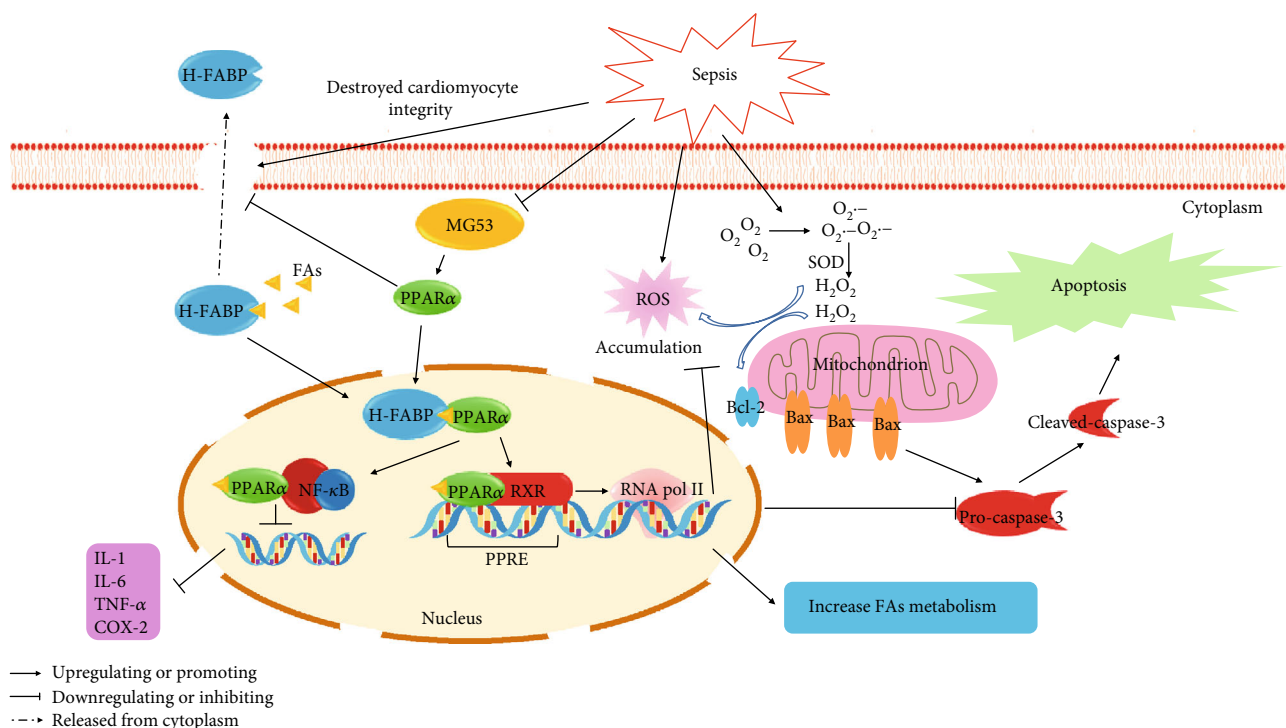


FIGURE 8: Schematic of the proposed mechanism involved in the protective effects of MG53 on PPAR α in SIMD rats. Sepsis caused the H-FABP released from cardiomyocyte plasma and downregulated MG53 and PPAR α protein levels. Endogenously, ROS were overproduced resulting in the activation of the caspase-3-dependent apoptosis pathway. Also, large amounts of inflammatory cytokines (IL-1, IL-6, and TNF- α) were generated due to the activation of some proinflammatory pathways (such as NF- κ B) after SIMD. The supplementation of MG53 upregulated PPAR α , attenuated cardiomyocyte damage, and prevented H-FABP release. H-FABP facilitated FAs transfer and activated PPAR α . PPAR α exhibited an anti-inflammatory effect through the inhibition of proinflammatory signaling pathways, such as NF- κ B. Also, PPAR α heterodimerized with RXR, banded to PPRE, and then recruited RNA Pol II to regulate gene function to play a crucial part in antioxidant stress, antiapoptosis, and promoting FAs metabolism. RXR = retinoid X receptor; RNA Pol II = RNA polymerase II; PPRE = PPAR response element; FAs = fatty acids.

Data Availability

The datasets generated during and/or analyzed during the current study are available from the corresponding author on reasonable request.

Conflicts of Interest

The authors report no conflict of interest.

Authors' Contributions

Xue Han, Daili Chen, and Ning Liufu contributed equally to this study. Xue Han, Weifeng Yao, and Minghi Cao designed the study. Xue Han, Daili Chen, Ning Lifu, and Fengtao Ji performed the experiment. All authors wrote and approved the manuscript. Xue Han, Daili Chen, Ning Lifu, and Fengtao Ji helped in data collection and interpretation. Weifeng Yao performed the statistical analysis.

Acknowledgments

The study was supported in part by grants from the Natural Science Foundation of China (No. 81900578 for Xue Han), the Medical Scientific Research Foundation of Guangdong

Province of China (No. A2018054 for Xue Han), and the Guangdong Basic and Applied Basic Research Foundation (No. 2019A1515011101 for Xue Han).

References

- [1] M. Singer, C. S. Deutschman, C. W. Seymour et al., "The third international consensus definitions for sepsis and septic shock (sepsis-3)," *Journal of the American Medical Association*, vol. 315, no. 8, pp. 801–810, 2016.
- [2] US CDC, "Sepsis. Data & Reports," 2018, January 2019, <https://www.cdc.gov/sepsis/datareports/index.html>.
- [3] T. Evans, "Diagnosis and management of sepsis," *Clinical Medicine*, vol. 18, no. 2, pp. 146–149, 2018.
- [4] E. Antonucci, E. Fiaccadori, K. Donadello, F. S. Taccone, F. Franchi, and S. Scolletta, "Myocardial depression in sepsis: from pathogenesis to clinical manifestations and treatment," *Journal of Critical Care*, vol. 29, no. 4, pp. 500–511, 2014.
- [5] A. Zaky, S. Deem, K. Bendjelid, and M. M. Treggiari, "Characterization of cardiac dysfunction in sepsis: an ongoing challenge," *Shock*, vol. 41, no. 1, pp. 12–24, 2014.
- [6] X. Lv and H. Wang, "Pathophysiology of sepsis-induced myocardial dysfunction," *Military Medical Research*, vol. 3, no. 1, p. 30, 2016.

- [7] A. Rhodes, L. E. Evans, W. Alhazzani et al., “Surviving sepsis campaign: international guidelines for management of sepsis and septic shock: 2016,” *Intensive Care Medicine*, vol. 43, no. 3, pp. 304–377, 2017.
- [8] M. M. Levy, L. E. Evans, and A. Rhodes, “The surviving sepsis campaign bundle: 2018 update,” *Intensive Care Medicine*, vol. 44, no. 6, pp. 925–928, 2018.
- [9] B. Tan, J. J. M. Wong, R. Sultana et al., “Global case-fatality rates in pediatric severe sepsis and septic shock: a systematic review and meta-analysis,” *JAMA Pediatrics*, vol. 173, no. 4, pp. 352–362, 2019.
- [10] K. R. Walley, “Sepsis-induced myocardial dysfunction and mammalian target of rapamycin signalling pathways,” *The Canadian Journal of Cardiology*, vol. 35, no. 7, pp. 809–812, 2019.
- [11] X. Hu and R. P. Xiao, “MG53 and disordered metabolism in striated muscle,” *Biochimica et Biophysica Acta (BBA) - Molecular Basis of Disease*, vol. 1864, no. 5, pp. 1984–1990, 2018.
- [12] C. Cai, H. Masumiya, N. Weisleder et al., “MG53 nucleates assembly of cell membrane repair machinery,” *Nature Cell Biology*, vol. 11, no. 1, pp. 56–64, 2009.
- [13] N. Weisleder, N. Takizawa, P. Lin et al., “Recombinant MG53 protein modulates therapeutic cell membrane repair in treatment of muscular dystrophy,” *Science Translational Medicine*, vol. 4, no. 139, article 139ra85, 2012.
- [14] P. Duann, H. Li, P. Lin et al., “MG53-mediated cell membrane repair protects against acute kidney injury,” *Science Translational Medicine*, vol. 7, no. 279, article 279ra36, 2015.
- [15] Y. Jia, K. Chen, P. Lin et al., “Treatment of acute lung injury by targeting MG53-mediated cell membrane repair,” *Nature Communications*, vol. 5, no. 1, p. 4387, 2014.
- [16] Y. Yao, B. Zhang, H. Zhu et al., “MG53 permeates through blood-brain barrier to protect ischemic brain injury,” *Oncotarget*, vol. 7, no. 16, pp. 22474–22485, 2016.
- [17] F. Guan, T. Huang, X. Wang et al., “The TRIM protein mitsugumin 53 enhances survival and therapeutic efficacy of stem cells in murine traumatic brain injury,” *Stem Cell Research & Therapy*, vol. 10, no. 1, p. 352, 2019.
- [18] J. Liu, H. Zhu, Y. Zheng et al., “Cardioprotection of recombinant human MG53 protein in a porcine model of ischemia and reperfusion injury,” *Journal of Molecular and Cellular Cardiology*, vol. 80, pp. 10–19, 2015.
- [19] W. Yao, H. Li, X. Han et al., “MG53 anchored by dysferlin to cell membrane reduces hepatocyte apoptosis which induced by ischaemia/reperfusion injury in vivo and in vitro,” *Journal of Cellular and Molecular Medicine*, vol. 21, no. 10, pp. 2503–2513, 2017.
- [20] C. M. Cao, Y. Zhang, N. Weisleder et al., “MG53 constitutes a primary determinant of cardiac ischemic preconditioning,” *Circulation*, vol. 121, no. 23, pp. 2565–2574, 2010.
- [21] Y. Zhang, F. Lv, L. Jin et al., “MG53 participates in ischaemic preconditioning through the RISK signalling pathway,” *Cardiovascular Research*, vol. 91, no. 1, pp. 108–115, 2011.
- [22] T. M. A. Adesanya, M. Russell, K. H. Park et al., “MG53 protein protects aortic valve interstitial cells from membrane injury and fibrocalcific remodeling,” *Journal of the American Heart Association*, vol. 8, no. 4, article e009960, 2019.
- [23] F. Liu, R. Song, Y. Feng et al., “Upregulation of MG53 induces diabetic cardiomyopathy through transcriptional activation of peroxisome proliferation-activated receptor α ,” *Circulation*, vol. 131, no. 9, pp. 795–804, 2015.
- [24] S. W. Standage, B. G. Bennion, T. O. Knowles et al., “PPAR α augments heart function and cardiac fatty acid oxidation in early experimental polymicrobial sepsis,” *American Journal of Physiology-Heart and Circulatory Physiology*, vol. 312, no. 2, pp. H239–H249, 2017.
- [25] Y. Tang, F. Soroush, S. Sun et al., “Protein kinase C-delta inhibition protects blood-brain barrier from sepsis-induced vascular damage,” *Journal of Neuroinflammation*, vol. 15, no. 1, p. 309, 2018.
- [26] V. R. More, C. R. Campos, R. A. Evans et al., “PPAR- α , a lipid-sensing transcription factor, regulates blood-brain barrier efflux transporter expression,” *Journal of Cerebral Blood Flow and Metabolism*, vol. 37, no. 4, pp. 1199–1212, 2017.
- [27] S. Yang, M. Zhou, I. H. Chaudry, and P. Wang, “Novel approach to prevent the transition from the hyperdynamic phase to the hypodynamic phase of sepsis: role of adrenomedullin and adrenomedullin binding protein-1,” *Annals of Surgery*, vol. 236, no. 5, pp. 625–633, 2002.
- [28] Z. Bian, Q. Wang, X. Zhou et al., “Sustained elevation of MG53 in the bloodstream increases tissue regenerative capacity without compromising metabolic function,” *Nature Communications*, vol. 10, no. 1, p. 4659, 2019.
- [29] Y. Kakihana, T. Ito, M. Nakahara, K. Yamaguchi, and T. Yasuda, “Sepsis-induced myocardial dysfunction: pathophysiology and management,” *Journal of Intensive Care*, vol. 4, no. 1, p. 22, 2016.
- [30] R. Rezar, P. Jirak, M. Gschwandtner et al., “Heart-type fatty acid-binding protein (H-FABP) and its role as a biomarker in heart failure: what do we know so far?,” *Journal of Clinical Medicine*, vol. 9, no. 1, p. 164, 2020.
- [31] F. G. Soriano, M. C. Guido, H. V. Barbeiro, E. G. Caldini, C. B. Lorigados, and A. C. Nogueira, “Endotoxemic myocardial dysfunction: subendocardial collagen deposition related to coronary driving pressure,” *Shock*, vol. 42, no. 5, pp. 472–479, 2014.
- [32] E. Goldstein and M. Lipsitch, “The relation between prescribing of different antibiotics and rates of mortality with sepsis in US adults,” *BMC Infectious Diseases*, vol. 20, no. 1, p. 169, 2020.
- [33] K. R. Walley, “Sepsis-induced myocardial dysfunction,” *Current Opinion in Critical Care*, vol. 24, no. 4, pp. 292–299, 2018.
- [34] W. Liu, G. Wang, C. Zhang et al., “MG53, a novel regulator of KCHIP2 and Ito, f, plays a critical role in electrophysiological remodeling in cardiac hypertrophy,” *Circulation*, vol. 139, no. 18, pp. 2142–2156, 2019.
- [35] L. Xu, H. Wang, F. Jiang, H. Sun, and D. Zhang, “LncRNA AK045171 protects the heart from cardiac hypertrophy by regulating the SP1/MG53 signalling pathway,” *Aging (Albany NY)*, vol. 12, no. 4, pp. 3126–3139, 2020.
- [36] H. Chen, X. Wang, X. Yan, X. Cheng, X. He, and W. Zheng, “LncRNA MALAT1 regulates sepsis-induced cardiac inflammation and dysfunction via interaction with miR-125b and p38 MAPK/NF κ B,” *International Immunopharmacology*, vol. 55, pp. 69–76, 2018.
- [37] M. N. Lyngbakken, P. L. Myhre, H. Røsjø, and T. Omland, “Novel biomarkers of cardiovascular disease: applications in clinical practice,” *Critical Reviews in Clinical Laboratory Sciences*, vol. 56, no. 1, pp. 33–60, 2019.
- [38] Y. X. Chen and C. S. Li, “The prognostic and risk-stratified value of heart-type fatty acid-binding protein in septic patients in the emergency department,” *Journal of Critical Care*, vol. 29, no. 4, pp. 512–516, 2014.

- [39] T. T. Fan, X. Y. Feng, Y. Z. Yang, F. Gao, and Q. Liu, "Down-regulation of PI3K- γ in a mouse model of sepsis-induced myocardial dysfunction," *Cytokine*, vol. 96, pp. 208–216, 2017.
- [40] G. Lippi, F. Schena, M. Montagnana, G. L. Salvagno, and G. C. Guidi, "Influence of acute physical exercise on emerging muscular biomarkers," *Clinical Chemistry and Laboratory Medicine*, vol. 46, no. 9, pp. 1313–1318, 2008.
- [41] N. S. Tan, N. S. Shaw, N. Vinckenbosch et al., "Selective cooperation between fatty acid binding proteins and peroxisome proliferator-activated receptors in regulating transcription," *Molecular and Cellular Biology*, vol. 22, no. 14, pp. 5114–5127, 2002.
- [42] M. Pawlak, P. Lefebvre, and B. Staels, "Molecular mechanism of PPAR α action and its impact on lipid metabolism, inflammation and fibrosis in non-alcoholic fatty liver disease," *Journal of Hepatology*, vol. 62, no. 3, pp. 720–733, 2015.
- [43] N. Bougarne, B. Weyers, S. J. Desmet et al., "Molecular actions of PPAR α in lipid metabolism and inflammation," *Endocrine Reviews*, vol. 39, no. 5, pp. 760–802, 2018.
- [44] K. Drosatos, N. M. Pollak, C. J. Pol et al., "Cardiac myocyte KLF5 regulates Ppara expression and cardiac function," *Circulation Research*, vol. 118, no. 2, pp. 241–253, 2016.
- [45] S. Li, B. Yang, Y. Du et al., "Targeting PPAR α for the treatment and understanding of cardiovascular diseases," *Cellular Physiology and Biochemistry*, vol. 51, no. 6, pp. 2760–2775, 2019.
- [46] H. Luo, J. Wang, D. Liu et al., "The lncRNA H19/miR-675 axis regulates myocardial ischemic and reperfusion injury by targeting PPAR α ," *Molecular Immunology*, vol. 105, pp. 46–54, 2019.
- [47] L. Ibarra-Lara, L. G. Cervantes-Pérez, F. Pérez-Severiano et al., "PPAR α stimulation exerts a blood pressure lowering effect through different mechanisms in a time-dependent manner," *European Journal of Pharmacology*, vol. 627, no. 1–3, pp. 185–193, 2010.
- [48] Y. Peng, Q. Li, L. Zhang, M. Bai, and Z. Zhang, "Peroxisome proliferator-activated receptor α plays an important role in the expression of monocyte chemoattractant protein-1 and neointimal hyperplasia after vascular injury," *PPAR Research*, vol. 2012, Article ID 970525, 7 pages, 2012.
- [49] R. Paumelle, J. T. Haas, N. Hennuyer et al., "Hepatic PPAR α is critical in the metabolic adaptation to sepsis," *Journal of Hepatology*, vol. 70, no. 5, pp. 963–973, 2019.
- [50] F. Guan, X. Zhou, P. Li et al., "MG53 attenuates lipopolysaccharide-induced neurotoxicity and neuroinflammation via inhibiting TLR4/NF- κ B pathway in vitro and in vivo," *Progress in Neuro-Psychopharmacology & Biological Psychiatry*, vol. 95, p. 109684, 2019.
- [51] J. Chen, J. Lai, L. Yang et al., "Trimetazidine prevents macrophage-mediated septic myocardial dysfunction via activation of the histone deacetylase sirtuin 1," *British Journal of Pharmacology*, vol. 173, no. 3, pp. 545–561, 2016.

Research Article

Electroacupuncture Pretreatment Attenuates Intestinal Injury after Autogenous Orthotopic Liver Transplantation in Rats via the JAK/STAT Pathway

Lili Jia , Wenli Yu , Hongli Yu, and Yiqi Weng

Department of Anesthesiology, Tianjin First Center Hospital, Tianjin 300192, China

Correspondence should be addressed to Wenli Yu; yzxwenliyu@163.com

Received 18 April 2020; Revised 5 June 2020; Accepted 15 July 2020; Published 4 August 2020

Guest Editor: Weifeng Yao

Copyright © 2020 Lili Jia et al. This is an open access article distributed under the Creative Commons Attribution License, which permits unrestricted use, distribution, and reproduction in any medium, provided the original work is properly cited.

Background. Liver transplantation induces self-injury and affects remote organs, such as the lung, kidney, and intestine. Postoperative intestinal dysfunction has been associated with prolonged hospitalization and affects a patient's health and quality of life. Electroacupuncture (EA) has been proven effective in multiple organ protection. However, the potential mechanism underlying the protective effects of EA on intestinal injury after liver transplantation remains unclear. **Methods.** After establishing an autogenous orthotopic liver transplantation (AOLT) model, we studied the effects of EA pretreatment on intestinal injury after AOLT. We used the JAK2-specific inhibitor AG490 to explore the underlying mechanism. Histological analysis and apoptosis assays were used to evaluate intestinal injury. Oxidative stress index and inflammatory response were also measured after AOLT. Furthermore, we detected the phosphorylation levels of JAK2, STAT1, and STAT3 by Western blot. **Results.** We found that pretreatment with EA alleviated intestinal injury after AOLT, as shown by HE staining and TUNEL methods. EA pretreatment inhibited the expressions of p-JAK2, p-STAT1, and p-STAT3 in the intestines after AOLT. Upon treatment with JAK2-specific inhibitor AG490, intestinal injury was balanced. **Conclusion.** The data indicated EA pretreatment alleviated intestinal injury after AOLT by inhibiting the JAK/STAT signaling pathway. These results provide basic evidence to support the potential therapeutic efficacy of EA.

1. Introduction

Liver transplantation is the most effective method to address end-stage liver diseases. During the past few decades, remote organ injury has been widely studied during liver transplantation. Liver transplantation not only induced self-injury but also affected remote organs, such as the lung, kidney, and intestine [1–4]. With the development of surgical techniques, postoperative mortality and morbidity significantly reduced in recent years. However, postoperative intestinal dysfunction remains associated with prolonged hospitalization and affects a patient's health and quality of life. Therefore, numerous studies have been conducted on the prevention of intestinal injury, from clinical trials to animal studies. Based on Nozato et al.'s study [5], we established an autogenous orthotopic liver transplantation (AOLT) model in rats, which can well imitate the clinical surgery process. Although

previous studies have explored various methods and drugs in ischemia organ injury, reported side effects have limited these studies from applying to clinical practice.

Acupuncture is a traditional Chinese medical treatment and is simple to perform, safe, and reliable. Electroacupuncture (EA) has been proven effective in multiple organ protection [6–8]. A previous study showed that excessive inflammation and oxidative stress response play vital roles in intestinal injury after liver ischemia-reperfusion [9]. Another study showed that EA protects against liver injury after liver ischemia-reperfusion [10]. Zusanli (ST36) is a widely used acupoint in humans to exert anti-inflammatory effects during acupuncture for treating pain or ischemia-reperfusion conditions [11, 12]. Herein, we used the ST36 acupoint to assess its protective effect against intestinal injury after AOLT in rats. Although EA has been increasingly used to treat various diseases, the mechanism remains unknown.

The Janus kinase/signal transducer and activator of the transcription (JAK/STAT) signaling pathway is involved in a wide range of distinct cellular processes, including inflammation, apoptosis, cell-cycle control, and development [13]. The JAK/STAT pathway comprises a family of receptor-associated cytosolic tyrosine kinases (JAKs) that phosphorylate tyrosine residues on bound transcription factors (STATs). JAK-mediated tyrosine phosphorylation of STAT family members enables the translocation of these transcription factors to the nucleus and leads to an augmentation of gene transcription [14, 15]. However, it is unclear whether the JAK/STAT signaling pathway is involved in EA pretreatment to prevent intestinal injury after AOLT. Based on the protective effect of EA on various tissues, our study is aimed at exploring the effect of EA on intestinal injury induced by AOLT in rats and at investigating the underlying mechanisms.

2. Methods and Materials

2.1. Animals. A total of 40 adult male Sprague-Dawley rats (220-250 g) were purchased from the People's Liberation Army Military Academy of Medical Sciences Laboratory Animal Center. The animals were housed in 12 h light-dark cycles with controlled room temperature and were fed with regular rat chow and water ad libitum but were fasted 12 h before experiments. Animals were randomly assigned into five groups: group A, sham operated (sham group); group B, autogenous orthotopic liver transplantation (AOLT group); group C, pretreated with EA (ST36, 1-2 mA, 2-100 Hz, 30 min) for 3 days+AOLT (EA+AOLT group); group D, pretreated with EA for 3 days+sham operated (EA+sham group); and group E, pretreated with EA for 3 days+AG490 (5 mg/kg, i.p., Selleck, USA) 30 min before establishing the AOLT model (EA+AOLT+AG490 group). The dosage was determined from a previous study [1]. The experimental procedures were conducted following the Guide for the Care and Use of Laboratory Animals and approved by the Institutional Animal Care and Use Committee.

2.2. Animal Model. A rat AOLT model was established using a previously reported method [5]. Anesthesia was induced by inhalation of 3.0-4.0% isoflurane and maintained 1.5-2.0% isoflurane inhalation. During surgery, all rats were free to breathe O₂ and were prone on a heating blanket. Rats in the sham group underwent laparotomy without performing AOLT as control. Total liver ischemia was induced by clamping the hepatic artery, the portal vein, suprahepatic vena cava (SHVC), and intrahepatic vena cava (IHVC). After clamping, the portal vein and IHVC were cannulated with a polyethylene tube, and the liver was perfused through the portal vein with 500 mL of heparinized cold saline (Jiangsu Wanbang Biochemical Pharmaceutical Co., Ltd., China) (2.5 IU/mL) to wash out all blood from the liver. The tubes were removed after perfusion, and the openings of tube insertion were closed. The SHVC and IHVC were then declamped immediately after repairing the vessels. After 45 min, the clamps were removed to allow the return of blood flow to the liver. After 6 h, the animals were euthanized by administering CO₂ inhalation. Blood samples and intestinal tissue biopsies were

taken. The tissues were fresh frozen for histological and biochemical evaluation. (Figure 1).

2.3. EA Pretreatment. Previous studies have shown that treatment with diluted 100 Hz and 2 Hz alternating frequency (2/100 Hz) EA stimulation of the ST36 acupoint can alleviate the inflammatory response caused by Complete Freund's adjuvant (CFA) [16, 17]. Zusanli acupoint is located 5 mm beneath the capitulum fibulae and lateral posterior to the knee joint. We performed EA pretreatment as described in a previous study [18]. Two acupuncture needles (diameter, 0.25 mm; length, 30 mm) were inserted into bilateral ST36 acupoints. Then, the two acupuncture needles were connected to the output of a Master-9 Pulse Stimulator (AMPI, Israel). EA parameters were set as follows: bidirectional symmetric square wave. The intensity was adjusted to induce moderate muscle contraction of the hind limb (1-2 mA), and the EA groups were subjected to EA with alternating frequencies and pulse waves. EA was applied 30 min/day from day 1 to day 3 (Figure 1).

2.4. Histological Examination. Formalin-fixed intestinal tissue was dehydrated, embedded in paraffin, and sliced into 4 μ m thick sections, which were stained with hematoxylin and eosin (HE). The damage of intestinal mucosal cells was analyzed by the Chiu score method [19]: 0—normal mucosa, 1—the tip of the hair on the top of the subcutaneous gap increases, 2—moderate separation of the epithelium and lamina, 3—when there are a large number of villi on both sides of the top of the villi with partial villi, 4—villous damage with a large number of inherent layer of capillary exposed, and 5—inherent layer damage of bleeding and ulcers.

2.5. Apoptosis Assay. To detect the apoptotic positive cells, terminal deoxynucleotidyl transferase-mediated digoxigenin-labeled UTP nick end labeling assay (TUNEL) was performed using an ApopTag peroxidase in situ cell death detection kit (Roche, Basal, Switzerland). Briefly, the 4 μ m thick paraffin sections were deparaffinized, treated with 0.1% TritonX-100, and incubated at 37°C for 8 min in a humidified atmosphere. PBS wash was performed 3 times. Then, the sections were further incubated with a mixture of marker and enzyme solution at 37°C for 1 h. PBS wash was performed 3 times, and the samples were observed under a fluorescence microscope (Olympus, Japan) at 450-550 nm. Five high-power fields were randomly selected to determine the percentage of apoptotic cells.

2.6. Enzyme-Linked Immunosorbent Assay (ELISA). Blood samples were collected from all rats. The serum levels of tumor necrosis factor- α (TNF- α), high-mobility group box-1 (HMGB-1), intestinal fatty acid-binding protein (IFABP), and endotoxin (LPS) were examined using an ELISA kit (Shanghai Baiwo Co., Ltd., China) according to the manufacturer's instructions [20].

2.7. Wet/Dry (W/D) Ratio of the Intestine. To test the edema of intestinal after AOLT 6 h following reperfusion, 5 cm of ileum tissue at 2 cm from the back of the blind was harvested, cleaned by removing blood and water, and weighed. Then, the sample was incubated at 70°C for 24 h and weighed.

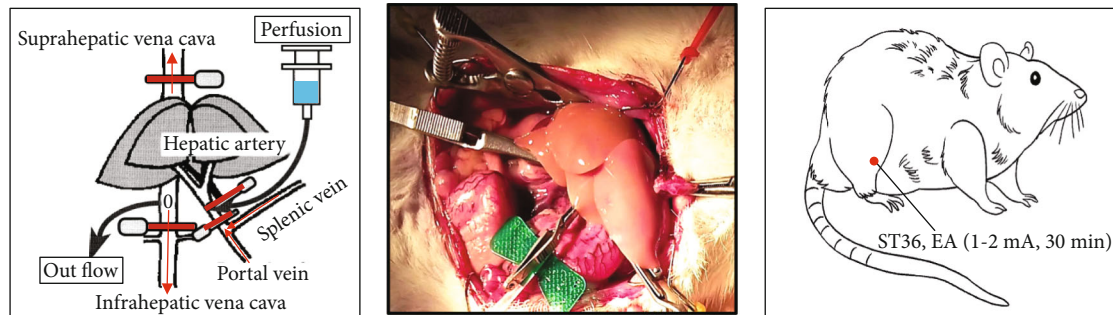


FIGURE 1: The autogenous orthotopic liver transplantation (AOLT) model in rats and electroacupuncture pretreatment on rats.

The *W/D* ratio was calculated as the ratio of the wet weight to the dry weight of the intestine.

2.8. Oxidative Stress. The levels of malondialdehyde (MDA) and superoxide dismutase (SOD) were determined using assay kits (Nanjing Institute Co., Ltd.) according to the manufacturer's instructions [20]. The tissue MDA level was determined by the Esterbauer and Cheeseman method based on its reaction with thiobarbituric acid at 90–100°C; absorbance was measured at 532 nm. MDA reacts with thiobarbituric acid (TBA) and produces a pink pigment, which has a maximum absorption at 532 nm. The value of each sample was obtained from the standard curve and was expressed as $\mu\text{mol/g}$ tissue. SOD activity was measured according to the Paoletti and Mocali method. In this assay, superoxide anion was generated from molecular oxygen in the presence of EDTA, manganese II chloride, and mercaptoethanol. Nicotinamide adenine dinucleotide phosphate oxidation was linked to the availability of superoxide anions in the medium.

2.9. Immunohistochemistry. Immunohistochemical staining of the intestinal tissue was performed on formalin-fixed paraffin sections using a microwave-based technique. The 4 μm thick sections of the fixed intestines were dewaxed with xylene, hydrated in graded concentrations of ethanol, and treated with 0.3% hydrogen peroxide for 10 min to quench endogenous peroxidase. The sections were heated in a microwave oven in sodium citrate (pH = 6.0) at 95–99°C for 15 min and then cooled at room temperature. The sections were incubated in 5% blocking serum for 30 min and then in primary antibodies (Cleaved Caspase-3: 1 : 1 000, from Cell Signaling Technology, Beverly, MA, USA) at 4°C overnight. They were subsequently incubated with biotinylated secondary antibodies for 30 min and finally counterstained with hematoxylin.

2.10. Western Blot. The protein lysates were prepared from frozen tissues in ice-cold RIPA buffer (Sigma-Aldrich). The extracted protein was separated in a 10% sodium dodecyl sulfate- (SDS-) PAGE and then electrophoretically transferred to a nitrocellulose membrane (Hybond, Amersham Biosciences, Little Chalfont, UK). Membranes were blocked with 5% nonfat milk powder in TBS for 1 h at room temperature. These membranes were subjected to immunoblot analysis with antibodies to JAK2, p-JAK2, STAT1, p-STAT1, STAT3, and p-STAT3. The protein antibody immune

complexes were detected with horseradish peroxidase-conjugated secondary antibodies and enhanced chemiluminescence reagents (Pierce Biotechnology, Rockford, IL). GAPDH was used as an internal control to calculate the ratio of optical density, and values were compared with those of sham controls.

2.11. Statistical Analysis. All values are given as the mean \pm SD. Statistical analysis was carried out using GraphPad Prism 8.0 software (GraphPad Software, USA). One-way analysis of variance was used to compare the measurement data between groups. $P < 0.05$ was considered significant.

3. Results

3.1. EA Pretreatment Significantly Decreases Intestinal Histology Injury. To examine the protective effect of EA pretreatment against intestinal injury after AOLT, each rat was analyzed by histopathology, and the intestinal mucous damage score was calculated. A normal histological structure was observed in the sham group by HE staining. Severe disruption of structural integrity in brush border, including loss of mucus, villi, and widespread necrotic area, was observed in the AOLT group. However, these damages were improved in the EA pretreatment group. The intestinal mucous damage score significantly increased in the AOLT group compared with the sham group. EA pretreatment combined with AG490 improved intestinal damage; no significant differences were observed between the EA+sham group and the EA+AOLT+AG490 group (Figures 2).

3.2. EA Pretreatment Alleviates *W/D* Ratio of the Intestine. To test intestinal edema after AOLT, we calculated the *W/D* ratio changes in all groups. As shown in Table 1, EA pretreatment significantly reduced the *W/D* ratio caused by AOLT. When compared with the AOLT group, the intestinal *W/D* ratio decreased in the EA+sham and EA+AOLT+AG490 groups. The EA+sham group did not show a significant difference from the sham group (Table 1, Figure 3).

3.3. EA Pretreatment Decreases Intestinal Inflammatory Reaction and Oxidative Stress. As aforementioned, EA application was shown to protect against intestinal injury following AOLT. However, the underlying mechanisms remain unknown. Severe intestinal damage was found to be accompanied by oxidative stress and inflammatory reaction

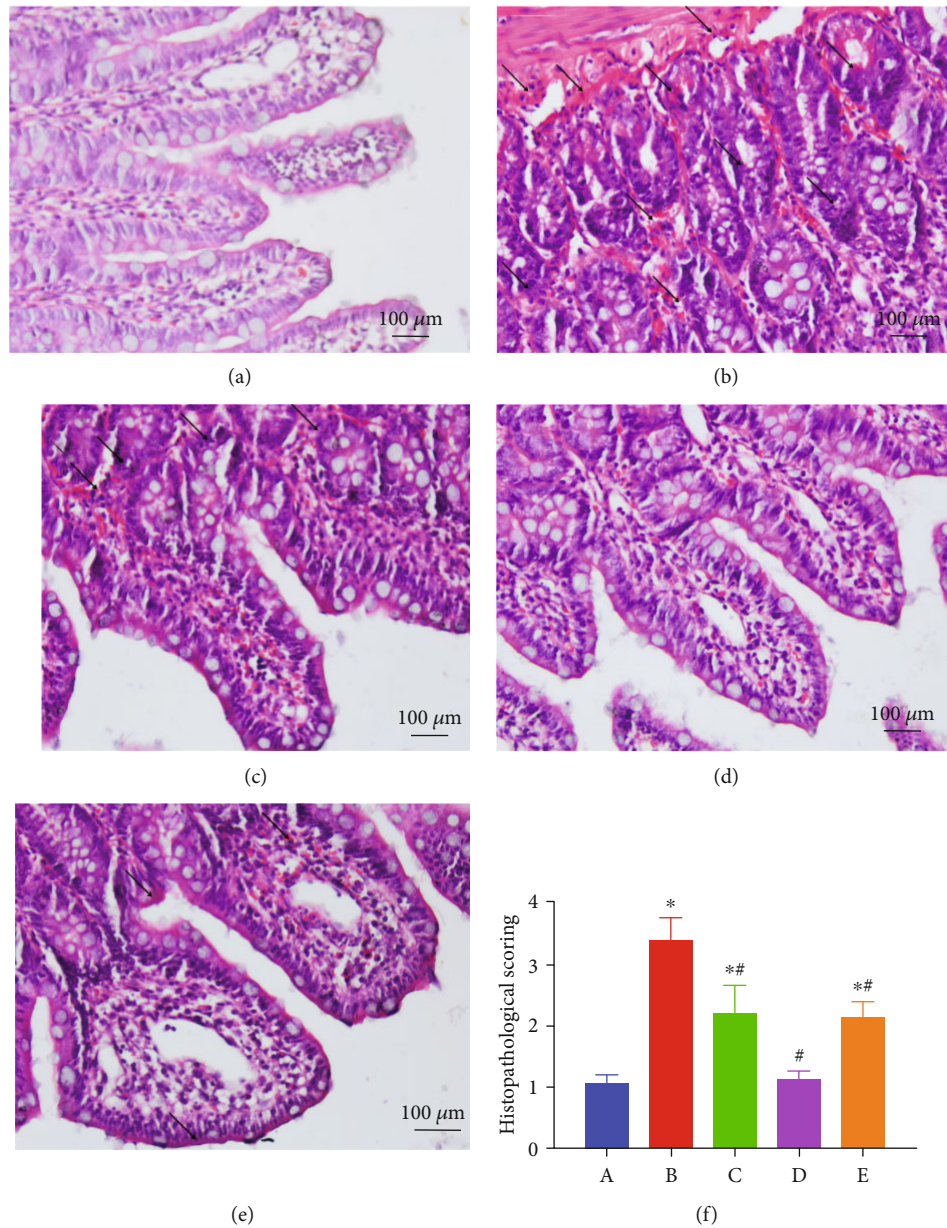


FIGURE 2: EA pretreatment significantly decreases intestinal histology injury (magnification, $\times 200$). Representative microphotographs were taken from the intestine of the sham (a), AOLT (b), EA+AOLT (c), EA+sham (d), and EA+AOLT+AG490 (e) groups at the time point of 6 h after AOLT in rats. (f) Histopathological scoring was calculated in each group: (A–E) the sham, AOLT, EA+AOLT, EA+sham, and EA+AOLT+AG490 groups. Data were represented as the mean \pm SD ($n = 8$, per group). * $P < 0.05$ vs. the sham group. # $P < 0.05$ vs. the AOLT group.

TABLE 1: W/D ratio of experiment rats ($n = 8$, $\bar{x} \pm s$).

Groups	W/D ratio
Sham	3.89 ± 0.81
AOLT	$9.35 \pm 0.13^*$
EA+AOLT	$5.85 \pm 0.55^{*#}$
EA+sham	$3.70 \pm 0.57^{\#}$
EA+AOLT+AG490	$4.45 \pm 0.41^{\#}$

Data presented are the mean \pm SD. * $P < 0.05$ vs. the sham group. # $P < 0.05$ vs. the AOLT group.

activation. The levels of TNF- α , HMGB-1, iFABP, LPS, and MDA increased markedly in the AOLT group. However, the application of EA effectively balanced oxidative stress and inflammatory reactions. The levels of TNF- α , HMGB-1, iFABP, LPS, and MDA decreased, whereas the level of SOD increased in EA+AOLT group. In the EA+sham group, EA had no effect on oxidative stress and inflammatory response, which were comparable with the results observed in the sham group. Results from the EA+AOLT+AG490 group were also similar to those from the EA+sham group (Figures 4 and 3).

3.4. EA Pretreatment Inhibits Intestinal P-JAK2, P-STAT1, and P-STAT3 Protein Expressions.

The JAK/STAT pathway

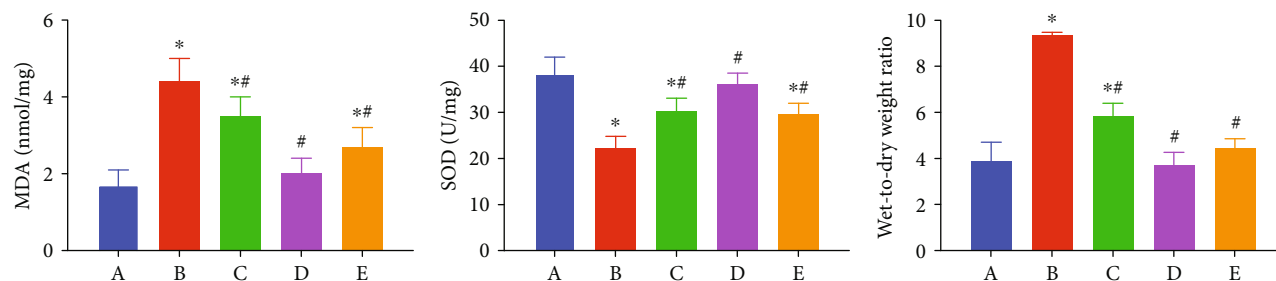


FIGURE 3: Effects of EA on the plasma level of MDA, SOD, and the W/D ratio following AOLT-induced intestinal injury. The levels of plasma MDA, SOD, and the W/D ratio were measured at 6 h following AOLT. (A–E) The sham, AOLT, EA+AOLT, EA+sham, and EA+AOLT+AG490 groups. Data were represented as the mean \pm SD ($n = 8$, per group). * $P < 0.05$ vs. the sham group. ** $P < 0.05$ vs. the AOLT group.

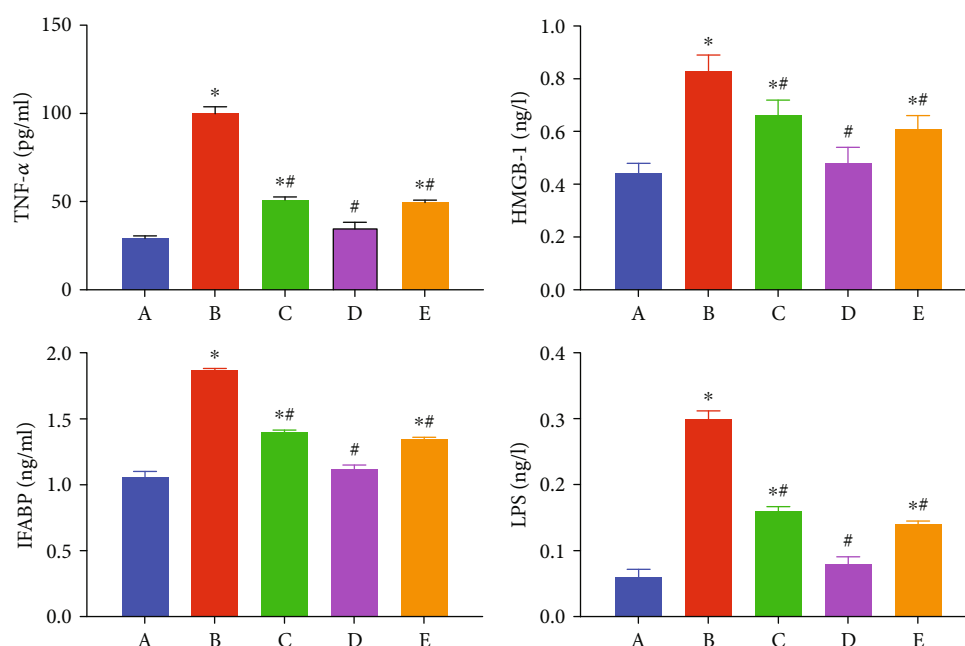


FIGURE 4: Effects of EA on the plasma level of TNF- α , HMGB-1, IFABP, and LPS following AOLT induced intestinal injury. The levels of plasma TNF- α , HMGB-1, IFABP, and LPS were measured at 6 h following AOLT. (A–E) The sham, AOLT, EA+AOLT, EA+sham, and EA+AOLT+AG490 groups. Data were represented as the mean \pm SD ($n = 8$, per group). * $P < 0.05$ vs. sham group. ** $P < 0.05$ vs. the AOLT group.

plays a vital role in regulating the immune response. Western blot analysis was performed to demonstrate the effect of EA on JAK/STAT pathway proteins. JAK2, STAT1, and STAT3 proteins were mainly expressed in intestinal cells. The expressions of p-JAK2, p-STAT1, and p-STAT3 proteins significantly increased in intestines subjected to AOLT ($P < 0.05$ vs. the sham group). However, EA application decreased the expression of p-JAK2, p-STAT1, and p-STAT3 proteins ($P < 0.05$ vs. the AOLT group). Treatment with AG490 reduced the expressions of p-JAK2, p-STAT1, and p-STAT3 proteins ($P < 0.05$ vs. the AOLT group). These results demonstrated that EA inhibited the JAK/STAT signaling pathway in intestinal injury after AOLT. The JAK/STAT signaling pathway was active in the AOLT group (Figure 5).

3.5. EA Pretreatment Decreases the Expression of Cleaved Caspase-3 in the Intestine. From the immunohistochemical staining, intense staining for active Cleaved Caspase-3 in

the cytoplasm of epithelial cells of rats subjected to AOLT was observed. However, very few Cleaved Caspase-3 immunoreactive cells were observed in the sham and EA+sham groups. These results again showed the tissue-protective effect of EA against intestinal injury after AOLT (Figure 6). When pretreated with EA and AG490, the EA+sham and EA+AOLT+AG490 groups did not show a significant difference from the sham group.

3.6. EA Pretreatment Attenuates Intestinal Epithelial Cell Apoptosis. TUNEL assay was used to evaluate the apoptosis of tubular epithelial cells induced by AOLT. A large number of apoptotic epithelial cells were visible in the intestines subjected to AOLT ($P < 0.05$ vs. the sham group). EA application was associated with the occurrence of apoptosis of epithelial cells, which was less than that observed with the AOLT group ($P < 0.05$). In the EA+sham group, EA treatment had no effect on apoptotic epithelial cells, comparable with the sham

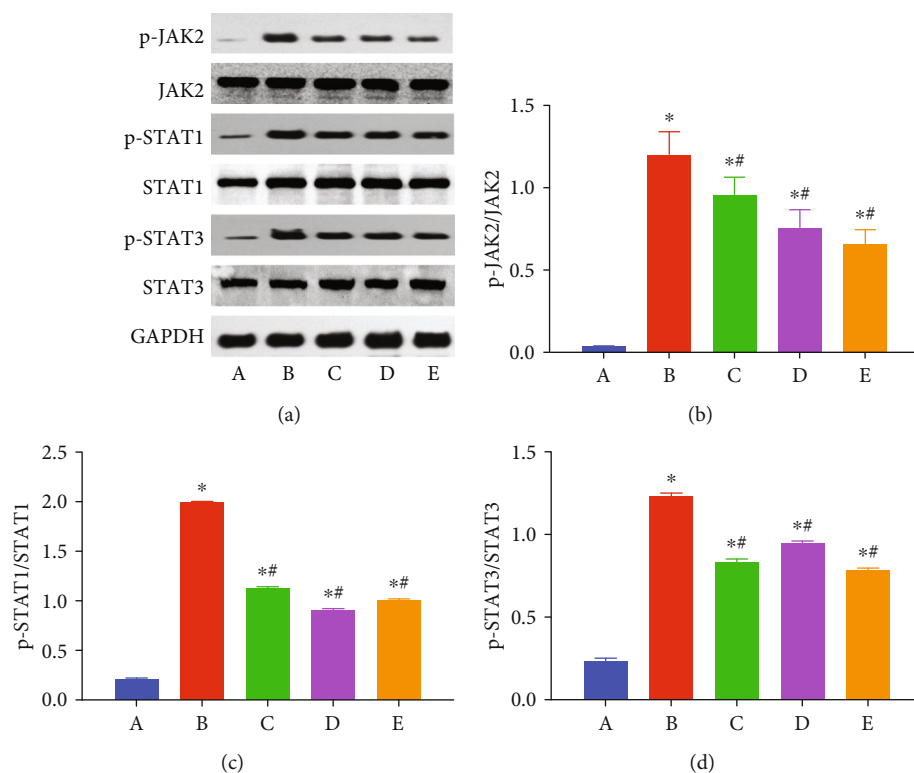


FIGURE 5: EA inhibited the phosphorylations of JAK2, STAT1, and STAT3. Representative Western blots for the phosphorylations of JAK2, STAT1, and STAT3 (a) of the intestine were detected after 6 h of AOLT; (A–E) The sham, AOLT, EA+AOLT, EA+sham, and EA+AOLT +AG490 groups. Densitometry analysis of Western blots for the ratio of p-JAK2/JAK2 (b), p-STAT1/STAT1 (c), and p-STAT3/STAT3 (d). Data were represented as the mean \pm SD ($n = 8$, per group). * $P < 0.05$ vs. the sham group. # $P < 0.05$ vs. the AOLT group.

group. The EA+AOLT+AG490 group had similar results as the sham group (Figure 7).

4. Discussion

We found that AOLT-induced intestinal injury in rats. We determined whether EA affected the results. Pretreatment with EA alleviated intestinal injury after AOLT, as shown by HE staining and TUNEL methods. Compared with the sham group, the EA+sham group did not produce adverse reactions as normal rats. We explored the potential mechanisms underlying EA pretreatment. EA pretreatment inhibited the expressions of p-JAK2, p-STAT1, and p-STAT3 in intestines after AOLT. When treated with JAK2-specific inhibitor AG490, intestinal injury was balanced. This indicated that EA pretreatment alleviated intestinal injury after AOLT by inhibiting the JAK/STAT signaling pathway and provides basic evidence supporting its potential therapeutic efficacy (Figure 8).

AOLT blocks the return of venous blood in the lower extremities, which induces a systemic response and a release of harmful substances that may damage remote organs, including the intestines [21–24]. After AOLT in rats, blood flow is blocked, and intestinal injury undergoes two processes: ischemia and secondary reperfusion injury [20]. Due to intestinal hyperemia and congestion during liver transplantation, intestinal peristalsis and barriers are often impaired. Intestinal erogenous endotoxin and bacteria enter

the blood or lymphatic system and are transferred to other organs, which may lead to multiple organs dysfunction and systemic inflammatory response [25]. Intestinal injury is a complex, multifactorial, and pathophysiological process that involves dysfunction of bacterial translocation, absorption, and production of reactive oxygen species, cytokines, nitric oxide, and initiates multiorgan dysfunction syndrome [4, 26]. A recent study found that intestinal barrier destruction was widely observed during liver transplantation [27]. Other studies have also explored the possible mechanism of intestinal injury caused by liver transplantation. TLR4/NF- κ B signaling pathway activation-induced cell apoptosis was involved in intestinal injury during liver transplantation [28]. In our study, we found that the intestinal injury score increased after AOLT. Our previous study showed that AOLT induced remote organ injury after 6 h reperfusion, and the inflammatory response was obvious [29]. Therefore, in the present study, we selected 6 h after reperfusion to measure the intestinal injuries caused by AOLT.

Numerous strategies have been designed to reduce intestinal injury after AOLT [30]. Although some drugs have been successfully used to reduce intestinal injury in animal models, few can be used in clinical settings or may not be available during operations. Acupuncture has been used to control weight [31], reduce epilepsy [32], improve learning and memory disorders [33], and reduce pain [34–37]. EA is a complementary alternative medicine approach and involves applying an electrical current to acupuncture points.

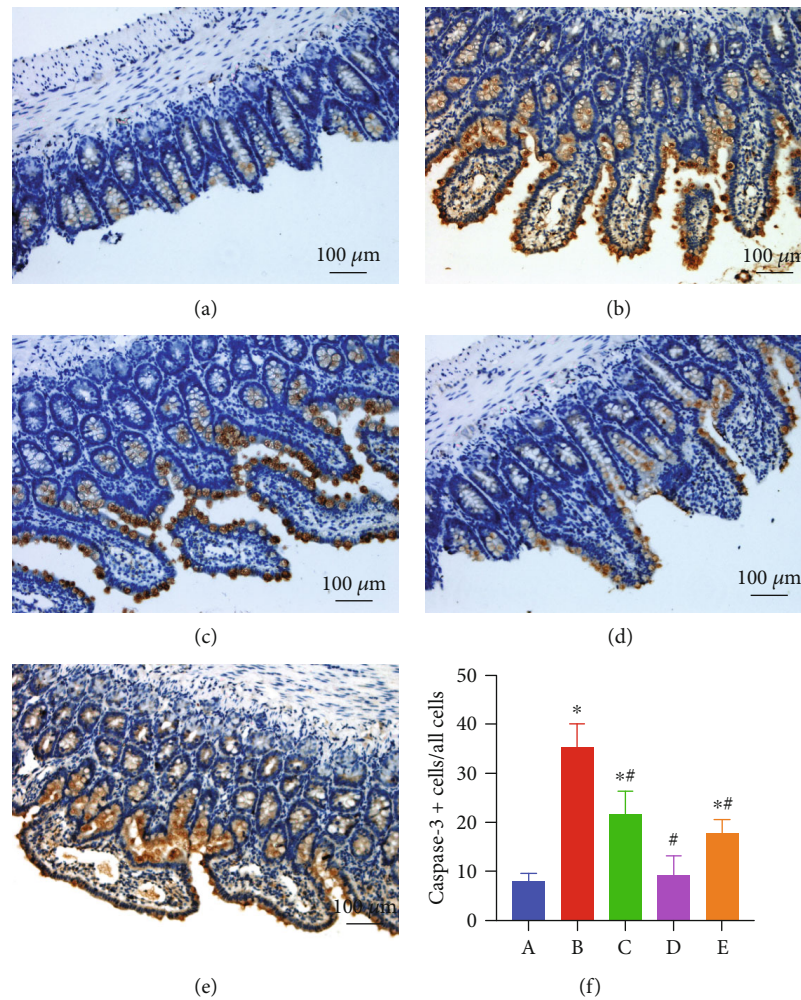


FIGURE 6: The effect of EA on AOLT induced Cleaved Caspase-3 of intestinal cells (magnification, $\times 200$). Representative microphotographs were taken from the intestine of the sham (a), AOLT (b), EA+AOLT (c), EA+sham (d), and EA+AOLT+AG490 (e) groups at the time point of 6 h after AOLT. (f) Quantification of Cleaved Caspase-3 positive cells were counted in each group: (A–E) the sham, AOLT, EA+AOLT, EA+sham, and EA+AOLT+AG490 groups.

Zusanli is an important acupuncture point commonly used in acupuncture practices to promote blood circulation and can also cure peripheral soft tissue inflammation and ischemia-reperfusion [6, 38–41]. Indeed, several studies have demonstrated that EA significantly attenuated apoptosis in the brain, heart, and intestinal ischemia-reperfusion [42–44]. In our study, inflammatory reaction markers (TNF- α , HMGB-1) and oxidative stress factors (MDA) increased significantly in the AOLT group. However, in the EA+AOLT group, apoptosis of epithelial cells resulting from the intestinal injury was significantly decreased. Caspase-3, which participates in the apoptosis pathway in the intestinal mucosa, was also markedly reduced in the EA+AOLT group, which confirmed the decreased disruption of the structural integrity of intestinal mucosa, as observed by HE staining. This study evaluated the protective and antiapoptotic effects of EA on intestinal architecture and apoptosis in intestinal injury.

JAK/STAT is involved in many pathophysiological processes in the body [45, 46]. JAK2 is a member of the Janus kinase family and is involved in immune, hematopoietic,

neural, and other signal transduction systems [47]. A recent study showed that EA has a protective effect on focal cerebral ischemia by inhibiting JAK2 phosphorylated activation in rats [48]. AG490 is a specific inhibitor of JAK2 which can inhibit the activation of JAK2 and downregulate the phosphorylation of STATs. The JAK/STAT signaling pathway is involved in ischemia-reperfusion processes. Our previous study showed that the JAK/STAT signaling pathway was inhibited by propofol in the hippocampus [29]. To confirm the hypothesis that the JAK/STAT signaling pathway participated in regulating apoptotic process in our model, AG490 was given in the EA+AOLT group. Our study showed that EA+AG490 significantly improved intestinal apoptosis and reduced the expression of Cleaved Caspase-3 protein following AOLT. Our data also showed significantly decreased expressions of p-JAK2 in the EA and EA+AG490 groups, accompanied by the downregulation of STAT1 and STAT3 phosphorylation. Our results indicated that EA significantly protected intestinal injury after AOLT in rats by inhibiting the activation of the JAK/STAT signaling pathway.

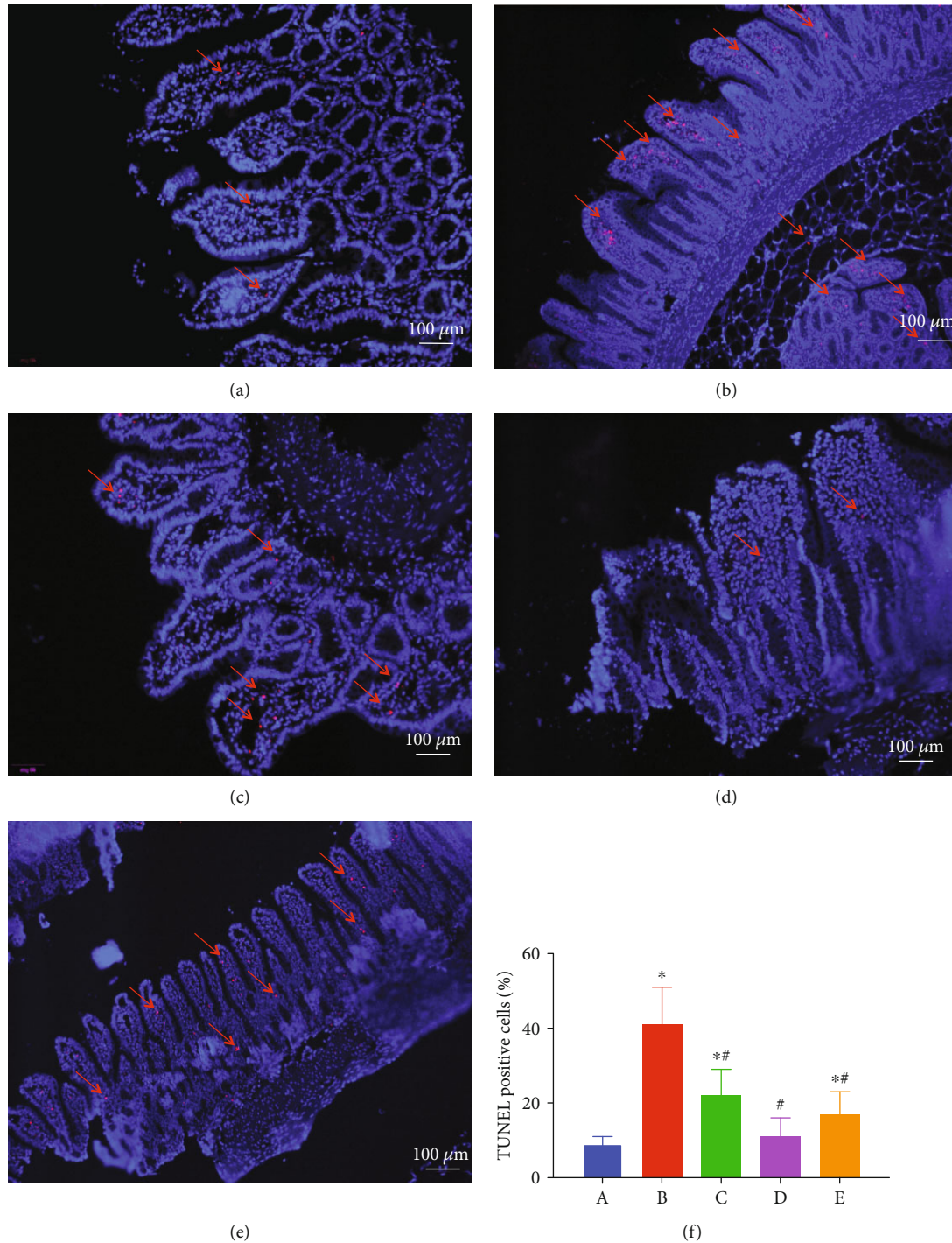


FIGURE 7: The effect of EA on AOLT induced apoptosis of intestinal cells (magnification, $\times 200$). Representative microphotographs were taken from the intestine of the sham (a), AOLT (b), EA+AOLT (c), EA+sham (d), and EA+AOLT+AG490 (e) groups at the time point of 6 h after AOLT. Apoptosis was evaluated by TUNEL staining. Quantification of TUNEL-positive cells was counted following AOLT (f). * $P < 0.05$ vs. the sham group. # $P < 0.05$ vs. the AOLT group.

Taken together, intestinal injury contributed to the damage of intestinal function and histological structure and enhanced the apoptosis of intestinal epithelial cells and the expression of protein Cleaved Caspase-3. We demonstrated that EA pretreatment attenuated intestinal injury by inhibiting the JAK/STAT signaling pathway in a rat AOLT model. Zusanli is a classic and preferred acupoint

for treating gastrointestinal diseases and is widely used in clinical practice. Its therapeutic effect is recognized by many medical workers and patients. EA is a branch of acupuncture and moxibustion therapy. Compared with classic acupuncture, it has many advantages, such as good therapeutic effects, a wide range, ease of stimulation control, and continuous needle movements [49]. However, there

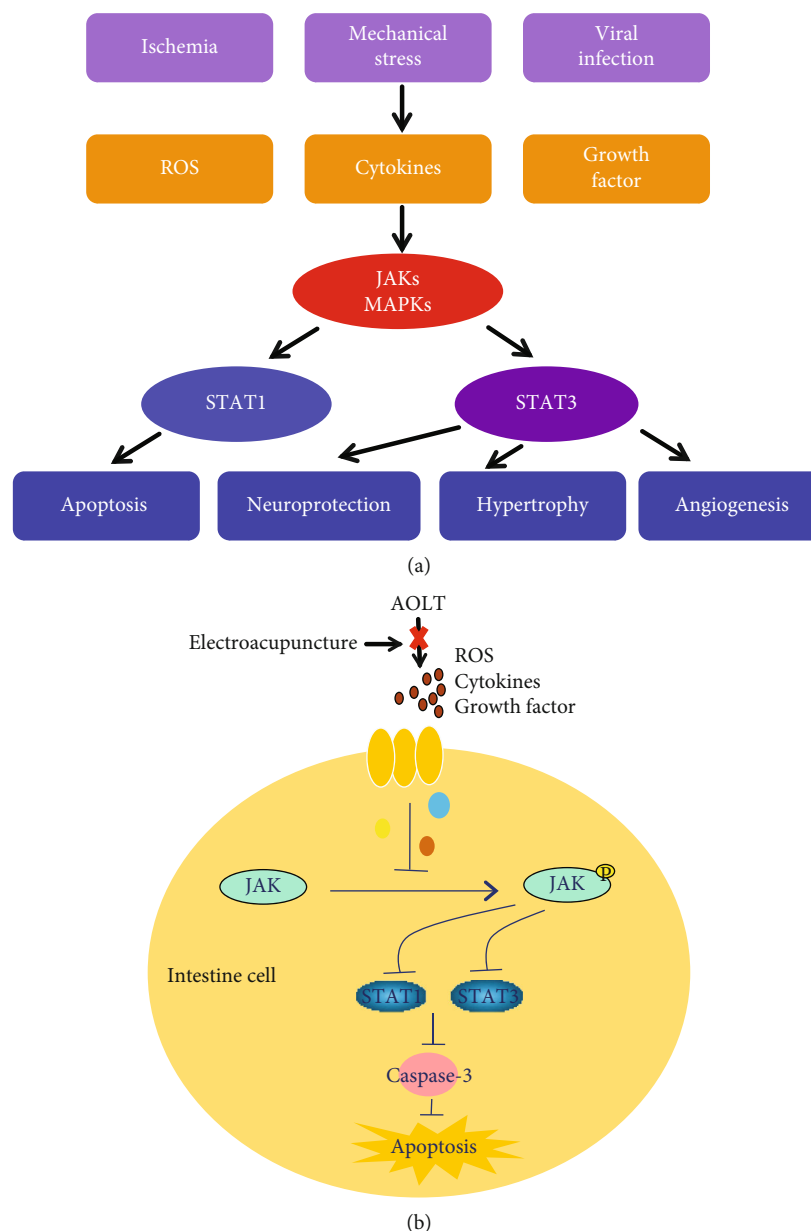


FIGURE 8: The possible mechanism of EA on AOLT induced apoptosis of intestine (a). The possible mechanism involved in the JAK/STAT pathway (b). EA pretreatment may have protective effects on AOLT-induced intestine injury by inhibiting JAK/STAT pathway.

are several limitations to our study. This study was based on our previous study; we could have used gene sequencing technology to explore the involved mechanism. Then, we would explore the mechanism *in vivo* and investigate whether this mechanism functioned at the cellular level. Finally, we need to apply this technique in clinical practice. To make progress on this front, our research team has begun a single-center study on the protective effect of EA pretreatment on postoperative organs.

In conclusion, our study showed that EA reduced intestinal injury against AOLT, at least in part through its inhibitory effects on the injury-induced activation of the JAK/STAT signaling pathway. If extrapolated to a clinical setting, EA has the potential to serve as a clinical strategy for preventing perioperative intestinal injury after AOLT.

Data Availability

The data used to support the findings of this study are available from the corresponding author upon request.

Conflicts of Interest

The authors declare that there is no conflict of interest regarding the publication of this paper.

Authors' Contributions

Lili Jia designed and wrote this paper, Hongli Yu and Yiqi Weng provided the technical assistance, and Wenli Yu offered the guidance of this study.

Acknowledgments

The paper was financially supported by the Natural Science Foundation of Tianjin (18JCYBJC27500 and 17JCYBJC28000), the Tianjin Clinical Key Discipline Project (Anesthesiology), and 2019 Tianjin First Central Hospital Academy Project (2019CF09).

References

- [1] Y. Si, H. Bao, L. Han et al., “Dexmedetomidine protects against renal ischemia and reperfusion injury by inhibiting the JAK/STAT signaling activation,” *Journal of Translational Medicine*, vol. 11, no. 1, p. 141, 2013.
- [2] J. Shen, G. Fu, L. Jiang, J. Xu, L. Li, and G. Fu, “Effect of dexmedetomidine pretreatment on lung injury following intestinal ischemia-reperfusion,” *Experimental and Therapeutic Medicine*, vol. 6, no. 6, pp. 1359–1364, 2013.
- [3] X. K. Zhang, X. P. Zhou, Q. Zhang, and F. Zhu, “The preventive effects of dexmedetomidine against intestinal ischemia-reperfusion injury in Wistar rats,” *Iranian Journal of Basic Medical Sciences*, vol. 18, no. 6, pp. 604–609, 2015.
- [4] C. Nastos, K. Kalimeris, N. Papoutsidakis et al., “Global consequences of liver ischemia/reperfusion injury,” *Oxidative Medicine and Cellular Longevity*, vol. 2014, Article ID 906965, 13 pages, 2014.
- [5] E. Nozato, M. Shiraishi, T. Miyaguni et al., “In situ perfusion of the liver under portosystemic shunt in rats: a stable model of cold ischemia for orthotopic liver transplantation,” *Transplantation Proceedings*, vol. 30, no. 7, pp. 3718–3720, 1998.
- [6] Y. Geng, D. Chen, J. Zhou, H. Jiang, and H. Zhang, “Role of cholinergic anti-inflammatory pathway in treatment of intestinal ischemia-reperfusion injury by electroacupuncture at Zusanli,” *Evidence-based Complementary and Alternative Medicine*, vol. 2017, Article ID 6471984, 5 pages, 2017.
- [7] M. Cai, J. H. Lee, and E. J. Yang, “Electroacupuncture attenuates cognition impairment via anti-neuroinflammation in an Alzheimer’s disease animal model,” *Journal of Neuroinflammation*, vol. 16, no. 1, p. 264, 2019.
- [8] Y. Li, C. Yin, X. Li et al., “Electroacupuncture alleviates paclitaxel-induced peripheral neuropathic pain in rats via suppressing TLR4 signaling and TRPV1 upregulation in sensory neurons,” *International Journal of Molecular Sciences*, vol. 20, no. 23, p. 5917, 2019.
- [9] N. Yun, J. W. Kang, and S. M. Lee, “Protective effects of chlorogenic acid against ischemia/reperfusion injury in rat liver: molecular evidence of its antioxidant and anti-inflammatory properties,” *The Journal of Nutritional Biochemistry*, vol. 23, no. 10, pp. 1249–1255, 2012.
- [10] Y. Li, Y. Chen, X. Zhang et al., “Protective effect of electroacupuncture on liver ischemia-reperfusion injury in rats,” *Experimental and Therapeutic Medicine*, vol. 16, no. 2, pp. 1373–1380, 2018.
- [11] M. V. R. Scognamiglio-Szabó, G. H. Bechara, S. H. Ferreira, and F. Q. Cunha, “Effect of various acupuncture treatment protocols upon sepsis in Wistar rats,” *Annals of the New York Academy of Sciences*, vol. 1026, no. 1, pp. 251–256, 2004.
- [12] W. Geng, L. Cai, K. Han et al., “Electroacupuncture pretreatment alleviates cerebral ischemia-reperfusion injury by increasing GSK-3 β phosphorylation level via adenosine A1 receptor,” *BioMed Research International*, vol. 2020, Article ID 6848450, 9 pages, 2020.
- [13] J. J. O’Shea, M. Gadina, and R. D. Schreiber, “Cytokine signaling in 2002,” *Cell*, vol. 109, no. 2, pp. S121–S131, 2002.
- [14] S. Negoro, K. Kunisada, E. Tone et al., “Activation of JAK/STAT pathway transduces cytoprotective signal in rat acute myocardial infarction,” *Cardiovascular Research*, vol. 47, no. 4, pp. 797–805, 2000.
- [15] A. Das, F. N. Salloum, D. Durrant, R. Ockaili, and R. C. Kukreja, “Rapamycin protects against myocardial ischemia-reperfusion injury through JAK2-STAT3 signaling pathway,” *Journal of Molecular and Cellular Cardiology*, vol. 53, no. 6, pp. 858–869, 2012.
- [16] J. Q. Fang, J. Y. du, Y. Liang, and J. F. Fang, “Intervention of electroacupuncture on spinal p38 MAPK/ATF-2/VR-1 pathway in treating inflammatory pain induced by CFA in rats,” *Molecular Pain*, vol. 9, 2013.
- [17] S. Katsuyama, H. Mizoguchi, H. Kuwahata et al., “Involvement of peripheral cannabinoid and opioid receptors in β -caryophyllene-induced antinociception,” *European Journal of Pain*, vol. 17, no. 5, pp. 664–675, 2013.
- [18] J. Zhou, Y. Jin, R. Ma et al., “Electroacupuncture alleviates experimental chronic inflammatory pain by inhibiting calcium voltage-gated channel-mediated inflammation,” *Evidence-based Complementary and Alternative Medicine*, vol. 2020, Article ID 7061972, 10 pages, 2020.
- [19] C. J. Chiu, A. H. McArdle, R. Brown, H. J. Scott, and F. N. Gurd, “Intestinal mucosal lesion in low-flow states. I. A morphological, hemodynamic, and metabolic reappraisal,” *Archives of Surgery*, vol. 101, no. 4, pp. 478–483, 1970.
- [20] L. M. Gonzalez, A. J. Moeser, and A. T. Blikslager, “Animal models of ischemia-reperfusion-induced intestinal injury: progress and promise for translational research,” *American Journal of Physiology. Gastrointestinal and Liver Physiology*, vol. 308, no. 2, pp. G63–G75, 2015.
- [21] B. Erenoglu, H. S. Gokturk, T. Kucukkartallar et al., “Mechanical intestinal cleansing and antibiotic prophylaxis for preventing bacterial translocation during the Pringle maneuver in rabbits,” *Surgery Today*, vol. 41, no. 6, pp. 824–828, 2011.
- [22] D. L. Liu, B. Jeppsson, C. H. Hakansson, and R. Odselius, “Multiple-system organ damage resulting from prolonged hepatic inflow interruption,” *Archives of Surgery*, vol. 131, no. 4, pp. 442–447, 1996.
- [23] P. A. Clavien, H. Petrowsky, M. L. DeOliveira, and R. Graf, “Strategies for safer liver surgery and partial liver transplantation,” *The New England Journal of Medicine*, vol. 356, no. 15, pp. 1545–1559, 2007.
- [24] S. A. W. G. Dello, K. W. Reisinger, R. M. van Dam et al., “Total intermittent Pringle maneuver during liver resection can induce intestinal epithelial cell damage and endotoxemia,” *PLoS One*, vol. 7, no. 1, article e30539, 2012.
- [25] M. Ge, X. Chi, A. Zhang et al., “Intestinal NF-E2-related factor-2 expression and antioxidant activity changes in rats undergoing orthotopic liver autotransplantation,” *Oncology Letters*, vol. 6, no. 5, pp. 1307–1312, 2013.
- [26] D. L. Carden and D. N. Granger, “Pathophysiology of ischaemia-reperfusion injury,” *The Journal of Pathology*, vol. 190, no. 3, pp. 255–266, 2000.
- [27] X. Tian, Z. Yang, F. Luo, and S. Zheng, “Gut microbial balance and liver transplantation: alteration, management, and prediction,” *Frontiers in Medicine*, vol. 12, no. 2, pp. 123–129, 2018.
- [28] D.-D. Yuan, X.-J. Chi, Y. Jin et al., “Intestinal injury following liver transplantation was mediated by TLR4/NF- κ B activation-

- induced cell apoptosis," *Molecular Medicine Reports*, vol. 13, no. 2, pp. 1525–1532, 2016.
- [29] L. Jia, F. Wang, X. Gu et al., "Propofol postconditioning attenuates hippocampus ischemia-reperfusion injury via modulating JAK2/STAT3 pathway in rats after autogenous orthotopic liver transplantation," *Brain Research*, vol. 1657, no. 15, pp. 202–207, 2017.
- [30] R. Bahde and H. U. Spiegel, "Hepatic ischaemia-reperfusion injury from bench to bedside," *The British Journal of Surgery*, vol. 97, no. 10, pp. 1461–1475, 2010.
- [31] Y. Li, P. Adamek, H. Zhang et al., "The cancer chemotherapeutic paclitaxel increases human and rodent sensory neuron responses to TRPV1 by activation of TLR4," *The Journal of Neuroscience*, vol. 35, no. 39, pp. 13487–13500, 2015.
- [32] P. Flood, J. M. Sonner, D. Gong, and K. M. Coates, "Isoflurane hyperalgesia is modulated by nicotinic inhibition," *Anesthesiology*, vol. 97, no. 1, pp. 192–198, 2002.
- [33] P. M. Cornett, J. A. Matta, and G. P. Ahern, "General anesthetics sensitize the capsaicin receptor transient receptor potential V1," *Molecular Pharmacology*, vol. 74, no. 5, pp. 1261–1268, 2008.
- [34] S. J. Raithel, M. R. Sapio, M. J. Iadarola, and A. J. Mannes, "Thermal A- δ nociceptors, identified by transcriptomics, express higher levels of anesthesia-sensitive receptors than thermal C-fibers and are more suppressible by low-dose isoflurane," *Anesthesia and Analgesia*, vol. 127, no. 1, pp. 263–266, 2018.
- [35] M. J. Caterina, M. A. Schumacher, M. Tominaga, T. A. Rosen, J. D. Levine, and D. Julius, "The capsaicin receptor: a heat-activated ion channel in the pain pathway," *Nature*, vol. 389, no. 6653, pp. 816–824, 1997.
- [36] C.-Y. Chen, C.-N. Lin, R.-S. Chern, Y.-C. Tsai, Y.-H. Chang, and C.-H. Chien, "Neuronal activity stimulated by liquid substrates injection at zusanli (ST36) acupoint: the possible mechanism of aquapuncture," *Evidence-based Complementary and Alternative Medicine*, vol. 2014, Article ID 627342, 7 pages, 2014.
- [37] S. I. Choi, J. Y. Lim, S. Yoo, H. Kim, and S. W. Hwang, "Emerging role of spinal cord TRPV1 in pain exacerbation," *Neural Plasticity*, vol. 2016, Article ID 5954890, 10 pages, 2016.
- [38] A. Villegas-Bastida, R. Torres-Rosas, L. A. Arriaga-Pizano, J. Flores-Estrada, A. Gustavo-Acosta, and M. A. Moreno-Eutimio, "Electrical stimulation at the ST36 acupoint protects against sepsis lethality and reduces serum TNF levels through vagus nerve- and catecholamine-dependent mechanisms," *Evidence-based Complementary and Alternative Medicine*, vol. 2014, Article ID 451674, 8 pages, 2014.
- [39] S. Hu, M. H. du, H. M. Luo et al., "Electroacupuncture at Zusanli (ST36) prevents intestinal barrier and remote organ dysfunction following gut ischemia through activating the cholinergic anti-inflammatory-dependent mechanism," *Evidence-based Complementary and Alternative Medicine*, vol. 2013, Article ID 592127, 10 pages, 2013.
- [40] M.-H. Du, H. M. Luo, Y. J. Tian et al., "Electroacupuncture ST36 prevents postoperative intra-abdominal adhesions formation," *The Journal of Surgical Research*, vol. 195, no. 1, pp. 89–98, 2015.
- [41] L. Zhang, H. Wang, Z. Huang et al., "Inhibiting effect of electroacupuncture at Zusanli on early inflammatory factor levels formed by postoperative abdominal adhesions," *Evidence-based Complementary and Alternative Medicine*, vol. 2014, Article ID 950326, 5 pages, 2014.
- [42] Y. Geng, D. Chen, J. Zhou et al., "Synergistic effects of electroacupuncture and mesenchymal stem cells on intestinal ischemia/reperfusion injury in rats," *Inflammation*, vol. 39, no. 4, pp. 1414–1420, 2016.
- [43] R. Torres-Rosas, G. Yehia, G. Peña et al., "Dopamine mediates vagal modulation of the immune system by electroacupuncture," *Nature Medicine*, vol. 20, no. 3, pp. 291–295, 2014.
- [44] D. Grech, Z. Li, P. Morcillo et al., "Intraoperative low-frequency electroacupuncture under general anesthesia improves postoperative recovery in a randomized trial," *Journal of Acupuncture and Meridian Studies*, vol. 9, no. 5, pp. 234–241, 2016.
- [45] J. J. O'Shea, M. Gadina, and R. D. Schreiber, "Cytokine signaling in 2002: new surprises in the Jak/Stat pathway," *Cell*, vol. 109, no. 2, pp. S121–S131, 2002.
- [46] K. Imada and W. J. Leonard, "The JAK-STAT pathway," *Molecular Immunology*, vol. 37, no. 1-2, pp. 1–11, 2000.
- [47] L. A. Wang, H. Bi, H. R. Ji, Y. P. Wang, and Z. M. Du, "Effect of lumbrokinase on JAK-STAT pathway in rat brain during cerebral ischemia and reperfusion," *Zhongguo Yao Xue Za Zhi*, vol. 44, no. 24, pp. 1862–1865, 2009.
- [48] R. Liu, N. Xu, W. Yi, K. Huang, and M. Su, "Electroacupuncture effect on neurological behavior and tyrosine kinase-JAK 2 in rats with focal cerebral ischemia," *Journal of Traditional Chinese Medicine*, vol. 32, no. 3, pp. 465–470, 2012.
- [49] Y. X. Gen, D. Cheng, J. Lu, M. Q. Chen, H. D. Zhang, and J. Zhou, "Effects of electroacupuncture at Zusanli (ST36) on mucosal barrier repair in rats with intestinal ischemia reperfusion injury," *Journal of Emergency in Traditional Chinese Medicine*, vol. 25, no. 7, pp. 1300–1302, 1315, 2016.

Research Article

MiR-181c-5p Promotes Inflammatory Response during Hypoxia/Reoxygenation Injury by Downregulating Protein Tyrosine Phosphatase Nonreceptor Type 4 in H9C2 Cardiomyocytes

Sheng Wang ¹, Liang Ge,^{2,3} Dengwen Zhang,¹ Lin Wang,² Hao Liu,⁴ Xiaodong Ye,² Wanling Liang,⁵ Jun Li,⁶ Haichun Ma ³, Yin Cai ², and Zhengyuan Xia ^{2,6,7}

¹Department of Anesthesiology, Guangdong Cardiovascular Institute, Guangdong Provincial People's Hospital, Guangdong Academy of Medical Sciences, Guangdong, China

²Department of Anesthesiology, The University of Hong Kong, Hong Kong SAR, China

³Department of Anesthesiology, The First Hospital, Jilin University, Jilin, China

⁴Department of Cardiology, The Second Affiliated Hospital of Guangzhou Medical University, Guangzhou Institute of Cardiovascular Disease, Guangdong, China

⁵Department of Pharmacology and Pharmacy, The University of Hong Kong, Hong Kong SAR, China

⁶Department of Anesthesiology, The Second Affiliated Hospital and Yuying Children's Hospital, Wenzhou Medical University, Wenzhou, China

⁷Department of Anesthesiology, Affiliated Hospital of Guangdong Medical University, Zhanjiang, China

Correspondence should be addressed to Yin Cai; caiyin1987@gmail.com and Zhengyuan Xia; zyxia@hku.hk

Received 24 February 2020; Revised 25 May 2020; Accepted 29 June 2020; Published 26 July 2020

Guest Editor: Margaret H Hastings

Copyright © 2020 Sheng Wang et al. This is an open access article distributed under the Creative Commons Attribution License, which permits unrestricted use, distribution, and reproduction in any medium, provided the original work is properly cited.

Background. Constitutive nuclear factor kappa B (NFκB) activation has been shown to exacerbate during myocardial ischemia/reperfusion (I/R) injury. We recently showed that miR-181c-5p exacerbated cardiomyocytes injury and apoptosis by directly targeting the 3'-untranslated region of protein tyrosine phosphatase nonreceptor type 4 (PTPN4). However, whether miR-181c-5p mediates cardiac I/R injury through NFκB-mediated inflammation is unknown. Thus, the present study aimed to investigate the role of miR-181c-5p during myocardial I/R injury and explore its mechanism in relation to inflammation in H9C2 cardiomyocytes. **Methods and Results.** In hypoxia/reoxygenation (H/R, 6 h hypoxia followed by 6 h reoxygenation)-stimulated H9C2 cardiomyocytes or postischemic myocardium of rat, the expression of miR-181c-5p was significantly upregulated, which was concomitant increased NFκB activity when compared to the nonhypoxic or nonischemic control groups. This is indicative that miR-181c-5p may be involved in NFκB-mediated inflammation during myocardial I/R injury. To investigate the potential role of miR-181c-5p in H/R-induced cell inflammation and injury, H9C2 cardiomyocytes were transfected with the miR-181c-5p agomir. Overexpression of miR-181c-5p significantly aggravated H/R-induced cell injury (increased lactate dehydrogenase (LDH) level) and exacerbated NFκB-mediated inflammation (greater phosphorylation and degradation of IκBα, phosphorylation of p65, and increased levels of proinflammatory cytokines tumor necrosis factor α (TNFα), interleukin (IL)-6, and IL-1β). In contrast, inhibition of miR-181c-5p by its antagomir transfection *in vitro* had the opposite effect. Furthermore, overexpression of miR-181c-5p significantly enhanced lipopolysaccharide-induced NFκB signalling. Additionally, knockdown of PTPN4, the direct target of miR-181c-5p, significantly aggravated H/R-induced phosphorylation and degradation of IκBα, phosphorylation of p65, and the levels of proinflammatory cytokines. PTPN4 knockdown also cancelled miR-181c-5p antagomir mediated anti-inflammatory effects in H9C2 cardiomyocytes during H/R injury. **Conclusions.** It is concluded that miR-181c-5p may exacerbate myocardial I/R injury and NFκB-mediated inflammation *via* PTPN4, and that targeting miR-181c-5p/PTPN4/NFκB signalling may represent a novel strategy to combat myocardial I/R injury.

1. Introduction

Ischemic heart disease is one of the major causes of death worldwide [1, 2]. During cardiac ischemia/reperfusion (I/R) injury, cellular damage such as excessive apoptosis can result in protease and danger-associated molecular patterns that favours a proinflammatory environment through the activation of nuclear factor kappa B (NF κ B) [3]. In the ischemic heart, prolonged activation of NF κ B is generally considered to be detrimental by eliciting signals that trigger chronic inflammation through enhanced elaboration of proinflammatory cytokines, including interleukin (IL)-6, IL-1 β , and tumor necrosis factor α (TNF α), leading to cardiac injury [4, 5]. Constitutive NF κ B activation has been demonstrated in various models of experimental myocardial ischemia and reperfusion [3, 6]. *In vivo* transfer of NF κ B decoy oligodeoxynucleotides to bind transcriptional factor, blocking inflammatory gene activation, reduced the extent of myocardial infarction following reperfusion [7]. Thus, a strategy that can inhibit excessive NF κ B-mediated inflammation should be an effective therapy to combat ischemic heart disease.

The miR-181 family (including miR-181a, miR-181b, miR-181c, and miR-181d) plays diverse roles in regulating various cellular and biological processes through posttranscriptional regulation of target genes [8–12]. Accumulating evidence suggests a central role for the miR-181 family in inflammation by regulating target proteins involved in critical inflammatory signalling pathways, such as NF κ B signalling [13, 14]. For example, miR-181b can reduce inflammation through targeting the 3' untranslated region of the importin- α 3 (a protein critical for the translocation of NF κ B from the cytoplasm to the nucleus), further inhibiting the activation of NF κ B signalling pathway [14]. In addition, previous study has demonstrated that miR-181c-5p (named miR-181c in other studies) can directly target the 3' untranslated region of TNF α mRNA, suppressing its mRNA and protein expression in rat microglial cells after ischemia injury [15]. However, the anti-inflammatory effect of miR-181c-5p in neuroinflammation was challenged as miR-181c-5p exacerbated brain injury in acute ischemic stroke [16]. Thus, it is still unclear whether miR-181c-5p exerts pro- or anti-inflammatory effect in the context of I/R in general, and in myocardial I/R injury in specific.

We have recently shown that miR-181c-5p exacerbated hypoxia/reoxygenation (H/R)-induced cardiomyocyte injury and apoptosis via targeting protein tyrosine phosphatase nonreceptor type 4 (PTPN4) [17]. Of note, PTPN4 suppresses Toll-like receptor 4/NF κ B signalling in mouse peritoneal macrophages [18]. However, it is unknown whether or not PTPN4 may inhibit NF κ B-mediated proinflammatory responses in cardiomyocytes. During myocardial I/R injury, the cardiac resident cells, such as cardiomyocytes may elaborate proinflammatory cytokines in response to various stimuli and thus favour a proinflammatory environment. Therefore, the present study aimed to determine whether or not miR-181c-5p enhances NF κ B-mediated inflammation via inhibiting PTPN4 during cardiac I/R injury by using rat origin cardiomyocytes (H9C2) subjected to H/R stimulation.

2. Materials and Methods

2.1. Cell Culture. The rat origin H9C2 cardiomyocytes were purchased from the American Type Culture Collection (ATCC, Manassas, VA, USA). The H9C2 cells were maintained in Dulbecco's Modified Eagle's Medium (DMEM, ThermoFisher Scientific, MA, USA) supplemented with 10% fetal bovine serum (FBS, Biosera, Kansas City, MO, USA) and 1% penicillin/streptomycin (100 U/ml, ThermoFisher Scientific). All cells were cultured in a humidified atmosphere containing 5% CO₂-95%O₂ at 37°C.

2.2. Cell Treatment. The H9C2 cardiomyocytes were seeded into six-well plate (2×10^5 cell/well) overnight and transfected with micrON rno-miR-181c-5p agomir (50 nM, RIBOBIO, Guangzhou, China), micrOFF rno-miR-181c-5p antagomir (50 nM, RIBOBIO), small RNA (siRNA) against PTPN4 (50 nM, RIBOBIO), or their negative controls using Lipofectamine 2000 (Invitrogen, Carlsbad, CA, USA) for 24 h according to the manufacturer's instructions. The subgroups of these cardiomyocytes were subsequently subjected to H/R or lipopolysaccharide (LPS, 3 μ g/ml, 21 h, Sigma) stimulation before harvesting. H/R stimulation was achieved as previously described [19]. Briefly, the H9C2 cardiomyocytes were cultured with DMEM medium (no glucose or FBS) for 6 h in a humidified Plexiglas chamber containing 95% N₂ and 5% CO₂. The cells were then exposed to fresh culture medium and room air atmosphere containing 5% CO₂ and 95% O₂ for an additional 6 h to achieve reoxygenation. The transfection effects were verified by detecting the expression of miR-181c-5p, mRNA, or protein expression of PTPN4 through real-time polymerase chain reaction (PCR) or Western blotting.

2.3. Measurement of Lactate Dehydrogenase (LDH) Activity. The content of LDH, which was released in the culture medium, was measured by LDH cytotoxicity assay kit (Roche, Germany) according to the manufacturer's instructions.

2.4. In Vivo Left Anterior Descending Artery Ligation Model. All experimental procedures were approved by The University of Hong Kong Committee on the Use of Live Animals for Teaching and Research. Male adult Sprague-Dawley rats (8 weeks of age) were anesthetized with ketamine (100 mg/kg) and xylazine (10 mg/kg). The *in vivo* myocardial I/R injury model was induced by occluding the left anterior descending (LAD) artery with a 7-0 silk suture for 30 min followed by 2 h of reperfusion [20]. A sham operation was performed by passing a silk thread under the LAD without occlusion. Myocardial infarct size (IS) was measured by using Evans blue/TTC (1% 2, 3, 5-triphenyltetrazolium chloride) staining and expressed as a percentage of the area at risk (AAR). At the harvest time, the heart was quickly collected for further measurement of miRNA, mRNA, and protein expression.

2.5. Real-Time Polymerase Chain Reaction. Total RNA was extracted from H9C2 cardiomyocytes or rat heart tissues using RNAiso Plus (Takara, Japan) and reverse transcribed to cDNA with PrimeScript RT Master Mix kit (Takara), according to the manufacturer's instructions. For reverse

transcription of miR-181c-5p or U6 (served as an internal reference), specific Bulge-Loop™ miRNA primers (Ribobio) were used instead of the random primers which were included in the PrimeScript RT Master Mix kit. Quantitative real-time PCR was performed with a SYBR green master mix (Takara) on an Applied Biosystems Prism 7000 sequence detection system (Applied Biosystems, Foster City, CA, USA) as previously described [21]. Gene-specific primers were as follows: rat IL-6 forward: 5'-ACTTCACAAGTCGGAGGCTT-3', reverse: 5'-AGTGCATCATCGCTGTTTCAT-3'; rat IL-1 β forward: 5'-TACCTATGTCTTGCCCGTGA-3', reverse: 5'-ATCATC CCACGAGTCACAGAGG-3'; rat TNF α forward: 5'-TCTC AAAACTCGAGTGACAAGC-3', reverse: 5'-GGTTGTCTT TGAGATCCATGC-3'; rat PTPN4 forward: 5'-CCCTCT TCCCCTGAAAAGTC-3', reverse: 5'-TCATGGGTGTG TTCTGCAAT-3'; rat β -actin forward: 5'-AGGCCAACG GTGAAAAGATG-3', reverse: 5'-ACCAGAGGCATACA GGGACAA-3'. Relative mRNA or miRNA levels were quantified by using the $2^{-\Delta\Delta Ct}$ method and normalized to those of β -actin or U6, respectively.

2.6. Western Blotting. H9C2 cardiomyocytes or frozen heart tissues were homogenized in lysis buffer (Sigma) supplemented with Protease inhibitor cocktail tablet (Roche) and Phosphatase inhibitor cocktail tablet (Roche). Equal protein amounts were loaded and separated by 10% sodium dodecyl sulfate polyacrylamide gel electrophoresis and transferred onto polyvinylidene difluoride membranes for immunoblot analysis as previously described [22]. Antibodies against I κ B α (1:1000), phospho-I κ B α (Ser^{32/36}) (1:1000), p65 (1:1000), phospho-p65 (Ser⁵³⁶) (1:1000), GAPDH (1:1000), and β -tubulin (1:3000) were purchased from Cell Signaling Technology and used as primary antibodies. Primary antibody against PTPN4 antibody (1:1000) was purchased from Novus. Horseradish peroxidase-conjugated antimouse (1:3000) or antirabbit (1:3000) secondary antibodies were purchased from Cell Signaling Technology. The blots were visualized with Amersham™ ECL Western Blotting Detection Reagent (GE Healthcare) and subsequently exposed to X-ray film (Carestream, NY, USA). Image J software (National Institutes of Health, MD, USA) was used to quantify the optical densities of the immunoreactive bands.

2.7. Statistical Analysis. All data are presented as means \pm standard error of means (S.E.M.). Comparison between groups was carried out by two-tailed unpaired Student's *t*-test, one-way ANOVA, or two-way ANOVA followed by Bonferroni post hoc test, where appropriate, using the GraphPad Prism 8.0 software (San Diego, CA, USA). In all comparisons, *P* value less than 0.05 was considered as statistically significant difference.

3. Results

3.1. miR-181c-5p Was Upregulated Concomitantly with Enhanced NF κ B Activity in Posthypoxic H9C2 Cardiomyocytes and Postischemic Myocardium of Rat. We have previously reported that the expression of miR-181c-5p in H/R-stimulated H9C2 cardiomyocytes or postischemic myocardium of

rat was significantly increased when compared to control groups [17]. Of note, the current study further demonstrated that upregulation of miR-181c-5p (Figure 1(a)) was paralleled by enhanced NF κ B activity, as evidenced by enhanced degradation of I κ B α and phosphorylation of I κ B α (Ser^{32/36}) and p65 (Ser⁵³⁶) (Figure 1(b)) in H/R-stimulated H9C2 cardiomyocytes. Furthermore, in the *in vivo* myocardial I/R model, increased myocardial infarction size (Figure 1(c)) was accompanied by upregulation of miR-181c-5p (Figure 1(d)) and enhanced NF κ B activity (Figure 1(e)), suggesting that miR-181c-5p may be involved in the NF κ B-mediated proinflammatory responses of cardiomyocytes during the pathology of myocardial I/R injury.

3.2. Overexpression of miR-181c-5p Exacerbated NF κ B-Mediated Inflammation in H9C2 Cardiomyocytes in Response to H/R Stimulation. To determine the role of miR-181c-5p in NF κ B-mediated inflammation in cardiomyocytes under hypoxic condition, the effect of miR-181c-5p on the key enzymes in the NF κ B signalling pathway and the expression of NF κ B-dependent genes were examined in H9C2 cardiomyocytes by using gain-of-function experiments. Overexpression of miR-181c-5p was achieved by transfection of miR-181c-5p agomir into H9C2 cardiomyocytes, which resulted in significant increases in the expression of miR-181c-5p (Figure 2(a)) and in the levels of H/R-stimulated release of LDH (Figure 2(b)), which were consistent with our previous report [17]. Overexpression of miR-181c-5p did not alter the presence of total p65 but significantly enhanced the degradation of I κ B α and increased the level of phosphorylated I κ B α (Ser^{32/36}) and phosphorylated p65 (Ser⁵³⁶) in response to H/R stimulation (Figure 2(c)). Furthermore, the H/R-stimulated induction of NF κ B-mediated proinflammatory cytokines (including IL-1 β , IL-6, and TNF α) was further increased in the presence of overexpression of miR-181c-5p by 58%, 72%, and 435%, respectively (Figure 2(d)). Taken in conjunction, these observations suggested that miR-181c-5p can exacerbate H/R-induced NF κ B signalling by facilitating the phosphorylation of I κ B α and p65, and thus lead to augmentation of NF κ B transcription activity.

3.3. Inhibition of miR-181c-5p Suppressed NF κ B-Mediated Inflammation in H9C2 Cardiomyocytes in Response to H/R Stimulation. To consolidate the proinflammatory effect of miR-181c-5p on NF κ B signalling in cardiomyocytes, antinegative control (the negative control of miR-181c-5p antagomir) or miR-181c-5p antagomir was transfected into H9C2 cardiomyocytes and subsequently subjected to normoxia or H/R stimulation. As anticipated, inhibition of miR-181c-5p significantly attenuated the H/R-induced LDH leakage (Figure 3(a)). In normoxia group, there was a trend towards an increased expression of phosphorylation of I κ B α (Ser^{32/36}) in miR-181c-5p antagomir-transfected H9C2 cells, which however did not reach statistical significance (Figure 3(b)). Upon H/R stimulation, inhibition of miR-181c-5p significantly suppressed the degradation of I κ B α and reduced the phosphorylation of I κ B α (Ser^{32/36}) and p65 (Ser⁵³⁶) (Figure 3(b)). Moreover, inhibition of miR-181c-5p significantly suppressed

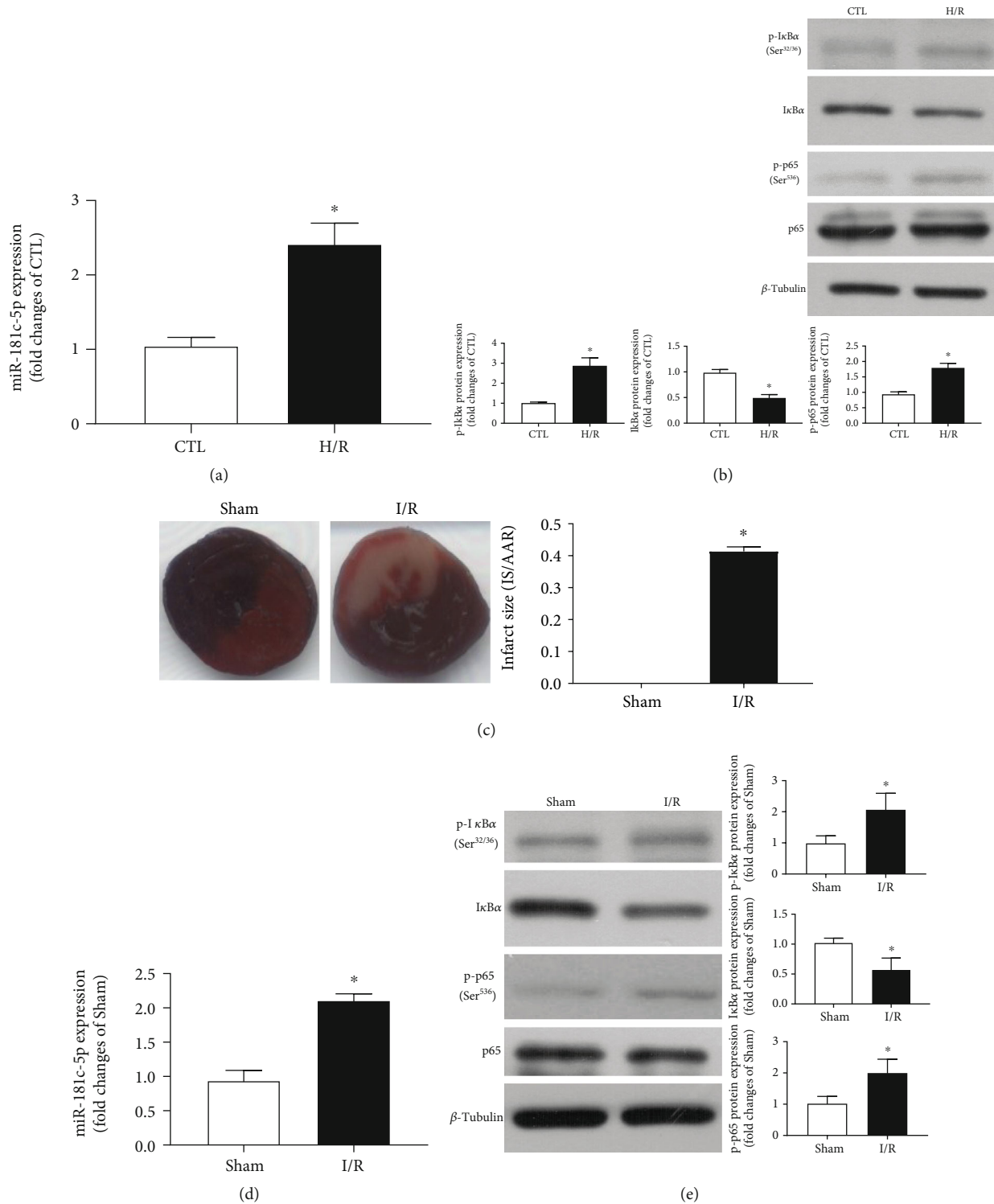


FIGURE 1: miR-181c-5p was upregulated concomitantly with enhanced NF κ B activity in posthypoxic H9C2 cardiomyocytes and postischemic myocardium of rat. (a) Increased expression of miR-181c-5p in hypoxia/reoxygenation (H/R, 6 h hypoxia followed by 6 h reoxygenation) stimulated H9C2 cardiomyocytes. (b) Representative Western blots of phosphorylated I κ B α (Ser^{32/36}), I κ B α , phosphorylated p65 (Ser⁵²⁶), p65, and β -tubulin in the H/R-stimulated H9C2 cardiomyocytes. In the *in vivo* model, myocardial I/R (30 minutes of left anterior descending artery occlusion and 2 hours of reperfusion in rats) induced significant increased postischemic myocardial infarction size (c) and upregulation of miR-181c-5p (d). (e) Representative Western blots of phosphorylated I κ B α (Ser^{32/36}), I κ B α , phosphorylated p65 (Ser⁵²⁶), p65, and β -tubulin in postischemic myocardium of rat. Protein presence of phosphorylated I κ B α (Ser^{32/36}), I κ B α , and phosphorylated p65 (Ser⁵²⁶) was normalized to I κ B α , β -tubulin, and p65, respectively. Data are shown as means \pm SEM; * P < 0.05 vs. CTL or Sham (two-tailed unpaired Student's *t*-test), n = 5.

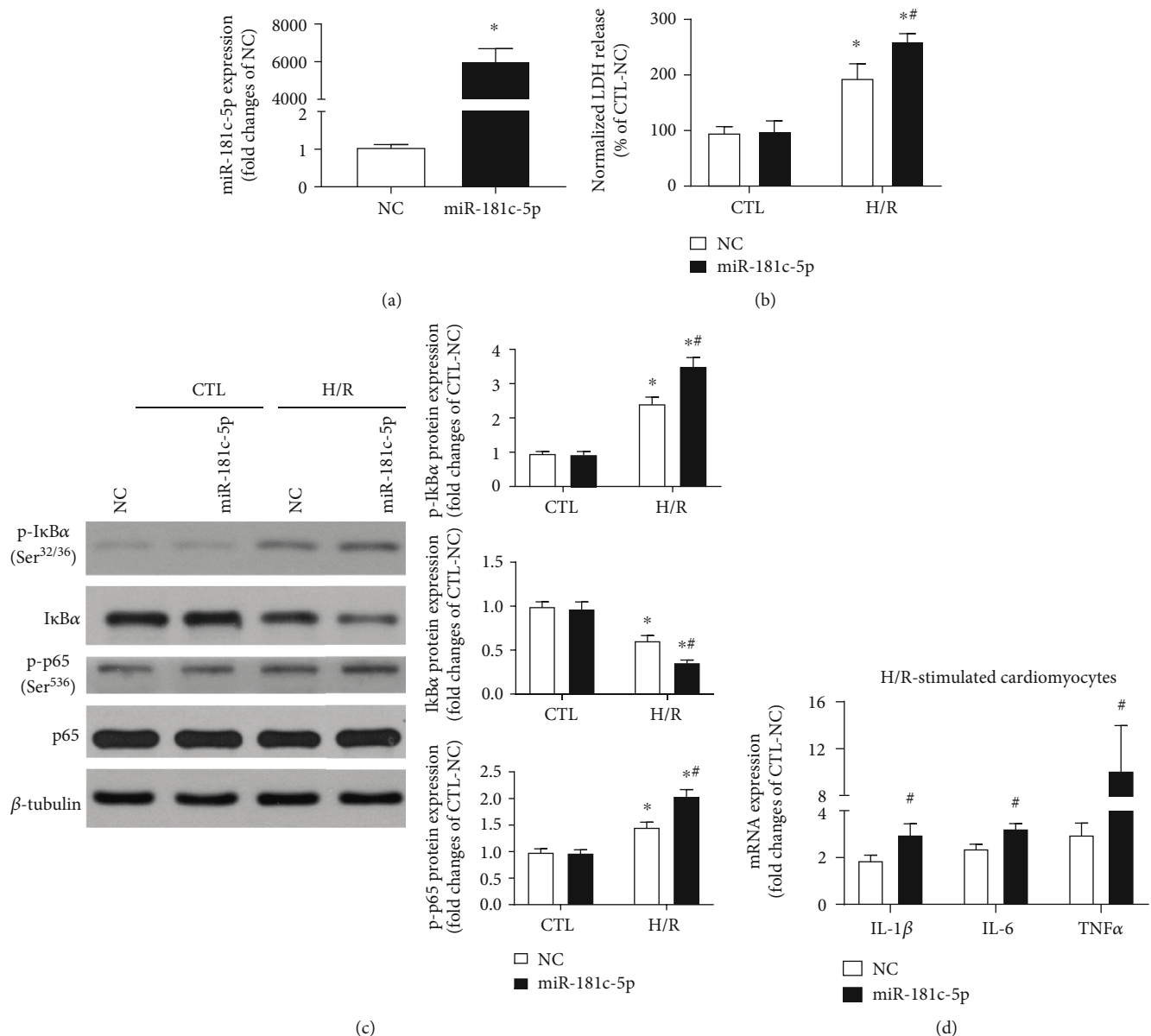


FIGURE 2: Overexpression of miR-181c-5p exacerbated NFκB-mediated inflammation in H9C2 cardiomyocytes in response to H/R stimulation. miR-181c-5p agomir (miR-181c-5p) transfection resulted in significant overexpression of miR-181c-5p in H9C2 cardiomyocytes (a), and overexpression of miR-181c-5p exacerbated the H/R-induced LDH release (b). (c) Representative Western blots of phosphorylated IκBα (Ser^{32/36}), IκBα, phosphorylated p65 (Ser⁵²⁶), p65, and β-tubulin in the NC- or miR-181c-5p agomir-transfected H9C2 cardiomyocytes with or without H/R stimulation. Protein presence of phosphorylated IκBα (Ser^{32/36}), IκBα, and phosphorylated p65 (Ser⁵²⁶) was normalized to IκBα, β-tubulin, and p65, respectively. (d) mRNA expression of NFκB-dependent genes, including IL-1β, IL-6, and TNFα in the NC- or miR-181c-5p agomir-transfected H9C2 cardiomyocytes with H/R stimulation. mRNA levels are expressed as fold changes against those mRNA expressions in NC-transfected H9C2 cardiomyocytes with no stimulation. Data are shown as means ± SEM; **P* < 0.05 vs. CTL, #*P* < 0.05 vs. NC agomir (NC) (two-tailed unpaired Student's *t*-test in (a, d) and two-way ANOVA followed by Bonferroni test in (b, c)), *n* = 5.

the H/R-induced mRNA expression of NFκB-mediated genes, including IL-1β, IL-6, and TNFα by 43%, 48%, and 40%, respectively (Figure 3(c)). Taken together, these findings indicated that inhibition of miR-181c-5p suppresses H/R-induced NFκB signalling in H9C2 cardiomyocytes.

3.4. miR-181c-5p Exacerbated LPS-Induced NFκB Signalling in H9C2 Cardiomyocytes. To further explore whether or not

miR-181c-5p could exacerbate NFκB-mediated proinflammatory responses in cardiomyocytes, experiments were performed using another stimulus—LPS, which has been proved to induce NFκB-dependent proinflammatory cytokines in cardiomyocytes [23, 24]. In response to LPS stimulation, the expression of miR-181c-5p was significantly increased to a level over 2-fold of that of unstimulated cells (Figure 4(a)), suggesting that miR-181c-5p may be involved

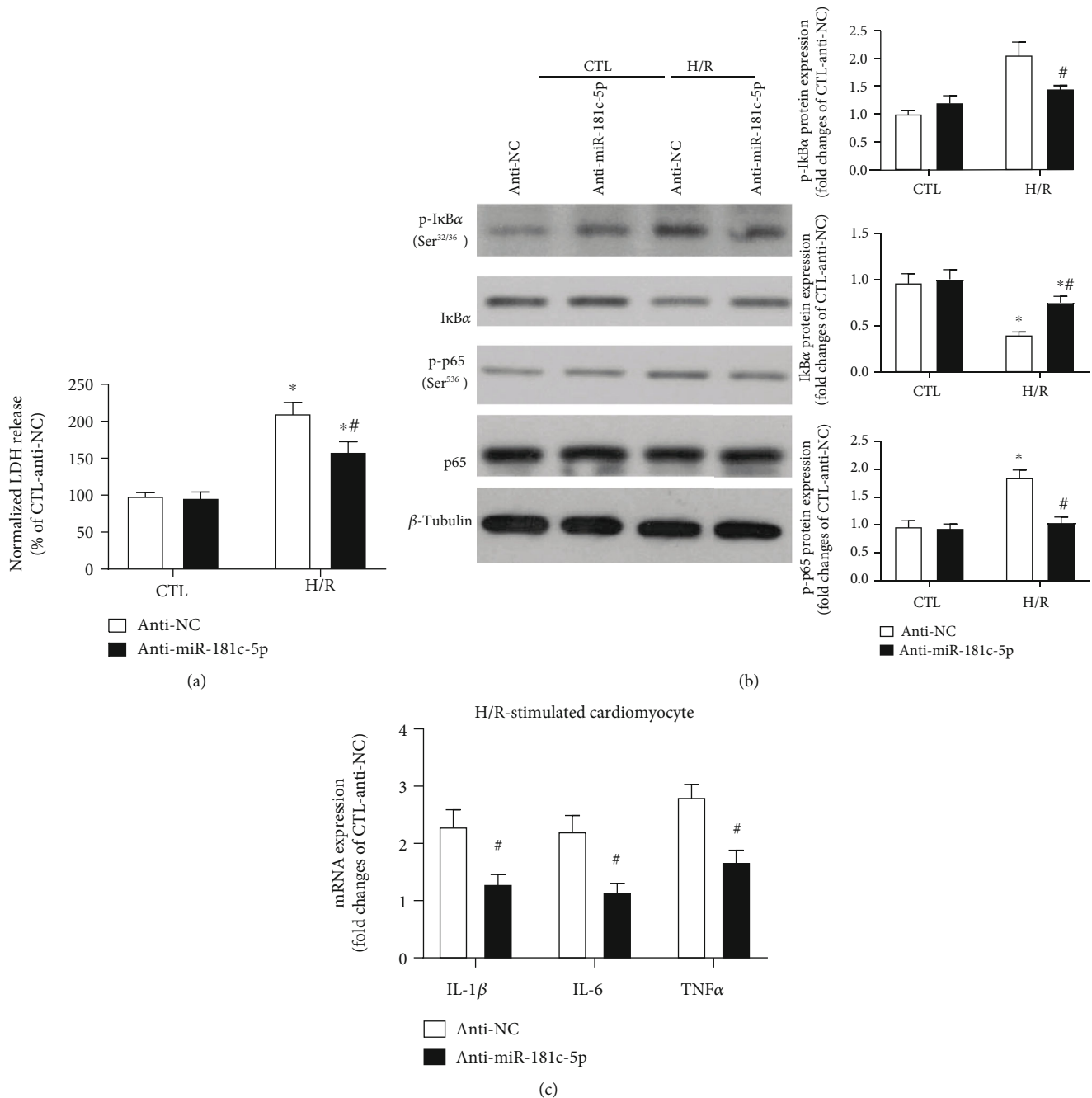


FIGURE 3: Inhibition of miR-181c-5p suppressed NF κ B-mediated inflammation in H9C2 cardiomyocytes in response to H/R stimulation. Inhibition of miR-181c-5p attenuated the H/R-induced LDH release (a). (b) Representative Western blots of phosphorylated I κ B α (Ser^{32/36}), I κ B α , phosphorylated p65 (Ser⁵²⁶), p65, and β -tubulin in the anti-NC- or miR-181c-5p antagonist (anti-miR-181c-5p)-transfected H9C2 cardiomyocytes with or without H/R stimulation. Protein presence of phosphorylated I κ B α (Ser^{32/36}), I κ B α and phosphorylated p65 (Ser⁵²⁶) was normalized to I κ B α , β -tubulin, and p65, respectively. (c) mRNA expression of NF κ B-dependent genes, including IL-1 β , IL-6, and TNF α in the anti-NC- or anti-miR-181c-5p-transfected H9C2 cardiomyocytes with H/R stimulation. mRNA levels are expressed as fold changes against those mRNA expressions in anti-NC-transfected H9C2 cardiomyocytes with no stimulation. Anti-NC: negative control of miR-181c-5p antagonist; data are shown as means \pm SEM; * P < 0.05 vs. CTL, # P < 0.05 vs. NC antagonist (anti-NC) (two-way ANOVA followed by Bonferroni test in (a–c) and two-tailed unpaired Student's t -test in (d)), n = 5.

in the proinflammatory responses of cardiomyocytes to LPS stimulation. In the unstimulated H9C2 cells, there was a trend towards a reduced phosphorylation of I κ B α (Ser^{32/36}) in miR-181c-5p agomir-transfected H9C2 cells, which however did not reach statistical significance (Figure 4(b)). Fur-

thermore, overexpression of miR-181c-5p significantly enhanced LPS-induced degradation of I κ B α and phosphorylation of I κ B α (Ser^{32/36}) and p65 (Ser⁵³⁶) (Figure 4(b)). In contrast, inhibition of miR-181c-5p significantly attenuated LPS-induced degradation of I κ B α and phosphorylation of

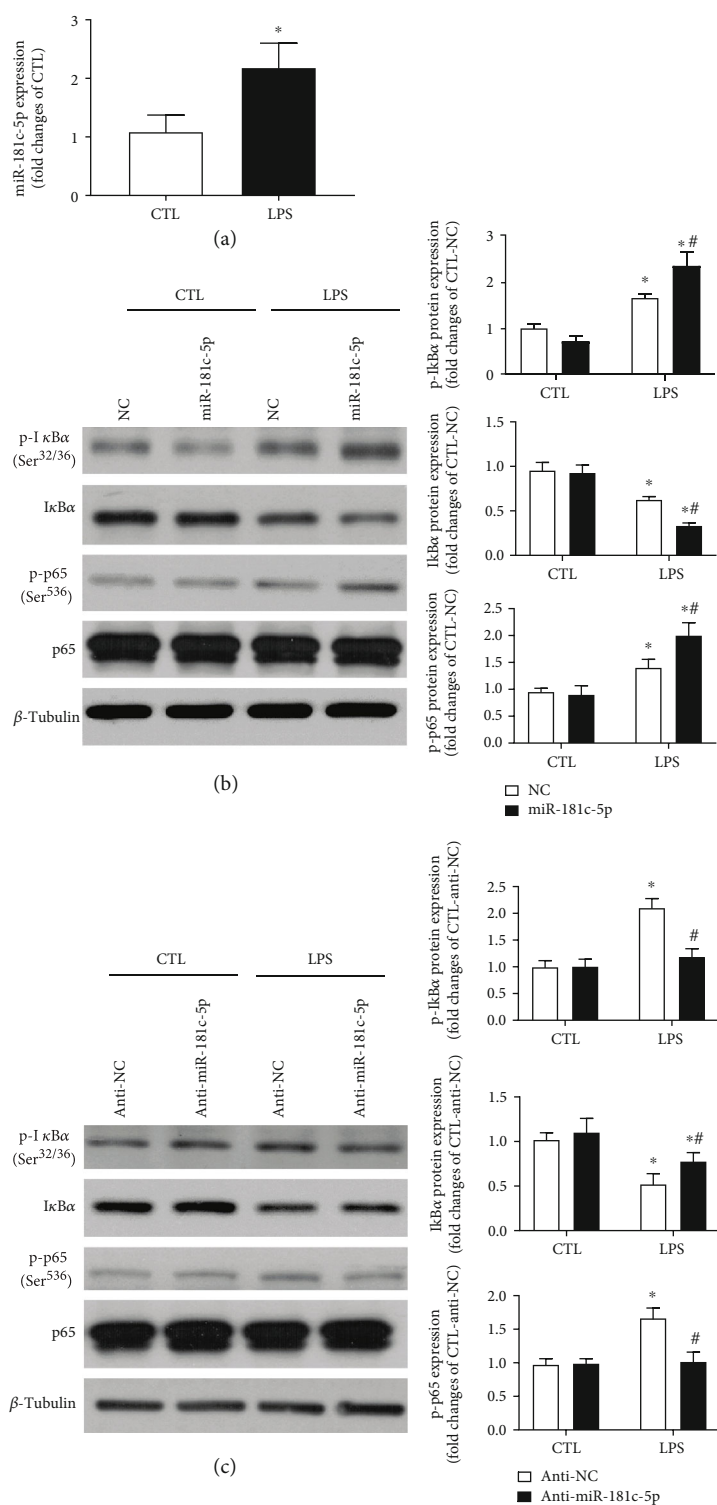


FIGURE 4: miR-181c-5p exacerbated LPS-induced NFκB signalling in H9C2 cardiomyocytes. Increased expression of miR-181c-5p in lipopolysaccharide (LPS, 3 μg/ml, 21 h) stimulated H9C2 cardiomyocytes (a). (b) Representative Western blots of phosphorylated IκBα (Ser^{32/36}), IκBα, phosphorylated p65 (Ser⁵²⁶), p65, and β-tubulin in the NC- or miR-181c-5p agomir-transfected H9C2 cardiomyocytes with or without LPS stimulation. (c) Representative Western blots of phosphorylated IκBα (Ser^{32/36}), IκBα, and phosphorylated p65 (Ser⁵²⁶), p65, and β-tubulin in the anti-NC- or miR-181c-5p antagonist (anti-miR-181c-5p)-transfected H9C2 cardiomyocytes with or without LPS stimulation. Protein presence of phosphorylated IκBα (Ser^{32/36}), IκBα, and phosphorylated p65 (Ser⁵²⁶) was normalized to IκBα, β-tubulin, and p65, respectively. Anti-NC: negative control of miR-181c-5p antagonist; data are shown as means ± SEM; **P* < 0.05 vs. CTL, #*P* < 0.05 vs. NC agomir (NC) or NC antagonist (anti-NC) (two-tailed unpaired Student's *t*-test in (a) and two-way ANOVA followed by Bonferroni test in (b, c), *n* = 5.

I κ B α (Ser^{32/36}) and p65 (Ser⁵³⁶) (Figure 4(c)). Taken together, these results suggested that miR-181c-5p enhances NF κ B signalling in response to LPS stimulation in H9C2 cardiomyocytes.

3.5. Reduction of PTPN4 Mediated the Proinflammatory Effect of miR-181c-5p in H9C2 Cardiomyocytes. We have previously reported that miR-181c-5p can directly bind to the 3'-untranslated region of PTPN4 [17]. Consistently, overexpression of miR-181c-5p leads to significant reduction of protein expression of PTPN4 in cardiomyocytes (Figure 5(a)). In addition, the expressions of PTPN4 mRNA and protein were both significantly reduced in the H/R or LPS-treated H9C2 cells when compared with unstimulated cells (Figures 5(b)–5(e)). Furthermore, the levels of PTPN4 mRNA and protein were also significantly suppressed in the postischemic myocardium of rat (Figures 5(f) and 5(g)), indicating that PTPN4 may be the potential target of miR-181c-5p. The protein level of PTPN4 was also measured in the H9C2 cells transfected with miR-181c-5p agomir or antagomir with or without H/R stimulation. Overexpression of miR-181c-5p led to significant reduction of PTPN4 at basal condition, and the PTPN4 expression was further reduced in miR-181c-5p agomir-transfected cells after H/R stimulation (Figure 5(h)). In contrast, inhibition of miR-181c-5p led to significant increment of PTPN4 in both basal and H/R-stimulated condition (Figure 5(i)). Taken together, these observations lend further support to the interpretation that PTPN4 is the downstream target of miR-181c-5p.

Although emerging evidence has demonstrated that PTPN4 inhibits Toll-like receptor 4/NF κ B signalling in mouse peritoneal macrophages [18], it is still unclear whether or not PTPN4 suppresses NF κ B-mediated proinflammatory responses in cardiomyocytes, especially in the context of H/R-stimulation. To further explore whether PTPN4 knockdown can reproduce the proinflammatory effect of miR-181c-5p, PTPN4 knockdown model was established in H9C2 cardiomyocytes by using siRNA technology, and these cells were subsequently subjected to normoxia or H/R stimulation. Transfection of PTPN4 siRNA significantly reduced the endogenous protein levels (Figure 6(a)) of PTPN4 in H9C2 cells when compared with mock-transfected cells. As anticipated, PTPN4 knockdown significantly enhanced H/R-induced degradation of I κ B α , phosphorylation of I κ B α (Ser^{32/36}) and p65 (Ser⁵³⁶) (Figure 6(b)), and mRNA expression of NF κ B-mediated proinflammatory cytokines (including IL-1 β , IL-6, and TNF α) (Figure 6(c)). To strengthen the notion that reduction of PTPN4 mediates the proinflammatory effect of miR-181c-5p during H/R-induced cell injury, the H9C2 cells were cotransfected with miR-181c-5p antagomir and PTPN4 siRNA and subjected to H/R stimulation. Transfection of miR-181c-5p antagomir alone significantly attenuated phosphorylation of I κ B α (Ser^{32/36}), degradation of I κ B α , and phosphorylation of p65 (Ser⁵³⁶) upon H/R stimulation, while cotransfection of miR-181c-5p antagomir and PTPN4 siRNA cancelled the anti-inflammatory effect of miR-181c-5p antagomir, as evidenced by enhanced phosphorylation of I κ B α (Ser^{32/36}), degradation of I κ B α , and phosphorylation of p65 (Ser⁵³⁶) (Figure 6(d)). Collec-

tively, these results demonstrated that miR-181c-5p may exacerbate NF κ B signalling pathway and thus aggravate cardiomyocyte inflammation and cell injury by directly targeting PTPN4 expression in H9C2 cardiomyocytes.

4. Discussion

Given the detrimental effect of the sustained NF κ B activation in the ischemic heart disease [5, 6], examining ways to attenuate excessive NF κ B-mediated inflammation is of clinical interest to combat cardiac I/R injury. The present study demonstrated that the NF κ B activity was significantly increased, with concomitantly upregulated miR-181c-5p level in the postischemic myocardium and H/R-stimulated H9C2 cardiomyocytes when compared to the control groups, suggesting that increased level of miR-181c-5p may be involved in the NF κ B-mediated inflammation during myocardial I/R injury. Indeed, overexpression of miR-181c-5p exacerbated H/R-induced cell injury (greater LDH leakage), and its proinflammatory effect in cardiomyocytes involves activation of NF κ B signalling pathway, as evidenced by enhanced degradation of I κ B α , increased level of phosphorylated I κ B α (Ser^{32/36}) and phosphorylated p65 (Ser⁵³⁶), and augmented expression of proinflammatory cytokines in response to H/R stimulation. In contrast, inhibition of miR-181c-5p *in vitro* had the opposite effect in NF κ B-mediated inflammation. Of note, neither overexpression nor inhibition miR-181c-5p altered the phosphorylated I κ B α (Ser^{32/36}) or total I κ B α at basal condition. The proinflammatory effect of miR-181c-5p may require the suppression or elevation of some other molecules during H/R. Indeed, in response to H/R, multiple signalling pathways were altered, such as hypoxia-inducible factor 1- α (HIF-1 α) [20] and cyclooxygenase-2 (COX-2) [19], both of which are involved in the H/R-induced inflammation. However, whether HIF-1 α , COX-2, or other molecules work as cofactors and participate in the proinflammatory effect of miR-181c-5p are still unclear and warrants further investigation. Taken together, these results indicated that miR-181c-5p enhances NF κ B-mediated inflammation in cardiomyocytes in response to H/R stimulation.

In addition to explore the role of miR-181c-5p in H/R stimulation induced inflammation, LPS was used in the present study as another stimulus to activate NF κ B signalling pathway in H9C2 cardiomyocytes. In response to LPS stimulation, I κ B α is phosphorylated at serine 32 and 36, followed by ubiquitination and proteasome-mediated degradation [25, 26], leading to the dissociation of I κ B α from NF κ B. The activated NF κ B moves into the nucleus and binds to specific sequences of DNA κ B sites resulting in the transcription of NF κ B-mediated genes [25, 26]. As a component of the bacterial cell wall, LPS has been widely used to establish sepsis model *in vivo* and *in vitro*, because LPS induces profound inflammation and pathological consequences similar to those found during sepsis [27, 28]. Sepsis, an acute inflammatory disease, is a life-threatening condition that follows bacterial infection [29, 30]. Cardiac dysfunction could be an important consequence of sepsis/septic shock and contributes to the high mortality because of the elevated inflammation [29, 30]. In the present study, overexpression of miR-181c-

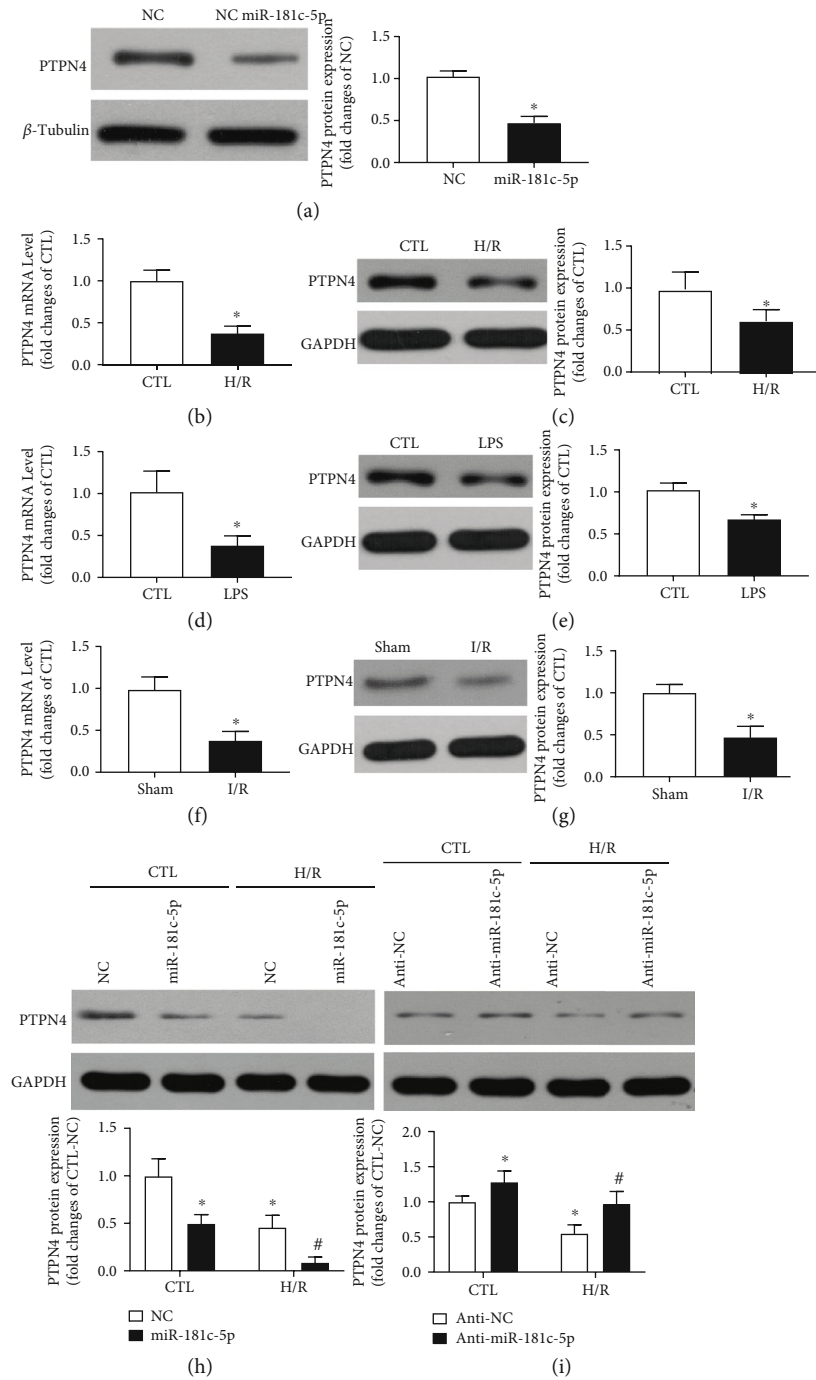


FIGURE 5: PTPN4 is the potential target of miR-181c-5p. Overexpression of miR-181c-5p results in reduced levels of protein expression (a) of PTPN4 in H9C2 cardiomyocytes. (b) mRNA and (c) protein expression in H9C2 cardiomyocytes with or without H/R stimulation. (d) mRNA and (e) protein expression in H9C2 cardiomyocytes with or without LPS stimulation. (f) mRNA and (g) protein expression in the postischemic myocardium of rat. Representative Western blots of PTPN4 and GAPDH in the miR-181c-5p agomir (h) or antagonist (i)-transfected H9C2 cardiomyocytes with or without H/R stimulation. Protein presence of PTPN4 was normalized to β -tubulin or GAPDH. mRNA levels are expressed as fold changes against the mRNA expression in H9C2 cardiomyocytes with no stimulation or myocardium in Sham group. Anti-NC: negative control of miR-181c-5p antagonist; data are shown as means \pm SEM; * P < 0.05 vs. NC agomir (NC) vs. CTL or vs. Sham or vs. CTL-NC agomir (NC) or vs. CTL-NC antagonist (anti-NC), # P < 0.05 vs. H/R-NC or vs. H/R- anti-NC (two-tailed unpaired Student's t -test in (a–g) and two-way ANOVA followed by Bonferroni test in (h, i)), n = 5.

5p further enhanced LPS-induced NF κ B signalling, whereas inhibition of miR-181c-5p attenuated LPS-stimulated NF κ B activation. These observations not only consolidate the pro-inflammatory effect of miR-181c-5p in cardiomyocytes but also

open an exciting research field to investigate the role of miR-181c-5p in cardiac dysfunction during the pathogenesis of sepsis and/or in during the likewise inflammation subsequent to myocardial I/R. To the best of our knowledge, the

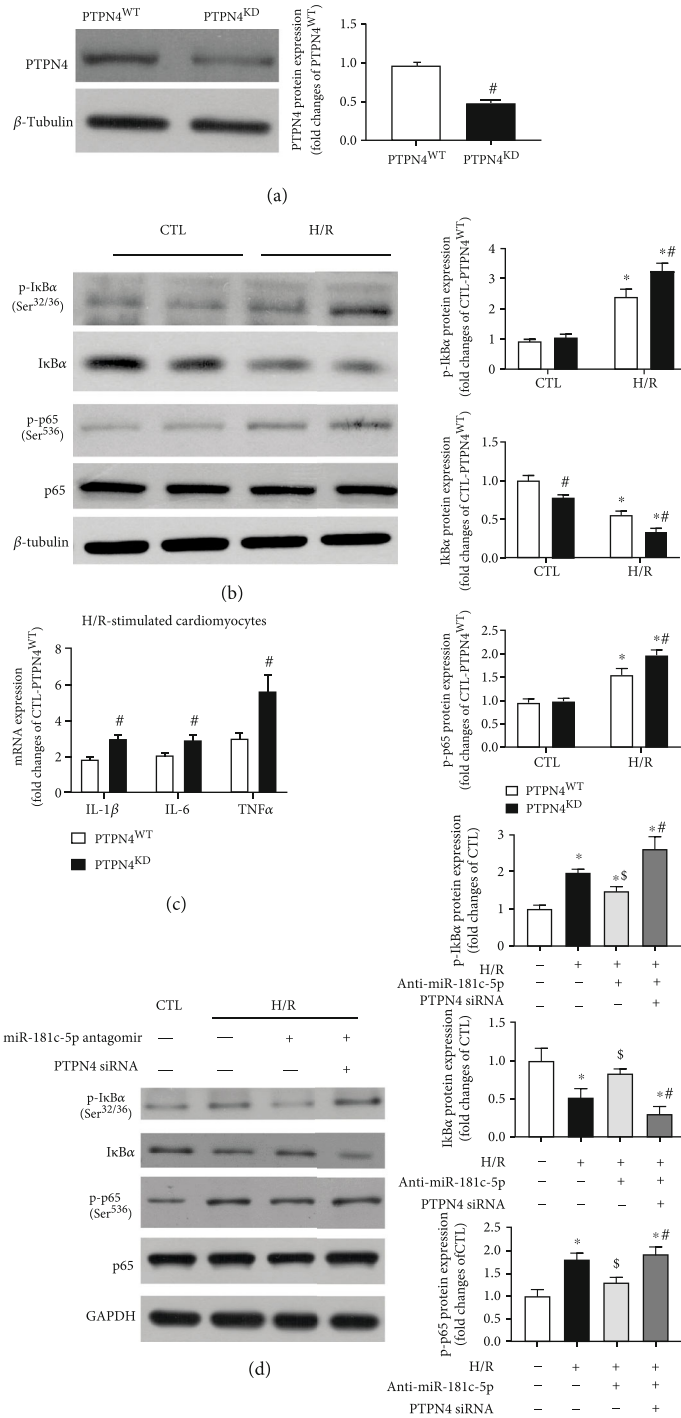


FIGURE 6: Reduction of PTPN4 mediated the proinflammatory effect of miR-181c-5p in H9C2 cardiomyocytes. (a) Transfection of cells with PTPN4 siRNA (PTPN4^{KD}) resulted in significant reduction of PTPN4 protein level in H9C2 cardiomyocytes. (b) Representative Western blots of phosphorylated IκBα (Ser^{32/36}), IκBα, phosphorylated p65 (Ser⁵²⁶), p65, and β-tubulin in the scramble siRNA or PTPN4 siRNA transfected H9C2 cardiomyocytes with or without H/R stimulation. (c) mRNA expression of NFκB-dependent genes, including IL-1β, IL-6, and TNFα in the scramble siRNA or PTPN4 siRNA-transfected H9C2 cardiomyocytes with H/R stimulation. mRNA levels are expressed as fold changes against those mRNA expressions in scramble siRNA-transfected H9C2 cardiomyocytes with no stimulation. (d) Representative Western blots of phosphorylated IκBα (Ser^{32/36}), IκBα, phosphorylated p65 (Ser⁵²⁶), p65, and GAPDH in the H9C2 cardiomyocytes cotransfected with miR-181c-5p antagonist and PTPN4 siRNA and subjected to H/R stimulation. Protein presence of phosphorylated IκBα (Ser^{32/36}), IκBα, and phosphorylated p65 (Ser⁵²⁶) was normalized to IκBα, β-tubulin/GAPDH, and p65, respectively. Data are shown as means ± SEM; *P < 0.05 vs. CTL or vs. NC agomir (NC) or no treatment group, #P < 0.05 vs. PTPN4^{WT} or vs. H/R +miR-181c-5p antagonist, \$P < 0.05 vs. H/R (two-tailed unpaired Student's *t*-test in (a, c), two-way ANOVA followed by Bonferroni test in (b), and one-way ANOVA followed by Bonferroni test in (d)), *n* = 5.

proinflammatory effect of miR-181c-5p in sepsis, especially sepsis-induced myocardial dysfunction has not been explored yet but is worth further investigation.

In response to different stimuli, besides to the classical phosphorylation sites of I κ B α at serine 32 and 36, phosphorylation of I κ B α at tyrosine residue 42 also mediates the degradation of I κ B α and the subsequent NF κ B activation [31, 32]. In a T lymphocytic cell line (EL4), mutation of Ser^{32/36} in I κ B α had no effect on H₂O₂-induced NF κ B activation, but mutation of tyrosine 42 abolished NF κ B activation by H₂O₂ [31]. Consistently, the cardiac NF κ B activation was completely blocked in a murine model which expressed the mutant I κ B α (S32A, S36A, Y42F) in a cardiac-specific manner, while in the mice expressed two mutant I κ B α (S32A, S36A), the NF κ B activation was only partially blocked (70-80%), indicating that phosphorylation of I κ B α at tyrosine residue 42 mediates NF κ B activation independent of Ser^{32/36} phosphorylation in I κ B α [32]. In addition, in HepG2 liver cells, in response to TNF α , activated cytosolic calpains has been shown to degrade I κ B α and activate NF κ B signalling independently of the ubiquitin-proteasome pathway [33]. In the present study, overexpression of miR-181c-5p leads to the phosphorylation of I κ B α at Serine 32 and 36, I κ B α degradation and NF κ B activation in H9C2 cells in response to H/R. However, whether or not miR-181c-5p may affect the phosphorylation of I κ B α at tyrosine residue 42 or cytosolic calpains activity is still unclear and merits further studies.

During the course of our study, we noticed that there are some studies reported that miR-181c-5p can attenuate excessive neuroinflammation through directly targeting the 3'-untranslated region of TNF α mRNA, suppressing its mRNA and protein expression in rat microglial cells after ischemia injury [15], which is opposite to our findings that miR-181c-5p exerts proinflammatory effect through enhanced NF κ B signalling in cardiomyocytes. The different cell types (BV-2 microglial cells vs. H9C2 cardiomyocytes) could be the main explanation regarding the discrepancy between our and others' study. The proinflammatory effect of miR-181c-5p may be cell specific. Similarly, the inhibitory effect of miR-181b (another member in miR-181 family) on NF κ B activation was specific to endothelial cells but not observed in other cell types, such as peripheral blood mononuclear cells [14]. Additionally, the expression pattern of miR-181c-5p varies in different cell types in response to stimulation. In oxygen-glucose deprivation activated BV-2 cells, there was significantly reduced level of miR-181c-5p in a time-dependent manner when compared with nonstimulated cells [15]. However, in the present study, in H9C2 cardiomyocytes, the expression of miR-181c-5p was significantly upregulated in response to H/R or LPS stimulation. Furthermore, in our study, transfection with miR-181c-5p agomir leads to an approximately 6000-fold increase of miR-181c-5p level, whereas there is only 20-fold increase of miR-181c-5p in others' work [15], which may also be viewed as a discrepancy between our and others' study. Moreover, the unaltered mRNA expression of TNF α in the H9C2 cardiomyocytes with miR-181c-5p overexpression also rules out the possibility that miR-181c-5p can directly target 3'-untranslated

region of TNF α mRNA in the current experimental setting. In addition, loss of miR-181c-5p in the mitochondrial compartment shows cardioprotective effects during myocardial I/R injury [34]. In another study, miR-181c-5p aggravates brain injury in acute ischemic stroke through enhancement of apoptosis of microglia and neurons [16]. Taken together, these studies provide additional evidence that miR-181c-5p may play detrimental (proinflammatory) roles during ischemic attack.

We recently reported that miR-181c-5p exacerbates cardiomyocytes injury and apoptosis by directly targeting the 3'-untranslated region of PTPN4 [17]. This target was substantiated through several lines of evidence: (1) overexpression of miR-181c-5p results in the significantly reduction of protein level of PTPN4 in H9C2 cardiomyocytes, which has also been repeated in the present study; (2) significant reduction of mRNA and protein level of PTPN4 in H9C2 in H/R or LPS-treated H9C2 cardiomyocytes and postischemic myocardium of rat; (3) complementary sequence of miRNA-181c-5p was located on the positions from 4915 to 4921 or from 6333 to 6339 (or both) on the 3' UTR of rat PTPN4 mRNA, and there were 7 pairs of Watson-Crick match; (4) mutation of miR-181c-5p binding sites blocked miR-181c-5p-mediated repression of PTPN4 in 293T cells [17]; (5) PTPN4 knockdown recapitulated the proapoptotic effect of miR-181c-5p in H9C2 cardiomyocytes. In addition to its reported effects in protecting against cell apoptosis, PTPN4 has been also reported to suppress Toll-like receptor 4 and may inhibit its downstream NF κ B signalling in mouse peritoneal macrophages [18]. These findings prompted us to hypothesize that miR-181c-5p may enhance NF κ B-mediated inflammation through targeting PTPN4 in H9C2 cardiomyocytes. In line with this speculation, siRNA-mediated knockdown of PTPN4 expression reproduced the proinflammatory effect of miR-181c-5p on NF κ B signalling in cardiomyocytes, as evidenced by the increased H/R-induced degradation of I κ B α , phosphorylation of I κ B α (Ser^{32/36}) and p65 (Ser⁵³⁶), and mRNA expression of NF κ B-mediated proinflammatory cytokines (including IL-6, IL-1 β , and TNF α). Furthermore, cotransfection with miR-181c-5p antagomir and PTPN4 siRNA cancelled the anti-inflammatory effect of miR-181c-5p antagomir. Taken in conjunction, these findings implicate that miR-181c-5p may serve as a regulator of NF κ B-mediated inflammation through targeting PTPN4 in H9C2 cardiomyocytes. It is still unclear whether or not miR-181c-5p targets PTPN4 and exerts proinflammatory effect *in vivo* during I/R injury and warrants investigation in the future study by using miR-181c-5p knockout/overexpression mice.

5. Conclusion

In conclusion, the present study demonstrates that miR-181c-5p is involved in the enhanced NF κ B-mediated inflammation through targeting PTPN4 during myocardial I/R injury or H/R-stimulated cardiomyocyte injury. These observations suggest that increased miR-181c-5p level may serve as a potential risk factor, and future studies will focus on the potential clinical use of miR-181c-5p to combat inflammatory diseases, including ischemic heart disease.

Data Availability

The data used to support the findings of this study are available from the corresponding author upon request.

Conflicts of Interest

The authors declare that there is no conflict of interest regarding the publication of this article.

Authors' Contributions

Sheng Wang and Liang Ge conceived and designed the study, performed experiments, and analysed the data. Dengwen Zhang, Lin Wang, Hao Liu, Xiaodong Ye, and Wanling Liang performed some experiments and analysed the data. Jun Li and Haichun Ma participated in the experiment design and the interpretation of results. Yin Cai and Zhengyuan Xia designed the experiments, analysed the data, and wrote/revised the manuscript. Sheng Wang and Liang Ge contributed equally to this work.

Acknowledgments

The authors' research was supported by General Research Fund (17123718M, 17158616M, 17118619M), Research Grants Council of Hong Kong), National Natural Science Foundation of Jilin (No. 20190201061 JC), The National Natural Science Foundation of China (No. 81970228, 81800245), Guangdong Natural Science Foundation (2018A030313535), and National Key Research and Development Program (2018YFC2001803). The funders had no role in study design, data collection and analysis, decision to publish, or preparation of the manuscript.

References

- [1] I. Y. Elgendy, D. Mahtta, and C. J. Pepine, "Medical therapy for heart failure caused by ischemic heart disease," *Circulation Research*, vol. 124, no. 11, pp. 1520–1535, 2019.
- [2] L. Pang, Y. Cai, E. H. C. Tang, M. G. Irwin, H. Ma, and Z. Xia, "Prostaglandin E receptor subtype 4 signaling in the heart: role in ischemia/reperfusion injury and cardiac hypertrophy," *Journal Diabetes Research*, vol. 2016, article 1324347, 10 pages, 2016.
- [3] J. W. Kim, Y. C. Jin, Y. M. Kim et al., "Daidzein administration *in vivo* reduces myocardial injury in a rat ischemia/reperfusion model by inhibiting NF- κ B activation," *Life Sciences*, vol. 84, no. 7-8, pp. 227–234, 2009.
- [4] R. Dhingra, J. A. Shaw, Y. Aviv, and L. A. Kirshenbaum, "Dichotomous actions of NF- κ B signaling pathways in heart," *Journal of Cardiovascular Translational Research*, vol. 3, no. 4, pp. 344–354, 2010.
- [5] J. W. Gordon, J. A. Shaw, and L. A. Kirshenbaum, "Multiple facets of NF- κ B in the heart: to be or not to NF- κ B," *Circulation Research*, vol. 108, no. 9, pp. 1122–1132, 2011.
- [6] Y. C. Jin, C. W. Kim, Y. M. Kim et al., "Cryptotanshinone, a lipophilic compound of *Salvia miltiorrhiza* root, inhibits TNF- α -induced expression of adhesion molecules in HUVEC and attenuates rat myocardial ischemia/reperfusion injury *in vivo*," *European Journal of Pharmacology*, vol. 614, no. 1-3, pp. 91–97, 2009.
- [7] R. Morishita, T. Sugimoto, M. Aoki et al., "*In vivo* transfection of *cis* element "decoy" against nuclear factor- κ B binding site prevents myocardial infarction," *Nature Medicine*, vol. 3, no. 8, pp. 894–899, 1997.
- [8] Y. Jiang, Y. Gong, N. Lin, and W. Qiu, "Expression of miR-181a and TGF- β 2 in lens epithelial cells of patients with cataractous retinal detachment and its clinical significance," *Experimental and Therapeutic Medicine*, vol. 17, no. 6, pp. 4435–4440, 2019.
- [9] F. J. Li, C. L. Zhang, X. J. Luo, J. Peng, and T. L. Yang, "Involvement of the MiR-181b-5p/HMGB1 pathway in Ang II-induced phenotypic transformation of smooth muscle cells in hypertension," *Aging and Disease*, vol. 10, no. 2, pp. 231–248, 2019.
- [10] J. Ai, C. Gong, J. Wu et al., "MicroRNA-181c suppresses growth and metastasis of hepatocellular carcinoma by modulating NCAPG," *Cancer Management and Research*, vol. 11, pp. 3455–3467, 2019.
- [11] H. Wang, J. Li, H. Chi et al., "MicroRNA-181c targets Bcl-2 and regulates mitochondrial morphology in myocardial cells," *Journal of Cellular and Molecular Medicine*, vol. 19, no. 9, pp. 2084–2097, 2015.
- [12] K. L. Fan, M. F. Li, F. Cui et al., "Altered exosomal miR-181d and miR-30a related to the pathogenesis of CVB3 induced myocarditis by targeting SOCS3," *European Review for Medical and Pharmacological Sciences*, vol. 23, no. 5, pp. 2208–2215, 2019.
- [13] X. Sun, A. Sit, and M. W. Feinberg, "Role of miR-181 family in regulating vascular inflammation and immunity," *Trends in Cardiovascular Medicine*, vol. 24, no. 3, pp. 105–112, 2014.
- [14] X. Sun, B. Icli, A. K. Wara et al., "MicroRNA-181b regulates NF- κ B-mediated vascular inflammation," *The Journal of Clinical Investigation*, vol. 122, no. 6, pp. 1973–1990, 2012.
- [15] L. Zhang, L. Y. Dong, Y. J. Li, Z. Hong, and W. S. Wei, "The microRNA miR-181c controls microglia-mediated neuronal apoptosis by suppressing tumor necrosis factor," *Journal of Neuroinflammation*, vol. 9, no. 1, p. 211, 2012.
- [16] Q. Ma, H. Zhao, Z. Tao et al., "MicroRNA-181c exacerbates brain injury in acute ischemic stroke," *Aging and Disease*, vol. 7, no. 6, pp. 705–714, 2016.
- [17] L. Ge, Y. Cai, F. Ying et al., "miR-181c-5p exacerbates hypoxia/reoxygenation-induced cardiomyocyte apoptosis via targeting PTPN4," *Oxidative Medicine and Cellular Longevity*, vol. 2019, Article ID 1957920, 15 pages, 2019.
- [18] W. Huai, H. Song, L. Wang et al., "Phosphatase PTPN4 preferentially inhibits TRIF-dependent TLR4 pathway by dephosphorylating TRAM," *Journal of Immunology*, vol. 194, no. 9, pp. 4458–4465, 2015.
- [19] L. Pang, Y. Cai, E. H. C. Tang et al., "Cox-2 inhibition protects against hypoxia/reoxygenation-induced cardiomyocyte apoptosis via Akt-dependent enhancement of iNOS expression," *Oxidative Medicine and Cellular Longevity*, vol. 2016, Article ID 3453059, 17 pages, 2016.
- [20] X. Mao, T. Wang, Y. Liu et al., "N-acetylcysteine and allopurinol confer synergy in attenuating myocardial ischemia injury via restoring HIF-1 α /HO-1 signaling in diabetic rats," *PLoS One*, vol. 8, no. 7, article e68949, 2013.
- [21] Y. Cai, F. Ying, E. Song et al., "Mice lacking prostaglandin E receptor subtype 4 manifest disrupted lipid metabolism

- attributable to impaired triglyceride clearance,” *The FASEB Journal*, vol. 29, no. 12, pp. 4924–4936, 2015.
- [22] Y. Cai, F. Ying, H. Liu et al., “Deletion of Rap1 protects against myocardial ischemia/reperfusion injury through suppressing cell apoptosis via activation of STAT3 signaling,” *The FASEB Journal*, vol. 34, no. 3, pp. 4482–4496, 2020.
- [23] Q. Ren, S. Zhao, C. Ren, and Z. Ma, “Astragalus polysaccharide alleviates LPS-induced inflammation injury by regulating miR-127 in H9c2 cardiomyoblasts,” *International Journal of Immunopathology and Pharmacology*, vol. 31, 2018.
- [24] S. Franceschelli, M. Pesce, A. Ferrone et al., “Biological effect of licochalcone C on the regulation of PI3K/Akt/eNOS and NF- κ B/iNOS/NO signaling pathways in H9c2 cells in response to LPS stimulation,” *International Journal of Molecular Sciences*, vol. 18, no. 4, p. 690, 2017.
- [25] Y. Cai, G. K. Sukhova, H. K. Wong et al., “Rap1 induces cytokine production in pro-inflammatory macrophages through NF κ B signaling and is highly expressed in human atherosclerotic lesions,” *Cell Cycle*, vol. 14, no. 22, pp. 3580–3592, 2015.
- [26] S. Ghosh, M. J. May, and E. B. Kopp, “NF- κ B and Rel proteins: evolutionarily conserved mediators of immune responses,” *Annual Review of Immunology*, vol. 16, no. 1, pp. 225–260, 1998.
- [27] M. Gao, X. Wang, X. Zhang et al., “Attenuation of cardiac dysfunction in polymicrobial sepsis by MicroRNA-146a is mediated via targeting of IRAK1 and TRAF6 expression,” *Journal of Immunology*, vol. 195, no. 2, pp. 672–682, 2015.
- [28] K. Drosatos, A. Lymperopoulos, P. J. Kennel, N. Pollak, P. C. Schulze, and I. J. Goldberg, “Pathophysiology of sepsis-related cardiac dysfunction: driven by inflammation, energy mismanagement, or both?,” *Current Heart Failure Reports*, vol. 12, no. 2, pp. 130–140, 2015.
- [29] M. W. Merx and C. Weber, “Sepsis and the heart,” *Circulation*, vol. 116, no. 7, pp. 793–802, 2007.
- [30] F. Fattahi and P. A. Ward, “Complement and sepsis-induced heart dysfunction,” *Molecular Immunology*, vol. 84, pp. 57–64, 2017.
- [31] S. Schoonbroodt, V. Ferreira, M. Best-Belpomme et al., “Crucial role of the amino-terminal tyrosine residue 42 and the carboxyl-terminal PEST domain of I κ B α in NF- κ B activation by an oxidative stress,” *Journal of Immunology*, vol. 164, no. 8, pp. 4292–4300, 2000.
- [32] M. Brown, M. McGuinness, T. Wright et al., “Cardiac-specific blockade of NF-kappaB in cardiac pathophysiology: differences between acute and chronic stimuli in vivo,” *American Journal of Physiology-Heart and Circulatory Physiology*, vol. 289, no. 1, pp. H466–H476, 2005.
- [33] Y. Han, S. Weinman, I. Boldogh, R. K. Walker, and A. R. Brasier, “Tumor necrosis Factor- α -inducible I κ B α proteolysis mediated by cytosolic m-Calpain,” *The Journal of Biological Chemistry*, vol. 274, no. 2, pp. 787–794, 1999.
- [34] S. Das, M. Kohr, B. Dunkerly-Eyring et al., “Divergent effects of miR-181 family members on myocardial function through protective cytosolic and detrimental mitochondrial microRNA targets,” *Journal of the American Heart Association*, vol. 6, no. 3, 2017.